

1-5-2012

Metal complexes of non-heme ligands: biological applications

Jai Prakash
Wayne State University,

Follow this and additional works at: http://digitalcommons.wayne.edu/oa_dissertations

 Part of the [Chemistry Commons](#)

Recommended Citation

Prakash, Jai, "Metal complexes of non-heme ligands: biological applications" (2012). *Wayne State University Dissertations*. Paper 518.

This Open Access Dissertation is brought to you for free and open access by DigitalCommons@WayneState. It has been accepted for inclusion in Wayne State University Dissertations by an authorized administrator of DigitalCommons@WayneState.

METAL COMPLEXES OF NON-HEME LIGANDS: BIOLOGICAL APPLICATIONS

by

JAI PRAKASH

DISSERTATION

Submitted to the Graduate School

of Wayne State University,

Detroit, Michigan

in partial fulfillment of the requirements

for the degree of

DOCTOR OF PHILOSOPHY

2012

MAJOR: CHEMISTRY (Organic)

Approved by:

Advisor

Date

DEDICATION

To my beloved parents and my family

ACKNOWLEDGEMENT

Firstly, I would like to thank my advisor Prof. Jeremy J. Kodanko for his support and guidance throughout my graduate studies. He was an excellent mentor and has always guided me not only in the scientific front but has also advised me on my future career prospects. I was always impressed with his scientific knowledge and his commitment towards research. I would like to thank him for his patience while teaching in the lab. I have learnt a lot under his guidance. In addition, I would also like to thank him for all the group outings (not to forget places on Cass) and discussion we used to have.

I would like to take this opportunity to thank my committee members Dr. Mary K. Pflum, Dr. Matthew J. Allen and Dr. Timothy L. Stemmler for all their time and valuable suggestions. I would like to thank them for being there for me whenever I needed them.

I would like to thank my collaborator Dr. Q. Ping Dou from Karmanos Cancer Institute, Wayne State University, for his valuable discussions, and allowing me to use the facilities in his lab, which helped me a lot to finish my graduate studies. I would also like to thank Sara, graduate student from his lab for all her help.

I would like to thank Lumigen Instrument Center (LIC) staff members of Wayne State University, especially Dr. Bashar Ksebati, Dr. Brian Shay and Dr. Lew Hryhorczuk for their help and support with the NMR and Mass instruments. I would also like to thank Dr. Mary Jane Heeg for her help with X-ray crystal structure.

I would also like to thank the official staff members of the Chemistry department, Melissa Barton, Mary Wood, Diane Klimas, Erin Bachert, Debbie McCreless and Bernie

Miesik. They were very helpful and very efficient. I would also like to thank Nestor for being there whenever I needed his help regarding computer matters.

I would like to thank all my previous lab members Dr. Anil, Dr. Ashley, Dr. Ahmed, Dr. Nitin, Mirvat, Selma and Casey along with all undergraduates who made the lab a pleasant place to work. Special thank to my present group members Tomasz, Eric and Raj for all their support and encouragement till the end. I had a wonderful time with all of them whether it's in the lab or outside.

I would like to thank my friends from Wayne State University who have made my stay in the graduate school enjoyable. I had very good time playing cricket that made my stress go away.

Finally, I would like to thank my parents and family for their support and trust on me. They have always supported me in every front of my life. I would like to thank Shreyashi for all her love and support. Lastly, I would like to thank the almighty god for the blessings throughout the graduate life.

TABLE OF CONTENTS

Dedication.....	ii
Acknowledgements.....	iii
List of Tables.....	ix
List of Figures.....	x
List of Abbreviations.....	xv
Chapter 1. Introduction.....	1
1.1. Background.....	1
1.2. Heme ligands	
1.2.1. Heme-enzymes in oxidation.....	2
1.2.2. Mechanism of heme-catalysis.....	3
1.2.3. Synthetic heme ligands and their applications.....	4
1.2.4. Drawback.....	5
1.3. Non-heme ligands.....	5
1.3.1. Non-heme enzymes in oxidation.....	5
1.3.2. Mechanism of non-heme enzyme catalysis.....	6
1.3.3. Synthetic non-heme ligands.....	7
1.3.3.1. Application.....	8
1.3.3.1.1. Oxidation of organic substrates.....	8
1.3.3.1.1.1. Generation and characterization of ferryls.....	8
1.3.3.1.1.2. Oxidation by ferryls.....	9
1.3.3.1.2. DNA oxidation.....	11
1.3.3.1.3. Protein oxidation.....	13

1.3.3.1.3.1. Human carbonic anhydrase-I.....	16
1.3.3.1.3.2. Serine proteases.....	18
1.3.3.1.3.3. Proteasome.....	20
1.3.3.1.4. Enzyme inhibition.....	21
1.3.3.1.4.1. Stoichiometric vs. catalytic inhibitors.....	21
1.3.3.1.4.1. Metal complexes as catalytic inhibitors.....	22
1.3.3.1.5. Glutathionylation of cobalamin (Cbl) model complexes.....	22
1.4. Thesis Statement.....	25
Chapter 2. Inactivation of Carbonic Anhydrase-I and Serine Proteases by Non-Heme Iron Complexes.....	29
2.1. Introduction.....	29
2.2. Inactivation of carbonic anhydrase-I.....	32
2.2.1. Results.....	32
2.2.1.1 Inhibitor design.....	32
2.2.1.2. Inhibitor synthesis.....	34
2.2.1.3. Inhibition studies.....	35
2.2.1.4. Inactivation studies.....	36
2.2.1.5. Characterization of products.....	38
2.2.2 Discussion.....	40
2.3. Inactivation of serine proteases.....	42
2.3.1. Results.....	42
2.3.1.1. Synthesis of Ligand.....	42
2.3.1.2. Generation and characterization of ferryl species.....	43
2.3.1.3. Enzymatic inactivation with ferryl compounds.....	44

2.3.1.4. Characterization of products.....	47
2.3.1.5. Enzymatic inactivation with ferrous complexes and H ₂ O ₂	51
2.3.1.6. Mechanistic studies.....	55
2.3.2. Discussion.....	60
2.4. Conclusions and future directions.....	64
2.5. Experimental section.....	65
Chapter 3. Inhibition of 20S Proteasome by Non-Heme Iron Complexes.....	75
3.1. Introduction.....	75
3.2. Results.....	77
3.2.1. IC ₅₀ determination.....	77
3.2.2. Mechanistic studies.....	79
3.2.2.1. Time-dependent inactivation.....	79
3.2.2.2. ROS scavenger.....	82
3.2.2.3. <i>In cellulo</i> studies.....	83
3.3. Discussion.....	84
3.4. Conclusions and future directions.....	86
3.5. Experimental section.....	86
Chapter 4. Synthesis, Characterization and Glutathionylation of Cobalamin Model Complexes [Co^{III}(N4PyCO₂Me)Cl]Cl₂ and [Co^{III}(BnCDPy3)Cl]Cl₂.....	89
4.1. Introduction.....	89
4.2. Results.....	91
4.2.1. Synthesis of [Co ^{III} (N4PyCO ₂ Me)Cl]Cl ₂	91
4.2.2. UV-vis spectroscopic data.....	91
4.2.3. ¹ H-NMR and ¹³ C-NMR spectroscopic data.....	92

4.2.4. High-resolution mass spectrometric data.....	93
4.2.5. X-ray crystallography data.....	94
4.2.6. Molar conductivity data.....	97
4.2.7. Glutathionylation of the cobalt complexes.....	98
4.3. Discussion.....	108
4.4. Conclusions and future directions.....	111
4.5. Experimental section.....	112
Chapter 5. Conclusions and Future Directions.....	116
Appendix A.....	122
Appendix B.....	136
Appendix C.....	147
References.....	152
Abstract.....	177
Autobiographical Statement.....	179

LIST OF TABLES

Table 2.1. IC ₅₀ values for inhibition of CA-I for compounds 1 and 4 , their metal complexes and free metal ions.....	36
Table 2.2. IC ₅₀ values (μM) for the inhibition of trypsin and chymotrypsin by ligands 8 and 7 and their respective ferrous (9 and 10) and ferryl (11 and 12) complexes.....	46
Table 3.1. IC ₅₀ values (μM) for inhibition of chymotrypsin-like (CT), trypsin-like (T) and peptidylglutamyl peptide hydrolyzing-like (PGPH) activity of 20S proteasome by ligands 1 and 2 and their respective ferrous complexes (3 and 4) along with iron metal ion control.....	78
Table 4.1. Crystal data and structure refinement for 3 ·MeOH·EtOH.....	95
Table 4.2. Selected bond lengths (Å) of 3	96
Table 4.3. Selected bond angles (°) of 3	96
Table 4.4. Molar conductivities for 3 in H ₂ O at 298 ± 2 K.....	97
Table 4.5. Initial rates of reaction of 3 (0.5 mM) with GSH (15 mM) as a function of pH.....	101

LIST OF FIGURES

Figure 1.1. Structure of protoheme IX.....	3
Figure 1.2. Proposed mechanism of the hydroxylation of organic substrates by CP450.....	4
Figure 1.3. Structures of synthetic porphyrin ligands.....	5
Figure 1.4. Coordination around metal center in non-heme iron enzymes a) protocatechuate 3,4-dioxygenase (3,4-PCD) b) 2,3-dihydroxy- biphenyl 1,2-dioxygenase (BphC) c) lipoxygenases (SLO-1) and d) isopenicillin N synthase (IPNS, Mn-substituted).....	6
Figure 1.5. Proposed mechanism of TauD catalysis.....	7
Figure 1.6. Non-heme ligands.....	8
Figure 1.7. Oxidation of organic substrates by non-heme iron ferryls.....	11
Figure 1.8. Structure of bleomycin (BLM).....	12
Figure 1.9. DNA cleavage by “activated bleomycin” in aerobic condition.....	12
Figure 1.10. Structures of molecules mimicking the metal-binding unit of bleomycin...	12
Figure 1.11. Co(III)-cyclen, and their derivatives a and b	14
Figure 1.12. Palladium complexes involved in the peptide cleavage in Cytochrome c.....	14
Figure 1.13. Mechanism of CO ₂ hydration catalyzed by CA.....	17
Figure 1.14. Mode of inhibition of sulfonamides and SCN ⁻	17
Figure 1.15. Sulfonamide based CAs inhibitors.....	18
Figure 1.16. The catalytic triad in serine proteases.....	19
Figure 1.17. Trypsin inhibitors.....	19
Figure 1.18. Chymotrypsin inhibitors.....	19
Figure 1.19. Proteasome 26S showing catalytic (core) and regulatory unit with ubiquitinated protein inside it.....	20
Figure 1.20. Structures of various proteasome inhibitors.....	21

Figure 1.21. Mode of action of stoichiometric and catalytic inhibitors.....	21
Figure 1.22. Structures of natural cobalamines.....	24
Figure 2.1. Structure of ligands used in the inactivation studies.....	32
Figure 2.2. (a) Molecular modelling representation of $[\text{Fe}^{\text{IV}}(\text{O})(\mathbf{4})]^{2+}$ docked in the active site of CA-I. (b) Space-filling representation of $[\text{Fe}^{\text{IV}}(\text{O})(\mathbf{4})]^{2+}$ docked in the active site of CA-I.....	34
Figure 2.3. Inhibition of CA-I by $\text{Fe}^{\text{II}}\cdot\mathbf{4}$	36
Figure 2.4. Plot of CA-I activities vs. time of preincubation at 37 °C in the presence of the reductant DTT.....	37
Figure 2.5. SDS-PAGE analysis (12%), stained with Coomassie blue, of CA-I (20 μM) incubated at 37 °C for 3 h at pH = 8.0, in 12.5 mM Tris buffer containing 75 mM NaCl and 10 mM DTT.....	39
Figure 2.6. Deconvoluted ESI-MS spectra of CA-I after treatment with Fe^{II} (spectrum a) or $\text{Fe}^{\text{II}}\cdot\mathbf{4}$ (spectrum b) in the presence of DTT.....	39
Figure 2.7. (a) Figure showing location of oxidized histidine (H67, H64, H200 and H243), tryptophan (W16 and W243) and methionine (M241) residues of CA-I (shown in red) with respect to the active site and the docked inhibitor $[\text{Fe}^{\text{IV}}(\text{O})(\mathbf{4})]^{2+}$	40
Figure 2.8. UV-vis spectra of ferrous and ferryl complexes in H_2O : (a) 9 (red) and 10 (blue); (b) 11 (red) and 12 (blue).....	44
Figure 2.9. IC_{50} plots with ferryl species 11 (red \blacktriangle) and 12 (blue \blacklozenge) for trypsin (a) and chymotrypsin (b).....	45
Figure 2.10. (a) SDS-PAGE analysis (16%), stained with Coomassie blue, of trypsin (20 μM) incubated at room temperature for 1 h at pH = 6.0, in a 10 mM acetate buffer containing 150 mM NaCl.....	47
Figure 2.11. LC chromatograms (top) and deconvoluted MS spectra (bottom) of trypsin (spectrum a) and after treatment with 12 (spectrum b) or 11 (spectrum c).....	49
Figure 2.12. LCMS chromatograms (top) and deconvoluted MS spectra (bottom) of chymotrypsin (spectrum a) and after treatment with 12 (spectrum b) or 11 (spectrum c).....	50
Figure 2.13. Trypsin (graph a) and chymotrypsin (graph b) activities as a function of added H_2O_2	52

Figure 2.14. SDS-PAGE analysis (16%), stained with silver, of (a) trypsin and (b) chymotrypsin (1 μM), pulsed with H_2O_2 (40 μM) every 10 min in presence of 10 (20 μM) at room temperature at pH = 6.0, in a 10 mM acetate buffer containing 150 mM NaCl.....	54
Figure 2.15. Inactivation of trypsin in the presence of ROS scavengers (azide, D-mannitol, and imidazole).....	56
Figure 2.16. Carbonyl content (nmol/mg of protein) as a function of pulsed H_2O_2 (0-500 μM) for enzymes (20 μM) trypsin (blue ●) and chymotrypsin (red ▲) in the presence of 10 (50 μM).....	57
Figure 2.17. Bar graphs showing the compositions of five natural amino acids present in the oxidized proteins samples isolated from single-turnover (ferryls 11 and 12 in green and gold, respectively) and catalytic conditions (9 or 10 plus H_2O_2 in red and blue, respectively) for trypsin (a) and chymotrypsin (b).....	59
Figure 2.18. Surface models of trypsin and chymotrypsin with tyrosine residues near the active site highlighted in red.....	62
Figure 3.1. Polydentate nitrogen-containing ligands.....	77
Figure 3.2. Binding and oxidation mode of action of iron complexes for 20S proteasome inactivation.....	79
Figure 3.3. Time-dependent inactivation of the purified 20S proteasome.....	80
Figure 3.4. Model illustrating the coordination sphere around iron centers of the ferrous complexes derived from (a) Bn-TPEN and (b) TPEN.....	81
Figure 3.5. Inactivation of the purified 20S proteasome by ferrous complex 4 in the presence of ROS scavengers (azide and D-mannitol).....	82
Figure 3.6. Effect of compounds 1-4 on apoptosis induction in PC-3 cells.....	83
Figure 4.1. Structures of polypyridyl N5 pentadentate ligands 1 and 2 , and glutathione.....	91
Figure 4.2. UV-vis spectrum of 3 in MeOH (1 mM) at 298 ± 2 K.....	92
Figure 4.3. ^1H -NMR (left) and ^{13}C -NMR (right) spectrum of 3 in CD_3OD	93
Figure 4.4. Calculated (top) and observed (bottom) high-resolution mass Spectra (HRMS) for the dication $[\text{Co}^{\text{III}}(\text{N4PyCO}_2\text{Me})\text{Cl}]^{2+}$ of 3	93
Figure 4.5. ORTEP diagram of the dication $[\text{Co}^{\text{III}}(\text{N4PyCO}_2\text{Me})\text{Cl}]^{2+}$	97

Figure 4.6. UV-vis spectral change for 3 (0.5 mM) on reaction with GSH (10 mM) in 100 mM acetate buffer at 298 ± 2 K (Inset: Abs vs. time plot for growth of peak at 323 nm).....	98
Figure 4.7. (a) Plot of initial rate (dA_{323}/dt) vs. [GSH] for substitution of Cl^- with GSH (0.5–25 mM) in 3 (0.5 mM) in 100 mM acetate buffer to form $[\text{Co}^{\text{III}}(\text{N4PyCO}_2\text{Me})(\text{SG})]^{2+}$. (b) Plot of initial rate (dA_{323}/dt) vs. [3] for substitution of Cl^- with GSH (4.0 mM) in 3 (0.5–4 mM) in 100 mM acetate buffer.....	99
Figure 4.8. Abs_{323} vs [GSH] plot, obtained from the equilibrated solutions of 3 (0.5 mM) and GSH (0.0–15 mM) kept at 298 ± 2 K for 2 h.....	100
Figure 4.9. $^1\text{H-NMR}$ spectra (6–10 ppm) of reaction mixture containing 3 (10 mM) and GSH (40 mM), after a time interval of 0 h (top), 16 h (middle) and 96 h (bottom) in D_2O	102
Figure 4.10. COSEY spectra (1–10 ppm) for the reaction of 3 (10 mM) with GSH (40 mM) in D_2O after 96 h.....	103
Figure 4.11. Calculated (top) and observed (bottom) high-resolution mass spectra (HRMS) for the dication $[\text{Co}^{\text{III}}(\text{N4PyCO}_2\text{Me})(\text{SG})]^{2+}$ of 5	104
Figure 4.12. UV-vis spectral change for 4 (0.5 mM) upon reaction with GSH (10 mM) in 100 mM acetate buffer pH 5.00 at 298 ± 2 K (Inset: Abs vs. time plot for growth of peak at 320 nm).....	105
Figure 4.13. (a) Plot of initial rate (dA_{320}/dt) vs. [GSH] for substitution of Cl^- with GSH (0.5–25.0 mM) in 4 (0.5 mM) in 100 mM acetate buffer. (c) Plot of initial rate (dA_{320}/dt) vs. [4] for substitution of Cl^- with GSH (25 mM) in 4 (0.25–1.5 mM) in 100 mM acetate buffer.....	106
Figure 4.14. Abs_{320} vs [GSH] plot, obtained from the equilibrated solutions of 4 (0.5 mM) and GSH (0.0–25.0 mM) kept at 298 ± 2 K for 3 h.....	106
Figure 4.15. Calculated (top) and observed (bottom) high-resolution mass spectra (HRMS) for the dication $[\text{Co}^{\text{III}}(\text{Bn-CDPy3})(\text{SG})]^{2+}$ of 6	107

LIST OF SCHEMES

Scheme 1.1. Fenton chemistry.....	2
Scheme 2.1. Synthesis of N4Py-sulfonamide inhibitor 4	35
Scheme 2.2. Synthesis of ligand 3CG-N4Py.....	42
Scheme 2.3. Conversion of Ac-Tyr-OH into Ac-DOPA-OH in presence of ferrous complex and H ₂ O ₂	60
Scheme 4.1. Synthesis of [Co ^{III} (N4PyCO ₂ Me)Cl]Cl ₂ (3).....	91

LIST OF ABBREVIATION

CP450.....	Cytochrome P450
MMO.....	Methane monooxygenase
SAMO.....	Secondary amine monooxygenase
IDO.....	Indoleamine 2,3-dioxygenase
TDO.....	Tryptophan 2,3-dioxygenase
TPP.....	<i>Meso</i> -tetraphenylporphyrin
PhIO.....	Iodosylbenzene
DNA.....	Deoxyribonucleic acid
3,4-PCD.....	Protocatechuate 3,4-dioxygenase
BphC.....	2,3-dihydroxybiphenyl 1,2-dioxygenase
SLO-1.....	Lipoxygenases
IPNS.....	Isopenicillin <i>N</i> synthase
EPR.....	Electron paramagnetic resonance
LMCT.....	Ligand-to-metal charge transfer
UV-vis.....	Ultraviolet visible
TauD.....	Taurine: α -ketoglutarate dioxygenase
Por.....	Porphyrin
TMC.....	Tetramethylcyclam
N4Py.....	1,1-Di(pyridin-2-yl)- <i>N,N</i> -bis(pyridin-2-ylmethyl) methanamine
DTT.....	Dithiothreitol
BPh ₄ ⁻	Tetraphenylborate
NADH.....	Nicotinamide adenine dinucleotide
TPA.....	Tris(pyridin-2-ylmethyl)amine

BQEN.....	<i>N</i> ¹ , <i>N</i> ² -Dimethyl- <i>N</i> ¹ , <i>N</i> ² -di(quinolin-8-yl)ethane-1,2-diamine
BPMEN.....	<i>N</i> ¹ , <i>N</i> ² -Dimethyl- <i>N</i> ¹ , <i>N</i> ² -bis(pyridin-2-ylmethyl)ethane-1,2-diamine
Bn-TPEN.....	<i>N</i> ¹ -benzyl- <i>N</i> ¹ , <i>N</i> ² , <i>N</i> ² -tris(pyridin-2-ylmethyl)ethane-1,2-diamine.
BLM.....	Bleomycin
Fe-BLMs.....	Iron bleomycins
ROS.....	Reactive oxygen species
EDTA.....	Ethylenediaminetetraacetic acid
CALI.....	Chromophore-assisted light inactivation
CAs.....	Carbonic anhydrases
PGPH.....	Peptidylglutamyl peptide hydrolyzing
Cbl.....	Cobalamin
MeCbl.....	Methylcobalamin
AdoCbl.....	Adenosylcobalamin
CoA.....	Coenzyme A
GSCbl.....	Glutathionylcobalamin
H ₂ OCbl ⁺	Aquacobalamin
Bpy.....	Bipyridine
GSH.....	Glutathione
N4PyCO ₂ Me.....	Methyl 6-[[[(dipyridin-2-ylmethyl)(pyridin-2-ylmethyl)-amino]methyl]nicotinate
¹ H-NMR.....	Proton nuclear magnetic resonance
¹³ C-NMR.....	Carbon-13 nuclear magnetic resonance
HRMS.....	High-resolution mass spectrometry

Bn-CDPy3.....	<i>Trans-N¹-benzyl-N¹,N²,N²-tris(pyridin-2-ylmethyl) cyclohexane-1,2-diamine</i>
VEGF.....	Vascular endothelial growth factor
VGRF2.....	VEGF receptor 2
SDS-PAGE.....	Sodiumdodecylsulfate polyacrylamide gel electrophoresis
ESI-MS.....	Electrospray ionization mass spectrometry
LC-MS.....	Liquid chromatography mass spectrometry
μ M.....	Micromolar
mM.....	Millimolar
nM.....	Nanomolar
M.....	Molarity
mg.....	Milligram
Mp.....	Melting point
IR.....	Infrared
HOCl.....	Hypochlorous acid
NaN ₃	Sodium azide
HPLC.....	High-pressure liquid chromatography
kD.....	Kilodalton
LRMS.....	Low-resolution mass spectrometry
DMF.....	Dimethylformamide
THF.....	Tetrahydrofuran
DMSO.....	Dimethylsulfoxide
mmol.....	Millimole
μ L.....	Microliter
RPM.....	Revolutions per minute

TFA.....	Trifluoroacetic acid
T _R	Retention time
MOPS.....	3-(<i>N</i> -morpholino)propanesulfonic acid
BAPNA.....	<i>N</i> - α -benzoyl-DL-arginine- <i>p</i> -nitroanilide
AMC.....	7-amino-4-methylcoumarin
Suc-LLVY-AMC.....	<i>N</i> -Succinyl-Leu-Leu-Val-Tyr-AMC
Z-LLE-AMC.....	<i>N</i> -Carboxybenzyl-Leu-Leu.Glu-AMC
Bz-VGR-AMC.....	<i>N</i> -Benzoyl-Val-Gly-Arg-AMC
TPEN.....	<i>N</i> ¹ , <i>N</i> ¹ , <i>N</i> ² , <i>N</i> ² -tetrakis(pyridin-2-ylmethyl)ethane-1,2-diamine
CT.....	Chymotrypsin
PC-3.....	Prostate cancer cell line
k.....	Rate constant
K _{obs}	Observed equilibrium constant
K _f	Formation constant
Py.....	Pyridine
PPM.....	Parts per million
2D-COSY.....	Two-dimensional correlation spectroscopy
Abs.....	Absorbance
mL.....	Milliliter
ϵ	Molar absorptivity (extinction coefficient)

CHAPTER 1

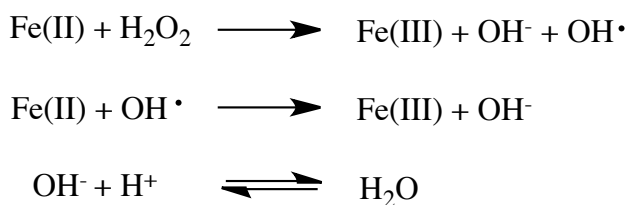
Introduction

1.1. Background

Selective aliphatic C-H functionalization under mild conditions is a significant challenge in the scientific community, and is still an active area of research due to its importance in the chemical industry.^{1,2} Natural abundance of hydrocarbons, mainly alkanes, in the form of natural gas and oil, make such transformations of great interest. Though the oxidation of C-H to C-OH is a thermodynamically favorable process with high enthalpy of reaction, the lack of proper reagents and inertness of hydrocarbons toward chemical transformations make it difficult to perform in a selective and efficient manner. Oxidants like KMnO_4 or $\text{K}_2\text{Cr}_2\text{O}_7$ are costly, not green and unselective, while environmentally friendly and cheap oxidants like O_2 or H_2O_2 are highly inefficient with extremely poor yields. Also, most cases require harsh reaction conditions like high temperature and pressure.

Given these challenges, it is interesting that nature performs C-H to C-OH reactions catalytically and efficiently with the help of metal-containing enzymes, termed metalloenzymes.³⁻⁵ A few examples of metalloenzymes involved in oxidative transformations are cytochrome P450, methane monooxygenases (MMO), catechol monooxygenases and Rieske dioxygenases. Most of these enzymes contain metal ions in their active sites and use bioavailable oxidants such as O_2 or H_2O_2 to oxidize molecules. Inspired by nature, scientists started using Fe complexes as catalysts to oxidize organic substrates in combination with O_2 or H_2O_2 .⁶⁻⁸ Even though, these reactions caused C-H oxidation of organic molecules to alcohols, the product obtained

were further prone to oxidative transformations like $C-OH \rightarrow C=O$. Moreover, these transformations were not selective. Thorough mechanistic investigation in these reactions led to the postulation that hydroxyl radical (OH^\bullet) is the key active species responsible for oxidation. The oxidation reaction with $Fe(II)$ and H_2O_2 is termed Fenton chemistry (Scheme 1.1).⁹ Though this chemistry has been well studied over decades and looks simple, there is still debate on the nature of active oxidant responsible for oxidation in such transformation.^{6,10-12}



Scheme 1.1. Fenton chemistry

To overcome the issue of selectivity and better understand the properties and reactivities of iron centers at enzymes active sites, researchers started making synthetic model complexes of heme-containing enzymes, specifically cytochrome P450, the well-established and well studied heme-enzyme involved in various oxidative transformations.^{13,14}

1.2. Heme ligands

1.2.1. Heme-enzymes in oxidation

Heme-containing enzymes catalyze a diverse array of chemical reactions in biology.¹⁵ The most important among them is the oxidation reaction. A few examples of heme-enzymes involved in oxidative transformations are cytochrome P450 (CP450), secondary amine monooxygenase (SAMO), indoleamine 2,3-dioxygenase (IDO) and tryptophan 2,3-dioxygenase (TDO). CP450 catalyzes the hydroxylation of organic

substrates,¹⁴ SAMO catalyzes the oxidative dealkylation of secondary amines to aldehydes and primary amines,^{16,17} and IDO and TDO both catalyze the conversion of L-tryptophan to *N*-formylkynurenine.^{18,19} They all contain heme prosthetic groups with iron bound to four nitrogen atoms from porphyrin ring (Figure 1.1), with the fifth coordination site occupied by either cysteine (CP450) or histidine residues (SAMO, IDO, TDO). The sixth position is available for oxidative transformations.

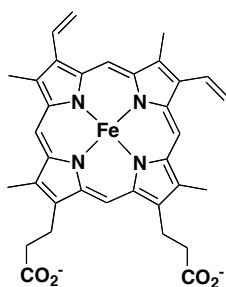


Figure 1.1. Structure of protoheme IX (adapted from ref.¹⁵)

1.2.2. Mechanism of heme-catalysis

In order to understand the catalytic reactions performed by heme-enzymes, with emphasis on exploring the nature of active oxidant, the hydroxylation of organic substrates by CP450 has been extensively studied in the past.^{14,20} The proposed mechanism of CP450 catalysis has been depicted in Figure 1.2.²¹ A high-valent Fe(IV)-oxo porphyrin π -cation radical ($[\text{Fe}^{\text{IV}}(\text{O})(\text{Por})]^{\bullet+} \leftrightarrow [\text{Fe}^{\text{V}}(\text{O})(\text{Por})]$) has been postulated as an active oxidizing species which transfers the oxygen atom to the organic substrate.

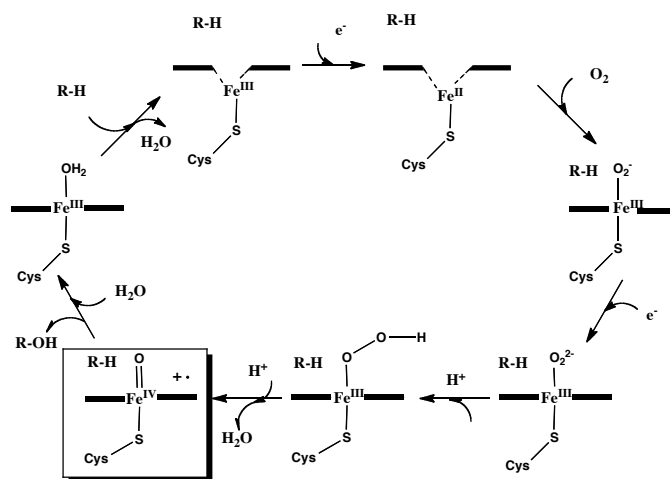


Figure 1.2. Proposed mechanism of the hydroxylation of organic substrates by CP450 (adapted from ref.²¹)

1.2.3. Synthetic heme-ligands and their applications

Synthetic iron-porphyrin complexes have been developed to mimic the functions of heme-enzymes. Because, it is synthetically challenging and time consuming to assemble the natural porphyrin, modified porphyrins based on *meso*-tetraphenylporphyrin (TPP) were synthesized.²² The structures of various porphyrin ligands are shown in Figure 1.3.⁷ Catalytic alkane hydroxylation and olefin epoxidation using synthetic Fe(III) porphyrin complexes were first illustrated by Groves and coworkers where Fe(TPP)Cl was used as catalyst along with iodosylbenzene (PhIO) as an oxidant.²³ Mechanistic investigations let them to identify the high-valent Fe(IV)-oxo porphyrin π -cation radical as the active oxidizing species.²⁴ Thereafter, a series of synthetic Fe(IV)-oxo porphyrin π -cation radical species were prepared and their reactivities were studied in various oxidative reactions.²⁵ These iron-porphyrins complexes were used as catalysts in alkane hydroxylation,^{23,24,26} alkene epoxidation,^{23,24,27} *N*- or *O*-dealkylation of aromatic amines or ethers,²⁸⁻³¹ oxygenation of

dialkyl sulfides^{32,33} or electron removal from phenol derivatives,³⁴ drugs,³⁵ or lignin.³⁶ They also find applications in DNA cleavage.³⁷

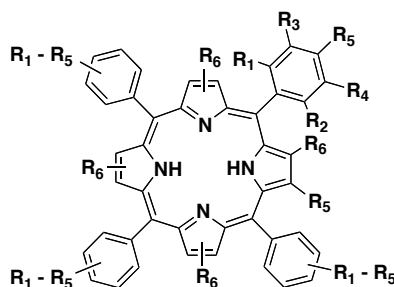


Figure 1.3. Structures of synthetic porphyrin ligands. H₂TPP: R₁ - R₅ = H, R₆ = H. H₂TMP: R₁ = R₂ = R₅ = Me, R₃ = R₄ = H, R₆ = H. H₂TPFPP: R₁ - R₅ = F. R₆ = H. H₂TDCPP: R₁ = R₂ = Cl, R₃ - R₅ = H, R₆ = H. H₂Br₈TDCPP: R₁ = R₂ = Cl, R₃ - R₅ = H, R₆ = Br. H₂Cl₈TDCPP: R₁ = R₂ = Cl, R₃ - R₅ = H, R₆ = Br. H₂Br₈TMP: R₁ = R₂ = R₅ = Me, R₃ = R₄ = H, R₆ = Br. H₂Cl₁₂TDCPP: R₁ = R₂ = R₅ = Me, R₃ = R₆ = Cl, R₄ = H. H₂F₈TPFPP: R₁ - R₅ = F, R₆ = F (adapted from ref.⁷)

1.2.4. Drawback

Though iron-porphyrin model complexes find their application as catalyst in selective oxidation of organic substrate and DNA damage, they suffer from several drawbacks. One of the biggest detriments to using heme ligands in oxidative transformations is the susceptibility of these ligands to oxidation.^{38,39} Moreover, though biologically available oxidants like O₂ or H₂O₂ had been used as oxidants, the more expensive iodosylbenzene was the choice of oxidant because it rendered higher yields and turnover numbers in these reactions.³⁹ This led scientists to explore non-heme metalloenzymes that also take part in catalyzing various oxidation reactions.

1.3. Non-heme ligands

1.3.1. Non-heme enzymes in oxidation

Like heme-enzymes, non-heme iron enzymes also catalyze a wide range of reactions in biology.^{3,5} A few examples of non-heme iron enzymes are MMO, Rieske

dioxygenases, catechol dioxygenases, lipoxygenases and isopenicillin N synthase (IPNS). MMO catalyzes the oxidation of methane into methanol,^{4,40,41} Rieske dioxygenases and catechol dioxygenases catalyze the degradation of aromatic rings,^{42,43} lipoxygenases catalyze the oxidation of unsaturated fatty acids into lipoxins and leukotrienes,⁴⁴ and IPNS take part in the biosynthesis of β -lactam antibiotics like penicillin.⁴⁵ The structures of the coordination sphere around the active sites of four crystallographically characterized mononuclear non-heme iron enzymes have been illustrated in Figure 1.4.

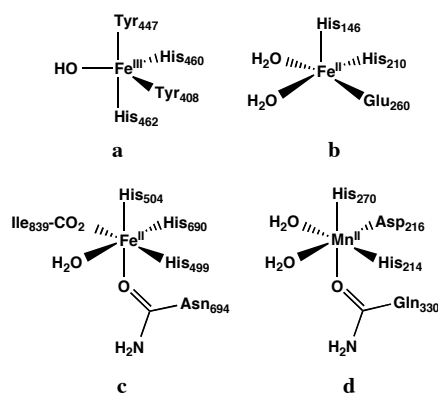


Figure 1.4. Coordination around metal center in non-heme iron enzymes a) protocatechuate 3,4-dioxygenase (3,4-PCD) b) 2,3-dihydroxybiphenyl 1,2-dioxygenase (BphC) c) lipoxygenases (SLO-1) and d) isopenicillin N synthase (IPNS, Mn-substituted) (adapted from ref.⁵)

1.3.2. Mechanism of non-heme enzyme catalysis

Unlike heme-enzymes, it is difficult to study the mechanism of non-heme enzyme catalysis as 1) they don't show the strong $\pi \rightarrow \pi^*$ transition, the signature transition of the porphyrin ligands, as they lack highly conjugated porphyrin system 2) they possess high spin Fe(II) centers with $S = 2$ (integer spin, non-Kramers ions) that generally are difficult to study using traditional EPR-related methods and 3) the ligand to metal charge transfer (LMCT) transitions fall in high energy region ($< 30000 \text{ cm}^{-1}$) making it difficult to

study using UV-vis spectroscopy.⁴⁶ Lack of suitable characterization techniques restricted our knowledge about the active intermediates being formed in non-heme iron enzymes responsible for the oxidation of organic substrates. Though people were speculating similar mechanisms in analogy with heme-enzymes, the existence of high valent Fe(IV)=O (or formally Fe(V)=O) without the porphyrin ligand was skeptical, because ligands around iron center in non-heme enzymes might not stabilize the high oxidation state of iron. However, recently scientists have managed to identify the key oxidizing species in several non-heme iron enzymes such as taurine: α -ketoglutarate dioxygenase (TauD), prolyl-4-hydroxylase, and halogenase CytC3 using various spectroscopic techniques like Mössbauer, Raman resonance and X-ray absorption spectroscopy.⁴⁷⁻⁴⁹ Like in heme-enzymes, non-heme Fe(IV)-oxo species have been found responsible for oxidizing organic substrates. The mechanism of TauD catalysis is shown in Figure 1.5.

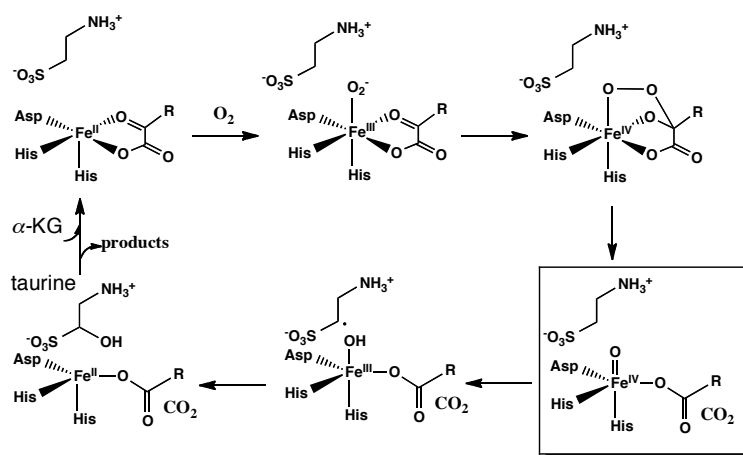


Figure 1.5. Proposed mechanism of TauD catalysis (adapted from ref.²¹)

1.3.3. Synthetic non-heme ligands

Synthetic model complexes of non-heme iron enzymes were explored to understand the chemical and physical properties of iron centers at the active site, with

emphasis on developing biomimetic catalysts for selective oxidation of the organic substrates. Structures of some non-heme ligands are shown in Figure 1.6.

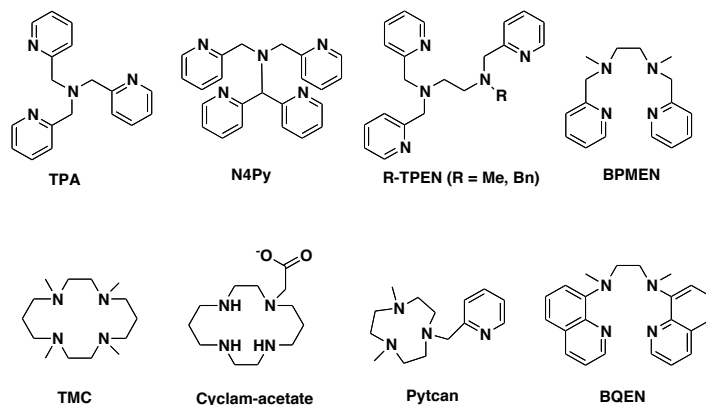


Figure 1.6. Non-heme ligands

1.3.3.1. Applications

Metal complexes of non-heme ligands find applications in a number of areas including small molecule oxidation, DNA cleavage, protein inhibition/inactivation and as models for biomolecules providing insight into their possible role in various biological pathways.

1.3.3.1.1 Oxidation of organic substrates

1.3.3.1.1.1. Generation and characterization of ferryls

Since the commencement of the mechanistic studies on the oxidation of organic substrates by heme enzyme CP450,^{14,20,21} the high-valent Fe(IV)-oxo porphyrin π -cation radical ($[\text{Fe}^{\text{IV}}(\text{O})(\text{Por})]^{\bullet+} \leftrightarrow [\text{Fe}^{\text{V}}(\text{O})(\text{Por})]$) has been postulated as an active oxidizing species. High-valent Fe(IV)-oxo porphyrin π -cation radicals were successfully synthesized and characterized later using iron-porphyrin model complexes.²⁴ However, the existence of high-valent Fe(IV)-oxo species in non-heme enzymes has recently been identified in taurine: α -ketoglutarate dioxygenase (TauD), prolyl-4-hydroxylase, and halogenase CytC3. In 1981, Wieghardt and coworkers, working with non-heme model

complexes, provided the first indirect evidence of high-valent Fe(IV)-oxo species when they treated $[\text{Fe}^{\text{III}}(\text{cyclam-acetato})(\text{CF}_3\text{SO}_3)]^+$ with O_3 in acetone and water at $-80\text{ }^\circ\text{C}$ to yield a green intermediate, characterized using Mössbauer as low spin Fe(IV)-oxo with $S = 1$.⁵⁰ The concrete proof of Fe(IV)-oxo species however, came from Que et al., when they isolated and reported the first crystal structure of the Fe(IV)-oxo complex of TMC ligand, $[\text{Fe}^{\text{IV}}(\text{O})(\text{TMC})]^{2+}$.⁵¹ $[\text{Fe}^{\text{IV}}(\text{O})(\text{TMC})]^{2+}$ was fully characterized using various spectroscopic techniques and X-ray crystallography. It is a low spin complex with $S = 1$ and there exists a double bond-like character between Fe and O with Fe-O bond length of 1.646 Å. Later, a number of Fe(IV)-oxo complexes were generated and characterized spectroscopically, along with X-ray crystal structure of $[\text{Fe}^{\text{IV}}(\text{O})(\text{N4Py})]^{2+}$ species.⁵²⁻⁵⁵ In general, high-valent Fe(IV)-oxo can be generated by treating iron complex of non-heme ligands with a series of oxygen donor atoms/oxidants such as PhIO,⁵¹ peracids,⁵² KHSO_5 ,⁵⁶ O_3 ,⁵⁰ and NaOX ($X = \text{Cl}, \text{Br}$)⁵⁷, hydroperoxides^{51,56} and molecular oxygen.⁵⁸ In the case of molecular oxygen, a reductant such as ascorbate, BPh_4 ⁻⁵⁹ or NADH ⁶⁰ is often required. Very recently, the perferryl species, Fe(V)-oxo has been identified for the first time by Costas, Cronin and co-workers using cryospray-assisted variable-temperature mass spectrometry (VT-MS) in the reaction between Fe(II) complex of tetradentate ligand Pytacn (Pytacn = 1-(2'-pyridylmethyl)-4,7-dimethyl-1,4,7-triazacyclononane) and H_2O_2 at $-40\text{ }^\circ\text{C}$ in acetonitrile. The active oxidant was characterized as HO-Fe(V)=O species and was capable of *cis*-dihydroxylating alkenes.⁶¹

1.3.3.1.1.2. Oxidation by ferryls

Iron complexes of non-heme ligands in conjugation with oxidants have been used to oxidize a number of organic molecules (alkanes, olefins, alcohol, aromatic

compounds, alkylaromatic compounds, thioanisoles, PPh₃, *N,N*-dialkylanilines) (Figure 1.7). The first highly stereospecific alkane hydroxylation using synthetic non-heme complex was shown in 1996 by Que and coworkers where [Fe^{II}(TPA)(CH₃CN)]²⁺ was used as catalyst in combination with H₂O₂. The active intermediate proposed in this transformation was [Fe(TPA)(η²-OOH)]²⁺.⁶² Later, a number of high-valent Fe(IV)-oxo species, termed ferryls, were generated and characterized, and were found to be highly efficient in selectively oxidizing small organic substrates. For example, [Fe^{IV}(O)(N4Py)]²⁺ oxidizes the organic substrates Ph₃CH, cumene, Ph-Et, Ph-Me, 2,3-dimethylbutane and cyclohexane albeit at different rates.⁵³ [Fe^{IV}(O)(BQEN)]²⁺, generated from [Fe^{II}(BQEN)](CF₃SO₃)₂ using CH₃CO₃H, was involved in oxidation of triphenylmethane, indan, tetralin, cumene, ethylbenzene, and benzyl alcohol.⁶³ A series of substituted hydroquinone substrates (H₂Q-X; X = H, ^tBu, Me, Cl, Br) were oxidized by [Fe^{IV}(O)(TMC)]²⁺. Alkynes had been oxidized by [Fe^{II}(TPA)(CH₃CN)₂]²⁺ or [Fe^{II}(BPMEN)(CH₃CN)₂]²⁺ and H₂O₂ systems. Oxidative *N*-alkylation was seen with [Fe^{IV}(O)(N4Py)]²⁺ and [Fe^{IV}(O)(TMC)]²⁺.⁶⁴ Aromatic compounds were oxidized by [Fe^{IV}(O)(N4Py)]²⁺ and [Fe^{IV}(O)(Bn-TPEN)]²⁺.⁶⁵ PPh₃ was oxidized using [Fe^{IV}(O)(TMC)]²⁺.⁵¹ Thioanisoles and benzyl alcohol were oxidized by [Fe^{II}(TMC)(OTf)₂]²⁺ in presence of air in a mixture of 1:1 CH₃CN and *tert*-butylether.⁵⁸ Aliphatic and aromatic alcohols were selectively oxidized to aldehydes by [Fe^{IV}(O)(TPA)]²⁺ and [Fe^{IV}(O)(N4Py)]²⁺.⁶⁶

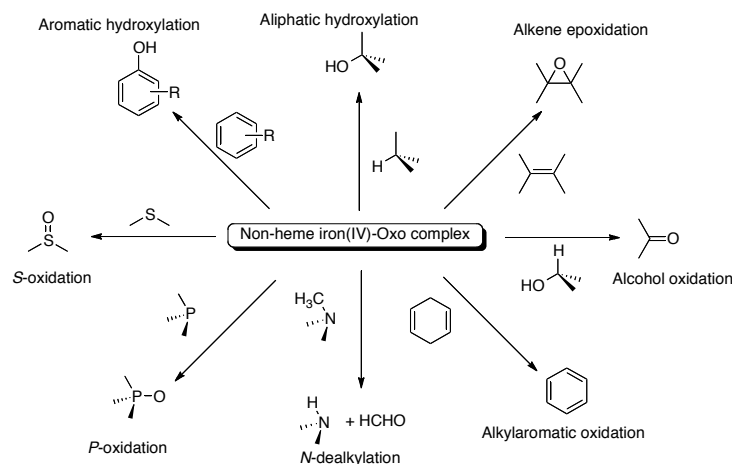


Figure 1.7. Oxidation of organic substrates by non-heme iron ferryls (adapted from ref.²¹)

1.3.3.1.2. DNA oxidation

To date, a number of metal complexes (iron, copper, nickel, zinc, rhodium and lanthanides) have been developed as DNA cleaving agents.⁶⁷⁻⁷⁵ The most promising of these are iron complexes of non-heme natural product, bleomycins (BLMs) that are being used in the treatment of various cancers (cervix, head, neck and testicular cancers).^{67,76} Iron-bleomycins (Fe-BLMs) can cleave both single- and double-stranded DNA efficiently and specifically under aerobic conditions.⁷⁷⁻⁷⁹ The efficacy of Fe-BLMs in DNA cleavage has been attributed to the presence of both a DNA-binding motif and a metal-binding unit in the same molecule (Figure 1.8). The active oxidant responsible for DNA damage, commonly termed as “activated BLM” has been identified a Fe(III)-OOH species.⁸⁰ The proposed mechanism of DNA cleavage with Fe-BLMs has been depicted in Figure 1.9. Inspired by the Fe-BLMs, a number of synthetic non-heme iron complexes mimicking the N5 binding motif of BLMs have been developed which cause oxidative DNA cleavage in presence of O_2 (Figure 1.10).⁸¹⁻⁸⁴

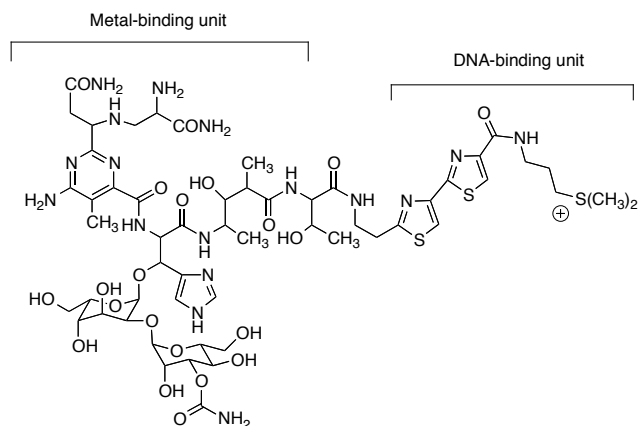


Figure 1.8. Structure of bleomycin (BLM)

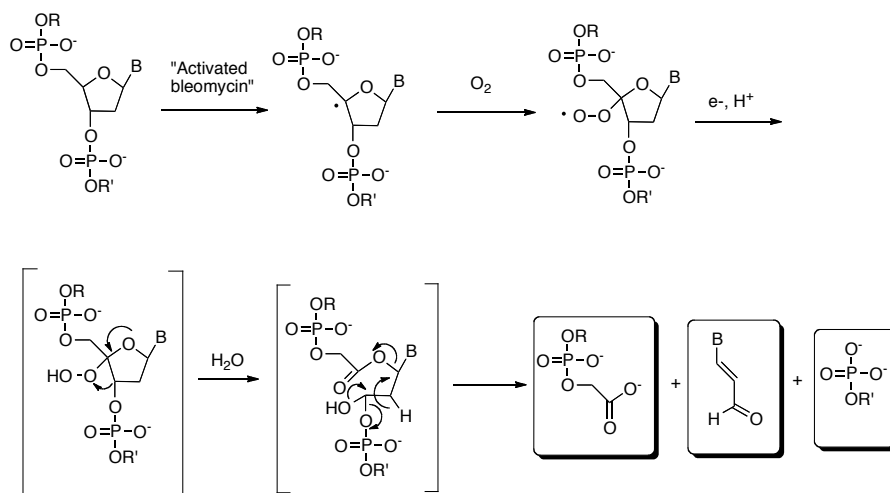


Figure 1.9. DNA cleavage by "activated bleomycin" in aerobic condition (adapted from ref.^{85,86})

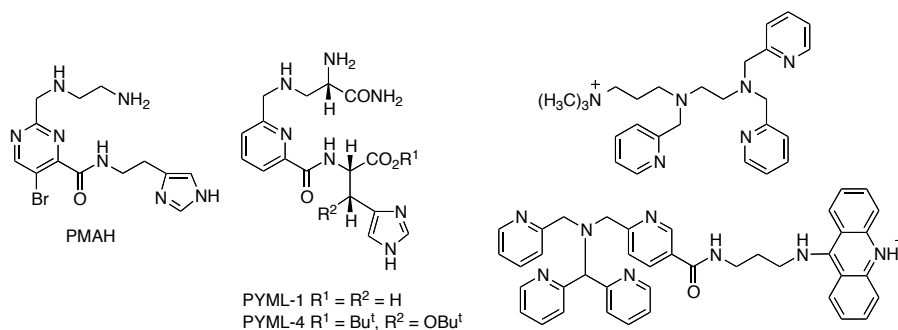


Figure 1.10. Structures of molecules mimicking the metal-binding unit of bleomycin

The inclusion of a DNA binding motifs like 9-aminoacridine, the ammonium group or 1,8-naphthalimide has led to increase in DNA cleavage efficiency. In some cases, the presence of an added reductant like DTT has been found to accelerate the rate of reaction as DTT accelerates the reduction of intermittent formed Fe(III) species to Fe(II), which is required for oxygen activation.⁸⁷

1.3.3.1.3. Protein oxidation

Metal complexes are ideal catalysts for targeting proteins because of their reactivity. Proteins can be inactivated either by hydrolyzing the amide bonds of the peptide backbone, or oxidatively cleaving the peptide backbone or oxidizing the amino acid side chains. Based on the modes of their inactivation, these complexes are classified into either hydrolytic complexes or oxidative complexes.

Examples of hydrolytic complexes include the copper(II) complex, $\text{Cu}([\text{9}]\text{aneN}_3)\text{Cl}_2$, ($[\text{9}]\text{aneN}_3 = 1,4,7\text{-triazacyclononane}$) that hydrolyzes the unactivated dipeptide Gly-Gly as well as the protein BSA at near physiological pH,⁸⁸ the Co(III) complexes ($[\text{Co}^{\text{III}}(\text{cyclen})]$ where cyclen = 1,4,7,10-tetraazacyclododecane and their derivatives, Figure 1.11) that cleave the soluble oligomer of amyloid β peptide ($\alpha\beta$), especially $\alpha\beta_{42}$ (composed of 42 amino acids) responsible for synaptic dysfunction of the brain nerves (Alzheimer disease)⁸⁹ and the palladium(II) complexes, $[\text{Pd}(\text{H}_2\text{O})_3(\text{OH})]^+$, $\text{cis-}[\text{Pd}(\text{en})(\text{H}_2\text{O})_2]^{2+}$, $\text{cis-}[\text{Pd}(\text{dtco})-(\text{H}_2\text{O})_2]^{2+}$, and $\text{cis-}[\text{Pd}(\text{dtco-OH})(\text{H}_2\text{O})_2]^{2+}$, where dtco is 1,5-dithiacyclooctane and dtco-OH is its 3-hydroxy derivative, that specifically cleave the amide bond at His18-Thr19 position in the enzyme Cytochrome c (Figure 1.12).⁹⁰

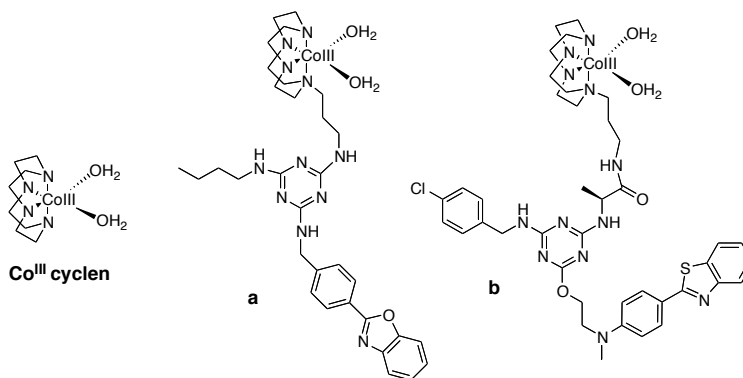


Figure 1.11. Co(III)-cyclen, and their derivatives **a** and **b**

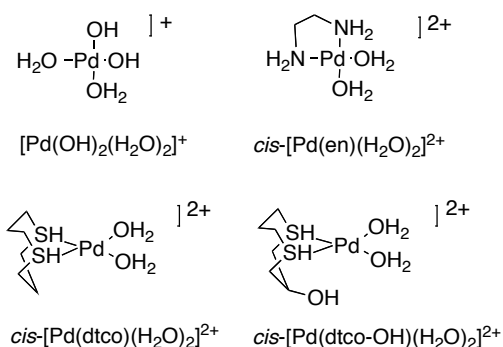


Figure 1.12. Palladium complexes involved in the peptide cleavage in Cytochrome c

Oxidative complexes can further be classified into two classes: ones that generate reactive oxygen species (ROS) like singlet oxygen, superoxide or hydroxyl radicals, and others that generate metal-based oxidants where the oxygen atom is attached to the metal center. The key difference between ROS and metal-based oxidants is that ROS are diffusible and can lead to scattered long distance damage (60-93 Å for $OH\cdot$)⁹¹ whereas the metal-based oxidants are non-diffusible and oxidation is localized and is limited only to close proximity around the metal center. Examples of ROS generating metal complexes include Fe(III)-EDTA based reagents that cleave the proteins calmodulin⁹² and streptavidin,⁹³ the Cu(I) complex of 1,10-phenanthroline that

oxidizes carbonic anhydrase⁹⁴ and the Ru(II) complexes of 2,2'-bipyridine ($[\text{Ru}^{\text{II}}(\text{bpy})]^{2+}$) that inactivate a variety of intra and extracellular proteins.^{95,96} The latter example uses chromophore-assisted light inactivation (CALI), generating singlet oxygen as an active oxidant leading to protein oxidation. Relative to ROS, the inactivation of proteins by metal-based oxidants has not been explored thoroughly, perhaps due to either the lack of ligands that can support the high-valent metal-based oxidant or the lack of spectroscopic techniques required to detect these reactive intermediates. For example, the Ni(II) and Cu(II) complexes derived from Gly-Gly-His tripeptide have been shown to oxidize calmodulin,⁹⁷ and angiotensin-converting enzyme, endothelin-converting enzyme¹⁹⁸ and carbonic anhydrase-I⁹⁹ respectively where the metal-based oxidants have been suggested to be involved in inactivation event. However, the exact nature of active oxidants has not been verified. Interestingly, with Cu(II) complexes above, the proteins were inactivated mainly due to the oxidation of the amino side chains of the proteins rather than cleavage of peptide backbone.

Even though metal-based oxidants such as high-valent Fe(IV)-oxo complexes of non-heme ligands have been well characterized, they find applications mainly in oxidizing small molecules and DNA cleavage. Proteins have not yet been targeted with these metal-based oxidants. Metal complexes based on iron are attractive reagents for protein targeting because iron is the one of most abundant transition metal in the human body and “chelatable iron,” also known as the labile iron pool,¹⁰⁰ is present at micromolar concentrations in the cytosol of mammalian cells,¹⁰¹⁻¹⁰⁶ so iron ions could be available to act as a cofactor in protein-targeting complexes. Another important factor that makes these iron-based reagents potent toward targeting proteins is that they can

react with bioavailable oxidants like O₂ or H₂O₂ in the cell to generate active species, which can oxidatively damage proteins. Extensive studies on oxidation of amino acids, the building blocks of proteins, in our laboratory, strengthen the possibilities of these iron complexes to oxidize full proteins.^{107,108} Since oxidation leads to irreversible (permanent) changes, tuning the properties of iron complexes (by tethering a protein-affinity ligand or varying ligands around the iron center) has great potential to render efficient (low concentrations) and catalytic inactivation of proteins. These factors motivated us to investigate protein inactivation using a series of non-heme iron complexes in the presence of oxidants. The proteins being targeted were human carbonic anhydrase-I, trypsin, chymotrypsin and the 20S proteasome.

1.3.3.1.3.1. Human carbonic anhydrase-I (CA-I)

Carbonic anhydrases (CAs) are a family of metalloenzymes that catalyze the reversible reaction between carbon dioxide (CO₂) and water to yield bicarbonate (HCO₃⁻) (Equation 1.1) and are known to be among the most active enzymes with a k_{cat}/K_m of $1.5 \times 10^8 \text{ M}^{-1} \text{ s}^{-1}$, almost approaching the diffusion-controlled limit.¹⁰⁹



This CO₂ to HCO₃⁻ interconversion helps regulate pH and CO₂ homeostasis in cells and tissues. The active sites of CAs consist of Zn²⁺ ion tetrahedrally bound by three histidine moieties (His 94, His 96, and His 119) and one water molecule/hydroxide ion. The mechanism of CO₂ hydration by CA has been depicted in Figure 1.13. These enzymes are mainly inhibited by the metal complexing anions and sulfonamides.^{110,111} Both of them inhibit CAs by binding to the Zn²⁺ ion, either by substituting the H₂O/OH⁻

molecule or by directly attaching to Zn^{2+} (Figure 1.14).¹¹¹⁻¹¹³ Sulfonamides inhibit CAs using the former mode with the nitrogen atom of the sulfonamide moiety coordinated to Zn^{2+} in a tetrahedral geometry, whereas anions like SCN^- add to the Zn^{2+} coordination sphere giving the trigonal-bipyramidal geometry.¹¹⁴ Several sulfonamide-based inhibitors of CAs are potential therapeutic agents and are used as antiglaucoma agents,^{110,115,116} antitumor agents,¹¹⁷ antithyroid agents,¹¹⁵ diuretic agents and antiepileptic agents¹¹⁸ (Figure 1.15).

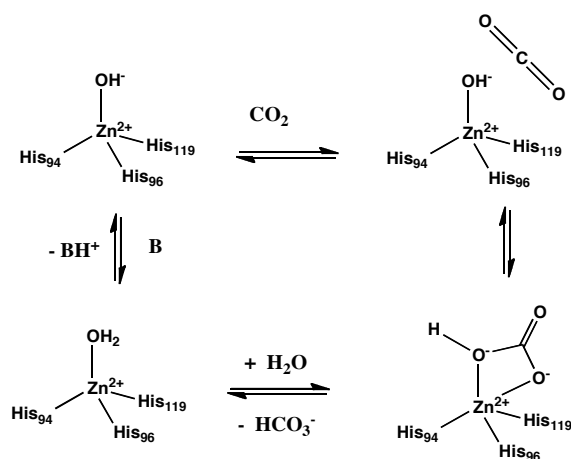


Figure 1.13. Mechanism of CO_2 hydration catalyzed by CA (adapted from ref.¹⁰⁹)

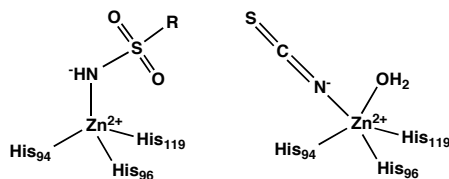


Figure 1.14. Mode of inhibition of sulfonamides and SCN^- (adapted from ref.¹⁰⁹)

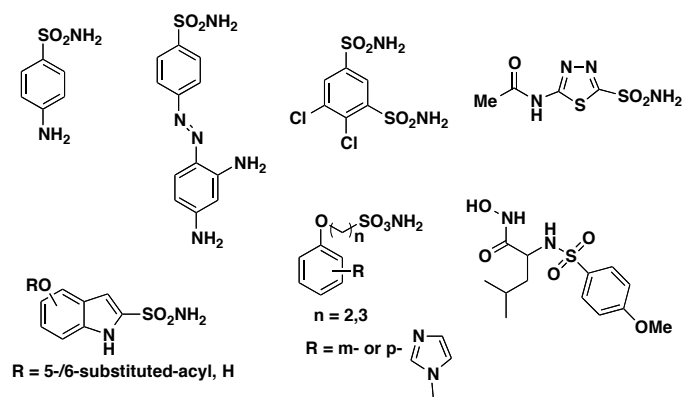


Figure 1.15. Sulfonamide based CAs inhibitors

1.3.3.1.3.2. Serine proteases (Trypsin and Chymotrypsin)

Trypsin and chymotrypsin belong to the family of serine proteases and catalyze the hydrolysis of the peptide backbones in proteins.¹¹⁹ Trypsin predominantly cleaves peptide chains at the carboxyl side of the amino acid, lysine or arginine, whereas chymotrypsin cleaves at the carboxyl side of amino acids tyrosine, phenylalanine or tryptophan. Both are biosynthesized in the pancreas as inactive precursor zymogens, trypsinogen (trypsin) and chymotrypsinogen (chymotrypsin). They possess a catalytic triad consisting of histidine, aspartate and serine residues.¹²⁰ These are connected through a series of hydrogen bonds making the serine residue highly nucleophilic (Figure 1.16). Most inhibitors of trypsin are based on amidine and guanidine moieties, as being positively charged, they interact and form salt bridges with negatively charged aspartate moiety residing in the S1 specificity pocket of trypsin (Figure 1.17).¹²¹⁻¹²⁶ On the other hand, most inhibitors of chymotrypsin contain hydrophobic moieties that are stabilized by hydrophobic interactions inside the S1 specificity pocket of chymotrypsin (Figure 1.18).¹²⁷⁻¹²⁹ Though trypsin and chymotrypsin themselves are not medicinal targets, several trypsin-like and chymotrypsin-like serine proteases are involved in

important biological processes like digestion, blood clotting and coagulation, and in diseases such as hypertension, arthritis, emphysema, Alzheimer's disease, and brain tumor growth.

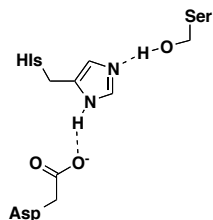


Figure 1.16. The catalytic triad in serine proteases

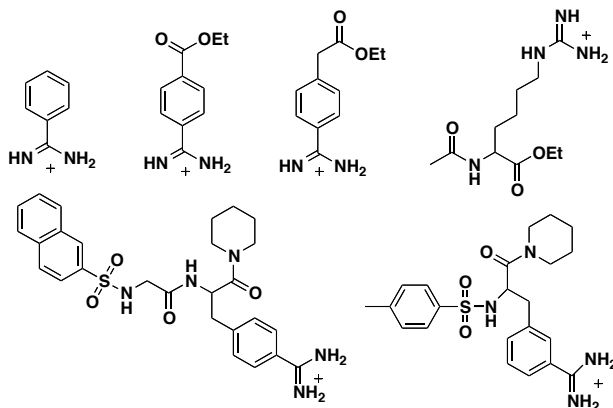


Figure 1.17. Trypsin inhibitors

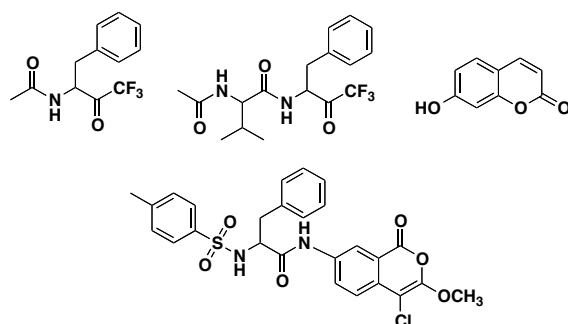


Figure 1.18. Chymotrypsin inhibitors

1.3.3.1.3.3. Proteasome

Proteasomes (26S proteasome) are large protein complexes of molecular weight approximately 12000 kD that catalyze the degradation of unwanted or damaged proteins inside the cell.¹³⁰ The proteins to be degraded are first tagged with a small protein called ubiquitin.^{131,132} This ubiquitination process is catalyzed by enzymes called ubiquitin ligases. The ubiquitinated proteins are then recognized by proteasomes which degrade the proteins into smaller peptides. The 26S proteasomes are cylindrically shaped and consist of catalytic subunits (core) and regulatory subunits (caps) (Figure 1.19).^{133,134}

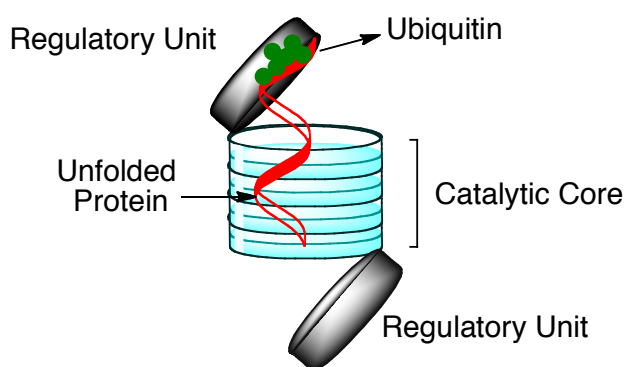


Figure 1.19. Proteasome 26S showing catalytic (core) and regulatory unit with ubiquitinated protein inside it (adapted from ref.¹³⁵)

The 20S proteasome, the catalytic core of 26S proteasome, performs three different type of peptidase activities (chymotrypsin like, trypsin-like and peptidylglutamyl peptide hydrolizing-like (PGPH))¹³⁶ whereas the 19S proteasome, the regulatory subunit of 26S proteasome, recognizes and allows the passage of the polyubiquitinated proteins to catalytic core for degradation. The ubiquitin-proteasome system is important for many biological processes such as cell cycle regulation, angiogenesis and response to

oxidative stress.¹³⁷ This system has also been an important target in cancer chemotherapy for decades. A number of small molecules and metal complexes have been developed as proteasome inhibitors which show potential anticancer activities (Figure 1.20).¹³⁸⁻¹⁴⁶

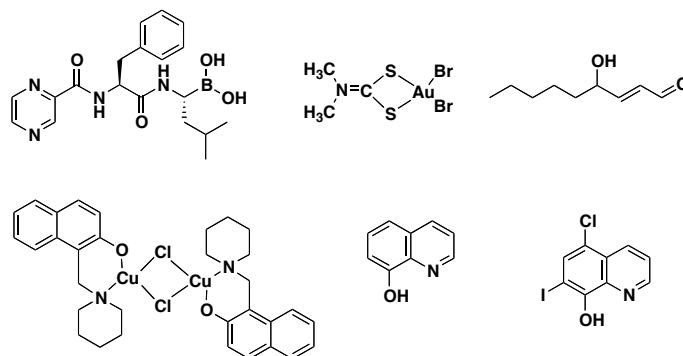


Figure 1.20. Structures of various proteasome inhibitors

1.3.3.1.4. Enzyme inhibition

1.3.3.1.4.1. Stoichiometric vs. catalytic inhibitors

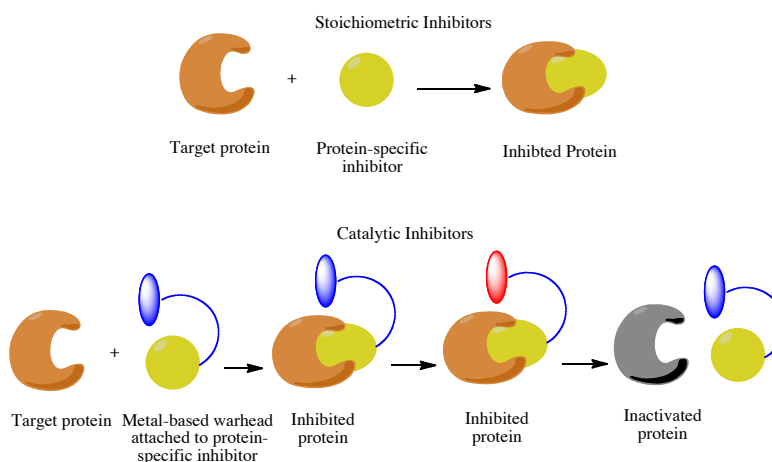


Figure 1.21. Mode of action of stoichiometric and catalytic inhibitors

Today's drug therapy uses the concept of enzyme inhibition to treat most human diseases. These are based on the principle of using stoichiometric amount of inhibitor

that binds to its target molecule one at a time. However, this inhibition mode has certain limitations. It is often difficult to identify highly potent and selective inhibitors for the target proteins. The mode of inhibition is the reversible and renders only temporary inactivation of the target molecule. Also, high concentrations of inhibitor may be required which may lead to off-target activity. To make enzyme inhibition more effective at lower concentrations, catalytic groups (warheads) need to be attached to these inhibitors, which would permanently and catalytically inactivate multiple target molecules (Figure 1.22).

1.3.3.1.4.2. Metal complexes as catalytic inhibitors

As discussed in the previous section, metal catalysts are ideal for targeting proteins because of their reactivities. Site-selective catalytic inactivation can be achieved by tethering either metal-binding units or metal complexes to the protein affinity ligands. Once these molecules bind to the specific position on proteins, metal complexes can selectively inactivate the proteins. Cowan and coworkers have used this strategy to catalytically inactivate CA-I.⁹⁹ They tethered Cu(II) complex to the benzene-sulfonamide group, a potent inhibitor of CA-I, which inactivated CA-I catalytically and selectively in presence of reductant like ascorbate. In another study, Kodadek and coworkers selectively inactivated proteasome by appending $[\text{Ru}(\text{bpy})]^{2+}$ complex to the site-specific peptoid ligand by irradiating light.⁹⁶

1.3.3.1.5. Glutathionylation of Cobalamin (Cbl) model complexes

In addition to iron, we also studied biomimetic reactions of cobalt complexes derived from non-heme ligands, including mimics of cobalamines (CbIs). Cobalamines are important class of biomolecules that are involved in various biological processes in humans, and deficiency of which may lead to diseases such as pernicious anemia, Alzheimer's disease, prostate cancer, myocardial infarction and cerebral strokes.¹⁴⁷⁻¹⁵³ As coenzymes, they participate in two major enzymatic reactions in mammals: methylcobalamin (MeCbl) mediated transfer of a methyl group from methyltetrahydrofolate to homocysteine by methionine synthase to generate methionine, and adenosylcobalamin (AdoCbl) mediated isomerization of methylmalonyl-CoA to succinyl-CoA, which is catalyzed by methylmalonyl-CoA mutase.¹⁵⁴⁻¹⁵⁷

CbIs are obtained through external diet in mammals, as they cannot synthesize them. Even when externally taken, these CbIs cannot pass through the cell plasma membrane, because they are highly polar. Therefore, mammals have developed a complex pathway for gastrointestinal absorption, blood transport and cellular uptake of dietary Cbl.¹⁵⁸ These pathways use cell surface receptors and Cbl-transport proteins.¹⁵⁹⁻¹⁶¹ However, Cbl is biosynthesized in microorganisms via both aerobic and anaerobic pathways. CbIs are comprised of N5 donor atom sets bound to the cobalt center (four equatorial corrin ring nitrogen atoms and one axial benzimidazole moiety) and vary according to the sixth donor group (X, Figure 1.21). Known derivatives of CbIs include MeCbl (X = Me), AdoCbl (X = 5'-deoxyadenosyl), aquacobalamin (X = H₂O) and cyanocobalamin (X = CN⁻), also known as vitamin B₁₂. Another important form of Cbl is thiolate-ligated glutathionylcobalamin (GSCbl), which has recently been isolated from cultured endothelial cells. GSCbl forms rapidly upon reaction of glutathione GSH, present in cells up to concentrations of 10 mM,^{162,163} with aquacobalamin (H₂OCbl⁺) and

has also been proposed as an intermediate in the biosynthesis of active cobalamin coenzymes, AdoCbl and MeCbl.¹⁶⁴ It was also suggested that GSCbl is a more direct precursor of the coenzyme promoting methyl synthase activity. Hence, GSCbl might be more effective than other cobalamines in treatment of conditions associated with hyperhomocysteinemia and oxidative stress, including dementia, arthritis, and cancer.^{149,165}

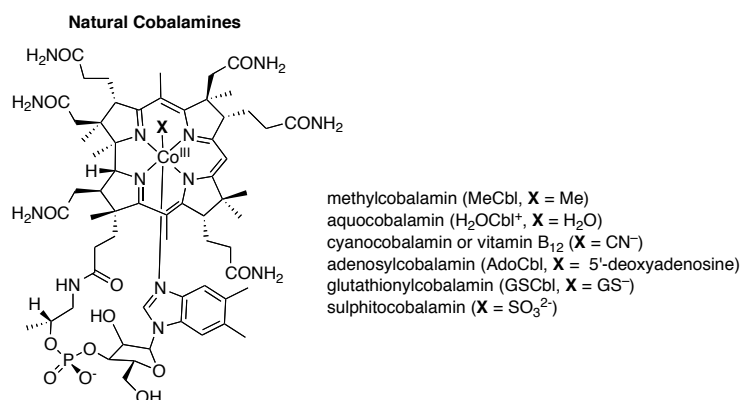


Figure 1.22. Structures of natural cobalamines

GSCbl has been synthesized,^{164,166-169} and well characterized through various spectroscopic techniques and X-ray crystallography.¹⁶⁹⁻¹⁷³ These studies confirm the thiolate ligation of the cysteine residue present in GSH to the Co(III) center in GSCbl. Detailed kinetic and thermodynamic studies of GSCbl formation from H_2OCbl^+ and GSH have been reported earlier and conclude that GSCbl formation from H_2OCbl^+ is both rapid and highly favorable.¹⁷⁴

A large number of Co(III) complexes as synthetic models for vitamin B₁₂ have been synthesized.¹⁷⁵⁻¹⁸⁶ Ligand substitution reactions with various nucleophiles (SCN^- , N_3^- , OH^- , CN^- , pyridine, 2-aminopyridine, diethoxyethylamine, NH_3 , 2-mercaptoethanol etc.) have been performed to gain insight into the reactivity at Co(III) center in vitamin

B₁₂ coenzyme. Brown et al. reported the kinetic and equilibrium studies for axial thiolate ligation of methylcobaloxime but the thiols used in ligation were 2-mercaptoethanol, S-methyl-2-mercaptoethanol, mercaptoacetate and methylmercaptoacetate.¹⁸⁷ Though, the interaction of glutathione with vitamin B₁₂ model complex [Me(Co^{III})(tn)H₂O] where tn = 2,3,9,10-tetramethyl-1,4,8,11-tetra-azaundeca-1,3,8,10-tetraen-11-ol-1-olato anion, had earlier been reported by Pellizer et al.,¹⁸⁸ a detailed kinetic and thermodynamic studies on glutathionylation has never been reported with synthetic vitamin B₁₂ model complexes. This motivated us to synthesize cobalt complexes of non-heme polypyridyl ligands mimicking the N5 coordination environments like that of Cbl, and perform their detailed kinetic and thermodynamic studies with glutathione.

1.4. Thesis statement

Selective C-H functionalization has always been a challenge, and the quest for developing suitable reagents that can perform such transformations under milder conditions still drive the research interest in this area. However, nature uses metalloenzymes (especially heme- and non-heme iron enzymes) to perform these reactions catalytically and selectively. Inspired by nature, many synthetic iron complex models based on heme- and non-heme ligands were developed to understand the chemical and physical properties, and reactivities of the iron center at the active sites of these enzymes. Various spectroscopic techniques were used to determine the nature of active oxidizing species responsible for oxidizing the organic substrates. High-valent Fe(IV)-oxo species had been identified as the key intermediate in both heme- and non-heme iron model complexes. Since iron-porphyrin complexes were susceptible to self-

oxidation, non-heme iron complexes got an edge toward exploration for non-heme iron based catalysts for oxidative transformations. High-valent Fe(IV)-oxo of non-heme iron complexes find applications in oxidation of a wide range of organic molecules such as alkane, olefins, aromatic compound, thioanisoles, *N*-deamination and sulfides. Fe-BLM and its synthetic model complexes can oxidatively cleave DNA. However, oxidation of proteins by non-heme iron complexes represents an underexplored area of research. This motivated us to investigate protein inhibition/inactivation by non-heme iron systems.

Apart from using non-heme iron complexes for oxidative chemistry, cobalt complexes of non-heme ligands provide excellent model systems for studying biomimetic reactions of biologically active cofactor, cobalamin or B₁₂, which consists of cobalt(III) ion bound by N5 donor set (from corrin and benzimidazole moiety) and vary according to sixth donor group (C, S, O), and catalyzes various significant biological processes. Glutathionylcobalamin (GSCbl), formed from aquacobalamin and GSH, is an important form of cobalamin present in the cell and has been proposed as an important intermediate in the biosynthesis of two of the active cobalamin coenzymes MeCbl and AdoCbl. GSCbl has also been suggested to be more effective than other cobalamines in treatment of conditions associated with hyperhomocysteinemia and oxidative stress, including dementia, arthritis, and cancer. Though a large number of cobalamin model complexes have been synthesized in the past, a detailed kinetic and thermodynamic study on glutathionylation has never been performed with these complexes. This inspired us to study the biomimetic reaction of glutathione with cobalamin model complexes formed from pentadentate non-heme ligands.

The overall goals of my research thesis are: 1) to explore the role of non-heme iron complexes towards protein inactivation and 2) to extend this chemistry towards cancer target 20S proteasome, and finally 3) to study mechanistic (kinetic and thermodynamic) details of glutathionylation of cobalamin model complexes, synthesized from non-heme ligands to give glutathionylated products.

Chapter 1 of my thesis deals with the overall introduction. First, heme-enzymes involved in oxidation were introduced and their modes of action were discussed. Mechanistic insights into heme-enzyme catalysis were provided using synthetic model complexes. Potential applications of these heme model complexes as catalysts were shown in various oxidative reactions. Susceptibility of heme complexes to self-degrade during oxidation led researchers to move toward non-heme iron enzymes. Mode of action and mechanistic details of non-heme iron enzyme catalysis using model complexes were provided. Applications of non-heme iron complexes in oxidation of various organic substrates, and DNA cleavage were summarized. The importance of non-heme iron complexes toward protein oxidation, which represents an underexplored area of research, has been outlined. Besides oxidation, the importance of non-heme ligands as a scaffold around cobalt centers, providing the N5 coordination sphere similar to found in biologically active cofactor cobalamin, and mimicking its behavior toward reaction with GSH (glutathionylation) has been mentioned.

In Chapter 2, the first section deals with the inactivation studies of carbonic anhydrase-I with iron complex of N4Py-sulfonamide inhibitor in presence of a reductant, dithiothreitol (DTT), where IC_{50} values were determined, time-dependent inactivation studies were performed and characterization of the oxidized products were illustrated by SDS-PAGE, ESI-MS and LC/MS/MS. The later section deals with the inactivation of

serine proteases, trypsin and chymotrypsin first with pre-generated ferryls and then with iron complexes in presence of H_2O_2 as an oxidant. The products of reactions in both the cases were characterized by SDS-PAGE, LC/MS and amino acid analysis. Further mechanistic studies were performed to investigate the mechanism of oxidation and to determine the nature of active oxidant responsible for the oxidation.

In Chapter 3, non-heme ligands N4Py and Bn-TPEN along with their iron complexes $[\text{Fe}^{\text{II}}(\text{N4Py})]^{2+}$ and $[\text{Fe}^{\text{II}}(\text{Bn-TPEN})]^{2+}$ were evaluated for their ability to inhibit 20S proteasome. IC_{50} values for inhibition of chymotrypsin-like, trypsin-like and PGPH-like activity of 20S proteasome were determined, followed by time-dependent inactivation studied with these ferrous complexes in absence and presence of DTT. Finally, to gain insight into the nature of oxidant, reactions were performed in the presence of radical scavengers. In addition, brief results of in vivo studies performed with prostate cancer PC-3 cells have been discussed.

In Chapter 4, a synthetic Co(III) model complex $[\text{Co}^{\text{III}}(\text{N4PyCO}_2\text{Me})\text{Cl}]\text{Cl}_2$, mimicking the N5 coordination sphere around Co(III) center in biologically active cobalamin was synthesized. The compound was fully characterized using various spectroscopic techniques (UV-vis, ^1H - and ^{13}C -NMR, HRMS) and X-ray crystallography. The molar conductivities of aqueous solutions of $[\text{Co}^{\text{III}}(\text{N4PyCO}_2\text{Me})\text{Cl}]\text{Cl}_2$ were also determined. The detailed kinetic and thermodynamic studies on the biomimetic reaction of the synthesized cobalamin model complex $[\text{Co}^{\text{III}}(\text{N4PyCO}_2\text{Me})\text{Cl}]\text{Cl}_2$ and one of its congener $[\text{Co}^{\text{III}}(\text{Bn-CDPy3})\text{Cl}]\text{Cl}_2$, with glutathione were performed in aqueous buffer. The second order rate constant k and observed equilibrium constant K_{obs} were calculated from the above data. Both glutathionylated products were further characterized in situ using ^1H -NMR and UV-vis spectroscopies, and HRMS.

CHAPTER 2

Inactivation of Carbonic Anhydrase-I and Serine Proteases by Non-Heme Iron Complexes

Copyright Permission: Portions of the text in this chapter were reprinted or adapted with permission from: Prakash, J.; Kodanko, J. J. *Inorg. Chem.* **2011**, *50*, 3934-3945. All rights to the work are retained by the authors and any reuse requires permission of the authors

2.1 Introduction

Enzyme inhibitors play a pivotal role in life sciences today, as reagents for chemical biology and as therapeutics for the treatment of human diseases. Inhibition is achieved by delivering molecules that bind selectively to targets and diminish enzyme activity. This inhibition can be reversible or irreversible. In the case of reversible inhibition, the inhibitor molecule binds tightly to the target using non-covalent interactions. Although this strategy is most common, it is reversible and can require high concentrations of inhibitor to achieve the desired effect, which can lead to off-target activities. Irreversible inactivation of the target enzyme, or suicide inhibition, involves formation of a covalent bond between the inhibitor molecule and target enzyme. Because of issues with toxicity and immunogenicity, suicide inhibition is less common in pharmaceuticals. Importantly, both of these strategies require a stoichiometric amount of the inhibitor.

An attractive method towards enzyme inhibition is to use metal-based reagents that generate either ROS or metal-based oxidants, diminishing enzyme activity through catalytic oxidation. Enzyme oxidation has great potential because of its irreversible

nature, and its ability to minimize the dose of inhibitors needed to have the desired effect. Damage to proteins by ROS has been well studied because of its significance in aging, neurodegenerative diseases, and radiation therapy.¹⁸⁹⁻¹⁹³ Early examples of catalysts that relied on the formation of ROS included Fe^{III}(EDTA)-based reagents for targeting calmodulin⁹² and streptavidin⁹³ which used O₂ and a reductant, as well as a Cu(I) complex of 1,10-phenanthroline tethered to a sulfonamide for targeting carbonic anhydrase⁹⁴ where oxidative cleavage of the peptide backbone was observed in the presence of O₂ and a reductant. Later work with chromophore-assisted light inactivation showed that proteins can also be inactivated selectively using singlet oxygen ¹O₂, generated by the metal-based chromophore [Ru^{II}(bpy)₃]²⁺,^{96,194} which showed an advantage over more traditional organic photosensitizers,¹⁹⁵⁻¹⁹⁷ which are susceptible to photobleaching. For example, [Ru^{II}(bpy)₃]²⁺ attached to HaloTag Protein upon irradiation to UV light can inactivate the protein Luciferase by producing singlet oxygen.⁹⁵ Similarly [Ru(bpy)₂]²⁺-peptoid conjugates have shown potent and selective inactivation of vascular endothelial growth factor (VEGF)-induced autophosphorylation of VEGF receptor 2 (VGRF2), and 26S proteasome upon photo-irradiation by means of generating singlet oxygen ¹O₂ as reactive oxidizing species.⁹⁶ Such peptoid derivatives provided a straightforward way to increase potency without resorting to extensive optimization of the inhibitor structure.⁹⁶ Importantly, selective targeting of intra- and extracellular proteins was demonstrated with this approach.

When compared with ROS, inactivation of proteins by metal-based oxidants represents an underexplored area of chemistry. Considering there were only a few examples of targeting proteins with metal-based oxidants,^{97,198,199} we found interest in

applying a set of iron complexes developed for small molecule oxidation for this purpose. Metal complexes based on iron are attractive reagents for protein targeting because iron is the most abundant transition metal in the human body and “chelatable iron,” also known as the labile iron pool,¹⁰⁰ is present at micromolar concentrations in the cytosol of mammalian cells,¹⁰¹⁻¹⁰⁶ so iron ions could be available to act as a cofactor in protein-targeting catalysts. Since studies with iron catalysts and proteins first began, EDTA has been the ligand of choice, especially for footprinting applications.²⁰⁰⁻²⁰⁵ However, others established that moving from carboxylate-rich ligands such as EDTA to more nitrogen-rich ligands resulted in better control and higher levels of selectivity in the oxidation of small molecules²⁰⁶ due to the action of metal-based oxidants, rather than ROS, specifically HO• through the Fenton reaction.²⁰⁷ Work in this area proved that iron-based oxidants, such as the well characterized high-valent Fe(IV)-oxo species $[\text{Fe}^{\text{IV}}(\text{O})(\text{N4Py})]^{2+}$,^{55,56,208} have spectacular applications in the selective oxidation of organic molecules^{53,56,64,65,209-213} and in mimicking non-heme protein active sites found in nature,^{21,214,215} including enzymes that are used to oxidize amino acids.^{48,216} We were further motivated to investigate these complexes as protein-targeting reagents because extensive investigations of bleomycin, an example of an iron-based catalytic drug that has been used for decades in cancer chemotherapy, as well as its model complexes, demonstrated that iron complexes can selectively oxidize and cleave DNA catalytically using bioavailable oxidants such as O₂ or H₂O₂.^{67,81,82,217-222} Yet the targeting of proteins with these reagents remained unexplored.

As a starting point to investigate protein-targeting with iron-based oxidants, our group demonstrated that the well characterized ferryl $[\text{Fe}^{\text{IV}}(\text{O})(\text{N4Py})]^{2+}$ oxidizes side

chains and cleaves the backbone of protected amino acids.^{107,108} However, questions remained regarding the reactivity of iron-based oxidants towards proteins, where the reactivities of amino acid residues could be dependent on the local protein structure and could differ from the model systems. Would a ferryl, which is typically more selective than HO•, be reactive enough to inactivate a protein, and if so, could this be done selectively? Could the parent Fe(II) complexes oxidize and inactivate enzymes in a catalytic and selective fashion using bioavailable oxidants, and if so would protein cleavage or side chain oxidation be observed? In order to address these questions, studies were performed commencing with inactivation of carbonic anhydrase-I with ferrous complex of N4Py-based sulfonamide inhibitor (Figure 2.1) in presence of a reductant dithiothreitol (DTT). Later, the reactivity of two ferryl complexes, the known ferryl $[\text{Fe}^{\text{IV}}(\text{O})(\text{N4Py})]^{2+}$ and a derivative containing a acylpropylguanidinium group for protein-binding named $[\text{Fe}^{\text{IV}}(\text{O})(3\text{CG-N4Py})]^{3+}$ for 3-carbon guanidinium (Figure 2.1), were evaluated for their ability to inactivate serine proteases trypsin and chymotrypsin under single turnover conditions. The starting ferrous complexes $[\text{Fe}^{\text{II}}(\text{N4Py})]^{2+}$ and $[\text{Fe}^{\text{II}}(3\text{CG-N4Py})]^{3+}$ were further combined with enzyme and treated with oxidants to determine if catalysis was possible. Results disclosed herein confirm for the first time that the new class of iron complexes that have extensive applications in the oxidation of small molecules can be applied to the selective targeting of proteins.

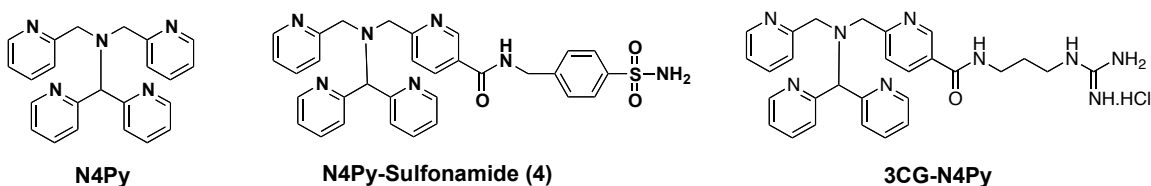


Figure 2.1. Structures of ligands used in the inactivation studies

2.2. Inactivation of carbonic anhydrase-I

2.2.1. Results

2.2.1.1. Inhibitor design

Designing the iron-based inhibitor for CA-I involved tethering a protein-affinity group, in this case an arylsulfonamide, to the iron-binding ligand N4Py. Simple arylsulfonamides are known to inhibit carbonic anhydrases effectively by displacing a zinc-bound hydroxide moiety found in the active site with a deprotonated sulfonamide or NH^- group. In order to keep the inhibitor most similar to the copper-based inhibitors of CA-I used in the past, a benzenesulfonamide group was chosen to anchor the inhibitor to the enzyme.

X-ray crystallographic data of CA-I bound to 4-aminobenzenesulfonamide (PDB ID 1CZM)²²³ were used to design the structure of the iron-based inhibitor. After inspecting the three-dimensional structure of the enzyme and attempting to dock several variants, linking a (4-methylamino)benzenesulfonamide to the N4Py ligand through an amide bond tether was deemed optimal (see structure **4**, Figure 2.1). An extra methylene unit was incorporated between the aryl ring of the sulfonamide and the amino group of the inhibitor, different from previous studies, which incorporated 4-aminobenzenesulfonamide,^{94,99} in order to prevent the bulky iron-bound N4Py unit from bumping into residues around the rim of the active site. Shown in Figure 2.2a are results from a molecular modelling study where the benzenesulfonamide portion of the inhibitor $[\text{Fe}^{\text{IV}}(\text{O})(\mathbf{4})]^{2+}$ was overlapped with the benzenesulfonamide of the original crystal structure. The space-filling representation shown in Figure 2.2b illustrates that the inhibitor can fit in the active site without creating unfavorable non-bonding interactions

with the surface of CA-I. Attempts were made to calculate binding energies with the inhibitor and CA-I using Monte Carlo methods. Results were judged to be unreliable, due to complications in assigning the appropriate partial charges on the iron-bound inhibitor and the lack of flexibility and solvation in the active site model.

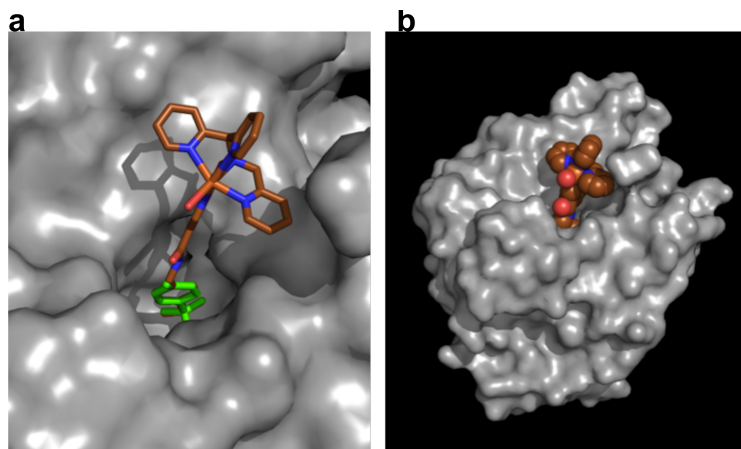
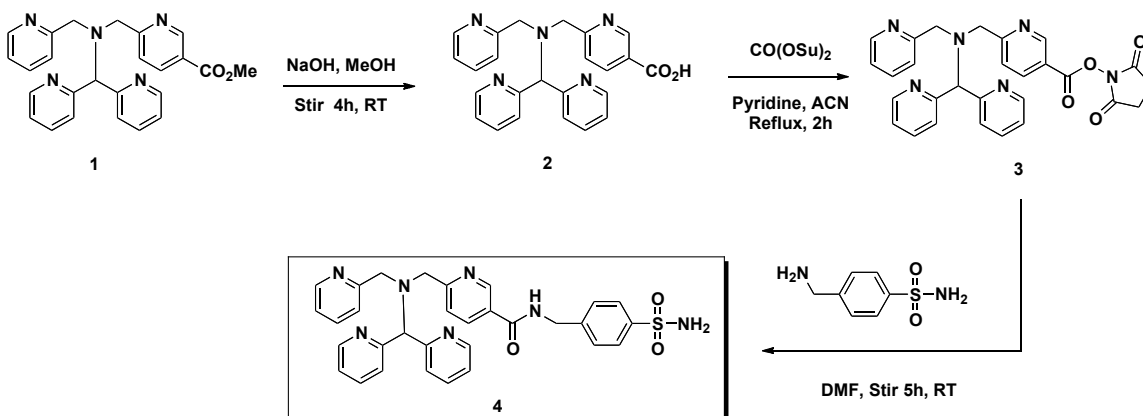


Figure 2.2. (a) Molecular modelling representation of $[\text{Fe}^{\text{IV}}(\text{O})(\mathbf{4})]^{2+}$ docked in the active site of CA-I. The structure of the original inhibitor, shown in green, was overlapped with the benzenesulfonamide group of $[\text{Fe}^{\text{IV}}(\text{O})(\mathbf{4})]^{2+}$. (b) Space filling representation of $[\text{Fe}^{\text{IV}}(\text{O})(\mathbf{4})]^{2+}$ docked in the active site of CA-I.

2.2.1.2. Inhibitor synthesis

The inhibitor designed in the previous section was synthesized in three steps starting from a known N4Py derivative, the ester N4PyCO₂Me **1** (Scheme 2.1).²²² Saponification of ester **1** using NaOH in MeOH furnished an acid **2** that was condensed with *N,N*-disuccinimidyl carbonate in a mixture of refluxing pyridine and MeCN, giving the unstable ester N4PyCO₂Su **3** in 84% yield and > 90% purity over the two steps. Reaction of the crude activated ester **3** with 4-(aminomethyl)benzenesulfonamide in DMF at room temperature furnished the inhibitor **4** in 54% yield. Development of a synthetic route to the succinimide ester N4PyCO₂Su was significant, because this versatile starting material can be used to link the N4Py ligand to various protein-binding

motifs under mild conditions.



Scheme 2.1. Synthesis of N4Py-sulfonamide inhibitor **4**

2.2.1.3. Inhibition studies

In order to evaluate the ability of the ligand **4** to inhibit CA-I, enzyme activities were determined in the presence of varied concentrations of free ligands **1** and **4**, as well as several metal complexes that were generated in situ (Figure 2.3 and Table 2.1). A concentration-dependent inhibition of CA-I was observed in all cases in assays that contained the ligand **4** (entries 1–3). Precomplexation of **4** with the metal ions Fe^{II} or Zn^{II} prior to conducting the assay did not change the inhibition dramatically, and IC₅₀ values were nearly identical in all three cases. The ligand N4PyCO₂Me **1** (Scheme 2.1), as well as its Fe^{II} or Zn^{II} complex, did not inhibit CA-I in the range of concentrations surveyed, giving a lower limit for the IC₅₀ values of >1000 mM, consistent with strong binding of the ligand **4** to CA-I due to the sulfonamide functional group of the inhibitor (entries 4–6), rather than the metal ion or N4Py moiety. Neither Fe^{II} nor Zn^{II} alone inhibited CA-I at the concentrations used in these assays (entries 7–8).

Table 2.1. IC₅₀ values for inhibition of CA-I for compounds **1** and **4** their metal complexes and free metal ions^a

Entry	Compound	IC ₅₀ (μM)
1	4	1.7 ± 0.1
2	Fe ^{II} · 4	1.1 ± 0.1
3	Zn ^{II} · 4	1.4 ± 0.4
4	1	> 1000
5	Fe ^{II} · 1	> 1000
6	Zn ^{II} · 1	> 1000
7	Fe ^{II}	> 1000
8	Zn ^{II}	> 1000

^a Metal complexes were generated in situ with using ligands **1** or **4** and Fe^{II}(NH₄)₂(SO₄)₂ or ZnCl₂. Enzyme (CA-I) concentration was 1.0 μM; substrate (4-nitrophenyl acetate) concentration was 1.0 mM. The reactions were conducted at pH = 8.0, in 12.5 mM Tris buffer containing 75 mM NaCl and 5% DMSO.

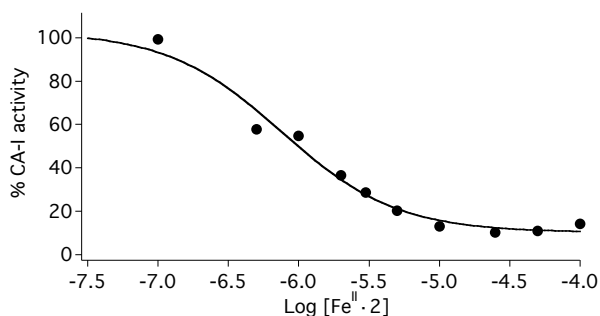


Figure 2.3. Inhibition of CA-I by Fe^{II}·**4**. Enzyme (CA-I) concentration was 1.0 μM; substrate (4-nitrophenylacetate) concentration was 1.0 mM. The reactions were conducted at pH = 8.0, in 12.5 mM Tris buffer containing 75 mM NaCl and 5% DMSO.

2.2.1.4. Inactivation studies

After gathering inhibition data, the inactivation of CA-I by Fe^{II}·**4** was examined. Following the method from the literature with copper-based metalloprotein,¹⁹⁸ CA-I (1 μM) was incubated in the presence of a subsaturating amount of inhibitor (1 μM) and enzyme activity was measured over time. A time-dependent inactivation of CA-I was

observed with $\text{Fe}^{\text{II}}\cdot\mathbf{4}$ in the presence of 0.5 mM dithiothreitol (DTT) at 37 °C (Figure 2.4). By measure of the assay, the activity changed from over 90% at $t = 0$ to under 40 % after 140 min under these conditions. Control experiments concluded that the rate of inactivation by 1 μM $\text{Fe}^{\text{II}}\cdot\mathbf{4}$ was significantly faster than the background rate of inactivation by either Fe^{II} alone or the control experiment with no metal ion added. In the absence of DTT, enzyme activities did not change significantly over time in the presence of $\text{Fe}^{\text{II}}\cdot\mathbf{4}$, Fe^{II} or the blank, confirming that loss of catalytic activity required a reductant to proceed. It was also noted that ascorbate as a reductant was not as effective as DTT. Therefore, a thiol-based reductant was ideal. Taken together, these observations are most consistent with reductive activation of dioxygen by the $\text{Fe}^{\text{II}}\cdot\mathbf{4}$ complex and subsequent oxidation and inactivation of CA-I, as witnessed in oxidative studies with DNA.^{219,222,224}

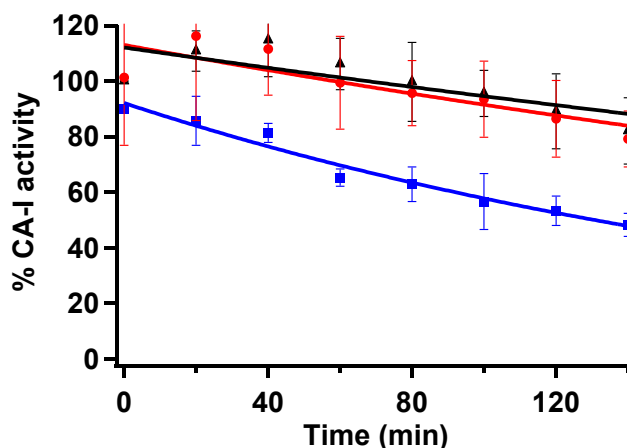


Figure 2.4. Plot of CA-I activities vs. time of preincubation at 37 °C in the presence of the reductant DTT. Enzyme (CA-I) concentration was 1.0 μM ; DTT concentration was 0.5 mM; H_2O was added as blank (\blacktriangle); concentration of Fe^{II} (\bullet) or $\text{Fe}^{\text{II}}\cdot\mathbf{4}$ (\blacksquare) was 1.0 μM . Reactions were conducted at pH = 8.0, in 12.5 mM Tris buffer containing 75 mM NaCl and 5% DMSO using a total volume of 1.5 mL. Activities, measured as initial velocities, were determined at each time interval by removing aliquots (100 μL) and adding the substrate 4-nitrophenylacetate (1 mM). Activities were converted to % CA-I activity, with 100% activity equal to the activity of the blank reaction in the absence of inhibitor $\mathbf{4}$ or Fe^{II} at $t = 0$.

2.2.1.5. Characterization of products

To gain insight into the mode of inactivation, CA-I products were analyzed by SDS-PAGE and ESI-MS. Incubation of CA-I with $\text{Fe}^{\text{II}}\cdot\mathbf{4}$ did not lead to cleavage of the protein backbone, as evidenced by SDS-PAGE analysis (Figure 2.5). No major fragments of the enzyme were observed in this case. Characterization of the CA-I inactivation products by ESI-MS revealed that several new products had formed, in the presence of $\text{Fe}^{\text{II}}\cdot\mathbf{4}$, all with higher molecular weights (Figure 2.6). These data are in good agreement with data from the copper metallopeptide used in the past,¹⁹⁸ and are consistent with oxidation of the protein by the addition of oxygen atoms to one or more amino acid side chains, rather than fragmentation of the protein backbone.⁹⁴

Nano LC/MS/MS analysis of trypsin and chymotrypsin digests of CA-I confirmed that the majority of oxidized residues were located in direct proximity of the active site, where $\text{Fe}^{\text{II}}\cdot\mathbf{4}$ is expected to bind. In total, ten oxidized residues were located through this analysis, including five histidines (H40, H64, H67, H200 and H243), which were oxidized to 2-oxo-histidine, four tryptophan residues (W16, W123 and W192), which were oxidized to formylkynurenine, and two methionine residues (M148 and M241), which were oxidized to methionine sulfoxide. Using the molecular model of $[\text{Fe}^{\text{IV}}(\text{O})(\mathbf{4})]^{2+}$, docked in the active site of CA-I (Figures 2.2), it was confirmed that eight of these residues were located near the active site, between 6-18 Å from the benzylic methylene carbon of the sulfanilamide inhibitor, which lies near the opening of the active site (Figure 2.7). In addition, two oxidized residues, H40 (~ 32 Å) and W192 (~ 25 Å), were located on the peripheral surface, similar to observations with the copper metallopeptide, which could indicate a secondary binding site for the inhibitor, or alternatively a non-specific surface oxidation.

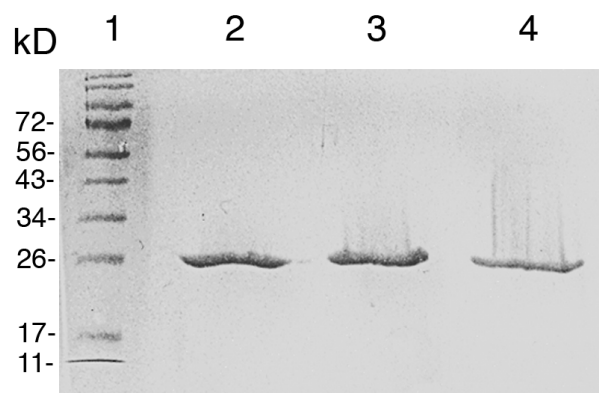


Figure 2.5. SDS-PAGE analysis (12%), stained with Coomassie blue, of CA-I (20 μ M) incubated at 37 °C for 3 h at pH = 8.0, in 12.5 mM Tris buffer containing 75 mM NaCl and 10 mM DTT. Cleavage products of CA-I were not observed. Lane 1: MW marker. Lane 2: enzyme only. Lane 3: Fe^{II} (20 μ M). Lane 4: Fe^{II}·4 (20 μ M).

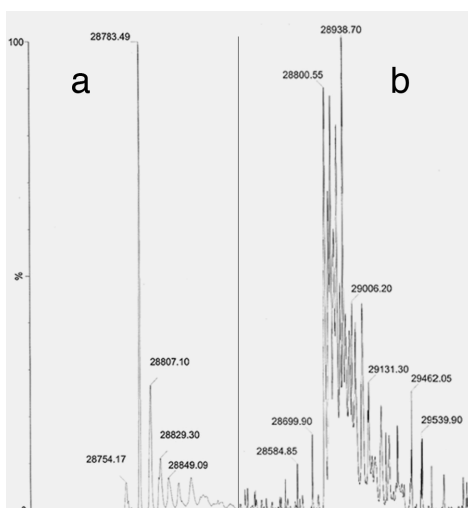


Figure 2.6. Deconvoluted ESI-MS spectra of CA-I after treatment with Fe^{II} (spectrum a) or Fe^{II}·4 (spectrum b) in the presence of DTT. Peaks observed at 28800 and 28939 in spectrum b are consistent with oxidation of CA-I. Reactions were conducted at 37 °C by incubating CA-I (20 μ M), Fe^{II} (40 μ M) or Fe^{II}·4 (40 μ M), DTT (20 mM) for 3 h before desalting and subjecting the samples to ESI-MS analysis.

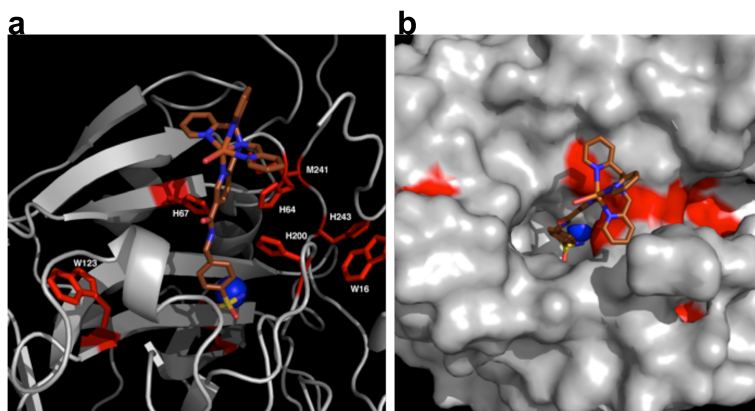


Figure 2.7. (a) Figure showing location of oxidized histidine (H67, H64, H200 and H243), tryptophan (W16 and W243) and methionine (M241) residues of CA-I (shown in red) with respect to the active site and the docked inhibitor $[\text{Fe}^{\text{IV}}(\text{O})(\mathbf{4})]^{2+}$. The zinc ion of the active site is represented as a blue sphere. (b) Surface model of CA-I docked with $[\text{Fe}^{\text{IV}}(\text{O})(\mathbf{4})]^{2+}$ showing oxidized residues near the active sites (in red)

The localized pattern of oxidized residues around the active site indicates that the inhibitor has some flexibility in its ability to oxidize residues. The ability of $\text{Fe}^{\text{II}}\cdot\mathbf{4}$ to transfer oxygen atoms to the protein could signify that the ferryl complex $[\text{Fe}^{\text{IV}}(\text{O})(\mathbf{4})]^{2+}$ might be the active oxidant, due to the fact that similar reactivity was demonstrated with $[\text{Fe}^{\text{IV}}(\text{O})(\text{N4Py})]^{2+}$ and protected amino acid derivatives.¹⁰⁷

2.2.2. Discussion

Results reported herein are significant as they confirm for the first time that the iron complex $\text{Fe}^{\text{II}}\text{N4Py}$ can oxidize proteins when tethered to a protein-affinity group. Though, the binding of iron to the N4Py-sulfonamide inhibitor **4** did not increase its efficiency to inhibit CA-I (infact they show similar IC_{50} values), the ferrous complex led to time-dependent inactivation of CA-I in presence of O_2 and a reductant DTT. The loss of CA-I activity over time was not seen with either Fe^{II} or $\text{Fe}^{\text{II}}\cdot\mathbf{4}$ in the absence of DTT confirming that $\text{Fe}^{\text{II}}\cdot\mathbf{4}$ and a reductant were needed to achieve efficient inactivation, consistent with a pathway involving the reductive activation of O_2 . Although the rate of

CA-I inactivation was slower compared with copper-peptide reagent used in the past,¹⁹⁸ the mode of their action seems to be similar i.e., oxidative inactivation. Oxidative mode of inactivation was further corroborated by SDS-PAGE and ESI-MS analysis. Absence of bands leading to cleavage products in SDS-PAGE, and presence of higher molecular weight peaks in ESI-MS concluded that CA-I was inactivated by the oxidation of their side chain amino acid residues rather than cleavage of the protein backbone. Additional evidence of oxidative damage came from LC/MS/MS analysis which illustrated that histidine and tryptophan residues near the active site were selectively oxidized. This localized pattern of oxidized amino acid residues also supports the role of metal-based oxidant responsible for the enzyme inactivation rather than diffusible ROS. Taken together, these make iron-based inhibitors as the potential candidates for *in vivo* applications that could emerge by taking advantage of the labile iron pool in the cell.

Unfortunately, the results from this study suffer the drawback of reproducibility. Though the data from time-dependent inactivation and SDS-PAGE were consistently reproduced, the oxidation results obtained from ESI-MS and LC/MS/MS were highly inconsistent. This may be due to the fact that we were largely relied on O₂ as source of oxidant in our studies which is not efficiently being activated by reductant. Another plausible reason that may lead to observed inconsistent results is that CA-I might be inactivated by non-oxidative pathways i.e., either blocking the activity of zinc at the active site by direct binding of inhibitor molecule or stripping off Zn²⁺ ion by the metal-binding N4Py moiety of the inhibitor.

This led us to move toward targeting other protein systems devoiding of metal center at the active site, mainly trypsin as it has been broadly studied in terms of its function and has well established crystal structure (PDB ID# 3ITI), and the use of

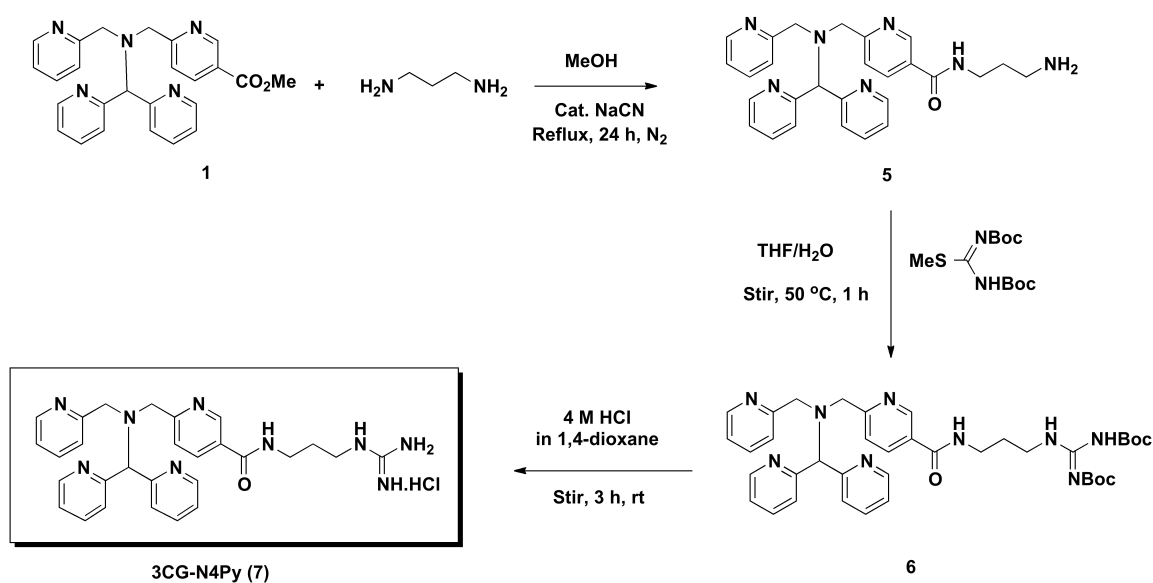
pregenerated ferryls and other suitable biological oxidant like H_2O_2 that has been used extensively in the past for oxidation chemistry.

2.3. Inactivation of serine proteases (trypsin and chymotrypsin)

2.3.1. Results

2.3.1.1. Synthesis of ligand 7

The N4Py derivative **7**, which contains a pendant acylpropylguanidinium group, was synthesized in three steps starting from the known ester **1** (Scheme 2.2).²²² Following a literature procedure, refluxing the methanolic solution of **3** and 1,3-diaminopropane in the presence of a catalytic amount of NaCN under a N_2 atmosphere gave the aminated product **5** in 77% yield.²²² The resultant primary amine **5** was treated with 1,3-bis(*tert*-butoxycarbonyl)-2-methyl-2-thiopseudourea in THF/ H_2O at 50 °C for 1 h, furnishing **6** in 88% yield. Compound **6** was deprotected by treatment with 4 M HCl in 1,4-dioxane for 3 h at room temperature, giving the ligand 3CG-N4Py (**7**) as a hydrochloride salt in quantitative yield.



Scheme 2.2. Synthesis of ligand 3CG-N4Py

2.3.1.2. Generation and characterization of ferryl species

The ferrous complexes **9** and **10** were generated in situ by adding 1 equiv of $\text{Fe}^{\text{II}}(\text{ClO}_4)_2$ to aqueous solutions of ligands and N4Py (**8**) and **7** respectively. The orange complexes **9** and **10** were characterized by UV-vis and $^1\text{H-NMR}$ spectroscopies and MS. UV-vis spectroscopy indicated similar data for **9** and **10** ($\epsilon_{380} = 1700 \text{ M}^{-1} \text{ cm}^{-1}$ with a shoulder at 460 nm and $\epsilon_{375} = 1700 \text{ M}^{-1} \text{ cm}^{-1}$ with a shoulder at 470 nm for **9** and **10**, respectively). $^1\text{H-NMR}$ spectra for **9** and **10** in D_2O were consistent with the complexes bearing high-spin $S = 2 \text{ Fe}^{\text{II}}$ centers. Broad resonances ranging from 150 to 20 ppm, well outside of the diamagnetic region, were observed for **9**. Complex **10** showed resonances within the same region, except that downfield resonances were split in two, which is consistent with the lower symmetry of **10** (C_1 symmetry) with respect to **9** (C_s symmetry) because of the acylpropylguanidinium group on the ligand 3CG-N4Py. Magnetic moments for **9** and **10** in D_2O were 4.4 and 4.5 μB , respectively, as determined by Evan's method, which are close to the expected spin-only values for a high-spin $\text{Fe}(\text{II})$ complex.²²⁵ Interestingly, treatment of **9** or **10** in D_2O with excess CH_3CN (50 equiv) caused a spin transition from high to low spin, as judged by $^1\text{H-NMR}$ spectroscopy, in which resonances between 200 and 20 ppm were no longer observed. In addition, a sharp drop in the magnetic moment, $< 0.2 \mu\text{B}$ for both samples, was observed by Evan's method. MS data for **9** in H_2O matched the formula $[\text{Fe}^{\text{II}}(\text{OH}_2)(\text{N4Py})]^{2+}$ as described previously,²²⁶ and data for **10** in H_2O showed a prominent molecular ion at m/z 300.5860, along with an isotope pattern that agreed with the molecular formula $[\text{Fe}^{\text{II}}(\text{Cl})(3\text{CG-N4Py})]^{2+}$, where chloride presumably binds to the iron center in place of H_2O because it is present as the counterion to the guanidinium

salt. Treatment of **9** with peracetic acid at 25 °C gave a pale-green species, $[\text{Fe}^{\text{IV}}(\text{O})(\text{N4Py})]^{2+}$ (**11**), in ~ 20 min with a maximum absorption wavelength at $\lambda_{\text{max}} = 680$ nm ($\epsilon = 170 \text{ M}^{-1} \text{ cm}^{-1}$), which agrees with the published data.²²⁷ A similar procedure was used to prepare the ferryl $[\text{Fe}^{\text{IV}}(\text{O})(3\text{CG-N4Py})]^{3+}$ (**12**; $\lambda_{\text{max}} = 675$ nm, $\epsilon = 170 \text{ M}^{-1} \text{ cm}^{-1}$; Figure 2.8) from **7**, where it took ~ 10 min for complete generation. Ferryl **12** was characterized by high-resolution electrospray ionization MS (ESI-MS), which displayed a prominent molecular ion at m/z 194.0682, along with a suitable isotopic pattern, consistent with a trication derived from the molecular formula $[\text{Fe}^{\text{IV}}(\text{O})(3\text{CG-N4Py})]^{3+}$.

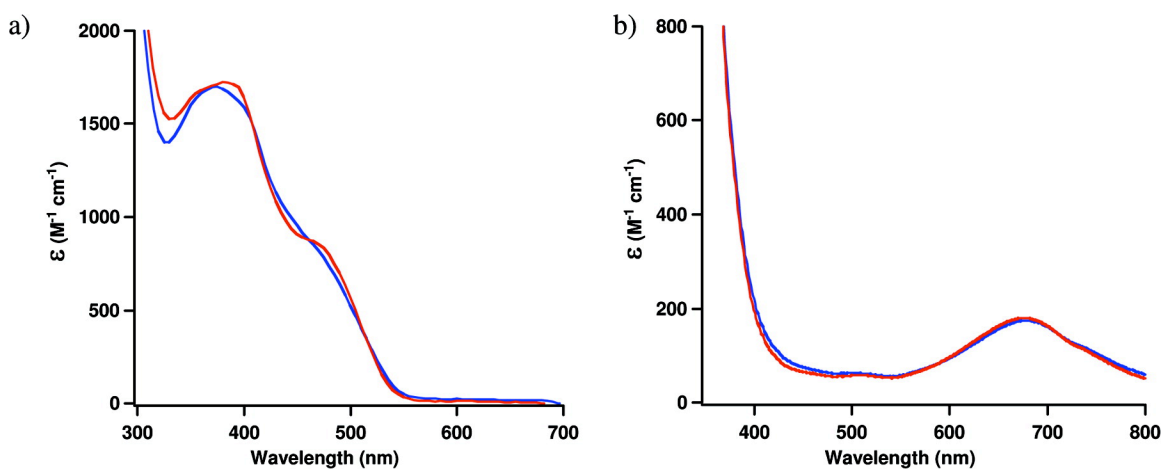


Figure 2.8. UV-vis spectra of ferrous and ferryl complexes in H_2O : (a) **9** (red) and **10** (blue); (b) **11** (red) and **12** (blue)

2.3.1.3. Enzyme inactivation with ferryl compounds

In order to evaluate the ability of the ferrous and ferryl complexes **7-12** to inactivate trypsin, the enzyme activities were determined in the presence of varied concentrations of these reagents along with controls, and IC_{50} values were calculated (Table 2.2). In these studies, trypsin ($1 \mu\text{M}$) was treated with each reagent (0 - $1000 \mu\text{M}$) in acetate buffer ($\text{pH} = 6.0$, 150 mM NaCl) at room temperature. After incubation for 1 h,

the enzyme activities were determined by addition of the chromogenic substrate BAPNA. These experiments indicated that ligands **8** and **7** inhibit trypsin in the mid-micromolar range (entries 1 and 2). Ligand **7** containing the propylguanidinium group was the more potent inhibitor. Despite the fact that $\text{Fe}^{\text{II}}(\text{ClO}_4)_2$ had no effect on the trypsin activity, the ferrous complexes **9** and **10** showed more potent inhibition than ligands alone (entries 3 and 4). Although peracetic acid inhibited trypsin, ferryls **11** and **12** were more potent oxidants (entries 5-7). Between the ferryls (Figure 2.9a), **12** ($\text{IC}_{50} = 54 \mu\text{M}$) was found to be a better oxidant than **11** ($\text{IC}_{50} = 71 \mu\text{M}$).

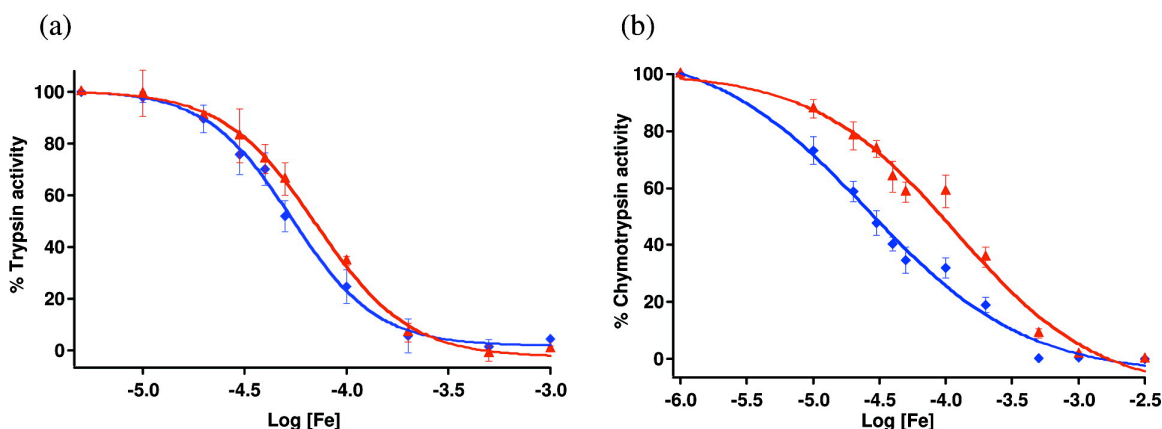


Figure 2.9. IC_{50} plots with ferryl species **11** (red \blacktriangle) and **12** (blue \blacklozenge) for trypsin (a) and chymotrypsin (b). The % enzyme activities at different concentrations were averaged out from three different independent runs, with 100% activity equal to the activity of the blank reaction in the absence of inhibitor and the error equal to the standard deviation of the data set. Enzyme (trypsin/chymotrypsin) concentration was $1.0 \mu\text{M}$; trypsin substrate *N*- α -Benzoyl-DL-arginine-4-nitroanilide hydrochloride and chymotrypsin substrate *N*-Succinyl-Ala-Ala-Pro-Phe-pNA concentrations were 1.0 mM . The reactions were conducted at $\text{pH} = 6.0$, in 10 mM acetate buffer containing 150 mM NaCl.

When inactivation studies were performed on chymotrypsin, different results were obtained (Table 2.2). Neither the ligands **8** and **7** nor the ferrous complexes **9** and **10** (entries 1-4) inhibited chymotrypsin in the range from 0 to $1000 \mu\text{M}$, with the exception of **10**, which inhibited chymotrypsin only at very high concentrations ($\text{IC}_{50} =$

790 μM). This observation is consistent with the loss of binding at the active site because the S1 pocket of chymotrypsin prefers hydrophobic groups as opposed to the charged propylguanidinium group of **7**. Despite the fact that ligands **8** and **7** and their iron complexes show only weak inhibition of chymotrypsin, both ferryls **11** and **12** (entries 6 and 7) inactivate chymotrypsin in a concentration-dependent fashion (Figure 2.9b). Between the two ferryls, again **12** was found to be a better oxidant, and a higher level of selectivity was observed between the ferryls with chymotrypsin versus trypsin. Binding of ferryl **12** near the active site is not likely because the S1 pocket prefers hydrophobic groups. Instead, the lower IC_{50} value of **12** compared to **11** may be attributed to favorable electrostatic interactions between the charged ferryl **12** and carboxylates on the surface of chymotrypsin, which are present in higher abundance than with trypsin.²²⁸

Table 2.2. IC_{50} values (μM) for the inhibition of trypsin and chymotrypsin by ligands **8** and **7** and their respective ferrous (**9** and **10**) and ferryl (**11** and **12**) complexes

Entry	Compound	Trypsin ^a	Chymotrypsin
1	N4Py (8)	493	>1000
2	3CG-N4Py (7)	354	1024
3	$[\text{Fe}^{\text{II}}(\text{OH}_2)(\text{N4Py})]^{2+}$ (9)	301	>1000
4	$[\text{Fe}^{\text{II}}(\text{OH}_2)(3\text{CG-N4Py})]^{3+}$ (10)	217	787
5	Peracetic acid	236	128
6	$[\text{Fe}^{\text{IV}}(\text{O})(\text{N4Py})]^{2+}$ (11)	71	119
7	$[\text{Fe}^{\text{IV}}(\text{O})(3\text{CG-N4Py})]^{3+}$ (12)	54	26
8	$\text{Fe}^{\text{II}}(\text{ClO}_4)_2$	>1000	>1000

^a Reaction conditions are mentioned in detail in Figure 2.9 footnote.

2.3.1.4. Characterization of products

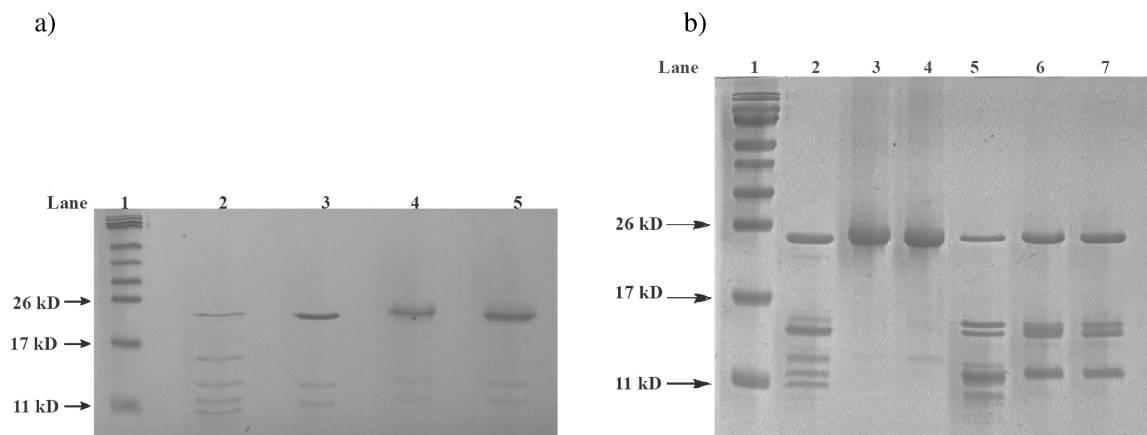


Figure 2.10. (a) SDS-PAGE analysis (16%), stained with Coomassie blue, of trypsin (20 μM) incubated at room temperature for 1 h at pH = 6.0, in a 10 mM acetate buffer containing 150 mM NaCl. A smeared band near 23 kD in lanes 3-5 showed oxidized enzyme. Lane 1: MW marker. Lane 2: enzyme only. Lane 3: peracetic acid (1000 μM). Lane 4: **11** (1000 μM). Lane 5: **12** (1000 μM). (b) SDS-PAGE analysis (16%), stained with Coomassie blue, of chymotrypsin (20 μM) incubated at room temperature for 1 h at pH = 6.0, in a 10 mM acetate buffer containing 150 mM NaCl. A smeared band near 25 kD in lanes 3 and 4 showed oxidized enzyme. Lane 1: MW marker. Lane 2: enzyme only. Lane 3: **11** (500 μM). Lane 4: **12** (500 μM). Lane 5: enzyme with DTT (100 mM). Lane 6: **11** (500 μM) with DTT (100 mM). Lane 7: **12** (500 μM) with DTT (100 mM). Equal amounts of protein were loaded in each lane.

To gain insight into the mode of inactivation, enzyme products were analyzed by SDS-PAGE (Figure 2.10), which confirmed that trypsin was oxidized but not cleaved extensively after treatment with ferryls **11** and **12**. Incubation of the protein alone for 1 h resulted in a major loss of intensity for the parent band at 23 kD and the formation of new bands with lower molecular weight, consistent with cleavage of the protein by autoproteolysis (Figure 2.10a). In contrast, enzyme samples treated with peracetic acid or ferryls **11** and **12** showed little or no cleavage of the protein, consistent with an inactivation event being faster than autoproteolysis of the enzyme. In the case of trypsin treated with peracetic acid (lane 3), a sharp, well defined band was observed at 23 kD,

whereas samples treated with the ferryl complexes showed a broad, smeared band (lanes 4 and 5) near the trypsin region (~ 23 kD), indicating a distribution of molecular weights near the parent mass of the enzyme.²²⁹

Similar results were obtained with chymotrypsin. In the control sample with enzyme alone, fragments with lower molecular weights were observed, which is consistent with autoprolysis (Figure 2.10b, lane 2). Autoprolysis was inhibited by peracetic acid, but the enzyme appeared as a sharp band. In contrast, broad smeared bands near the 25 kD region were observed for chymotrypsin treated with ferryls **11** and **12** (lanes 3 and 4). Fragments of lower molecular weight were not observed in lanes 3 and 4, indicating that inactivation of the enzyme was rapid and complete before autoprolysis began. Because chymotrypsin is composed of three subunits, α (1254 kD), β (13924 kD), and γ (10067 kD), which are linked by disulfides, the same three samples were treated with dithiothreitol (DTT) to determine if internal cross-links had formed between the subunits. Lane 5 with enzyme plus DTT showed three major fragments, plus new bands that were expected because of autoprolysis. Only three bands were observed in samples treated with ferryls **11** and **12** followed by DTT (lanes 6 and 7), which are consistent with the expected molecular weights for the subunits (β and γ) plus an additional band resulting from incomplete cleavage of the disulfide bond between the α and β subunits. Although the band at 14 kD could represent a covalent cross-link that was not cleaved by DTT, the sample of enzyme only treated under the same conditions shows the same pattern, suggesting that incomplete reduction of the disulfide bond between the α and β subunits occurred. However, bands at 14 and 11 kD in samples treated with ferryls **11** and **12** appear broad with respect to the same bands

observed in lane 5, as would be expected if the individual subunits were oxidized at the side chains and present as a distribution of masses near the parent region.

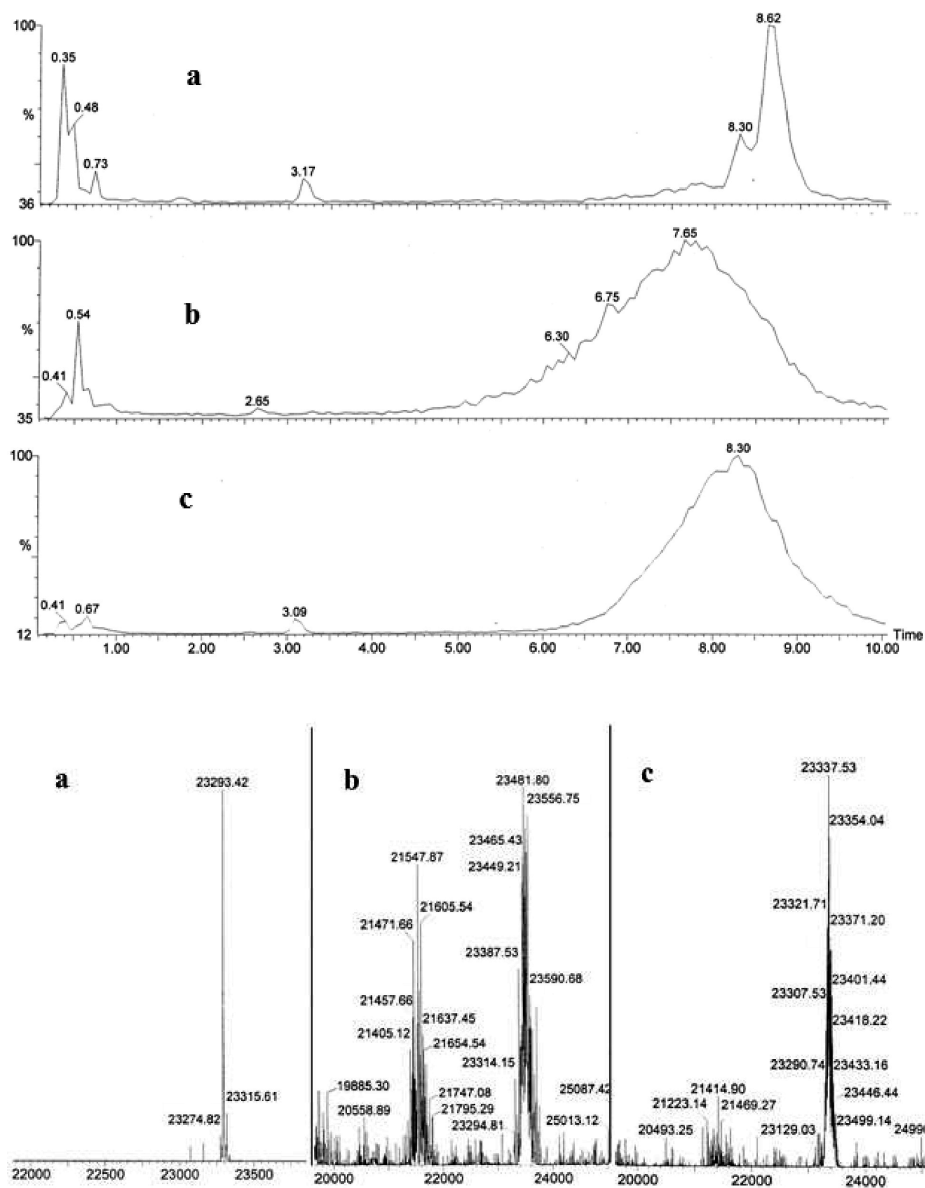


Figure 2.11. LC chromatograms (top) and deconvoluted MS spectra (bottom) of trypsin (spectrum a) and after treatment with **12** (spectrum b) or **11** (spectrum c). Reactions were conducted at room temperature by incubating trypsin (20 μ M) with **11** or **12** (1000 μ M) for 1 h before desalting and subjecting the samples to ESMS analysis.

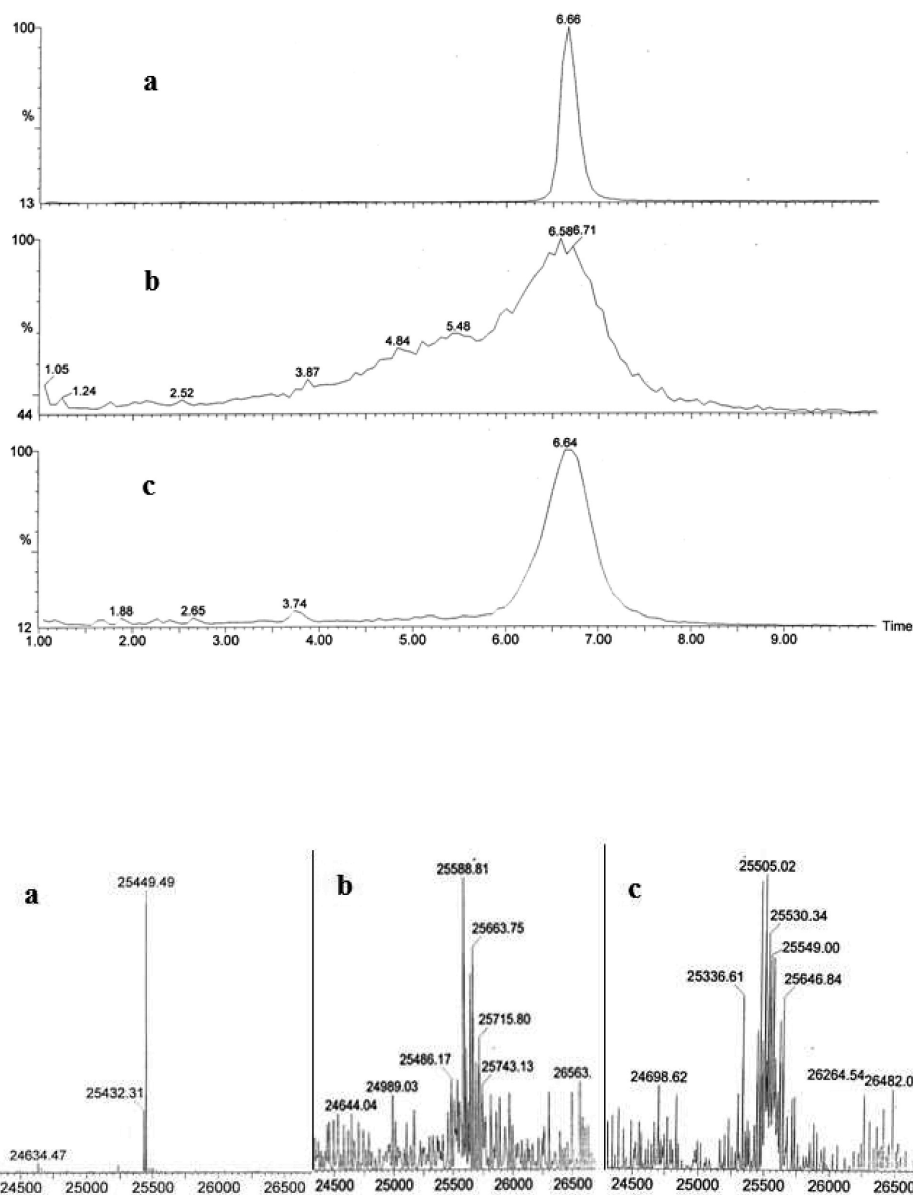


Figure 2.12. LCMS chromatograms (top) and deconvoluted MS spectra (bottom) of chymotrypsin (spectrum a) and after treatment with **12** (spectrum b) or **11** (spectrum c). Reactions were conducted at room temperature by incubating chymotrypsin ($20 \mu\text{M}$) with **11** or **12** ($1000 \mu\text{M}$) for 1 h before desalting and subjecting the samples to ESMS analysis.

LCMS chromatograms of trypsin ($20 \mu\text{M}$, not incubated), and trypsin incubated with the ferryls **11** and **12** ($1000 \mu\text{M}$) for 1 h at room temperature, show different retention times and product distributions for enzyme (control) versus enzymes treated with ferryls **11** and **12** (Figure 2.11). Integration of the peaks and deconvolution of the

MS spectra gave a single peak for the control sample with enzyme only, which corresponds to the MW of bovine trypsin (MW = 23293) and complex spectra for both samples treated with ferryls. For the treated samples, a distribution of molecular weights larger than that of trypsin was observed consistent with oxidation of the enzyme by the addition of multiple oxygen atoms to the protein, as evidenced by the difference between masses corresponding to 16 units. In the case of the sample treated with ferryl **12** (Figure 2.11, spectrum b), a second group of peaks was observed below the parent mass of trypsin, which is consistent with oxidation of trypsin and cleavage of a small fragment, approximately 2 kD in weight, most likely from the N terminus (vide infra). Similar results were observed for chymotrypsin. LCMS chromatograms of chymotrypsin (20 μ M) incubated with the ferryls **11** and **12** (1000 μ M) for 1 h at room temperature are shown in Figure 5 (Figure 2.12). The sample with enzyme only showed a sharp peak that was integrated and deconvoluted to a mass of 25449, whereas broad peaks were observed for samples treated with ferryls **11** and **12**. Again integration of these peaks gave complex spectra with peaks higher in masses than the chymotrypsin itself consistent with oxidation of protein.

2.3.1.5. Enzyme Inactivation with Ferrous Complexes and H₂O₂

After it was established that trypsin and chymotrypsin could be inactivated selectively with ferryls **11** and **12**, experiments were performed in which the enzymes were treated with ferrous complexes **9** and **10** prior to the addition of oxidant. These conditions were examined to determine if catalytic inactivation of the proteases was possible. When enzymes were incubated in the presence of **9** or **10** under an aerobic atmosphere, the enzyme activity did not change within reasonable time periods (< 6 h).

Similar results were obtained in the presence of the reductant ascorbate or DTT, which did not accelerate enzyme inactivation. Thus, these results confirm that enzyme inactivation of trypsin and chymotrypsin using O_2 as the oxidant, either in the presence or absence of reductant, is a relatively slow process with these iron complexes.²³⁰

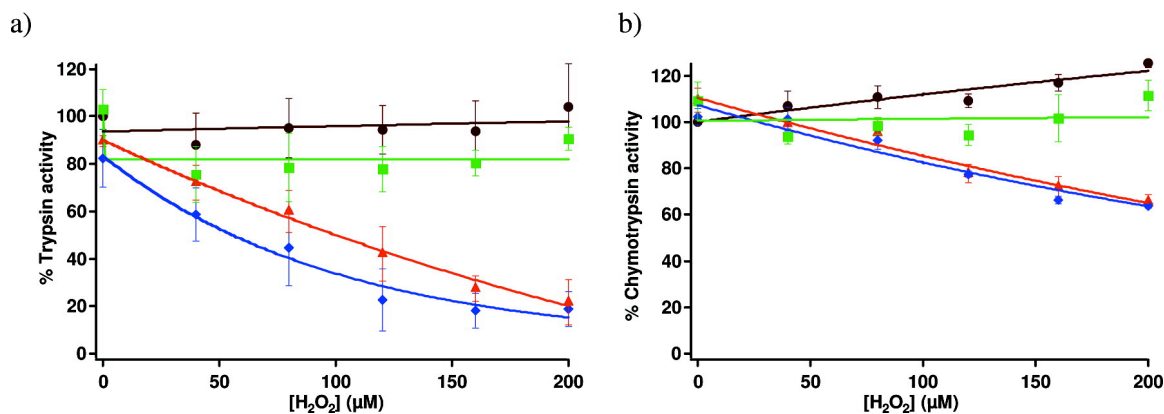


Figure 2.13. Trypsin (graph a) and chymotrypsin (graph b) activities as a function of added H_2O_2 . Samples containing enzyme only (brown ●, 1 μM) and enzyme treated with $Fe^{II}(ClO_4)_2$ (green ■), **9** (red ▲), or **10** (blue ◆) (20 μM) were pulsed with H_2O_2 every 10 min (40 μM per pulse). The reaction was performed in an acetate buffer of pH = 6.0 containing 150 mM NaCl. The activities were converted to % enzyme activity, with 100% activity equal to the activity of the blank reaction in the absence of inhibitor at $t = 0$. Data points are averages from three independent experiments, where errors are reported as standard deviations.

More promising results were obtained when H_2O_2 was used as the oxidant. For these experiments, solutions of trypsin (1 μM) and several iron species [$Fe^{II}(ClO_4)_2$, **9** or **10**, 20 μM] were pulsed with H_2O_2 (40 μM per pulse). Enzyme activities were determined by removing aliquots after each pulse (10 min between pulses) and plotted against the total amount of peroxide added (Figure 2.13a). Negligible changes in the activities were observed with trypsin alone and trypsin treated with $Fe^{II}(ClO_4)_2$. In the case of the sample treated with $Fe^{II}(ClO_4)_2$, the trypsin activity dropped immediately by $\sim 15\%$ after the first addition of H_2O_2 but did not drop further after the addition of more

H₂O₂, which is consistent with a Fenton reaction carried out by an iron species that was no longer viable after the first addition of the oxidizing reagent. In contrast, enzyme activities were lost in a concentration-dependent fashion with respect to H₂O₂ when pulsing was performed in the presence of **9** or **10**. In both cases, the activities were diminished by roughly 80% after the addition of 200 μM H₂O₂, 10 equiv with respect to the iron complexes. These data confirm that **10**, which contain the propylguanidinium group, inactivate trypsin more effectively than **9**. For example, after three additions of H₂O₂ (120 μM total), the trypsin activity dropped by 80% with **10** compared to 60% with **9**. The more efficient inactivation of trypsin with **10** compared to **9** confirms that selectivity can be gained between two iron complexes and is consistent with the protein-affinity group (propylguanidinium) of **10** directing the complex toward the protein, presumably the S1 pocket where Asp 189 may form a salt bridge with the guanidinium group.

When chymotrypsin was treated with H₂O₂ under the same conditions, controls with enzyme alone or enzyme plus Fe^{II}(ClO₄)₂ showed no significant changes after the addition of 200 μM H₂O₂ (Figure 2.13b). Again, the enzyme activity was lost in a concentration-dependent fashion when chymotrypsin was pulsed with H₂O₂ in the presence of **9** and **10**. However, the enzyme activities dropped only by ~ 35% in both cases after the addition of 200 μM H₂O₂, as opposed to 80% with trypsin. Selectivity was not observed between **9** and **10**. These data confirm that selective inactivation of trypsin over chymotrypsin can be observed with the iron complexes **9** and **10** in the presence of H₂O₂. Differences in reactivity for **9** and **10** with trypsin versus chymotrypsin parallel data from inhibition studies (Table 2.2, entries 3 and 4), where the complexes **9**

and **10** show more a potent inhibition of trypsin than chymotrypsin. The trend observed is consistent with the active reagents derived from **9** or **10** and H_2O_2 possessing a higher effective molarity for trypsin over chymotrypsin and causing more efficient oxidative damage.

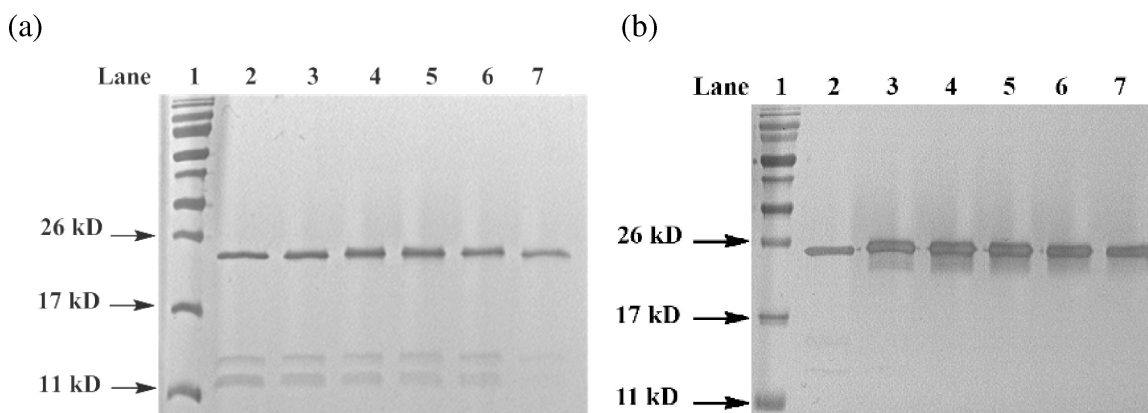


Figure 2.14. SDS-PAGE analysis (16%), stained with silver, of (a) trypsin and (b) chymotrypsin (1 μM), pulsed with H_2O_2 (40 μM) every 10 min in the presence of **10** (20 μM) at room temperature at pH = 6.0, in a 10 mM acetate buffer containing 150 mM NaCl. Smear bands near 23 kD in part a and 25 kD in part b in lanes 3-7 showed oxidized enzymes. Lane 1: MW marker. Lane 2: enzyme only. Lane 3: H_2O_2 (40 μM). Lane 4: H_2O_2 (80 μM). Lane 5: H_2O_2 (120 μM). Lane 6: H_2O_2 (160 μM). Lane 7: H_2O_2 (200 μM).

Analysis by LCMS and SDS-PAGE was used in order to characterize the enzyme products from trypsin and chymotrypsin. SDS-PAGE analysis of the enzymes (1 μM), pulsed with H_2O_2 (40 μM per pulse) every 10 min, in the presence of **10** showed an increase in the smearing of the band near the parent trypsin band (23 kD, Figure 2.14a) and the chymotrypsin band region (25 kD, Figure 2.14b) with added H_2O_2 , although smearing was less extensive than in the samples treated with ferryls **11** and **12**. This observation is consistent with a distribution of molecular weights after oxidation with **10** and H_2O_2 . Because other bands were not observed in either case, the oxidation with **10** and H_2O_2 does not lead to cleavage of the enzymes. The chromatograms of trypsin (1

μM) and chymotrypsin pulsed with H_2O_2 ($40 \mu\text{M}$ per pulse) in the presence of **9** or **10** ($20 \mu\text{M}$) at room temperature show different retention times and product distributions for enzyme (control) versus treated samples. Integration of the peaks and deconvolution of the MS spectra gave single peaks for the control samples with enzyme only, while complex spectra were obtained for samples where enzymes were pulsed with H_2O_2 in the presence of **9** or **10**, confirming that oxidation of the proteins occurred.

2.4.1.6. Mechanistic studies

Additional experiments were carried out to gain further insight into the nature of protein inactivation under single-turnover (ferryls **11** and **12**) and catalytic conditions (**9** or **10** plus H_2O_2). In particular, the identity of the active oxidant under catalytic conditions was in question. Both $\text{HO}\cdot$ (Fenton chemistry) and iron-based oxidants have been implicated in oxidation reactions when ferrous complexes such as **9** are treated with H_2O_2 , and the outcome varies according to the ligand set and the conditions of the experiment (*vide infra*).²³¹⁻²³³ To distinguish between Fenton chemistry ($\text{HO}\cdot$) and iron-based oxidants, control experiments were performed in the presence of reagents that scavenge ROS. When the inactivation of trypsin with **10** was performed in the presence of D-mannitol, a potent hydroxyl radical scavenger, inactivation was not inhibited with 0.1 mM D-mannitol and was only slightly inhibited with 20 mM D-mannitol, confirming that $\text{HO}\cdot$ can act as only a minor component of the inactivation pathway if at all (Figure 2.15 for trypsin). Thus, another oxidant was likely at play. Similar results were obtained in the presence of imidazole, a scavenger of the hydroxyl radical and $^1\text{O}_2$. Interestingly, inactivation was inhibited somewhat in the presence of NaN_3 ($0.1\text{-}1 \text{ mM}$), again in a concentration-dependent fashion. Although azide is a scavenger of $^1\text{O}_2$, it is known to

inhibit tyrosine nitration catalyzed by the heme enzyme myeloperoxidase.²³⁴ In this case, rather than quenching $^1\text{O}_2$, competitive binding of azide to the peroxidase iron center may poison the heme by blocking access to H_2O_2 .²³⁵ In support of this mode of inhibition, the binding of azide to **10** was confirmed by UV-vis titration of **10** with NaN_3 , which suggests that the action of peroxide with the iron catalyst can be inhibited by ligands that bind competitively to the sixth site of the iron center. Together, these results indicate that an oxidant other than $\text{HO}\cdot$ or $^1\text{O}_2$ is responsible for the inactivation of trypsin and chymotrypsin in the presence of **9** or **10** and H_2O_2 .

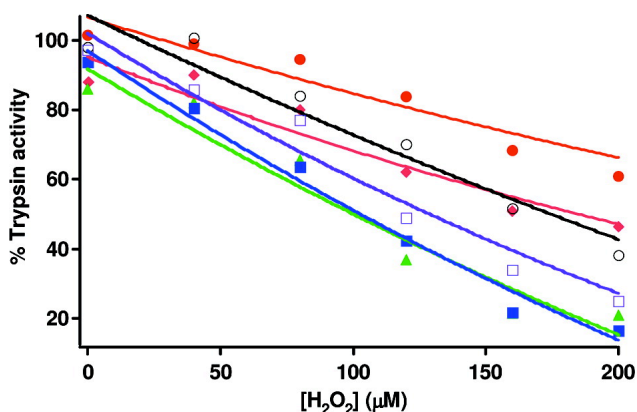


Figure 2.15. Inactivation of trypsin in the presence of ROS scavengers (azide, D-mannitol, and imidazole). The reactions were conducted at pH = 6.0, in a 10 mM acetate buffer containing 150 mM NaCl. Trypsin (1 μM) with **10** (20 μM) was pulsed with H_2O_2 (40 μM) in the presence of a buffer as a blank (blue ■) and ROS scavengers D-mannitol (0.1 mM, green ▲; 20 mM, black ●), imidazole (0.1 mM, purple □), and NaN_3 (0.1 mM, maroon ◆; 1.0 mM, red ●). Enzyme activities, where 100% activity is equal to the activity of the blank reaction in the absence of inhibitor at $t = 0$, were determined by removing aliquots before each pulse (10 min between pulses) and plotted against the total amount of peroxide added. Data points are averages from three independent experiments; errors were $\pm 5\%$.

The presence of ketones and aldehydes in proteins, known as the carbonyl content, is a key indicator of oxidative damage observed *in vitro* and *in vivo* during aging and under conditions of oxidative stress.²³⁶ Because normal proteins do not contain

ketone or aldehyde carbonyls that react electrophilically with hydrazine nucleophiles, the reagent 2,4-dinitrophenylhydrazine can be used to determine the overall protein carbonyl content resulting from protein oxidation. Following a literature method,²³⁶ the amount of carbonyl groups formed with trypsin and chymotrypsin (20 μM) was determined as a function of the pulsed H_2O_2 concentration in the presence of **10** (50 μM ; Figure 2.16). Similar results were obtained with **9**. In the case of both enzymes, an increase in the carbonyl content was observed that plateaued at 500 μM H_2O_2 to approximately 20 nmol/mg of protein. Because nearly identical results were obtained with trypsin and chymotrypsin, these data indicate that the formation of protein carbonyls is not coupled to the inactivation event imparted by **10** and H_2O_2 (Figure 2.13a,b). In fact, using the molecular weight of the proteins and the observed content of protein carbonyls, one can estimate that only four or five carbonyls are formed per protein out of 223 (trypsin) and 241 (chymotrypsin) residues when the proteins (20 μM) are treated with **10** (50 μM) and 500 μM H_2O_2 . Assuming that a single carbonyl is formed per oxidized residue, this modification accounts for less than 3% of all residues.

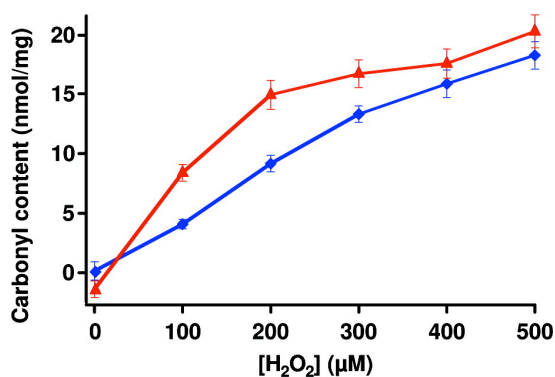


Figure 2.16. Carbonyl content (nmol/mg of protein) as a function of pulsed H_2O_2 (0-500 μM) for enzymes (20 μM) trypsin (blue ●) and chymotrypsin (red ▲) in the presence of **10** (50 μM). Data points are averages from three independent experiments, where the errors are reported as standard deviations.

The aforementioned results confirm that a unique oxidant must give preferential inactivation of trypsin over chymotrypsin under catalytic conditions. Attempts to analyze the oxidized proteins by LCMS/MS analysis were inconclusive due to low sequence coverage because the oxidized proteins did not respond well to digestion. Although LCMS/MS analysis can reveal information about the location of oxidized residues in proteins, it is difficult to obtain quantitative measurements of protein oxidation using this method. Therefore, amino acid analysis was performed on the oxidized samples, in order to determine which types of residues were affected by treatment of trypsin and chymotrypsin under the single-turnover (ferryls **11** and **12**) and catalytic conditions (ferrous complexes **9** and **10** plus H₂O₂) (Figure 2.17).

Strikingly, catalytic conditions produced a major modification in the levels of the amino acid tyrosine with respect to the control, while leaving other amino acid levels unchanged within the margin of error. Different results were obtained with the ferryls, where the levels of tyrosine, cysteine, and tryptophan were diminished significantly with respect to controls. These data are consistent with published model studies that indicated that cysteine, tyrosine, and tryptophan were the most reactive amino acids with **11**.¹⁰⁸ Results obtained in the single-turnover and catalytic conditions were not highly dependent on the ligand structure, suggesting that only a modest level of directability was achieved by attaching the propylguanidinium group to the N4Py ligand. These results confirm that catalytic conditions result in a milder form of oxidation than oxidation by the ferryls and support the hypothesis that an oxidant other than ferryl is acting in the presence of H₂O₂.

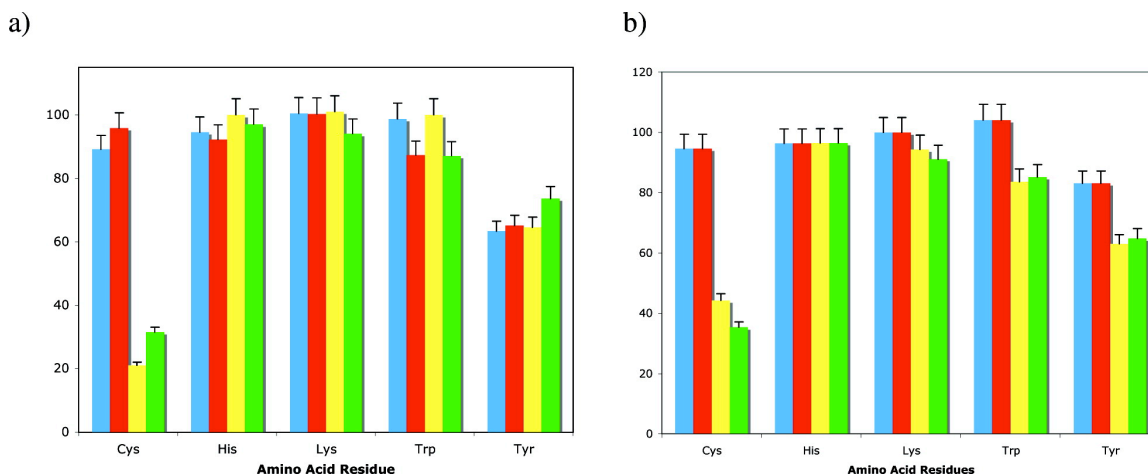
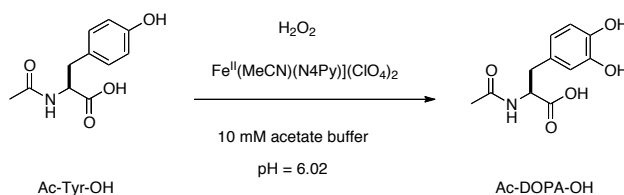


Figure 2.17. Bar graphs showing the compositions of five natural amino acids present in the oxidized proteins samples isolated from single-turnover (ferryls **11** and **12** in green and gold, respectively) and catalytic conditions (**9** or **10** plus H₂O₂ in red and blue, respectively) for trypsin (a) and chymotrypsin (b). Compositions are reported as percentages normalized with respect to the control experiments with no iron or oxidant added. Enzymes trypsin and chymotrypsin (20 μ M) were treated with ferryl **11** or **12** (1000 μ M) or with **9** or **10** (50 μ M) and pulsed with H₂O₂ (500 μ M total, 100 μ M per pulse). Standard errors are 10%. The results indicate that tyrosine was modified selectively in the case of catalytic conditions with **9** or **10** plus H₂O₂, whereas cysteine, tyrosine, and tryptophan were modified by ferryls **11** and **12**.

In order to gain insight into the reaction of the iron catalyst with tyrosine in the presence of H₂O₂, the oxidation of **13** was examined. Under the same conditions as those used in the enzyme experiments, the catechol product Ac-DOPA-OH (**14**) was observed as a major product by HPLC analysis (Scheme 2.3). Dityrosine, a common product of tyrosine oxidation resulting from oxidative coupling of the two phenol rings, was detected by fluorescence analysis of the crude reaction mixture but not by ESMS, suggesting that this product was present in only trace amounts. Importantly, chlorotyrosine was not detected by ESMS or HPLC analysis of the crude reaction mixture, which confirmed that oxidation of **13** was not due to the action of HOCl generated from H₂O₂ and chloride ion.^{237,238} Taken together, these observations are diagnostic and significant because catechol products are not formed when tyrosine derivatives are treated with the ferryl **11**, confirming that a different mechanism of action

takes place when H_2O_2 is used as the oxidant. In other words, ferryl **11** was not the active oxidant. To probe this further, the reaction was monitored by UV-vis spectroscopy. When the ferrous complex **9** was treated with 0.5 equiv of H_2O_2 under these conditions, bleaching occurred, which consumed the signature absorbance for Fe^{II} at 380 and 464 nm. However, ferryl **11** was not observed, suggesting that a ferric complex was formed instead (vide infra). When this mixture was treated with **13**, the yellow color of the starting ferrous complex returned and reached completion after approximately 10 min, as judged by UV-vis spectroscopy. If this reaction solution was treated again with peroxide, bleaching occurred again, and after ca. 10 min, the UV spectrum returned to its original intensity, suggesting that turnover was possible without significant loss of the starting ferrous complex. In conclusion, these results are consistent with the phenol ring of tyrosine being oxidized by an oxidant other than ferryl **11**, which is discussed in the following section.



Scheme 2.3. Conversion of Ac-Tyr-OH into Ac-DOPA-OH in presence of ferrous complex and H_2O_2

2.3.2. Discussion

Our results confirm that ferryls are potent and selective oxidants that inactivate serine proteases. The ferryls **11** and **12** were more powerful oxidants than peracetic acid. Selectivity was observed for a single ferryl between two enzymes (trypsin and chymotrypsin; Table 2.2, entry 7 vs. entry 8) but also for a single enzyme between two ferryls (Table 2.2, entries 7 and 8, trypsin vs. chymotrypsin). Ferryl **12** was most

effective in the inactivation of chymotrypsin with an IC_{50} value of 24 μ M. With both serine proteases, the oxidation of protein side chains occurred. Major cleavage products were not observed by SDS-PAGE or LCMS, confirming that cleavage of the protein backbone is a slow process relative to side-chain oxidation. In the oxidation of trypsin by **12**, LCMS analysis indicated a minor cleavage product consistent with a loss of approximately 2 kD, presumably at a glycine residue located near the active site, 20 residues from the N terminus of the enzyme. Therefore, these results are in good agreement with model studies that focused on protected amino acids,¹⁰⁸ which confirmed that activation of the α -CH bond of amino acids and resultant oxidative cleavage of the backbone are slow relative to side-chain oxidation with ferryl complexes. Furthermore, the results from the amino acid analysis of enzyme samples oxidized by the ferryls prove a direct correlation between the most reactive amino acids (cysteine, tyrosine, and tryptophan) in the model studies with Ac-AA-NHtBu substrates and the residues modified in the proteins trypsin and chymotrypsin. These results have relevance to biology because, under conditions of oxidative stress, ferryls such as ferrylmyoglobin can oxidize proteins.^{193,239-245} Observations reported herein reveal useful information about how proteins are modified and inactivated by ferryls. For example, when tyrosine and tryptophan residues are oxidized, as our results confirm, this type of oxidation is often irreversible.¹⁸⁹ In contrast, oxidative modification of cysteine residues can be reversed if disulfides are formed.²⁴⁶ However, when higher oxidation states of sulfur are obtained, such as sulfenic and sulfonic acid derivatives, oxidative damage becomes irreversible. The levels of cystic acid did not change in these studies between control and treated samples of enzyme, consistent with the oxidants presented herein forming products other than cystic acid.

Reasonable levels of selectivity were observed in the oxidation of trypsin and chymotrypsin catalyzed by **9** and **10** in the presence of H_2O_2 . However, as opposed to the single-turnover conditions where ferryl **12** was the most effective at inactivating chymotrypsin, catalytic conditions provided the most efficient inactivation of trypsin with both **9** and **10**. The advantage of incorporating iron and oxidant with the inhibitors **8** and **7** was clear. Upon addition of these two reagents, a ligand concentration of $20\ \mu\text{M}$ becomes more effective than $500\ \mu\text{M}$ inhibitor alone, which amplifies the effects of the ligand by almost 2 orders of magnitude. The results obtained from amino acid analysis prove that tyrosine residues of both proteins were selectively targeted under these conditions, with residues of trypsin being diminished to a greater extent (60% of control) than chymotrypsin (80%). These results suggest that iron complexes derived from N4Py mimic the action of myeloperoxidase, a heme enzyme produced by neutrophil granulocytes (white blood cells) that is known to oxidize tyrosine residues of proteins using H_2O_2 as the oxidant.²⁴⁷

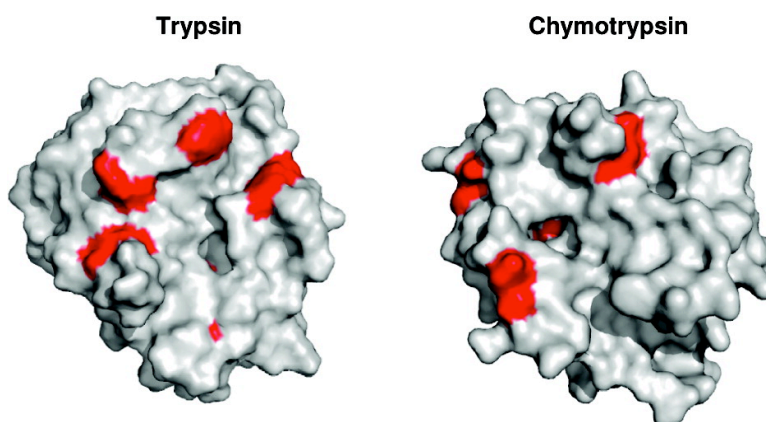


Figure 2.18. Surface models of trypsin and chymotrypsin with tyrosine residues near the active site highlighted in red. Trypsin contains four residues near the active site, whereas chymotrypsin contains three.

The selective inactivation of trypsin observed under catalytic conditions may be due to the active iron reagent obtained with H_2O_2 , giving a higher effective molarity with trypsin than with chymotrypsin. Alternatively, this selectivity could be due to an inherent sensitivity of trypsin over chymotrypsin to oxidation of its Tyr residues. Both enzymes have numerous tyrosine residues on the surface near the active site (Figure 2.18). The fact that ligands **8** and **7** were more effective at inhibiting trypsin than chymotrypsin, in the absence and presence of $\text{Fe}^{\text{II}}(\text{ClO}_4)_2$, supports the hypothesis that the active reagents derived from **9** and **10** bind tighter to trypsin than chymotrypsin. Furthermore, previous studies performed with $^1\text{O}_2$ confirmed that trypsin and chymotrypsin have similar sensitivity to oxidation, although the types of residues targeted in this case were likely different and were not confirmed.²⁴⁸ More studies in this area are needed, specifically over a larger group of enzymes such as the family of serine proteases, to discern between these two possibilities. Importantly, these studies suggest that incorporating protein affinity groups that bind tighter to enzyme targets and place iron catalysts in the vicinity of tyrosine residues has the potential to achieve protein inactivation at low concentrations.

The results with iron complexes and H_2O_2 indicate that a unique oxidant was responsible for the selective protease inactivation. Control experiments ruled out ROS such as $\text{HO}\cdot$ (Fenton chemistry) or $^1\text{O}_2$. The action of ferryls under these conditions is also unlikely because ferryls were not observed when the ferrous complexes **9** or **10** were treated with peroxide. Furthermore, studies in Table 2.1 prove that chymotrypsin is inactivated at lower ferryl concentrations than trypsin, so the opposite trend in selectivity would be expected under catalytic conditions if ferryls were operating. The action of a

different oxidant is also supported by the fact that catechol is observed in the oxidation of Ac-Tyr-OH (**13**) with H₂O₂. Catechols are not observed when tyrosine derivatives are treated with ferryl **11**; instead, hydrogen-atom transfer occurs to generate phenoxy radicals that decompose, presumably by polymerization.¹⁰⁸ Taking into account our results and data in the literature,²⁴⁹ we can conclude that another oxidant is likely to be generated under catalytic conditions. However, further mechanistic studies in this area are needed to differentiate between the potential pathways and to determine if there is an analogy between the chemistry reported herein and the action of the non-heme iron enzyme tyrosine hydroxylase^{216,250,251} or the heme enzyme myeloperoxidase.²⁴⁷ In any case, the effect of the ligand N4Py is clear in the inactivation experiments because Fe^{II}(ClO₄)₂ did not give the same level of dose-dependent inactivation with H₂O₂.

2.4. Conclusions and future directions

Non-heme iron complexes inactivate serine proteases selectively. Ferryls are potent oxidants that inactivate trypsin and chymotrypsin by oxidation of amino acid side chains rather than backbone cleavage, where the residues cysteine, tyrosine, and tryptophan are the most susceptible to oxidation. Oxidation of the proteases by ferrous complexes in the presence of hydrogen peroxide leads to the preferential inactivation of trypsin over chymotrypsin. In this case tyrosine residues are targeted, and data support action of a pathway unique from that of an Fe^{II}/Fe^{IV} cycle involving ferryl compounds. Importantly, these results suggest a promising future direction for the method presented herein where complexes that cycle between accessible oxidation states are used to target proteins. Although the scope of such a method may be limited with respect to ROS for attack on tyrosine residues, there are many proteins, including important

medicinal targets that contain crucial tyrosine residues near their active sites.

2.5. Experimental section

2.5.1. General considerations

All reagents were purchased from commercial suppliers and used as received. NMR spectra were recorded on a Varian FT-NMR Mercury-400 MHz Spectrometer. Mass spectra were recorded on a Micromass Quattro LC Triple-Quad mass spectrometer using an electrospray ionization source. IR spectra were recorded on a Nicolet FT-IR spectrophotometer. Enzymatic assays were performed on a TECAN Infinite M200 microplate reader. UV-vis spectra were recorded on a Varian Cary 50 spectrophotometer. Human carbonic anhydrase-I (product # C4396) and its substrate, 4-nitrophenyl acetate (product # N8130), were obtained from Sigma. Trypsin from bovine pancreas (product # T8003) and its substrate, *N*- α -benzoyl-DL-arginine-4-nitroanilide hydrochloride (catalog # 227740050), were obtained from Sigma and Acros Organics, respectively, and were used as received. Chymotrypsin (product # C4129) and its substrate *N*-succinyl-Ala-Ala-Pro-Phe-pNA (product # S7388) were obtained from Sigma. Absorbance data were collected on a GENios Pro, microplate reader, TECAN, using 96-well microplates. The compounds 1,1-dipyridin-2-yl-*N,N*-bis(pyridin-2-ylmethyl)methanamine (N4Py, **8**),²¹⁸ methyl 6-[[[(dipyridin-2-ylmethyl)(pyridin-2-ylmethyl)-amino]methyl]nicotinate (**1**),²²² and *N*-acetyltyrosine (**13**)²⁵² were synthesized using literature procedures.

2.5.2. Molecular modelling

Docking studies were performed with the program MacPyMOL using crystallographic data from 4-aminobenzenesulfonamide bound to CA-I (PDB ID 1CZM).

For these studies, a model of the ferryl inhibitor $[\text{Fe}^{\text{IV}}(\text{O})(\mathbf{4})]^{2+}$ was constructed using the program Spartan 04. Bond length and angle constraints were made on the $[\text{Fe}^{\text{IV}}(\text{O})(\text{N4Py})]^{2+}$ unit of the inhibitor using crystallographic data for the ferryl species before MM2 minimization of the overall structure $[\text{Fe}^{\text{IV}}(\text{O})(\mathbf{4})]^{2+}$ was carried out. After minimization, a pdb file of the inhibitor was exported from Spartan 04 and imported into MacPyMOL for docking in the active site of CA-I. Dihedral angles of the inhibitor were adjusted to place the inhibitor in the active site after overlapping benzenesulfonamide portions of the original inhibitor and $[\text{Fe}^{\text{IV}}(\text{O})(\mathbf{4})]^{2+}$. The dihedral angle of the amide bond of the inhibitor was maintained at 180° .

2.5.3. Inhibitor synthesis

Preparation of 6-(((dipyridin-2-ylmethyl)(pyridin-2-ylmethyl)amino)methyl)-N-(4-sulfamoylbenzyl)nicotinamide (4). Sodium hydroxide (2 N, 1 mL) was added dropwise to a solution of ester **1** (0.225 g, 0.481 mmol) in methanol (3 mL). This reaction mixture was stirred vigorously at rt. After 4 h, the reaction mixture was acidified to pH = 2 with 2 N HCl and then concentrated. Methanol (5 mL) was added to the remaining residue. The white solid formed was removed by filtration and the filtrate was concentrated to give slightly wet brown solid. The brown solid was dried under vacuum desiccator over P_2O_5 and KOH to give the acid **2** (0.24 g, quant.). LRMS (ESI) Calcd for $\text{C}_{28}\text{H}_{30}\text{N}_5\text{O}_2$ $[(\text{M}+\text{H})^+]$: m/z 468. Found: m/z 468.

DSC (250 mg, 0.98 mmol) and pyridine (195 μL , 2.43 mmol) were added to a solution of the crude acid **2** (100 mg, 0.243 mmol) in acetonitrile (25 mL) and stirred at 80°C under nitrogen. After 2 h, the reaction mixture was cooled to room temperature and concentrated to remove pyridine and acetonitrile. The remaining residue was dissolved in 5% NaHCO_3 (50 mL) and extracted with chloroform (50 mL x 3). The

organic layers were then combined, dried with anhydrous sodium sulfate, and concentrated to yield the corresponding *N*-hydroxysuccinimide ester **3** (104 mg, 84%) as a brown oil that was unstable to chromatography and used without further purification. $^1\text{H-NMR}$ (CDCl_3) δ 9.11 (d, $J = 2.4$ Hz, 1H), 8.53 (d, $J = 4.9$ Hz, 2H), 8.45 (d, $J = 4.1$ Hz, 1H), 8.21–8.31 (dd, $J = 2.4, 1.6$ Hz, 1H), 7.79 (d, $J = 8.1$, 1H), 7.42–7.69 (m, 6H), 7.06–7.15 (m, 3H), 5.34 (s, 1H), 4.09 (s, 2H), 3.95 (s, 2H), 2.87 (s, 4H); $^{13}\text{C-NMR}$ (CDCl_3) δ 168.9, 167.5, 160.9, 159.7, 159.1, 150.7, 149.2, 149.0, 137.8, 136.4, 126.4, 125.2, 124.0, 123.2, 122.8, 122.3, 122.0, 72.6, 57.9, 57.4, 25.6; LRMS (ESMS) calcd for $\text{C}_{28}\text{H}_{25}\text{N}_6\text{O}_4$ [(M+H) $^+$]: m/z 509. Found: m/z 509.

4-(aminomethyl)benzenesulfonamide (20 mg, 0.11 mmol) was added to a solution of *N*-hydroxysuccinimide ester **3** (54 mg, 0.11 mmol) and DMF (5 mL) and stirred for 5 h at room temperature. After 5 hours, the reaction mixture was concentrated *in vacuo* to remove DMF. Alumina gel chromatography (EtOAc, then MeOH) was used to purify the crude mixture. A brown oil was obtained after MeOH elution that was stirred with EtOAc and filtered. The inhibitor **4** precipitated upon addition of hexanes to the filtrate and was isolated as a tan amorphous solid (33 mg, 54%). $^1\text{H-NMR}$ (CD_3OD) δ 8.83 (d, $J = 1.8$ Hz, 1H), 8.46 (d, $J = 4.9$ Hz, 2H), 8.35 (d, $J = 4.3$, 1H), 8.12 (dd, $J = 2.2, 6.1$ Hz, 1H), 7.80–7.65 (m, 7H), 7.58–7.40 (m, 5H), 7.30–7.18 (m, 3H), 5.36 (s, 1H), 4.63 (s, 2H), 4.03 (s, 2H), 3.97 (s, 2H); $^{13}\text{C-NMR}$ (d_6 -DMSO) δ 172.9, 165.0, 162.7, 159.9, 159.2, 149.0, 148.9, 147.9, 143.5, 142.7, 136.6, 136.5, 135.6, 128.0, 127.6, 125.8, 123.7, 122.5, 122.2, 122.0, 71.4, 57.0, 56.6, 42.3; IR (film) 3583, 3219, 2922, 2851, 2360, 1705, 1651, 1592, 1569, 1537, 1469, 1433, 1260, 1158, 1036, 752 cm^{-1} ; LRMS (ESMS) calcd for $\text{C}_{31}\text{H}_{30}\text{N}_7\text{O}_3\text{S}$ [(M + H) $^+$]: m/z 580. Found: m/z 580.

Preparation of *tert*-Butyl-1-(6-[[[(Dipyridin-2-ylmethyl)(pyridin-2-ylmethyl)amino]methyl]pyridin-3-yl]-11,11-dimethyl-1,9-dioxo-10-oxa-2,6,8-triazadodecan-7-ylidencarbamate (6). A solution of *N*-(3-aminopropyl)-6-[[[(dipyridin-2-ylmethyl)(pyridin-2-ylmethyl)-amino]methyl]nicotinamide **5** (100 mg, 0.213 mmol) in a mixture of tetrahydrofuran (THF; 0.3 mL) and H₂O (20 μ L) was treated with a solution of 1,3-bis(*tert*-butoxycarbonyl)-2-methyl-2-thiopseudourea (61.8 mg, 0.213 mmol) in THF (0.2 mL) dropwise at room temperature. The reaction mixture was heated to 50 °C for 1 h and then concentrated in vacuo. The resulting crude reaction mixture was partitioned between CHCl₃ (5 mL) and a saturated aqueous solution of NaHCO₃ (5 mL). The organic layer was separated, dried over anhydrous Na₂SO₄, filtered, and concentrated to obtain **6** as a pale-yellow solid (131 mg, 88%). ¹H-NMR (CDCl₃): δ 11.50 (s, 1H), 9.07 (d, *J* = 1.6 Hz, 1H), 8.55-8.52 (m, 3H), 8.48 (d, *J* = 4.0 Hz, 1H), 8.29-8.26 (m, 1H), 8.16 (dd, *J* = 8.1 and 2.4 Hz, 1H), 7.71-7.56 (m, 7H), 7.24-7.07 (m, 3H), 5.29 (s, 1H), 3.99 (s, 2H), 3.93 (s, 2H), 3.47-3.41 (m, 4H), 1.74-1.72 (m, 2H), 1.48 (s, 9H), 1.28 (s, 9H). ¹³C-NMR (CDCl₃): δ 165.5, 163.2, 162.9, 159.8, 157.5, 153.2, 149.3, 149.1, 148.4, 136.4, 136.2, 135.5, 128.4, 123.9, 122.7, 122.2, 122.1, 121.9, 83.5, 79.7, 71.3, 57.2, 56.9, 36.9, 35.5, 30.3, 28.2, 28.0. IR (cm⁻¹): 3324, 3055, 2978, 2931, 2359, 2239, 1723, 1642, 1589, 1569, 1474, 1433, 1368, 1325, 1223, 1135, 1049, 1026, 995, 912, 855, 732, 645, 616. HRMS (ESI) Calcd for C₃₈H₄₇N₉O₅ [(M + Na)⁺]: *m/z* 732.3598. Found: *m/z* 732.3589.

Preparation of 6-[[[(Dipyridin-2-ylmethyl)(pyridin-2-ylmethyl)amino]-methyl]-*N*-(3-guanidinopropyl)nicotinamide hydrochloride (7). Compound **6** (100 mg, 0.141 mmol) was maintained with 4 M HCl in 1,4-dioxane (2 mL) for 3 h at room temperature.

The reaction mixture was concentrated to furnish **7** (100 mg) as a hygroscopic pale-yellow solid in quantitative yield as its hydrochloride salt. Stock solutions of **10** in H₂O (4 mM) were prepared from this solid for the following studies based on the quantitative yield in the conversion of **6** to **7**. ¹H-NMR (DMSO-*d*₆): δ 9.18 (s, 2H), 8.82 (d, *J* = 4.1 Hz, 1H), 8.62 (d, *J* = 4.1 Hz, 2H), 8.41 (d, *J* = 7.3 Hz, 1H), 8.27 (t, *J* = 7.3 Hz, 1H), 8.18-8.14 (m, 2H), 8.01 (br s, 1H), 7.92 (d, *J* = 8.1 Hz, 2H), 7.82 (d, *J* = 7.3 Hz, 2H), 7.69-7.62 (m, 4H), 6.06 (s, 1H), 4.44 (s, 2H), 4.26 (s, 2H), 3.37-3.33 (m, 2H), 3.23-3.21 (m, 2H), 1.76-1.73 (m, 2H). ¹³C-NMR (CD₃OD): δ 167.3, 161.4, 161.2, 161.1, 156.1, 156.0, 148.7, 147.5, 146.6, 143.3, 143.0, 138.5, 131.0, 127.8, 127.3, 126.7, 126.4, 124.8, 118.7, 115.8, 58.1, 55.9, 40.0, 38.2, 29.8. IR (cm⁻¹): 3105, 2359, 1674, 1539, 1469, 1435, 1320, 1200, 835, 798, 721. HRMS (ESI) Calcd for C₂₈H₃₂N₉O [(M + H)⁺]: *m/z* 510.2730. Found: *m/z* 510.2733.

2.5.4. Metal complexation (Fe^{II}·**4**)

The iron-inhibitor complex was prepared by adding a 10 mM solution of Fe^{II}(NH₄)₂(SO₄)₂ (3 mL) into a mixture of **4** (18 mg, 0.030 mmol) and H₂O (7 mL). The reaction mixture was stirred vigorously for 3 h until the inhibitor dissolved. The complex Fe^{II}·**4** was characterized in solution by UV-vis spectroscopy (λ_{max} 380 nm, ϵ = 1400 M⁻¹ cm⁻¹) which agrees well with data for the ferrous complex of N4Py (λ_{max} 390 nm, ϵ = 1500 M⁻¹ cm⁻¹) in aqueous solution. A 3 mM stock solution of Fe^{II}·**4** in H₂O was divided and frozen. Upon thawing, the quality of the solution was confirmed by UV-vis before each enzymatic assay.

2.5.5. Metal complexation (**9** and **10**) and ferryl generation

The iron-ligand complexes [Fe^{II}(OH₂)(N4Py)]²⁺ (**9**) and [Fe^{II}(Cl)(3CG-N4Py)]²⁺ (**10**) were prepared by adding 1 equiv of Fe^{II}(ClO₄)₂·*x*H₂O (100 mM stock solution in

H₂O) to H₂O solutions of **8** and **7**, respectively. Ferryls [Fe^{IV}(O)(N4Py)]²⁺ (**11**) and [Fe^{IV}(O)(3CG-N4Py)]³⁺ (**12**) were generated by adding 8 μ L of a 100 mM solution of peracetic acid in H₂O (2 equiv) to solutions of **9** and **10** (200 μ L, 2 mM).

2.5.6. CA-I activity assay

Human CA-I activity was measured by collecting absorbance measurements at 400 nm, using 4-nitrophenyl acetate as the substrate. The final volume used for the assay was 100 μ L (1 μ M CA-I and 1 mM substrate in Tris buffer (12.5 mM) containing 75 mM NaCl, pH = 8.0). Changes in absorbance were measured for 3 min at an interval of 6 sec. The stock solution of substrate was made in DMSO and added to initiate the assay. The final concentration of DMSO in the assay was kept at 5%.

2.5.7. CA-I inhibition assay

Inhibitors, used for inhibition of CA-I activity, were **4**, Fe^{II}·**4**, Zn^{II}·**4**, Fe^{II} and Zn^{II}. Enzyme was incubated with various concentrations of inhibitor for 5 min prior to initiating the assay by addition of substrate. The initial velocities, obtained from A₄₀₀ vs. time plot, were converted to % CA-I activity with respect to the control reaction containing no inhibitor. For each assay, % CA-I activity was plotted as a function of inhibitor concentration to obtain the dose-dependent curve, which was fit using a sigmoid equation to obtain the IC₅₀ value. Each IC₅₀ was computed using the average of three runs, with the error equal to the standard deviation.

2.5.8. Time-dependent inactivation of human CA-I activity

Enzyme (1 μ M) was incubated with inhibitor (1 μ M) and DTT (500 μ M) at 37 °C and a series of assays were performed at specified time intervals, with zero time equal to the start of incubation. For each activity measurement, the assay was initiated by adding substrate to an aliquot, taken out from the reaction mixture. Control reactions

with and without inhibitor and no DTT were performed simultaneously. The initial velocities were converted to % CA-I activities, with 100% equal to the enzyme activity from the control reaction with enzyme only at $t = 0$, and were plotted as a function of preincubation time.

2.5.9. Trypsin and chymotrypsin inactivation assay

The enzymatic assays were initiated by adding the substrate (*N*- α -benzoyl-DL-arginine-4-nitroanilide hydrochloride for trypsin and *N*-succinyl-Ala-Ala-Pro-Phe-pNA for chymotrypsin) to the solutions of enzyme containing varied concentrations of inhibitor (0-1000 μ M). The initial velocities, obtained from the A_{405} versus time plot, were converted to the percentage of enzyme activity (% enzyme activity) with respect to the control reaction containing no inhibitor. For each assay, % enzyme activity was computed using the average of three runs, with the error equal to the standard deviation, and plotted as a function of the inhibitor concentration. Data were fit using a sigmoidal equation to obtain the IC_{50} value.

2.5.10. Pulse experiments with H₂O₂

The enzyme (1 μ M) was incubated with $Fe^{II}(ClO_4)_2$, or **9** or **10** (20 μ M) (total volume 600 μ L), and H₂O₂ (5 \times 40 μ M) was added every 10 min. Enzyme activities were determined on aliquots removed from the solution as described above, 10 min after each addition of H₂O₂. Activities were adjusted for dilution prior to their conversion to % enzyme activity, with 100% activity equal to the activity of the blank reaction in the absence of inhibitor at $t = 0$. In control experiments, ROS scavengers D-mannitol, imidazole, and NaN₃ (see Figure 2.14) were added as aqueous solutions before the addition of H₂O₂.

2.5.11. Magnetic susceptibility measurements and NMR studies

The solution-phase magnetic moments of iron complexes **9** and **10** were determined by $^1\text{H-NMR}$ in a D_2O solvent following Evan's method using *tert*-butyl alcohol as the reference. A small capillary tube (closed at one end) was filled with a solution of D_2O and *tert*-butyl alcohol [50-75 μL , 7:1 (v/v)] and sealed. Solutions of **9** (4 mM, 0.016 mmol, 4 mL) and **10** (5 mM, 0.015 mmol, 3 mL) were made by mixing ligands **8** and **7** with 1 equiv of $\text{Fe}(\text{ClO}_4)_2$, respectively, in D_2O containing *tert*-butyl alcohol. The sealed capillary tubes were placed inside the NMR tubes, iron complex solutions (800 μL) were added, and $^1\text{H-NMR}$ spectra were recorded. For solution NMR studies, 10 mM solutions of ligands **8** and **7** were prepared in a D_2O solvent. Their iron complexes **9** and **10** were generated in situ by mixing 800 μL of ligand solutions **8** and **7**, with 10 μL of a 0.8 M $\text{Fe}(\text{ClO}_4)_2$ solution (203.8 mg, 0.8 mmol, 1 mL, 1 equiv) in D_2O , respectively. The samples were analyzed by $^1\text{H-NMR}$ spectroscopy after the addition of ligand, iron, and CH_3CN (21 μL , 50 equiv).

2.5.12. Liquid chromatography/Mass spectrometry (LCMS)

Analysis of protein samples. LCMS was performed on a Micromass QuattroLC triple quadrupole mass spectrometer with an electrospray/APCI source and Waters Alliance 2695 liquid chromatograph. Approximately 100 pmol of the sample was injected onto a Jupiter 5 μm C18 300 Å 50 × 2.0 mm column (Phenomenex) using an autosampler. Separation was achieved using a linear gradient of 20-30% (trypsin) and 20-40% (chymotrypsin) CH_3CN in water and a 0.1 % HCO_2H solution in water. A total of 80 μL of H_2O (blank) was injected after each sample to minimize any carryover from the previous sample. High-performance liquid chromatography (HPLC) was carried out at a flow rate of 0.6 mL min^{-1} with the column heated to 45 °C.

2.5.13. Carbonyl assay

The carbonyl contents of the oxidized enzyme samples were determined using the following literature method. Enzymes (20 μM) were treated with **9** or **10** (50 μM) and pulsed with varying amounts of H_2O_2 (100-500 μM , 100 μM per pulse). After pulsing, protein samples were precipitated with 20% (w/v) trichloroacetic acid, centrifuged (5 min, 25 °C, 6600 rpm), the supernatant was removed, and the precipitate was treated with 2,4-dinitrophenylhydrazine in 2 M HCl (10 mM, 500 μL). The samples were allowed to stand at room temperature for 1 h with vortexing every 10-15 min. Enzymes were precipitated with 20% trichloroacetic acid (500 μL) and centrifuged (5 min, 25 °C, 6600 rpm), the supernatant was discarded, and the pellet was washed three times with 1 mL of ethanol/ethyl acetate (1:1) to remove any free reagent. The sample was allowed to stand 10 min before centrifugation (5 min, 25 °C, 6600 rpm), and the supernatant was discarded each time. The precipitated enzyme was dissolved in 0.6 mL of a 6 M guanidine solution (pH = 2.3, 20 mM potassium phosphate), and the carbonyl contents were determined by UV-vis spectroscopy using the known molar extinction coefficient, $\epsilon_{360} = 22\,000\ \text{M}^{-1}\ \text{cm}^{-1}$.

2.5.14. Synthesis of **14**

A solution of Ac-Tyr-OH (**13**; 56 mg, 0.25 mmol) and $[\text{Fe}^{\text{II}}(\text{N4Py})(\text{CH}_3\text{CN})](\text{ClO}_4)_2$ (17 mg, 25 μmol) in a 10 mM acetate buffer (25 mL, pH = 6.0, 150 mM NaCl) was pulsed with H_2O_2 (50 $\mu\text{L} \times 5$, 10 mM total, 2 mM per pulse) every 10 min over the course of 1 h. The solution was frozen and lyophilized. The lyophilized powder was dissolved in water and filtered through Dowex 50WX4-100 ion-exchange resin to remove ligand and iron. The filtrate was frozen and lyophilized. The product **14** was

purified by HPLC (HPLC column Zorbax XDB-C18, 21.2 × 150 mm, 5 μm equipped with a guard column Zorbax XDB-C18, 21.2 mm, 5 μm, 0.1% TFA/MeOH 87:13, flow rate = 20 mL min⁻¹; T_R = 6.24 min); ¹H-NMR and MS data of isolated **14** matched the literature data for the known compound.²⁵³

CHAPTER 3

Inhibition of 20S Proteasome by Non-Heme Iron Complexes

Copyright Permission: Portions of the text in this chapter were reprinted or adapted with permission from: (a) Prakash, J.; Schmitt, S. M.; Dou Q. P. and Kodanko J. J. *Metallomics*, **2012**, *4*, 174-178. (b) Zou, J.; Schmitt, S. M.; Zhang Z.; Prakash, J.; Fan, Y.; Bi, C.; Kodanko, J. J.; Dou, Q. P. *J. Cell. Biochem.* **2012**, DOI: 10.1002/jcb.24132. All rights to the work are retained by the authors and any reuse requires permission of the authors.

3.1. Introduction

The ubiquitin-proteasome system plays a central role in the regulatory degradation of unfolded or unwanted proteins inside the cell, which would otherwise result in tumor growth and cancer.^{130,137} This makes the ubiquitin-proteasome system an important target in cancer chemotherapy. Though in the beginning, targeting ubiquitin-proteasome system for therapeutic was seen with great apprehension because of its essential role in normal cellular homeostasis, later work illustrated that proteasome inhibitors could induce apoptosis in cancer cells while at the same time show attenuated toxicity towards normal cells.²⁵⁴⁻²⁵⁶ Another feature that makes proteasome inhibitors even more promising as cancer chemotherapy agents is that cancer cells are more sensitive, as compared to normal cells, to apoptosis-inducing stimuli including proteasome inhibitors.²⁵⁷⁻²⁵⁹ For example, a boron-based peptidomimetic proteasome inhibitor bortezomib has recently been approved for the treatment of multiple myeloma and mantle cell lymphoma.^{138,139} A series of transition metal complexes based on nickel, copper, zinc, gold and gallium are in preclinical development and show promising

anticancer activities in live cells and animals.¹⁴⁰⁻¹⁴⁴ Most of these medicinal agents inhibit the proteasome by binding directly to the enzyme's catalytic subunits (20S core). However, another exciting strategy that has recently been utilized effectively towards enzyme inhibition is the use of metal-based reagents, either generating ROS or metal-based oxidants that diminish enzyme activity through catalytic oxidation.^{96,198,199,260} For example, $[\text{Ru}(\text{bpy})_2]^{2+}$ -peptoid conjugates have shown potent and selective inactivation of vascular endothelial growth factor (VEGF)-induced autophosphorylation of VEGF receptor 2 (VGRF2), and 26S proteasome upon photo-irradiation by means of generating singlet oxygen $^1\text{O}_2$ as reactive oxidizing species.⁹⁶ This strategy renders several advantages over traditional enzyme inhibition as mentioned in the previous section. It uses biologically relevant oxidants like H_2O_2 and O_2 , can be performed selectively in live cells, and is often irreversible in nature, and can reduce the concentration of inhibitor needed to provide the desired effect.

In this chapter, we describe a new iron-based approach towards the catalytic targeting of the proteasome that occurs spontaneously in the presence of a non-heme iron complex and air. The non-heme ligands used in our studies are pentadentate nitrogen-containing ligands N4Py and Bn-TPEN (Figure 3.1).^{208,218,222,261} These ligands were selected because they find applications in biology as they bind strongly to iron with dissociation constants in the pM-fM range. They can mobilize Fe^{II} from ferritin, the major intracellular storage site for iron suggesting that these ligands can access iron from the "labile iron pool" in cells.²⁶² The high valent iron (IV)-oxo complexes of these ligands have been shown to selectively oxidize small organic molecules.^{261,263-265} Recent studies from our laboratory have already established that iron complexes based on pentadentate ligands have applications in the area of amino acid, peptide and protein

oxidation.^{107,108,226,260} Because previous work with the proteasome demonstrated that the enzyme could be inactivated by oxidants,^{146,266,267} and by knowing the importance of proteasome in cancer therapy, we decided to examine the ability of these iron complexes to inactivate the proteasome. This chemistry was established against the purified 20S proteasome instead of 26S proteasome *in vitro*. 20S proteasome was selected against 26S proteasome because of the following reasons: (a) 20S proteasomal activity is similar to that of 26S proteasome since 19S cap increases the specificity but not potency; (b) purified 20S proteasome is cheaper and more stable than purified 26S proteasome.

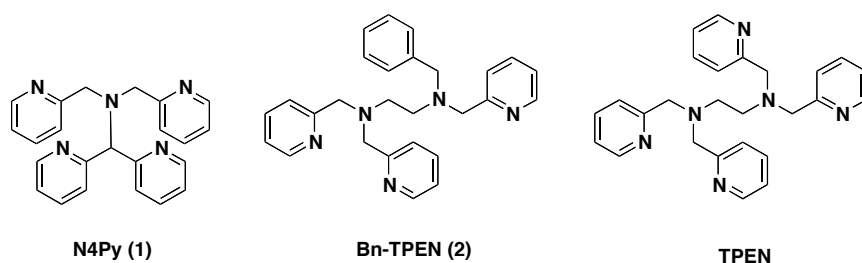


Figure 3.1. Polydentate nitrogen-containing ligands

3.2. Results

3.2.1. IC₅₀ determination

Studies commenced with evaluating the ability of ligands **1** and **2** and their ferrous complexes $[\text{Fe}^{\text{II}}(\text{OH}_2)(\text{N4Py})]^{2+}$ (**3**) and $[\text{Fe}^{\text{II}}(\text{OH}_2)(\text{Bn-TPEN})]^{2+}$ (**4**), to inhibit the chymotrypsin-like activity of the purified 20S proteasome. The ferrous complexes **3** and **4** were generated *in situ* by mixing equal equivalents of ligand **1** and **2** with iron(II) perchlorate salt, respectively. The purified 20S proteasome (0.5 nM, final concentration) was treated with varied concentrations (0–1000 mM) of **1–4**, along with

$\text{Fe}^{\text{II}}(\text{ClO}_4)_2 \cdot x\text{H}_2\text{O}$ as a control, in 100 mM MOPS buffer (pH = 7.4). Proteasome activities were measured using fluorescence spectroscopy and corresponding IC_{50} values were calculated (Table 3.1).

Table 3.1. IC_{50} values (μM) for inhibition of chymotrypsin-like (CT), trypsin-like (T) and peptidylglutamyl peptide hydrolyzing-like (PGPH) activity of 20S proteasome by ligands **1** and **2** and their respective ferrous complexes (**3** and **4**) along with iron metal ion control

Entry	Compound	CT ^a	T ^a	PGPH ^a
1	N4Py (1)	>1000	>1000	>1000
2	$[\text{Fe}^{\text{II}}(\text{OH}_2)(\text{N4Py})]^{2+}$ (3)	9.2	>1000	>1000
3	Bn-TPEN (2)	96	>1000	>1000
4	$[\text{Fe}^{\text{II}}(\text{OH}_2)(\text{Bn-TPEN})]^{2+}$ (4)	4.0	>1000	>1000
5	$\text{Fe}^{\text{II}}(\text{ClO}_4)_2$	>1000	nd ^b	>1000

^a The % proteasome activity at different concentrations was determined as the average from three independent experiments, with 100% activity equal to the fluorescence of the proteasome in the absence of inhibitor. Proteasome concentration was 0.5 nM; fluorogenic peptide substrates, Suc-LLVY-AMC (for proteasomal chymotrypsin-like activity), Bz-VGR-AMC (for proteasomal trypsin-like activity) and Z-LLE-AMC (for proteasomal peptidylglutamyl peptide hydrolyzing-like activity), concentrations were 20 μM . The reactions were conducted at pH = 7.4 in 100 mM MOPS buffer for 30 min at 37 °C. ^b nd = not determined.

The results indicated that ligand **1** was ineffective in inhibiting the chymotrypsin-like activity of the proteasome ($\text{IC}_{50} > 1000 \mu\text{M}$) but its ferrous complex **3** was a more potent inhibitor with an IC_{50} value of 9.2 μM (Table 3.1, entry 2). Similar results were observed for ligand **2** where its ferrous complex **4** was more potent than ligand **2**.

Ligand **2**, unlike ligand **1**, also inhibited the proteasome, albeit at a 25-fold higher concentration than its ferrous complex **4** (Table 3.1, entries 3 and 4). Despite the fact that $\text{Fe}^{\text{II}}(\text{ClO}_4)_2$ had no effect on proteasome activity (Table 3.1, entry 5), the ferrous complexes **3** and **4** showed more potent inhibition than the ligands alone. These results confirm that iron and the ligand together play a key role in proteasome inhibition. Similarly, IC_{50} values for inhibition of the trypsin- and PGPH-like activities of the proteasome were determined for compound **1–4**. To our surprise, the trypsin- and PGPH-like activities of the proteasome were not affected by these ferrous complexes, indicating a high level of selectivity by these ferrous complexes toward inhibition of chymotrypsin-like activity of the proteasome, which is consistent with oxidative inactivation.²⁶⁸

3.2.2. Mechanistic Studies

3.2.2.1. Time-dependent inactivation

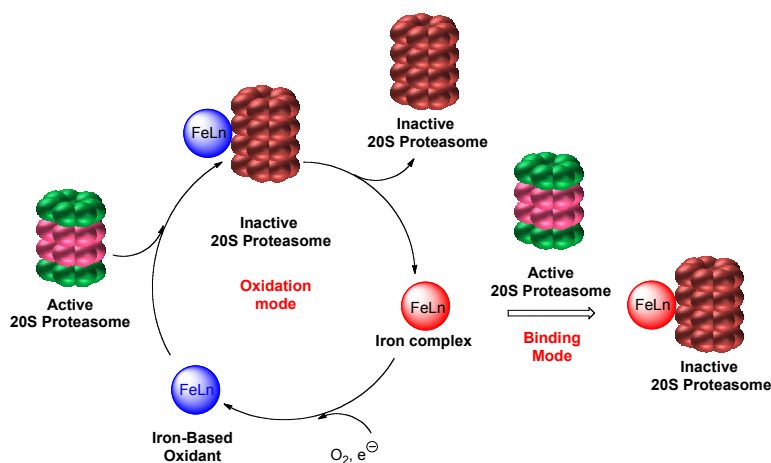


Figure 3.2. Binding and oxidation mode of action of iron complexes for 20S proteasome inactivation

Based on literature data, two possible pathways were considered for proteasome inhibition, either direct binding of the iron complexes to the $\beta 5$ subunits (responsible for the chymotrypsin activity) of the 20S proteasome,^{140,142} or alternatively oxidation of the enzyme (Figure 3.2).^{96,146,266,269} In order to gain insight into the mode of action, the 20S proteasome was incubated with ferrous complexes **3** and **4** (10 μ M) at room temperature under an aerobic atmosphere and the activities were determined as a function of incubation time. Proteasome activity did not change over time with **3**, suggesting that direct binding of the iron complex to the enzyme contributed to the observed inhibition (Figure 3.3a). In contrast, time-dependent inactivation was observed in the presence of **4**, where 20S proteasome activity was diminished from $\sim 70\%$ to $\sim 10\%$ over the course of 165 min at room temperature (Figure 3.3b). Time-dependent loss of proteasome activity was not observed with ligand **2** or with $\text{Fe}^{\text{II}}(\text{ClO}_4)_2$ alone, both in the presence and absence of the reductant dithiothreitol (DTT). However, proteasome activity was lowered, albeit slightly, with **4** in the presence of DTT, consistent with the reductive activation of O_2 playing a role in enzyme inactivation (Figure 3.3d).¹⁹⁸ This mode of action was further corroborated by the fact that time-dependent inhibition was not observed with $[\text{Fe}^{\text{II}}(\text{TPEN})]^{2+}$ (Figure 3.3c), in which all six coordination sites around the iron center are occupied (Figure 3.4). Blocking all six sites would inhibit access of O_2 to the iron center with respect to **4** which contains a labile H_2O , presumably allowing **4** to reach a coordinatively unsaturated state easier than $[\text{Fe}^{\text{II}}(\text{TPEN})]^{2+}$. It is important to note that the timescale for the decay of proteasome activity observed with **4** is too long to result from simple binding of the iron complex to the enzyme. Rates for association of small molecules with proteins are extremely fast ($k = 10^6\text{--}10^8 \text{ M}^{-1} \text{ s}^{-1}$),²⁷⁰ much faster than the time scale of the experiments (165 min).

Taken together, these results are consistent with **4** oxidizing the 20S proteasome over time, leading to its inactivation.

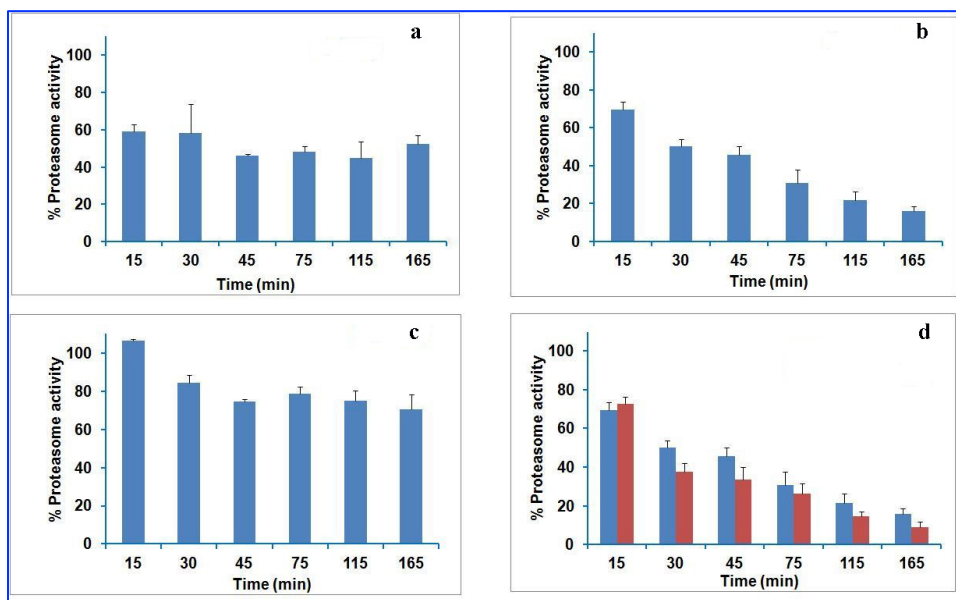


Figure 3.3. Time-dependent inactivation of the purified 20S proteasome. The reaction was performed by incubating the proteasome (0.5 nM) with 10 μ M of ferrous complexes **3** (a), **4** (b and d (blue) without DTT, d (red) with DTT, 250 μ M) and $[\text{Fe}^{\text{II}}(\text{TPEN})]^{2+}$ (c) in 100 mM MOPS buffer at pH = 7.4. The fluorescence intensity was converted to % CT-like activity, with 100% activity equal to fluorescence of the blank reaction containing proteasome, in the absence of the inhibitor at t = 0.

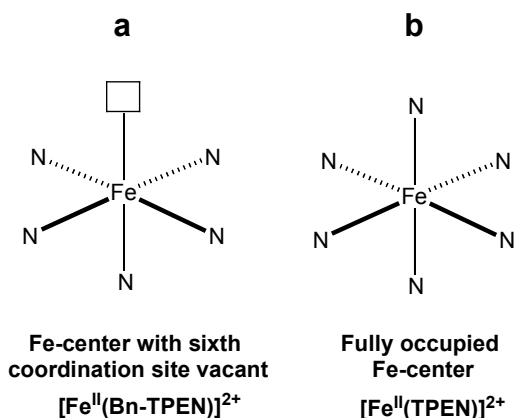


Figure 3.4. Model illustrating the coordination sphere around iron centers of the ferrous complexes derived from (a) Bn-TPEN and (b) TPEN. The sixth coordination site in model 'a' is vacant for redox chemistry.

3.2.2.2. ROS scavengers

In order to gain further insight into the nature of the oxidant, control experiments were performed in the presence of reactive oxygen species (ROS) scavengers. When the inactivation of the 20S proteasome with **4** was performed in the presence of NaN₃ (10 mM), a potent singlet oxygen (¹O₂) scavenger, 20S proteasome inhibition was still observed, precluding a major role for ¹O₂ (Figure 3.5).^{194,260} Similar results were obtained in the presence of D-mannitol (20 mM), a potent scavenger of the hydroxyl radical and superoxide,^{194,260} confirming that another oxidant apart from ROS is responsible for the time-dependent proteasome inhibition observed with **4**.

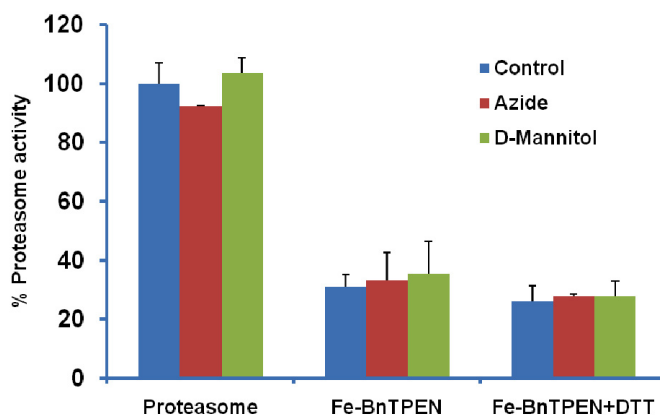


Figure 3.5. Inactivation of the purified 20S proteasome by ferrous complex **4** in the presence of ROS scavengers (azide and D-mannitol). The reactions were performed by incubating proteasome with **4** (10 μ M) in the presence/absence of DTT (250 μ M) for 80 min at rt in 100 mM MOPS buffer at pH = 7.4. The fluorescence intensity was converted to % CT-like proteasome activity, with 100% activity equal to fluorescence of blank reaction containing proteasome in the absence of inhibitor and additive. Data points are averages from three independent experiments, errors equal to the standard deviation of the data set.

These results suggest that a metal-based oxidant derived from **4** may be responsible for the loss of proteasome activity over time. Although the exact nature of

this oxidant has not been confirmed, activation of O_2 by non-heme iron complexes is known to generate Fe^{III} -superoxo, -hydroperoxo and Fe^{IV} -oxo species.^{59,60,271,272} Our own work proved that iron-based oxidants of this class inactivate the serine proteases trypsin and chymotrypsin efficiently.²⁶⁰ Furthermore, we have observed that **3** decomposes much slower than **4** under aerobic conditions, which agrees well with **4** activating O_2 at a faster rate than **3**, and with differences in time-dependent inhibition between **3** and **4** (Figure 3.3a and 3.3b). Therefore, faster oxidation of **4** may lead to a more rapid loss of the purified 20S proteasome activity over time under aerobic conditions.

3.2.2.3. *In cellulo* studies

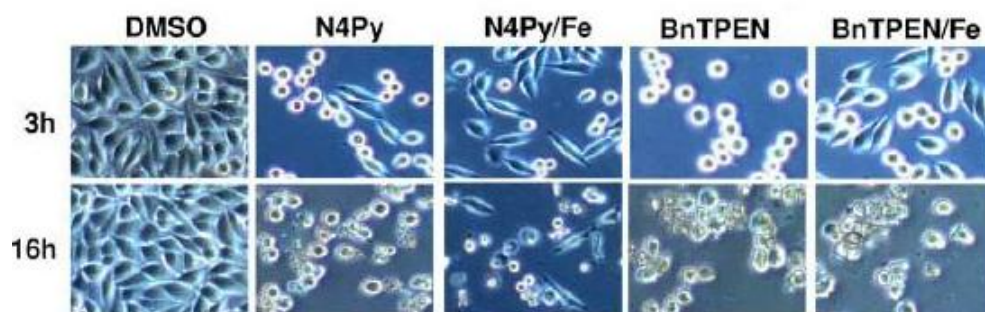


Figure 3.6. Effect of compounds **1–4** on apoptosis induction in PC-3 cells. Circular and elongated cells represent dead and live cells respectively.

Studies were conducted to gain insight into modes of action for compounds **1–4** in cells. PC-3 cells were incubated with these compounds and cell proliferation data were collected. These data, reported in another manuscript,²⁷³ indicate that compounds **1–4** elicit apoptotic effects and give rise to potent cell death (Figure 3.6). Proteasome inhibition, however, was not observed, presumably because cell death occurs at lower concentrations than proteasome inhibition. However, even though proteasome inhibition

was not observed in these live cell assays, it is important to note that the ligands and complexes **1–4** used in this study do not contain a proteasome-binding motif. Directing these compounds to the proteasome by attachment of a binding motif could lead to more potent proteasome inhibition, giving the possibility of inhibiting the proteasome before cell death occurs.

3.3. Discussion

Proteasome inhibitors can cause apoptosis in cancer cells and are promising candidates for the development of novel anti-cancer drugs. Though many potent proteasome inhibitors are either in preclinical or clinical trials for the treatment of one or other forms of cancer, most of them inhibit proteasome by binding to the central catalytic 20S subunit. For example, Bortezomib is a FDA approved drug. Studies reported herein are significant because these are indicative of oxidative inactivation of proteasomes that can be achieved spontaneously in the presence of non-heme iron complex and air. Though the *in vitro* studies with purified 20S proteasome led to its oxidative inactivation, *in cellulo* data pointed toward apoptotic induction leading to cell death prior to proteasome inhibition.

The ferrous complexes of ligand **1** and **2** show more potent inhibition ($IC_{50} < 10 \mu\text{M}$) towards chymotrypsin-like activity of proteasome than the ligands or the iron salt alone. These results are indicative of key role played by iron and the ligand together towards proteasome inhibition. Moreover, a high level of selectivity toward inhibition of chymotrypsin-like activity of proteasome was seen with these ferrous complexes as compared to trypsin- and PGPH-like activities of the proteasome. Mechanistic studies revealed two different modes of action of ferrous complexes towards proteasome

inhibition. Loss of 20S proteasome activity was not observed with **3** over time, suggesting inhibition through direct binding of the iron complex to the enzyme. In contrast, a time-dependent decay of proteasome activity was seen with ferrous complex **4** that was accelerated in presence of a reducing agent like DTT. This suggests reductive activation of O₂ and oxidation of the 20S proteasome as a mode of action. This mode of action was further supported by the fact that proteasome activity was not affected by [Fe^{II}(TPEN)]²⁺ over the course of reaction. [Fe^{II}(TPEN)]²⁺ is a coordinately saturated system with central Fe^{II} atom bound strongly by six N-atoms from the TPEN ligand, inhibiting access of O₂ to the iron center as compared to **4**, which contains a labile H₂O ligand at the sixth position.

The role of ROS as an active oxidant was precluded by the fact that reactive oxygen species scavengers (NaN₃ and D-mannitol) failed to block the inhibition of 20S proteasome by **4**, and hence, alternatively supported a unique oxidant being responsible for the time-dependent inhibition observed. Non-heme iron complexes are known to react with O₂ resulting in generation of high valent metal-based oxidants like Fe(IV)-oxo that selectively oxidize small organic molecules. Recent studies have provided strong evidence for the existence of perferryl species, commonly known as Fe(V)-oxo, and can be generated from similar ligand sets.⁶¹ However, the exact nature of the oxidizing species in this study is yet to be investigated.

To gain insight into the mode of action of compound **1-4** *in vivo*, cell proliferation and cell morphological changes were studied against PC-3 cells. The results have been discussed in detail in another manuscript. In brief, the compounds **1-4** were found to induce apoptosis that led to potent cell death. The role of proteasome inhibition in cell

death was precluded mainly because of the fact that cell death was seen at lower concentrations than the proteasome inhibition. However, by attaching proteasome-affinity groups to compound **1-4** may result into selective and potent proteasome inhibition prior to cell death.

3.4. Conclusions and future directions

In conclusion, non-heme ligands **1** and **2** and their iron complexes **3** and **4** were investigated for their ability to inhibit the purified 20S proteasome. Ferrous complexes **3** and **4** showed more potency in inhibiting the proteasome than the ligands and iron salts alone. Control experiments confirmed a key role for iron and ligands in enzyme inhibition. The time-dependent inactivation studies suggested that the ferrous complexes of N4Py and Bn-TPEN have different modes of action, either binding to the target enzyme, or alternatively enzyme oxidation. Investigations precluded the role of ROS and suggested that an iron-based oxidant was responsible for loss of proteasome activity observed. Studies are now underway to understand the biological activities of these complexes further and to extend this method of enzyme targeting towards achieving anticancer activities.

3.5. Experimental section

3.5.1. Materials and methods

3.5.1.1. Materials

N4Py (**1**),²¹⁸ Bn-TPEN (**2**)²⁷⁴ and TPEN²⁷⁵ were synthesized according to literature methods. Iron(II) perchlorate hydrate and dithiothreitol (DTT) were purchased from Sigma-Aldrich and Acros chemicals, respectively. Purified human 20S proteasome

and fluorogenic substrates, Suc-LLVY-AMC and Bz-VGR-AMC (for proteasomal chymotrypsin- and trypsin-like activities, respectively), were from Boston Biochem (Cambridge, MA) whereas the fluorogenic substrate Z-LLE-AMC (for proteasomal peptidylglutamyl peptide hydrolyzing-like activity) was from Calbiochem. Human 20S proteasome was aliquoted in buffer (1 M HEPES, 3 M NaCl, final concentration: 25 nM). The iron complexes $[\text{Fe}^{\text{II}}(\text{OH}_2)(\text{N4Py})]^{2+}$ (**3**) and $[\text{Fe}^{\text{II}}(\text{OH}_2)(\text{Bn-TPEN})]^{2+}$ (**4**) were generated *in situ* by treating ligands **1** and **2** in 100mM MOPS buffer (pH = 7.4) containing % DMSO with 1.0 equiv. of $\text{Fe}^{\text{II}}(\text{ClO}_4)_2 \cdot x\text{H}_2\text{O}$.

3.5.1.2. Purified 20S proteasomal inhibition assay

Purified human 20S proteasome (0.5 nM, final concentration) was incubated with 20 μM of a fluorogenic substrate, Suc-LLVY-AMC or Bz-VGR-AMC or Z-LLE-AMC (for proteasomal chymotrypsin-, trypsin- and peptidylglutamyl peptide hydrolyzing-like activities, respectively), in 100 μL assay buffer (100 mM MOPS buffer, pH = 7.4) for 30 min at 37 °C in the presence of inhibitor molecules at different concentrations (0–1000 μM). After incubation, proteasomal activities (production of hydrolyzed AMC) were measured with a Wallac Victor multilabel counter (PerkinElmer, Waltham, MA) with an excitation filter of 365 nm and emission filter of 460 nm. Background fluorescence was subtracted from the blank reaction. Activities were plotted against log [inhibitor] and fit to a sigmoidal curve to calculate IC_{50} values.

3.5.1.3. Time-dependent 20S proteasomal inactivation assay

Purified human 20S proteasome (0.5 nM, final concentration) was incubated at room temperature with 10 μM inhibitor in the presence or absence of DTT (250 μM) for

different time periods (0–165 min) in assay buffer (100 mM MOPS buffer, pH = 7.4). A fluorogenic substrate, Suc-LLVY-AMC (20 μ M), was added and the mixture was further incubated for 15 min at 37 °C. Proteasomal activities (production of hydrolyzed AMC) were measured with a Wallac Victor multilabel counter with an excitation filter of 365 nm and emission filter of 460 nm. In control experiments, reactive oxygen species scavengers D-mannitol (20 mM) and NaN_3 (10 mM) were added as aqueous solutions prior to treatment with the iron complexes.

CHAPTER 4

Synthesis, Characterization and Glutathionylation of Cobalamin Model Complexes $[\text{Co}^{\text{III}}(\text{N4PyCO}_2\text{Me})\text{Cl}]\text{Cl}_2$ and $[\text{Co}^{\text{III}}(\text{Bn-CDPy}_3)\text{Cl}]\text{Cl}_2$

Copyright Permission: Portions of the text in this chapter were reprinted or adapted with permission from: Prakash, J.; Kodanko, J. J. *Inorg. Chem.* **2012**, *51*, 2689-2698. All rights to the work are retained by the authors and any reuse requires permission of the authors

4.1. Introduction

Glutathionylcobalamin (GSCbl) forms rapidly upon reaction of glutathione (GSH) with aquacobalamin (H_2OCbl^+). Because of the fact that GSH is present in cells up to a concentration of 10 mM,^{162,163} GSCbl is thought to be an important form of cobalamin present in cells. GSCbl finds many applications in biology. For example, it has been shown that it can reverse the biological effects caused by NO ,²⁷⁶ and can induce potent antioxidant properties *in vitro*.²⁷⁷ GSCbl has also been proposed as an important intermediate in the biosynthesis of two of the active cobalamin coenzymes MeCbl and AdoCbl which are involved in transfer of a methyl group from methyltetrahydrofolate to homocysteine by methionine synthase to generate methionine, and isomerization of methylmalonyl-CoA to succinyl-CoA, catalyzed by methylmalonyl-CoA mutase, respectively.^{155-157,278,279} The former reaction is significant because it helps regenerate folate, which is essential for DNA synthesis, and at the same time reduces the concentration of homocysteine that is associated with various diseased states. The later reaction helps in metabolic pathways associated with consumption of branched and odd chain fatty acids. Moreover, GSCbl has been suggested to be more effective than other cobalamines in treatment of conditions associated with hyperhomocysteinemia and

oxidative stress, including dementia, arthritis, and cancer.^{149,164,165}

This inspired various researchers to study the formation of GSCbl from GSH and aquacobalamin.^{164,167,169,280} A large formation constant ($K_f = 5 \times 10^9 \text{ M}^{-1}$) and bimolecular rate constant as high as $163 \pm 8 \text{ M}^{-1} \text{ s}^{-1}$ have been reported recently, concluding that GSCbl formation from H_2OCbl^+ is both rapid and highly favorable.¹⁷⁴ The nature of this reaction suggests that any free intracellular H_2OCbl^+ (H_2OCbl^+ not attached to protein) is prone to conversion to GSCbl, as GSH is found up to 10 mM in concentration in most biological tissues. However, the extent of this facile conversion may be limited in cells by the fact that free Cbl is estimated to be $< 5 \%$.²⁸¹

Though a large number of cobalamin models complexes have been synthesized in the past, a detailed kinetic and thermodynamic study on glutathionylation has never been performed with these complexes. In this chapter, we report the interesting observation that glutathionylation is not unique to Cbl, but infact occurs readily with a series of other Co(III) complexes that mimic the structure of this important biological cofactor. In this study, the synthesis and characterization of a new Co(III) complex is described, which is derived from the polypyridyl pentadentate N5 ligand N4PyCO₂Me (**1**) (Figure 4.1). The complex $[\text{Co}^{\text{III}}(\text{N4PyCO}_2\text{Me})\text{Cl}]\text{Cl}_2$ (**3**), and related congener $[\text{Co}^{\text{III}}(\text{Bn-CDPy3})\text{Cl}]\text{Cl}_2$ (**4**), which contain a N5 coordination environments like that of Cbl, undergo biomimetic reactions with GSH to generate the species $[\text{Co}^{\text{III}}(\text{N4PyCO}_2\text{Me})(\text{SG})]^{2+}$ (**5**) and $[\text{Co}^{\text{III}}(\text{Bn-CDPy3})(\text{SG})]^{2+}$ (**6**), respectively. Species **5** and **6** were generated *in situ* and characterized in solution. Data for **5** and **6** are consistent with the cysteine thiolate in GSH binding to the Co(III) centers of these complexes. The kinetics and thermodynamic studies for glutathionylation of **3** and **4** are

reported, and relevance of these data to the analogous reaction with H_2OCbl^+ is discussed. To the best of our knowledge, this is the first example of synthetic Co(III) coordination complexes based on polypyridine ligands mimicking the behavior of Cbl and undergoing glutathionylation with GSH.

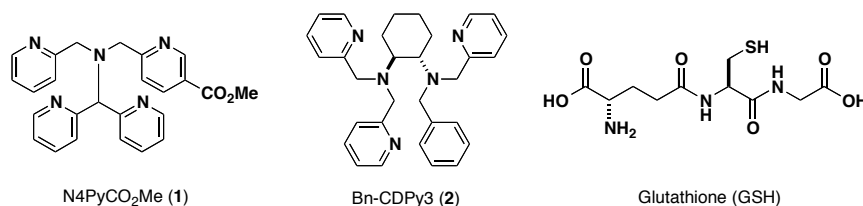
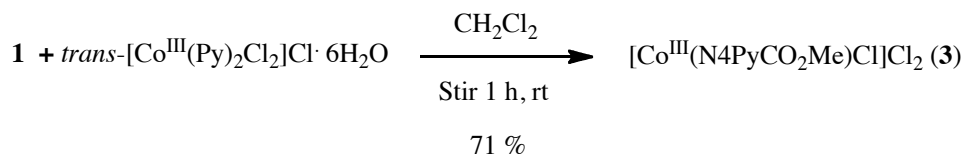


Figure 4.1. Structures of polypyridyl N5 pentadentate ligands **1** and **2**, and glutathione

4.2. Results

4.2.1. Synthesis of $[\text{Co}^{\text{III}}(\text{N4PyCO}_2\text{Me})\text{Cl}]\text{Cl}_2$ (**3**)

The Co(III) complex, $[\text{Co}^{\text{III}}(\text{N4PyCO}_2\text{Me})\text{Cl}]\text{Cl}_2$ (**3**), where N4PyCO₂Me (**1**) is methyl-6-(((di(pyridin-2-yl)methyl)(pyridin-2-ylmethyl)amino)methyl)nicotinate, was synthesized using the Co(III) starting material *trans*- $[\text{Co}^{\text{III}}(\text{Py})_4\text{Cl}_2]\text{Cl}\cdot 6\text{H}_2\text{O}$ ^{282,283} (Scheme 1). Ligand **1** was stirred with 1 equiv of *trans*- $[\text{Co}^{\text{III}}(\text{Py})_4\text{Cl}_2]\text{Cl}\cdot 6\text{H}_2\text{O}$ in CH_2Cl_2 for 60 min at room temperature resulting in the formation of **3** as a pink precipitate. This pink solid was further recrystallized by vapor diffusion of Et_2O into EtOH , followed by Et_2O into MeOH , giving pink crystals of **3** suitable for X-ray crystallographic analysis.



Scheme 4.1. Synthesis of $[\text{Co}^{\text{III}}(\text{N4PyCO}_2\text{Me})\text{Cl}]\text{Cl}_2$ (**3**)

4.2.2. UV-vis spectroscopic data

Typical of other low spin Co(III) complexes, the compound **3** shows two major absorption bands, λ_{max} , at 370 nm and 520 nm with molar extinction coefficient, ϵ , $340 \text{ M}^{-1} \text{ cm}^{-1}$ and $210 \text{ M}^{-1} \text{ cm}^{-1}$ in MeOH, respectively (Figure 4.2). These bands are assigned to transitions from the $^1A_{1g}$ ground state to the upper $^1T_{1g}$ and $^1T_{2g}$ states in the parent octahedral species, based on analogy with related Co(III) complexes.^{284,285}

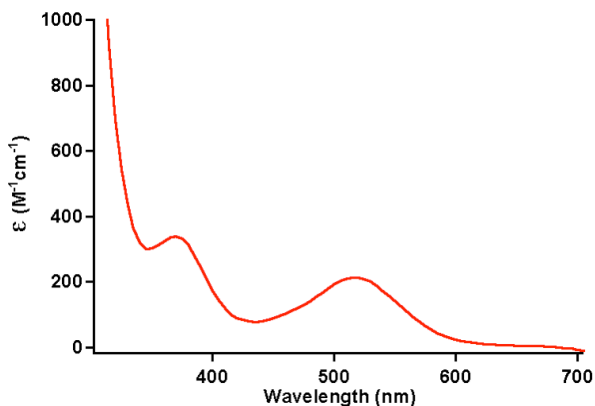


Figure 4.2. UV-vis spectrum of **3** in MeOH (1 mM) at $298 \pm 2 \text{ K}$

4.2.3. $^1\text{H-NMR}$ and $^{13}\text{C-NMR}$ spectroscopic data

The $^1\text{H-NMR}$ spectrum of **3** in CD_3OD revealed that resonances were sharp, well resolved, and lie between 3.9 and 9.9 ppm, consistent with a diamagnetic low spin Co(III) complex. Likewise, resonances observed in $^{13}\text{C-NMR}$ spectrum of **3** lie between 54–170 ppm. The most important features of these resonances, both in $^1\text{H-NMR}$ and $^{13}\text{C-NMR}$ spectra (Figure 4.3), are that they are shifted downfield in **3** when compared with the parent ligand **1**, consistent with the pyridine N-atoms remaining bound to the metal center in solution. Resonances assigned to the H-atoms located at the 2-position of the four pyridine rings shift by approximately 1 ppm when compared with the spectrum of **1**, consistent with the hypothesis that all four pyridine rings remain bound to the Co(III) center. Particularly striking is the 1.71 ppm downfield shift of the methine C-H

resonance, from 5.36 ppm in the parent ligand **1** to 7.07 ppm in the complex **3**. In addition, the four-methylene protons of the ligand become diastereotopic upon coordination to the metal center and each proton shows a unique resonance in the complex **3** (5.13–5.43 ppm). Typical coupling values of 16-19 Hz for geminal protons are observed, consistent with the chiral properties of **3**, which unlike symmetric complexes of N4Py, does not possess a mirror plane due to the ester substituent.

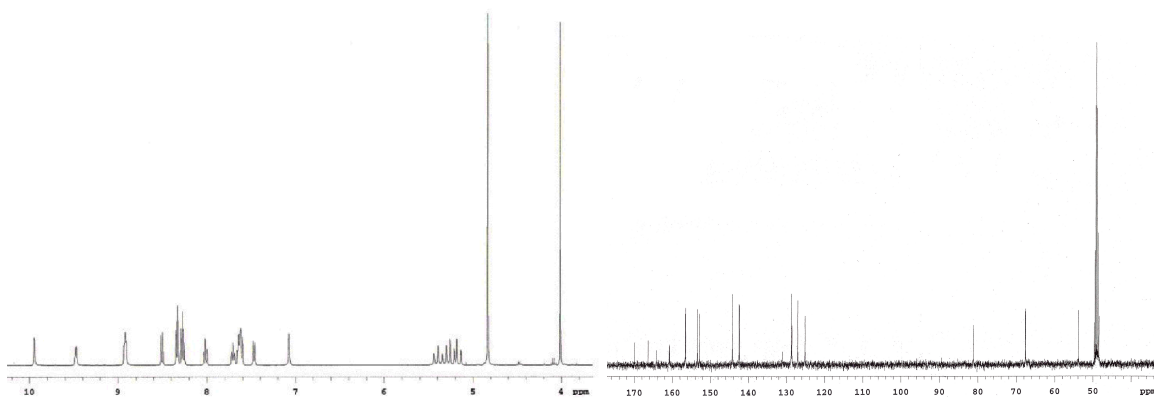


Figure 4.3. ^1H -NMR (left) and ^{13}C -NMR (right) spectrum of **3** in CD_3OD

4.2.4. High-resolution mass spectrometric data

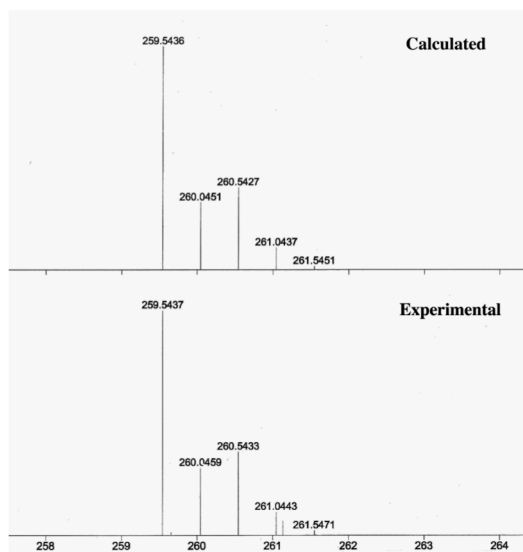


Figure 4.4. Calculated (top) and observed (bottom) high resolution mass spectra (ESMS) for the dication $[\text{Co}^{\text{III}}(\text{N4PyCO}_2\text{Me})\text{Cl}]^{2+}$ of **3**

The high-resolution electrospray ionization mass spectrum (ESI-MS) for **3** in H₂O solution reveals a prominent ion cluster with a dominant peak at m/z 259.5437. This cluster displayed an isotopic pattern that fits with molecular formula [Co^{III}(N4PyCO₂Me)Cl]²⁺ (Figure 4.4). It is noteworthy that the axially coordinated Cl⁻ ligand remains attached in solution.

4.2.5. X-ray crystallographic data

Crystallographic data for **3** are given in Table 4.1. Table 4.2 and Table 4.3 list selected bond lengths and bond angles, respectively. Complex **3** crystallized in the space group $P \bar{1}$, with $Z = 2$. Figure 4.5 shows an ORTEP diagram of the dication [Co^{III}(N4PyCO₂Me)Cl]²⁺. The Co(III) center of the dication [Co^{III}(N4PyCO₂Me)Cl]²⁺ has a N5Cl donor atom set. Bond lengths are consistent with a low-spin Co(III) ion. The octahedral geometry is slightly distorted, due to acute bite angles typical of 5-membered rings. The angles between Cl(1) and N(4-5) are approximately 3° smaller than angles involving N(2-3), resulting from the restriction of the common atom C(15). Even though the environments are dissimilar, bond lengths between Co(1) and all the five nitrogen donors of N4PyCO₂Me are nearly identical, varying from 1.930(2) to 1.938(2) Å, indicating that the ester moiety on the pyridine ring of the ligand does not affect the bond length between Co(1) and N(2) to a great extent. These Co-N lengths are decidedly short.²⁸⁶ Furthermore, the Co-Cl bond length (2.222 Å) is at the very shortest end of the recorded ranges for similar complexes, which may indicate a strong Co-Cl bond.²⁸⁷⁻²⁸⁹ The Co ion lies 0.171(1) Å out of the N4 equatorial plane towards the Cl atom (*cf.* Ru displacement of 0.263 Å in RuN4PyCl).²⁹⁰

Table 4.1. Crystal data and structure refinement for **3·MeOH·EtOH**

Empirical Formula	$C_{28}H_{33}Cl_3CoN_5O_4$
Formula weight	668.87
Crystal system	Triclinic
Space group	$P\bar{1}$
a (Å)	9.6350(3)
b (Å)	11.5595(4)
c (Å)	15.6403(5)
α (°)	97.695(2)
β (°)	106.955(1)
γ (°)	109.816(2)
V (Å ³)	1514.23(9)
Z	2
D _{calc} (mg/m ³)	1.467
Absorption coefficient, μ (mm ⁻¹)	0.874
F (000)	692
Crystal size (mm ³)	0.29 x 0.26 x 0.18
θ -range for data collection (°)	1.94 to 28.48
Limiting indices	$-12 \leq h \leq 12, -15 \leq k \leq 15$ $0 \leq l \leq 20$
Unique Reflections	36734 / 7571 [R (int) = 0.0342]
Goodness-of-fit on F_o^2	1.033
Final R indices [$I > 2\sigma(I)$]	R1 = 0.0450, wR2 = 0.1227
R indices (all data)	R1 = 0.0530, wR2 = 0.1269
Highest peak and deepest hole (e·Å ⁻³)	1.642 and -0.388

Table 4.2. Selected bond lengths (Å) of **3**.

Co(1)-N(3)	1.930(2)
Co(1)-N(1)	1.933(2)
Co(1)-N(5)	1.933(2)
Co(1)-N(4)	1.933(2)
Co(1)-N(2)	1.938(2)
Co(1)-Cl(1)	2.222(6)

Table 4.3. Selected bond angles (°) of **3**.

N(3)-Co(1)-N(1)	86.40(8)	N(3)-Co(1)-N(5)	89.50(8)
N(1)-Co(1)-N(5)	83.55(9)	N(3)-Co(1)-N(4)	169.66(9)
N(3)-Co(1)-N(2)	91.52(8)	N(1)-Co(1)-N(2)	86.35(8)
N(5)-Co(1)-N(2)	169.76(9)	N(4)-Co(1)-N(2)	89.35(8)
N(3)-Co(1)-Cl(1)	96.33(6)	N(1)-Co(1)-Cl(1)	175.84(6)
N(5)-Co(1)-Cl(1)	93.32(6)	N(4)-Co(1)-Cl(1)	93.81(6)
N(2)-Co(1)-Cl(1)	96.70(6)	C(1)-N(1)-Co(1)	110.1(1)
C(9)-N(1)-Co(1)	110.0(1)	C(15)-N(1)-Co(1)	98.9(1)
C(2)-N(2)-Co(1)	112.9(2)	C(6)-N(2)-Co(1)	127.7(2)
C(14)-N(3)-Co(1)	127.1(2)	C(10)-N(3)-Co(1)	113.6(2)
C(20)-N(4)-Co(1)	128.6(2)	C(16)-N(4)-Co(1)	111.3(2)
C(25)-N(5)-Co(1)	128.9(2)	C(21)-N(5)-Co(1)	111.0(2)

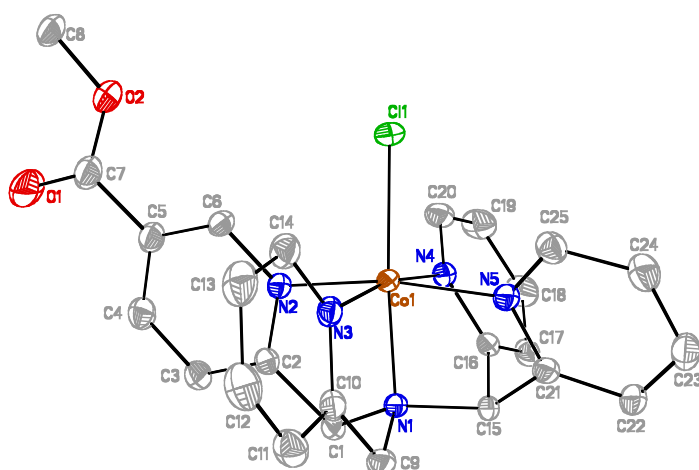


Figure 4.5. ORTEP diagram of the dication $[\text{Co}^{\text{III}}(\text{N4PyCO}_2\text{Me})\text{Cl}]^{2+}$, thermal ellipsoids are drawn at the 50 % probability. Hydrogen atoms and chloride counter ions have been omitted for clarity.

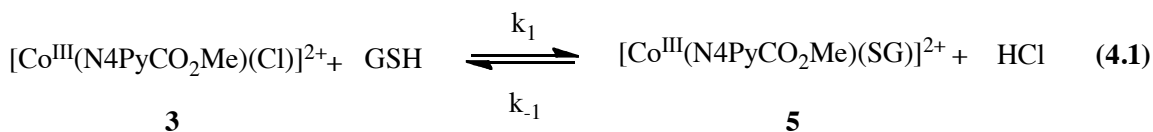
4.2.6. Molar conductivity data

Molar conductivity (Λ_{M}) values for **3** in H_2O range from 133–180 $\text{S cm}^2 \text{mol}^{-1}$ for concentrations ranging from 2.0–0.5 mM (Table 4.4). These data agree well with the data for other 2:1 electrolytes in H_2O .²⁹¹ Importantly, these data are consistent with the dication of **3** maintaining its structure in solution, and not undergoing rapid hydrolysis to form $[\text{Co}^{\text{III}}(\text{N4PyCO}_2\text{Me})(\text{H}_2\text{O})]^{3+}$, which would act as a 3:1 electrolyte.

Table 4.4. Molar conductivities for **3** in H_2O at $298 \pm 2 \text{ K}$

3 (mM)	Λ_{M} ($\text{S} \cdot \text{cm}^2 \cdot \text{mol}^{-1}$)
2.0	133
1.5	152
1.0	160
0.5	180

4.2.7. Glutathionylation of the cobalt complex **3**



$$K_{\text{obs}}(\mathbf{5}) = [\mathbf{5}]/([\mathbf{3}][\text{GSH}]) \quad (4.2)$$

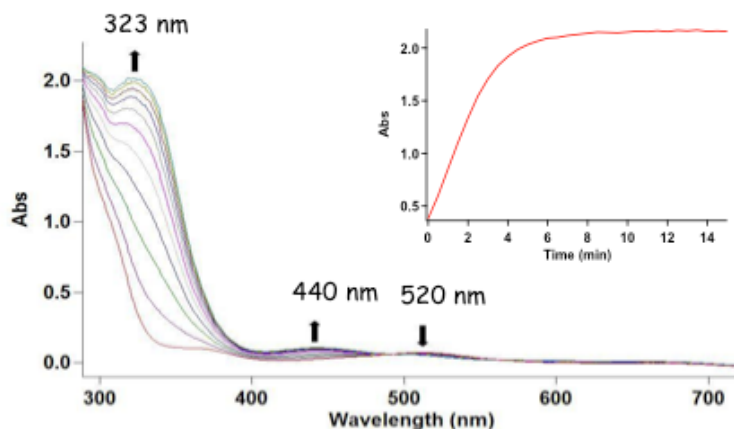


Figure 4.6. UV-vis spectral change for **3** (0.5 mM) on reaction with GSH (10 mM) in 100 mM acetate buffer at 298 ± 2 K (Inset: Abs vs time plot for growth of peak at 323 nm)

Treatment of the Co(III) complex **3** with GSH in 100 mM acetate buffer (pH 5.00, $I = 100$ mM (KNO_3)) resulted in a color change from pink to brown within minutes at room temperature. Upon following the reaction of **3** (0.5 mM) with GSH (10 mM) by UV-vis spectroscopy, the disappearance of a peak at 520 nm and appearance of two new peaks at 323 nm and 440 nm with a shoulder at 490 nm were observed, with two isosbestic points at 490 nm and 560 nm (Figure 4.6). These results are consistent with conversion of **3** into a new product without the formation of any long-lived intermediate. When the initial rates of the reaction (dA_{323}/dt) of **3** (0.5 mM) with GSH (0.5–25 mM) were plotted against the total concentration of GSH, a line passing through the origin can be fit, indicating the reaction (eq 4.1) to be first order with respect to GSH. A second

order rate constant, k_1 , of $9.3 \times 10^{-2} \text{ M}^{-1} \text{ s}^{-1}$ was obtained from these data (Figure 4.7a). Similarly, when the initial rates of reaction of GSH (4 mM) with **3** (0.5–5 mM) were plotted against concentration of **3**, a line passing through origin can be fit, indicating the reaction to be first-order also with respect to **3** and, from these data, a second-order rate constant, k_1 , of $10.8 \times 10^{-2} \text{ M}^{-1} \text{ s}^{-1}$ was obtained (Figure 4.7b). The values of k_1 obtained from both the plots were in good agreement within the experimental error confirming the reaction follows the rate law, $\text{Rate} = k_1[\mathbf{3}][\text{GSH}]$ under the condition used in this study. It is noteworthy that this reaction is approximately two orders of magnitude slower than the reaction of GSH with H_2OCbl^+ .¹⁷⁴

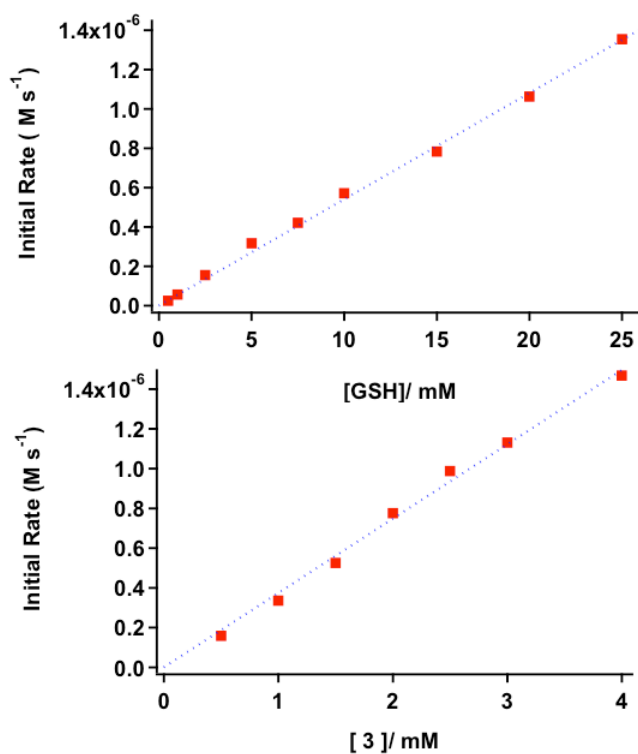


Figure 4.7. (a) Plot of initial rate (dA_{323}/dt) vs. [GSH] for substitution of Cl^- with GSH (0.5–25 mM) in **3** (0.5 mM) in 100 mM acetate buffer to form $[\text{Co}(\text{N4PyCO}_2\text{Me})(\text{SG})]^{2+}$. (b) Plot of initial rate (dA_{323}/dt) vs. [3] for substitution of Cl^- with GSH (4.0 mM) in **3** (0.5–4 mM) in 100 mM acetate buffer.

Next, the observed equilibrium constant was determined for the reaction of **3** with GSH (eq 4.2) in 100 mM acetate buffer (Figure 4.8). The value calculated for K_{obs} was $870 \pm 50 \text{ M}^{-1}$, which is approximately three orders of magnitude smaller than that of GSCbl ($9.5 \times 10^5 \text{ M}^{-1}$).¹⁷⁴

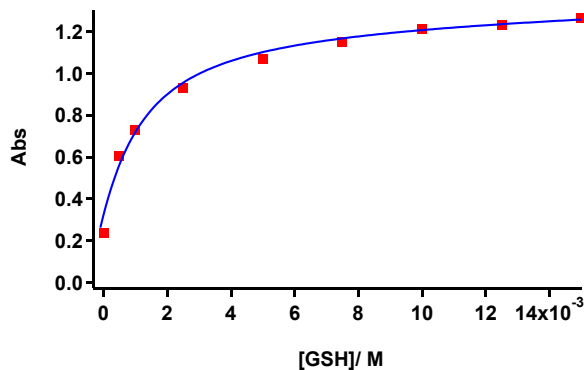


Figure 4.8. Abs₃₂₃ vs [GSH] plot, obtained from the equilibrated solutions of **3** (0.5 mM) and GSH (0.0–15 mM) kept at $298 \pm 2 \text{ K}$ for 2 h (The data was fit according to the literature method, fixing $[\mathbf{3}] = 5.0 \times 10^{-4} \text{ M}$, $A_{323}(\mathbf{3}) = 0.237$ and $A_{323}(\mathbf{5}) = 1.263$).¹⁷⁴

Further examination revealed that rates for glutathionylation of **3** showed a significant dependence on pH. Studies carried out between pH 4.0–8.0 confirmed that the rates for the substitution reaction increased with increase in pH (Table 4.5). This was expected, because the concentration of the more nucleophilic thiolate GS^- (pKa of thiol of GSH = 8.72)²⁹² increases with respect to the neutral thiol GSH at higher pH. It is important to note that conditions of these experiments are relevant to biology, because GSH is estimated to be present at concentrations much higher (up to 10^6) than H_2OCbl^+ in cells.

Table 4.5. Initial rates of reaction of **3** (0.5 mM) with GSH (15 mM) as a function of pH

Entry	Initial Rate of Reaction (M s ⁻¹)				
	pH 4.0 ^a	pH 5.0 ^a	pH 6.0 ^a	pH 7.0 ^b	pH 8.0 ^b
3 + GSH	1.78 x 10 ⁻⁷	1.46 x 10 ⁻⁶	5.31 x 10 ⁻⁶	3.44 x 10 ⁻⁵	nd

^a100 mM acetate buffer
^b100 mM phosphate buffer (*I* = 100 mM (KNO₃))
nd = not determined (Initial rate of the reaction was too fast to measure under the reaction condition)

The species [Co^{III}(N4PyCO₂Me)(SG)]²⁺ (**5**), obtained from reaction of **3** and GSH, was generated *in situ* and characterized further by UV-vis and ¹H-NMR spectroscopies and mass spectrometry. The *in situ* generated **5**, obtained from the reaction of **3** with GSH, shows two major absorption bands, one intense at 323 nm and other relatively weaker at 440 nm with shoulder at 490 nm (Figure 4.6). The intense peak at 323 nm is consistent with thiolate ligation to Co(III) in **5** and is assigned to S → Co(III) ligand-to-metal charge transfer (LMCT) transition based on analogy with other Co(III) complexes.^{187,293,294} The thiolate ligation in **5** was further corroborated by the fact that other thiols i.e., *N*-acetylcysteine and 2-mercaptoethanol upon reaction with **3**, gave similar absorption bands. The weaker band at 440 nm with shoulder at 490 nm can be due to a splitting of the ¹A_{1g} → ¹T_{1g} transition arising by a lowering of the symmetry from O_h, based on literature assignments.^{294,295} Using the maximum absorbance observed for reaction of **3** (0.5 mM) with GSH (10 mM), a molar extinction coefficient of ε₃₂₃ = 4300 M⁻¹ cm⁻¹, ε₄₄₀ = 280 M⁻¹ cm⁻¹ and ε₄₉₀ = 120 M⁻¹ cm⁻¹ was calculated for **5**, respectively.

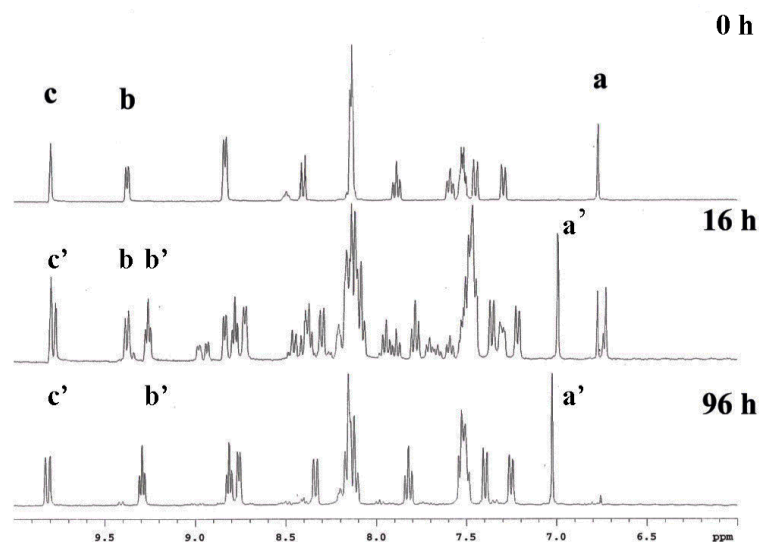


Figure 4.9. ^1H -NMR spectra (6-10 ppm) of reaction mixture containing **3** (10 mM) and GSH (40 mM), after a time interval of 0 h (top), 16 h (middle) and 96 h (bottom) in D_2O

^1H -NMR spectra were recorded at regular time intervals to follow the reaction of **3** (10 mM) with GSH (40 mM) in D_2O (Figure 4.9). At the beginning of the reaction, no immediate change was observed. As the time progressed over the course of 96 h,²⁹⁶ original resonances diminished and new resonances appeared. Major changes were noted with resonances at 6.6, 9.4 and 9.9 ppm (Figure 4.10, labeled **a-c**, respectively). The resonance at 6.6 ppm (**a**), assigned to the methine proton of the ligand $\text{N4PyCO}_2\text{Me}$, shifted to 7.0 ppm (**a'**) over time. A resonance assigned to the pyridyl protons of the ligand at 9.4 ppm (**b**) disappeared with concomitant growth of a new resonance at 9.2 ppm (**b'**). The resonance at 9.8 ppm (**c**) split to form two peaks (**c'**) with similar intensities. Based on the distance between the peaks (9.7 Hz), which are too large for ^1H - ^1H coupling in a pyridine ring, and the lack of cross peaks in 2D-COSY correlation spectrum (Figure 4.10), the two peaks are assigned as independent singlets rather than a doublet. This is consistent with the formation of a 1:1 mixture of diastereomers of **5**, which occurs because both starting materials are chiral, where **3** is

racemic and GSH is enantioenriched. Also, shifts in the peaks corresponding to Cys_α (4.5 → 4.3 ppm) and Cys_β (2.9 → 3.1 ppm) protons of GSH were observed, consistent with the direct thiolate ligation to the cobalt center.^{169,186} All resonances lie between 1-10 ppm region, confirming that **5** is a low-spin Co(III) complex. Furthermore, even after 96 h, resonances were still sharp and well defined, and no broadening occurred. This is consistent with a lack of paramagnetic impurities, as would be expected if diamagnetic **3** or **5** was reduced by GSH to form a Co(II) complex during the reaction. Less than 5% of the total GSH was oxidized to form GSSG, as judged by ¹H-NMR spectroscopy, which confirmed a negligible role for oxidation of GSH by atmospheric O₂ in this process, either uncatalyzed or catalyzed by **3**. Taken together, these data confirm that the reaction of **3** with GSH proceeds cleanly to generate **5** under these conditions.

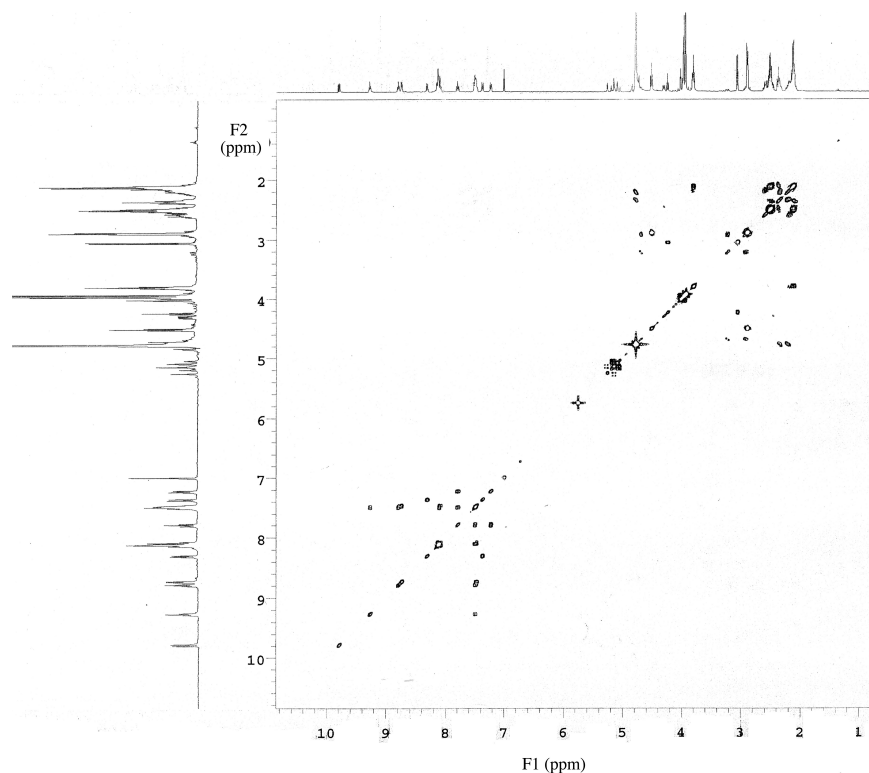


Figure 4.10. COSEY spectra (1 – 10 ppm) for the reaction of **3** (10 mM) with GSH (40 mM) in D₂O after 96 h

The high-resolution ESMS spectrum of **5** generated *in situ* displayed a prominent ion cluster with a peak at $m/z = 395.5974$. This cluster displayed an isotopic pattern that fits with molecular formula $[\text{Co}(\text{N4PyCO}_2\text{Me})(\text{SG})]^{2+}$ (Figure 4.11), albeit the intensities of calculated and experimental isotopic pattern do not correlate exactly. In this dication, the ligand derived from GSH is treated as a monoanion (i.e., GSH-H^+), as would be expected if the thiolate of GSH were deprotonated and bound to the Co(III) center of **5**. The difference in intensities from the calculated spectrum may indicate that **5** is partially reduced to form $[\text{Co}^{\text{II}}(\text{N4PyCO}_2\text{Me})(\text{GSH})]^{2+}$ under the harsh conditions of analysis (150 °C, 40V).

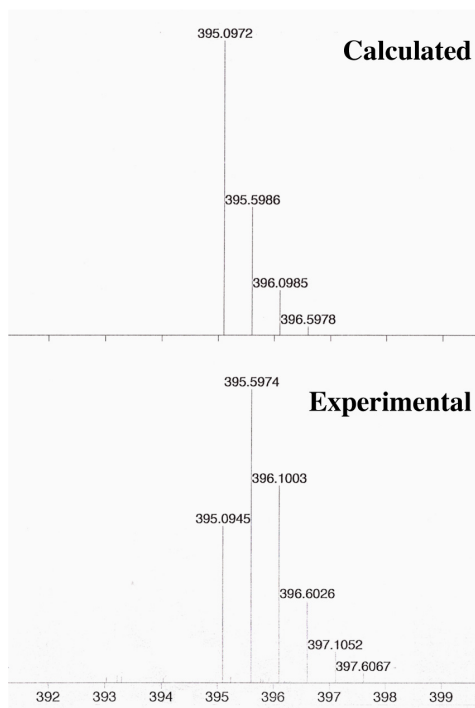


Figure 4.11. Calculated (top) and observed (bottom) high resolution mass spectra (HRMS) for the dication $[\text{Co}^{\text{III}}(\text{N4PyCO}_2\text{Me})(\text{SG})]^{2+}$ of **5**.

Like compound **3**, the Co(III) complex $[\text{Co}^{\text{III}}(\text{Bn-CDPy3})\text{Cl}]\text{Cl}_2$ (**4**) reacts with GSH in 100 mM acetate buffer to generate the species $[\text{Co}^{\text{III}}(\text{Bn-CDPy3})(\text{SG})]^{2+}$ (**6**). The reaction of **4** (0.5 mM) with GSH (10 mM) was followed by UV-vis spectroscopy over

time at 298 ± 2 K (Figure 4.12). As with **3**, the disappearance of a peak at 555 nm and appearance of two new peaks at 320 and 580 nm were observed, with shoulders at 500 and 450 nm. In addition two isosbestic points were present at 520 nm and 610 nm. The new peak at 320 nm is consistent with a $S \rightarrow \text{Co(III)}$ LMCT band, and with the thiolate of GSH binding to the Co(III) center of **6**.

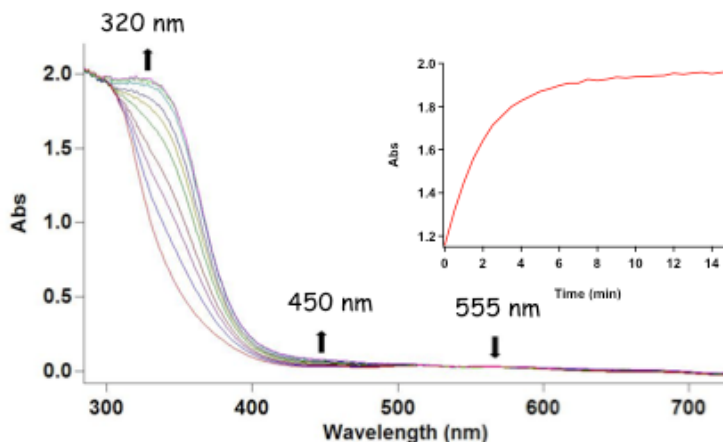


Figure 4.12. UV-vis spectral change for **4** (0.5 mM) upon reaction with GSH (10 mM) in 100 mM acetate buffer pH 5.00 at 298 ± 2 K (Inset: Abs vs time plot for growth of peak at 320 nm)

Kinetic and thermodynamic analysis indicated that the observed rates and equilibrium constant for formation of **6** were similar to **5**. The reaction of **4** with GSH follows the rate law, $\text{Rate} = k_2[\mathbf{4}][\text{GSH}]$ under the condition used in this study, the same as with **3**. The order of the reaction is unity with respect to both **4** and GSH as evidenced from the straight lines obtained when the initial rates of the reaction (dA_{320}/dt) of **4** (0.5 mM) with GSH (0.5–25 mM) were plotted against the total concentration of GSH (Figure 13a), and when the initial rates of the reaction (dA_{320}/dt) of GSH (25 mM) with **4** (0.25–1.5 mM) were plotted against the concentration of **4** (Figure 4.13b). Second-order rate constants, k_2 of $8.7 \times 10^{-2} \text{ M}^{-1} \text{ s}^{-1}$ and $8.0 \times 10^{-2} \text{ M}^{-1} \text{ s}^{-1}$ were obtained from the individual plots which are in good agreement within the experimental error.

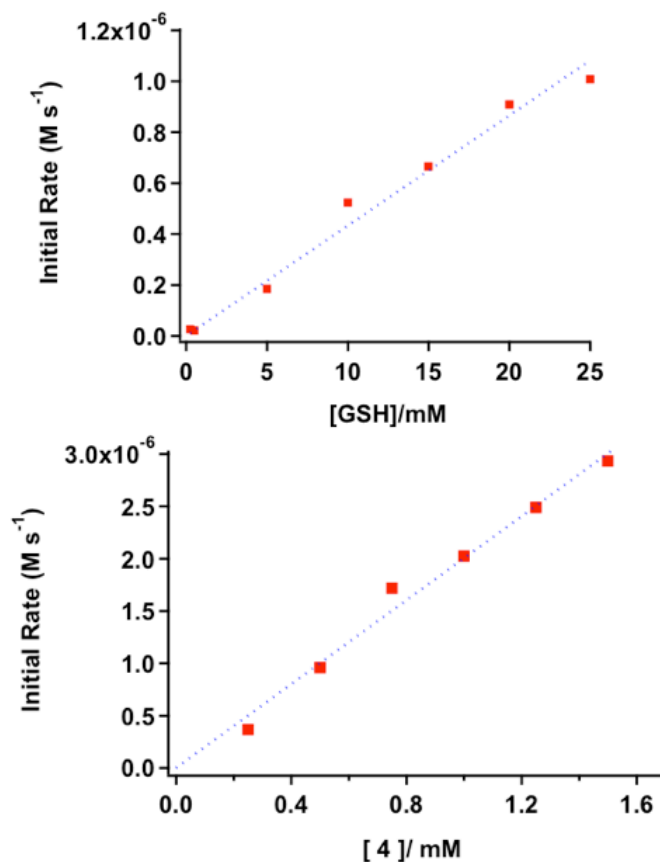


Figure 4.13. (a) Plot of initial rate (dA_{320}/dt) vs. [GSH] for substitution of Cl^- with GSH (0.5–25.0 mM) in **4** (0.5 mM) in 100 mM acetate buffer. (c) Plot of initial rate (dA_{320}/dt) vs. [4] for substitution of Cl^- with GSH (25 mM) in **4** (0.25–1.5 mM) in 100 mM acetate buffer.

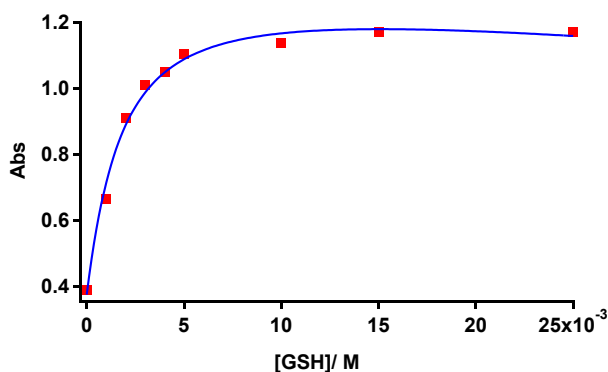


Figure 4.14. Abs₃₂₀ vs [GSH] plot, obtained from the equilibrated solutions of **4** (0.5 mM) and GSH (0.0–25.0 mM) kept at 298 ± 2 K for 3 h (The data was fit according to the literature method, fixing [4] = 5.0 × 10⁻⁴ M, A₃₂₀(**4**) = 0.378 and A₃₂₀(**6**) = 1.170).¹⁷⁴

A value of $740 \pm 47 \text{ M}^{-1}$ was obtained for the observed equilibrium constant, K_{obs} for formation of **6** compared to $870 \pm 50 \text{ M}^{-1}$ for **5** in 100 mM acetate buffer (Figure 4.14).

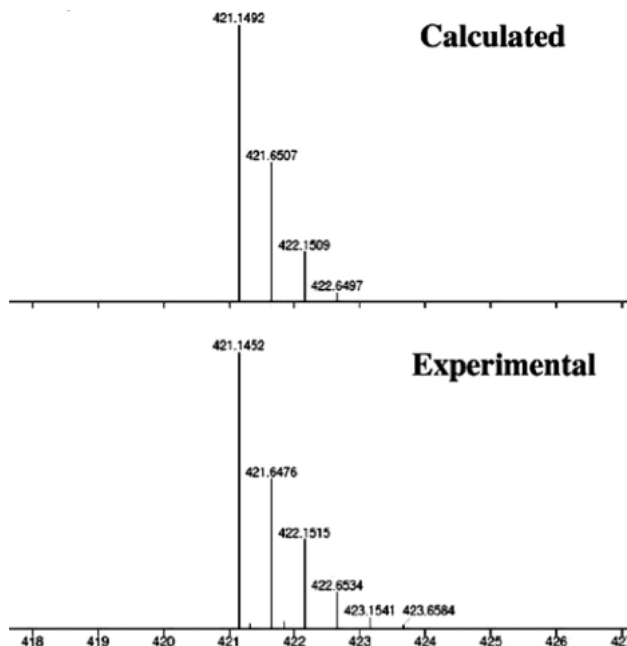


Figure 4.15. Calculated (top) and observed (bottom) high resolution mass spectra (HRMS) for the dication $[\text{Co}(\text{Bn-CDPy}_3)(\text{SG})]^{2+}$ of **6**.

The species $[\text{Co}^{\text{III}}(\text{Bn-CDPy}_3)(\text{SG})]^{2+}$ (**6**), obtained from reaction of **4** and GSH *in situ*, was characterized further by UV-vis, $^1\text{H-NMR}$ spectroscopies and mass spectrometry. Like **3**, new resonance peaks were observed when **4** (10 mM) was treated with GSH (40 mM) in D_2O , though the complete conversion of **4** into **6** was not observed. However, evolution of a new ion cluster with a dominant peak at $m/z = 421.1452$ was observed by ESMS, which agrees well with that expected for a dication with the chemical formula $[\text{Co}^{\text{III}}(\text{Bn-CDPy}_3)(\text{SG})]^{2+}$ of **6** (Figure 4.15). The timescale for evolution of this new peak correlated well with the timescale of the new peak at 320 nm from the kinetic experiments, consistent with its assignment as **6**. Using the maximum absorbance observed for reaction of **4** (0.5 mM) with GSH (10 mM), a molar extinction

coefficient of $\epsilon_{320} = 4300 \text{ M}^{-1} \text{ cm}^{-1}$ was calculated for **6**, which agrees with the intensity and wavelength of S \rightarrow Co(III) LMCT bands observed for **5** and other related complexes.^{187,293,294} Taken together, these data are consistent with **4**, which contains a N5 donor set like that of H_2OCbl^+ and **3**, undergoing glutathionylation. Thus, glutathionylation appears to be a general reaction of N5 donor Co(III) complexes that contain a labile coordination site, although reaction mechanisms and rates of glutathionylation differ between related complexes.

4.3. Discussion

Glutathionylation of Cbl to form GSCbl is an important reaction in biology. Although this process is well understood at the fundamental chemistry level,^{166,174,297} the role of GSCbl in Cbl metabolism and its applications in medicine are still being actively investigated. Studies reported herein are significant, because they are the first example of synthetic Co(III) model compounds bearing a unique polypyridyl ligand set mimicking the chemistry of Cbl and undergoing glutathionylation in a similar fashion to H_2OCbl^+ . Data for **5** and **6**, which were generated *in situ* and characterized in solution by $^1\text{H-NMR}$ (only **5**) and UV-vis spectroscopies and mass spectrometry, are consistent with ligation of the cysteine thiolate of GSH to the Co(III) centers, as occurs in GSCbl. This result was noteworthy as GSH though possesses three donor atoms (N, O and S) that can ligate to cobalt center, it selectively ligates through S atom in **5** and **6**. Despite the fact that **5**, **6** and GSCbl have similar structures, containing N5S donor atom sets and low-spin Co(III) centers, the formation of **5** and **6** occurs much slower (~ 100 times) than GSCbl at pH 5.0. The reaction of **3** or **4** with GSH was found to be bimolecular in nature, the order of reaction being unity with respect to each reactant. The pH

dependence studies (pH 4.0–8.0) further confirmed that the rates for the substitution reaction increase with increasing pH, as would be expected, because of the higher concentration of GS^- . This is different from H_2OCbl^+ , where the observed rate constants for the reaction of GSH with H_2OCbl^+ were found to decrease with increasing pH, presumably because of increase in concentration of hydroxycobalamine (HOcbl), which does not react with GSH and hence decreases the rate of reaction.¹⁷⁴ This same issue does not apply to **3** and **4**, which have chloride rather than H_2O bound at the sixth position. Discrepancies regarding the mechanism of the axial ligand substitution reactions of vitamin B_{12} , its derivatives, and model complexes have been seen in the literature. Since, octahedral Co(III) complexes are coordinately saturated systems with 18 e^- in their valence shells, the $\text{S}_{\text{N}}2$ (associative) type of mechanism for ligand substitution appears impervious. However, some authors have favored the associative mechanism²⁹⁸ whereas a limiting dissociative (D) mechanism²⁹⁹⁻³⁰³ or a dissociative interchange (I_{d}) mechanism³⁰⁴⁻³¹³ has been favored by others. High-pressure kinetic techniques³¹⁴⁻³¹⁶ can differentiate between D or I_{d} substitution mechanism.^{304,307-309,314-317} Further studies will be required to elucidate the exact mechanism of substitution of Cl^- in **3** and **4** by GSH. Nonetheless, kinetics of glutathionylation are clearly second-order.

In contrast to **3** and **4**, corrin and porphyrin-derived Co(III) complexes react much faster in ligand substitution reactions, where data suggests a dissociative interchange mechanism takes place.^{305,306,310} Difference in kinetics may be due to the nature of the ligand structure. In the delocalized structure of H_2OCbl^+ , the Co(III) oxidation state may be a formalism, where the complex is more like Co(II) due to delocalization into the corrin ring.³¹⁸⁻³²⁰ This idea was recently supported with Cbl derivatives. A significant

decrease in the rate of ligand substitution was observed with the stable yellow aquacyanocobyrinic acid heptamethyl ester, which contains less conjugation in corrin ligand than H_2OCbl^+ .³²¹ Even though the kinetics and reaction pathways for glutathionylation of H_2OCbl^+ differ from that of complexes **3** and **4**, it is significant that these synthetic model compounds mimic the chemistry of H_2OCbl^+ , which implies that Co(III) complexes related to Cbl used in biological studies may become glutathionylated in cell culture and *in vivo*, especially with complexes containing labile ligands such as chloride or H_2O . For example, the soluble oligomer of amyloid β peptide ($\alpha\beta$), especially $\alpha\beta_{42}$, responsible for synaptic dysfunction of the brain nerves (Alzheimer disease) are cleaved by $[\text{Co}^{\text{III}}(\text{cyclen})(\text{OH}_2)_2]$ derivatives,⁸⁹ and since these complexes contain two labile H_2O ligands, glutathionylation may render a competing reaction resulting in inefficacy of these complexes to hydrolyze these peptides. Similarly, potency of Co(III)-Ebox complex, a Co(III) Schiff base–DNA conjugate, to inhibit snail family zinc finger transcription factor may be diminished by glutathionylation at the cobalt center, affecting the binding of histidine (via ligand substitution of labile amine at Co(III) center), responsible for the inhibitory action.³²²⁻³²⁵

Glutathionylation of H_2OCbl^+ occurs readily and GSCbl is one of the most abundant forms of Cbl isolated from mammalian cells. Previous studies reported rate constants as high as $163 \pm 8 \text{ M}^{-1} \text{ s}^{-1}$ ($4.5 < \text{pH} < 11.0$) for the formation of GSCbl.¹⁷⁴ Unlike H_2OCbl^+ , compounds **3** and **4** react slower with GSH, with rate constants ranging between $8.3\text{-}9.3 \text{ M}^{-1} \text{ s}^{-1}$ respectively. The slower rates of formation for **5** and **6** may be attributed to differences in ligand structure. Unlike corrin rings or planar oxime/Schiff base ligands found in cobalamin or cobaloxime, which contain large planar conjugated

rings, the polypyridyl rings in **3** and **4** are perpendicular to the basal plane and can not adopt the same conformation, which may limit the amount of delocalization.

The observed equilibrium constants, K_{obs} for the formation of glutathionylated products **5** and **6** ranged between 740-870 M^{-1} , which are considerably smaller than earlier reported values of K_{obs} , for GSCbl formation, of $(9.5 \pm 0.9) \times 10^6 \text{M}^{-1}$ (pH 5.0, 25 °C),¹⁷⁴ $(\sim 5) \times 10^5 \text{M}^{-1}$ (pH 4.7, temperature not specified)²⁹⁷ and $(1.1 \pm 0.3) \times 10^5 \text{M}^{-1}$ (pH 5.0, 25 °C)²⁸⁰ and also K_{obs} , for [Me(Co)(tn)(SG)] formation where tn = 2,3,9,10-tetramethyl-1,4,8,11-tetra-azaundeca-1,3,8,10-tetraen-11-ol-1-olato anion, of $\sim 10^{6.6} \text{M}^{-1}$ (pH 7.0, temperature not specified).²⁹³ The high formation constants of thiolate-bound vitamin B₁₂ model complexes have been attributed to π -bonding from the ligand to the cobalt center. The lower values of K_{obs} for **5** and **6** may be attributed to weak interactions of thiolate ligands with Co(III) center, as a result of steric hindrance of GSH with N4PyCO₂Me and Bn-CDPy3 ligands on the cobalt center. Alternatively, backbonding could be lower because of electronic considerations. The lower value of K_{obs} for **6** as compared to **5** can also be explained because of the fact that the Co center is crowded in **6** as compared to **5** (based on crystallographic data), resulting in a weaker bonding interaction between the thiolate and Co(III) center. By changing the electronic structure of the ligand around Co(III) center, the kinetic and equilibrium parameters for glutathionylation may be tuned.

4.4. Conclusions and future directions

Glutathionylation of synthetic Co(III) model compounds **3** and **4** was reported that mimics the biological chemistry of Cbl. These compounds show similar chemistry to H_2OCbl^+ , although kinetic and thermodynamic parameters differ. Unlike H_2OCbl^+ , where

the Co(III) center is bound by the highly delocalized corrin ring and GSCbl formation is rapid and highly favorable, compounds **3** and **4** react slower with GSH in substitution reactions, and formation constants are not as strong. These results entail the importance of ligand structure toward tuning the special reactivity of H_2OCbl^+ . Nonetheless, the ease with which complexes such as **3** and **4** undergo gluathionylation suggests this may be a general reaction for cobalt complexes of this type. Understanding how facile gluathionylation is for synthetic cobalt complexes may lead to a better understanding of the behavior of these interesting metal complexes in biological systems, due to the natural abundance of GSH.

4.5. Experimental section

4.5.1. General considerations

All reagents were purchased from commercial suppliers and used as received. Ligands $\text{N4PyCO}_2\text{Me}$ (**1**)²²² and $(R,R)\text{-Bn-CDPy3}$ (**2**),²⁸⁷ and the complex $[\text{Co}(\text{Bn-CDPy3})\text{Cl}]\text{Cl}_2$ (**4**)^{287,326} were prepared using literature procedures. NMR spectra were recorded on a Varian FT-NMR Mercury- 400 MHz Spectrometer. Mass spectra were recorded on a Waters ZQ2000 single quadrupole mass spectrometer using an electrospray ionization source. IR spectra were recorded on a Nicolet FT-IR spectrophotometer. All reactions were performed under ambient atmosphere unless otherwise noted. Conductivity measurements were performed with an Omega portable conductivity meter (Model CDH-280). X-ray diffraction data were collected on a Bruker *APEX-II* diffractometer at 100K. Kinetic and thermodynamic studies have been performed in 100 mM acetate buffer (pH 5.0, $I = 100 \text{ mM (KNO}_3)$) unless otherwise noted.

4.5.2. Synthesis of [Co^{III}(N4PyCO₂Me)Cl]Cl₂ (**3**)

The compound, *trans*-[Co^{III}(Py)₄Cl₂]Cl·6H₂O,^{282,283} (277 mg, 0.470 mmol) was added to a solution of **1** (200 mg, 0.470 mmol) in CH₂Cl₂ (5 mL). The mixture was stirred for 60 min, during which time a light purple solid formed. The resultant solid was isolated by filtration in analytically pure form (173 mg, 71%). Single crystals of **3** suitable for X-ray crystallographic analysis were obtained by recrystallization of the purple precipitate from EtOH with Et₂O vapor diffusion, followed by isolation of the pink solid and recrystallization from MeOH with Et₂O vapor diffusion. Mp = 144-146 °C. ¹H-NMR (CD₃OD) δ 9.94 (s, 1H), 9.47 (d, *J* = 5.67 Hz, 1H), 8.90 (t, *J* = 8.92 Hz, 2H), 8.49 (dd, *J* = 6.48, 1.62 Hz, 1H), 8.25-8.34 (m, 4H), 7.99 (dt, *J* = 1.62, 7.19 Hz, 1H), 7.69 (t, *J* = 6.48, 1H), 7.6-7.66 (m, 3H), 7.46 (d, *J* = 8.1 Hz, 1H), 7.07 (s, 1H), 5.13-5.43 (m, 4H), 4.01 (s, 3H); ¹³C-NMR (CD₃OD) δ 169.9, 166.4, 160.8, 160.7, 156.5, 156.4, 153.38, 152.8, 144.2, 142.5, 142.4, 130.9, 128.7, 128.5, 127.0, 125.1, 81.1, 67.6, 67.5, 53.7 ppm; IR (KBr) 3588 (w), 3568 (w), 3407 (s), 2922 (m), 1735 (s), 1610 (s), 1300 (s) cm⁻¹; HRMS (ESMS) calc'd for C₂₅H₂₃O₂N₅CoCl (M²⁺) 259.5436, found: 259.5437. Anal. Calc. for C₂₅H₂₈Cl₃CoN₅O_{4.5} (2·2.5H₂O): C, 47.23; H, 4.44; N, 11.01. Found: C, 47.21; H, 4.19; N, 10.95.

4.5.3. Kinetic studies

Generation of the complexes [Co(N4PyCO₂Me)(SG)]²⁺ (**5**) and [Co(Bn-CDPy3)(SG)]²⁺ (**6**), formed *in situ* from reaction of GSH with **3** and **4** respectively, were followed spectrophotometrically. The solutions of **3** or **4** (1 mM, 50 μL, final concentrations = 0.5 mM,) in 100 mM acetate buffer were treated with solutions of GSH in the same buffer (50 μL, final concentration = 0-25 mM). Absorbance at 323 nm for formation of **5** and 320 nm for formation of **6**, respectively was recorded over a period of

2 h at 298 ± 2 K with a GENios Pro, microplate reader (TECAN) using a 96 well microplate. All data were collected in triplicate. Initial rates ($dA_{320/323}/dt$) were calculated from slopes obtained from linear portions of absorbance vs. time graphs for the first 5% of the reaction.

4.5.4. Determination of equilibrium constant (K_{obs})

The observed equilibrium constants for the formation of glutathionylated products **5** and **6** were determined by measuring the absorbances of equilibrated reaction mixtures containing cobalt complexes **3** or **4** (0.5 mM) and GSH (0-15 mM or 25 mM, respectively) in 100 mM acetate buffer. $A_{323/320}$ values were plotted against [GSH] and the data was fit according to literature methods.¹⁷⁴

4.5.5. $^1\text{H-NMR}$ spectroscopic studies

A solution of GSH (12.3 mg, 40.0 μmol) and **3** (5.91 mg, 10.0 μmol) or **4** (6.43 mg, 10.0 μmol) in D_2O (1 mL) was prepared. The reaction was monitored by $^1\text{H-NMR}$ spectroscopy at regular time intervals. The reaction was maintained at room temperature (298 ± 2 K) during the experiment.

4.5.6. X-ray crystallographic studies

Diffraction data were collected on a Bruker X8 APEX-II kappa geometry diffractometer equipped with Mo radiation and a graphite monochromator at 100 K. Frames were recorded for 10 s and 0.3 degree between frames. APEX-II and SHELX software^{327,328} were used in the collection and refinement of the model. Crystals of **3** appeared as red rhomboids. 36734 reflections were measured, of which 7571 were independent. Hydrogen atoms were placed in calculated positions. The asymmetric unit contains one coordination complex, two Cl anions, and one equivalent each of methanol and ethanol. The ethanol was disordered over two sites and described with partial

occupancies and isotropic thermal parameters. There is a network of hydrogen bonds linking the anions and solvates in the lattice.

Chapter 5

Conclusions and Future Directions

This chapter comprises of two sections, where the first section deals with the accomplishments of my research goals described at the beginning of the dissertation with suggestions to improve the present outcome of the research, and the second section entails the conclusions and future prospects highlighting the significance and scope of the research reported in this dissertation.

5.1. Research goal accomplishments and suggestions

5.1.1. Application of non-heme iron complexes in protein oxidation

Non-heme iron complexes were investigated for their ability to inactivate a series of proteins. The proteins being inactivated in these studies were human carbonic anhydrase-I (CA-I), serine proteases (trypsin and chymotrypsin) and 20S proteasome. Different non-heme ligands for iron complex formation were designed and synthesized to target different proteins. Proteins inactivation was achieved either by pre-generated ferryl (serine proteases) or by an iron complex in presence of O₂ and a reductant (CA-I and 20S proteasome) or H₂O₂ (serine proteases). Mode of action of these iron complexes to inactivate proteins was determined by characterizing the protein inactivation products using SDS-PAGE, ESI-MS, LC/MS and LC/MS/MS. These characterization techniques enabled me to confirm that CA-I is inactivated by an oxidation event that does not result in cleavage of the protein backbone where specific oxidation of His, Trp and Met residues, mostly localized around the active site, was achieved. The time-dependent inactivation of CA-I and 20S proteasome in presence of

O₂ and DTT was consistent with a pathway involving the reductive activation of O₂ playing a role in enzyme inactivation. The results obtained for CA-I inactivation were found irreproducible probably due to inefficacy of O₂ activation by the reductant DTT under the reaction condition used in this dissertation. This led us to move toward inactivating proteins with pre-generated ferryl and using relatively stronger bioavailable oxidant H₂O₂ replacing O₂. Ferryls were found potent oxidants inactivating trypsin and chymotrypsin by oxidation of amino acid side chains rather than protein backbone cleavage, similar to seen in CA-I oxidation. Amino acid analysis further confirmed that the residues Cys, Tyr and Trp were the most susceptible to oxidations. Oxidation of the proteases by ferrous complexes in the presence of hydrogen peroxide led to the preferential inactivation of trypsin over chymotrypsin where tyrosine residues were selectively oxidized. Further investigation into the details of active oxidant responsible for protein oxidation was achieved by performing the inactivation studies in presence of radical scavengers like NaN₃, D-mannitol and imidazole. The data precluded the role of ROS and supported that a metal-based oxidant was responsible for inactivation of proteins (serine proteases and 20S proteasome), though the nature of active oxidant was not confirmed. In case of seine proteases inactivation, extensive mechanistic studies (oxidation of Ac-Try-OH to Ac-DOPA-OH) led to conclude that a pathway unique from that of an Fe^{II}/Fe^{IV} cycle involving ferryl compounds was operative.

Overall, non-heme iron complexes, which find extensive application in oxidation of small organic molecules, amino acids and DNA, were shown to oxidize full proteins with mode of action primarily being oxidation of amino acid side chains rather than protein backbone cleavage where residues Cys, His, Trp, Tyr and Met were more prone

to oxidation and supporting the role of a metal-based oxidant responsible for inactivation of proteins. However, further investigation is required to unravel the exact nature of active oxidant.

5.1.2. Application of non-heme cobalt complexes as biomimetic model systems for cobalamin

Synthetic cobalt(III) model complexes derived from polypyridyl pentadentate non-heme ligands (N4PyCO₂Me and Bn-CDPy3), mimicking the N5 coordination environment around cobalt(III) center present in biologically important cofactor cobalamin (Cbl) or vitamin B₁₂ were investigated (kinetic and thermodynamic analysis) for their reaction with glutathione (GSH) to generate glutathionylated products similar to glutathionylcobalamin (GSCbl), an important form of Cbl present in the cell. The Co(III) model complexes were synthesized, and characterized using various experimental techniques including UV-vis, ¹H- and ¹³C-NMR spectroscopies, HRMS and X-ray crystallography. The reaction of these Co(III) model complexes with GSH followed second order kinetic (the order of reaction being unity with respect to each reactant). The rate of reaction was found to be dependent on pH where the rate increases with increase in pH. The second order rate constants calculated for the reaction of GSH with both the compounds showed that these reactions were ~ 100 times slower than the reaction of GSH with aquacobalamin. Also, the observed equilibrium constants were ~ 1000 times weaker than the observed equilibrium constants for the formation of GSCbl from aquacobalamin (H₂OCbl⁺) and GSH. The *in situ* generated glutathionylated products were further characterized using ¹H-NMR and UV-vis spectroscopies, and

HRMS. The thiolate-ligation from GSH in glutathionylated products was confirmed by $^1\text{H-NMR}$ and UV-vis spectroscopies.

Overall, synthetic Co(III) model complexes underwent facile glutathionylation reaction to generate thiolate-ligated glutathionylated products, though the kinetic and thermodynamic parameters differed from the reaction of GSH with aquacobalamin. Unlike aquacobalamin, these cobalt complexes reacted slower with GSH, and even the observed equilibrium constants were not stronger. Further work is needed to investigate the mechanism of this reaction to better understand the factors governing the reactivity of Co(III) center in these cobalamin model complexes, and render insight into the special reactivity of natural cobalamin.

5.2. Conclusions and future directions

The studies reported in this dissertation were aimed at exploring metal complexes derived from non-heme ligands as promising candidates for biological applications. In particular, inactivation of proteins using non-heme iron complexes, and understanding the reactivity of Co(III) center in synthetic cobalamin model complexes at the fundamental level via glutathionylation reaction were investigated. Both represent an underexplored area of research, which has not been investigated in details.

Through our studies, we have shown that non-heme iron complexes can inactivate a broad range of proteins (carbonic anhydrase-I, serine proteases (trypsin and chymotrypsin) and 20S proteasome). These results are significant because non-heme ligands bind tightly to iron with association constants in 10^{12} – 10^{15} M range and have the ability to mobilize Fe^{II} from ferritin, the major intracellular storage site for iron,

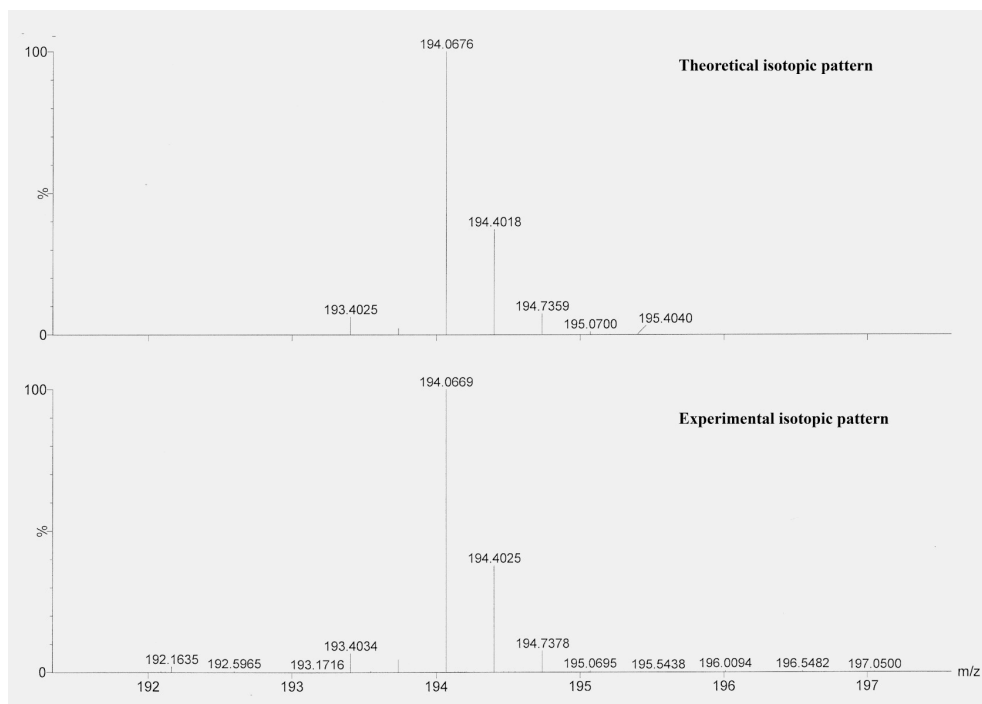
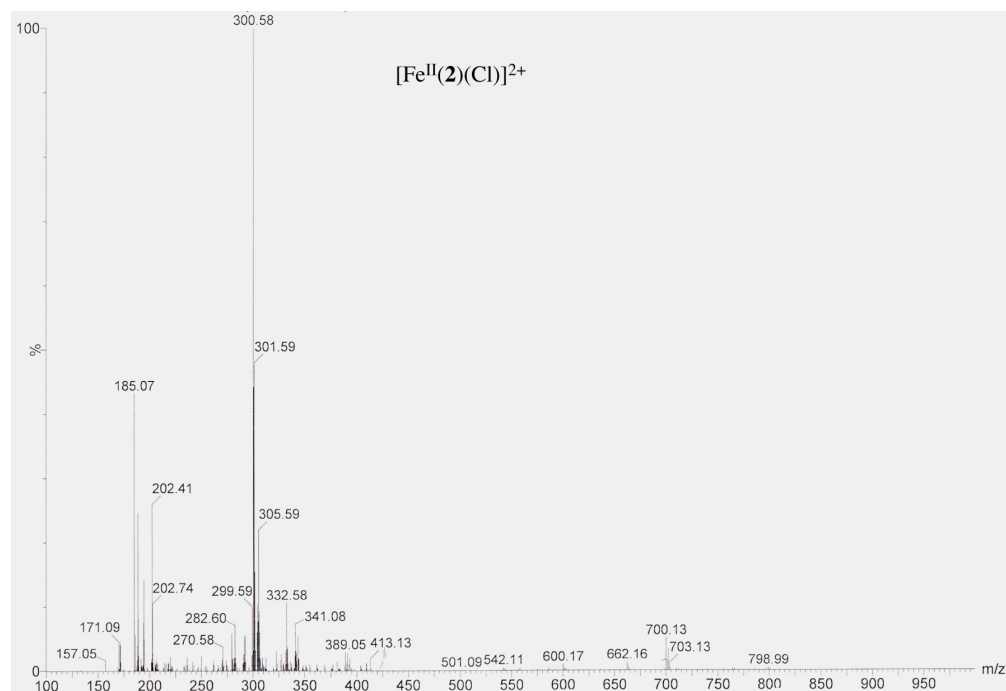
suggesting that such ligands could access iron in cells. Results from amino acid analysis for inactivation of serine protease under catalytic condition proved that tyrosine residues were selectively targeted. These results suggest that these complexes mimic the action of myeloperoxidases, a heme enzyme that is known to oxidize tyrosine residue of protein using H_2O_2 as the oxidant or even the tyrosine hydroxylase. This chemistry provides a promising future direction to target medically important target proteins that contain important tyrosine residues near the active site. Moreover, the use of H_2O_2 as an oxidant for inactivating proteins extend the scope of this study to perform *in cellulo* as H_2O_2 is a bioavailable oxidant, formed as a byproduct of aerobic respiration in cells. Due to the fact that the tumor cells produce high levels of H_2O_2 as compared to normal cells, these can be targeted selectively.^{329,330} This opens up a whole new paradigm for developing iron complexes as potential antitumor agents. My studies also established that incorporating protein-binding affinity group to non-heme iron complexes has the potential to inactivate proteins at lower concentrations. Results from amino acid analysis of enzymes, oxidized by ferryls find relevance to biology, because under conditions of oxidative stress, ferryls such as ferrylmyoglobin can oxidize proteins. Inactivation of proteasome by non-heme iron complexes make them potential therapeutic candidates toward anticancer agent, however the potency of these complexes to inactivate proteasome needs to be enhanced by attaching a binding motif that can direct these complexes selectively toward proteasomes in cell.

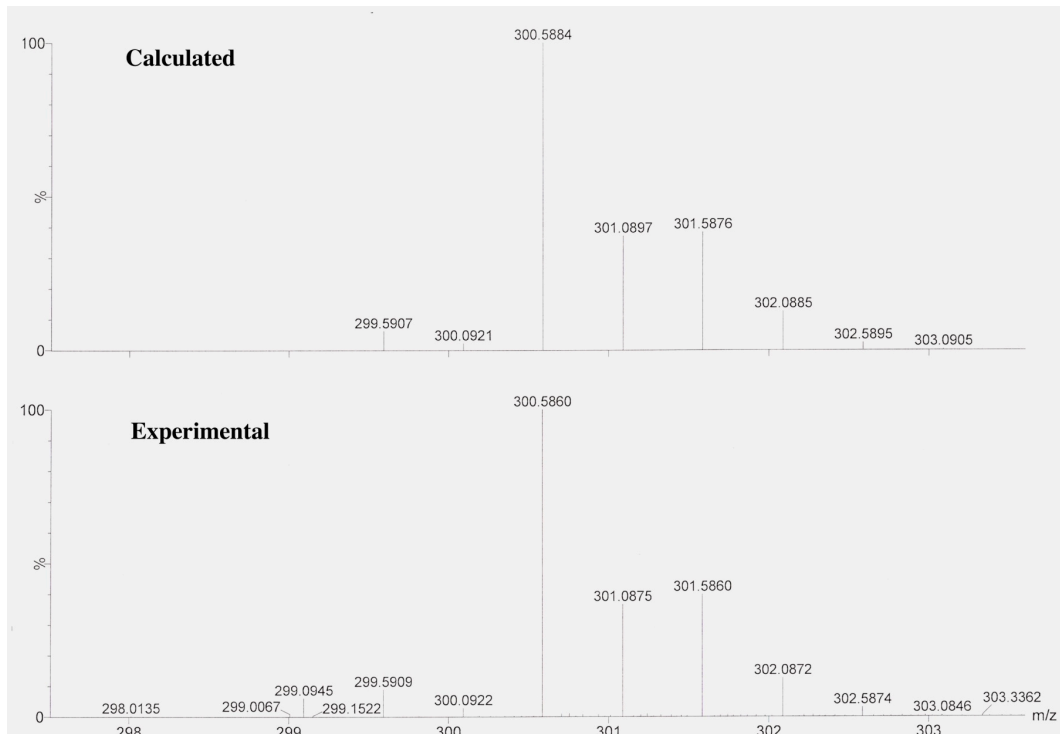
Besides the significance of non-heme ligands (as iron complexes) in protein oxidation, their Co(III) complexes find application as synthetic model systems for studying biologically important cofactor cobalamin. In this dissertation, I have reported

the first example of synthetic Co(III) model complexes derived from a unique polypyridyl non-heme ligand set, mimicking the chemistry of Cbl and undergoing glutathionylation in a similar fashion to aquacobalamin. However, the kinetic and thermodynamic parameter differs. As compared to H_2OCbl^+ , the slower rates of reaction of model cobalt complexes with GSH were attributed to difference in ligand structure around Co(III) center. Unlike highly conjugated planar corrin rings systems found in Cbl that make the Co(III) center in Cbl more like Co(II), the polypyridyl rings in model cobalt complexes adopt conformation orthogonal to the basal plane, limiting the extent of delocalization. The lower values of observed equilibrium constants for the formation of glutathionylated products could be attributed to the weak interaction of thiolate ligands with Co(III) center as a result of steric hindrance of GSH with non-heme ligands on the cobalt center. These results signify the importance of ligand structure tuning the special reactivity of H_2OCbl^+ . However, the facile glutathionylation of synthetic Co(III) model complexes suggest that this may represent a general reaction for cobalt complexes of this type. Higher abundance of GSH in cells may provide a competing reaction (glutathionylation) to the Co(III) complexes related to Cbl used in biological studies, especially with complexes containing labile ligands such as Cl^- or H_2O .

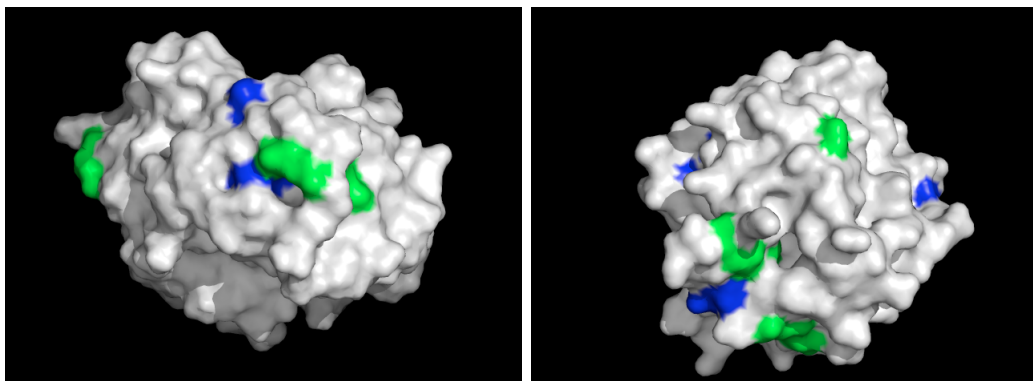
Overall, my dissertation work harnesses the potential of metal complexes (iron and cobalt) of non-heme ligands for their applications in oxidatively inactivating proteins, and understanding fundamental chemistry of important biological reaction, with future prospect of these metal complexes as excellent tools, and in the development of novel therapeutic agents.

APPENDIX A

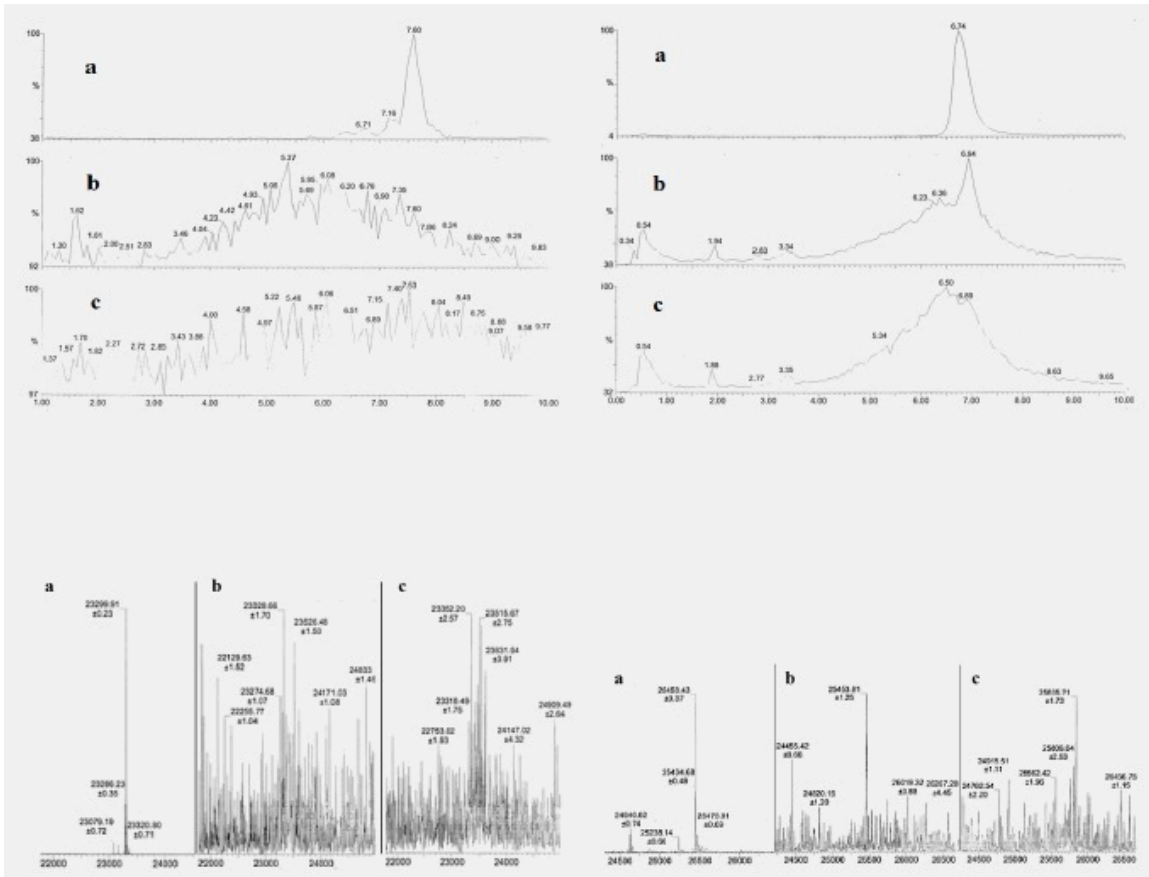
A1. HRMS data for $[\text{Fe}^{\text{IV}}(\text{O})(3\text{CG-N4Py})]^{3+}$ A2. HRMS of *in situ* generated iron complex $[\text{Fe}^{\text{II}}(3\text{CG-N4Py})\text{Cl}]^{2+}$ 

A3. HRMS data for $[\text{Fe}^{\text{II}}(\text{3CG-N4Py})(\text{Cl})]^{2+}$ 

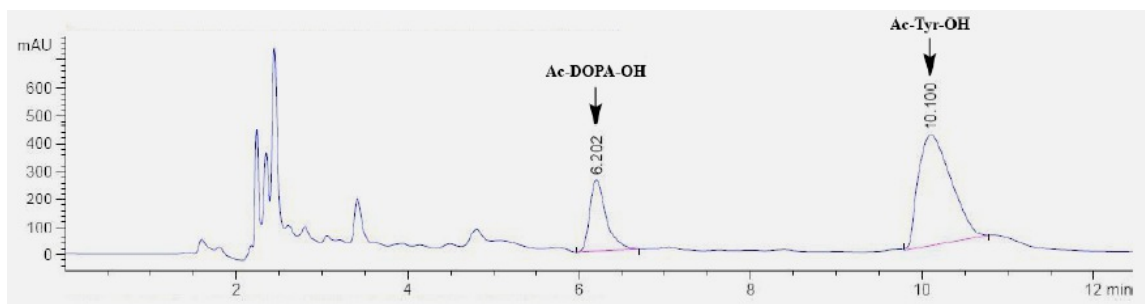
A4. Asp (blue) and Glu (green) residues on trypsin (left) and chymotrypsin (right) surface. Figures were constructed from the Protein Data Bank files 3MFJ (trypsin) and 4CHA (chymotrypsin).



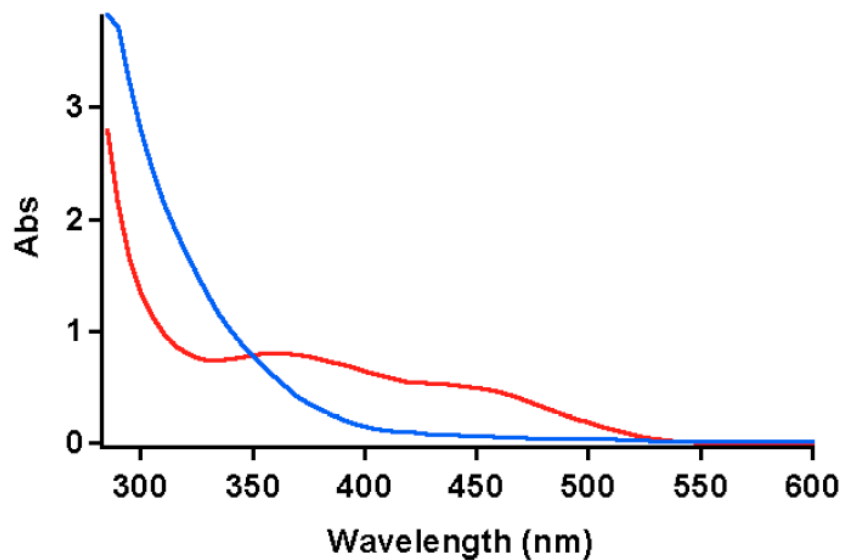
A5. Left Panels: LCMS chromatogram (top) and deconvoluted MS spectra (bottom) of trypsin (spectrum **a**) and after treatment with **10** (spectrum **b**) or **9** (**c**). Reactions were conducted at rt by incubating trypsin (1 μM) with **10** or **9** (20 μM) pulsed with H_2O_2 (40 μM) every 10 min, before desalting and subjecting the samples to LCMS analysis. Right panels: LCMS chromatogram (top) and deconvoluted MS spectra (bottom) of chymotrypsin (spectrum **a**) and after treatment with **10** (spectrum **b**) or **9** (spectrum **c**). Reactions were conducted at rt by incubating chymotrypsin (1 μM) with **10** or **9** (20 μM) and pulsed with H_2O_2 (40 μM) every 10 min, before desalting and subjecting the samples to LCMS analysis.



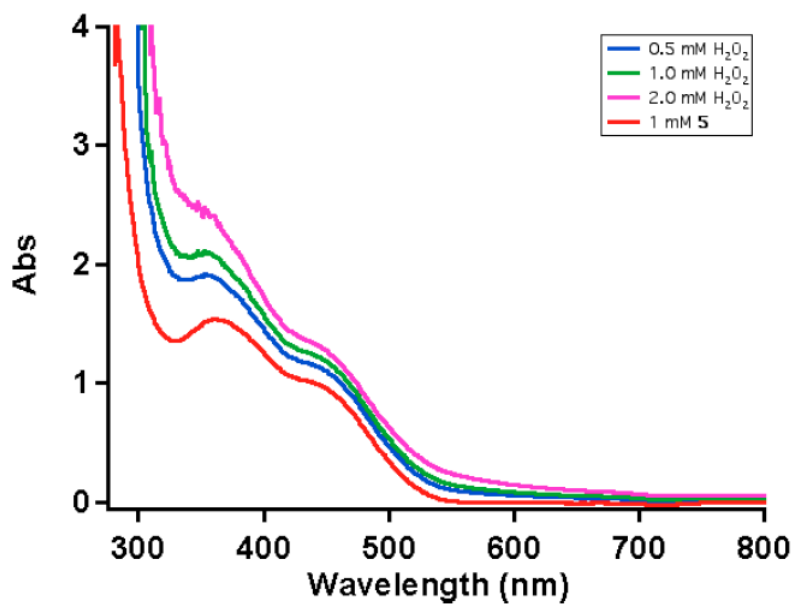
A8. HPLC chromatogram from the oxidation of **13** by $[\text{Fe}^{\text{II}}(\text{CH}_3\text{CN})(\text{N4Py})](\text{ClO}_4)_2$ and H_2O_2 shows Ac-DOPA-OH **14** as a major product



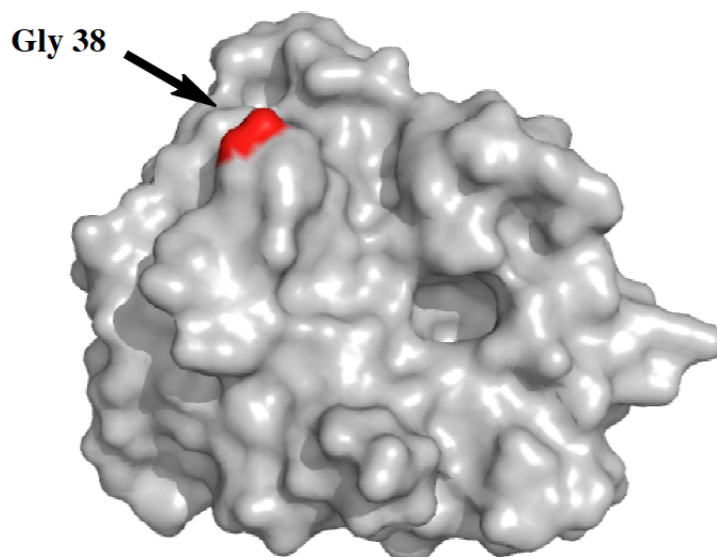
A9. Spectral change that occurs when solution of **9** in acetate buffer (0.5 mM, red) was treated with H_2O_2 (0.25 mM, blue).



A10. UV-vis spectral change of 1 mM solution of **9** (red) and Ac-Tyr-OH (**13**) in acetate buffer when the solution was pulsed with 0.5 mM (blue), 1.0 mM (green) and 2.0 mM (pink) H_2O_2 , respectively



A11. Proposed site of trypsin cleavage upon treatment with ferryl **12**. The residue Gly 38, highlighted in red is located near the active site.



A12. Amino acid analysis of trypsin (20 μM) pulsed with H_2O_2 (500 μM , total addition) in presence of **9** and **10** (50 μM)

Amino acid	Theoretical composition (%)	Experimental composition (%)	10	9
Ala	6.3	7.07	7.28	7.32
Arg	0.9	1.02	1.04	1.03
Asn/Asp	9.9	10.71	11.10	11.11
Cys	5.4	2.66	2.37	2.55
Gln/Glu	6.3	6.98	7.18	7.14
Gly	11.2	12.34	12.67	12.63
His	1.3	1.28	1.21	1.18
Ile	6.7	6.36	6.53	6.47
Leu	6.3	6.72	6.84	6.78
Lys	6.3	6.96	6.99	6.98
Met	0.9	0.62	0.64	0.67
Phe	1.3	1.56	1.57	1.52
Pro	3.6	4.15	4.18	4.19
Ser	15.2	14.6	14.81	14.81
Thr	4.5	4.53	4.65	4.63
Trp	1.8	0.79	0.78	0.69
Tyr	4.5	4.53	2.87	2.98
Val	7.6	6.91	7.02	7.02

A13. Amino acid analysis of chymotrypsin (20 μM) pulsed with H_2O_2 (500 μM , total addition) in presence of **9** and **10** (50 μM)

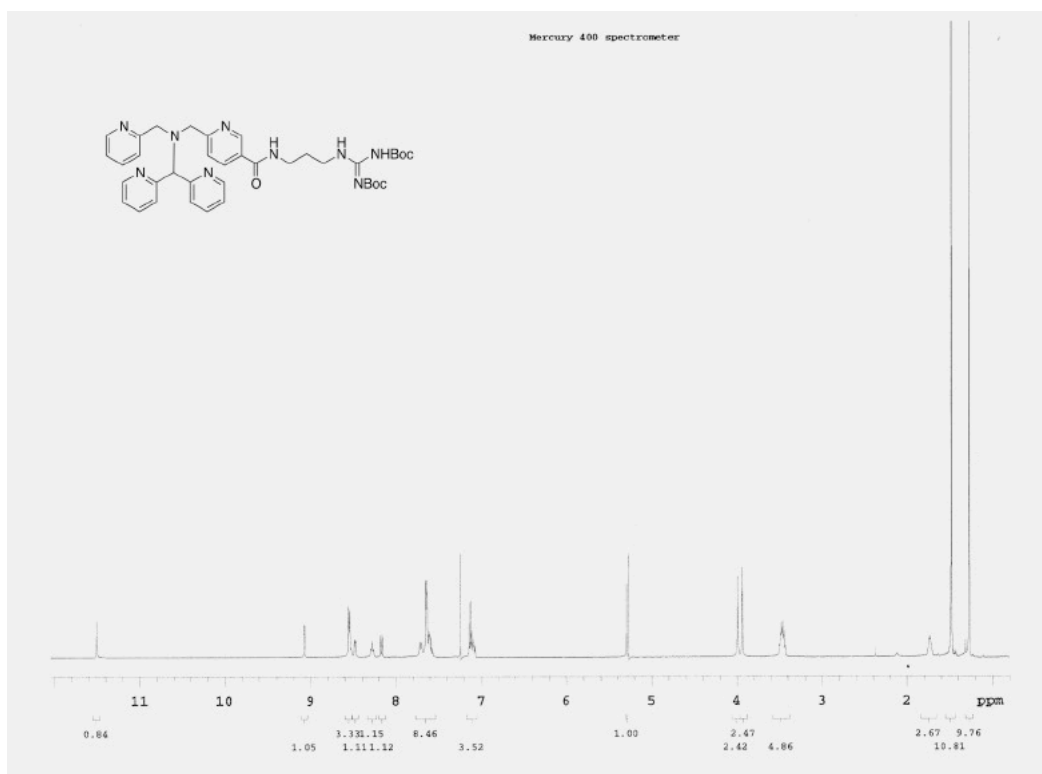
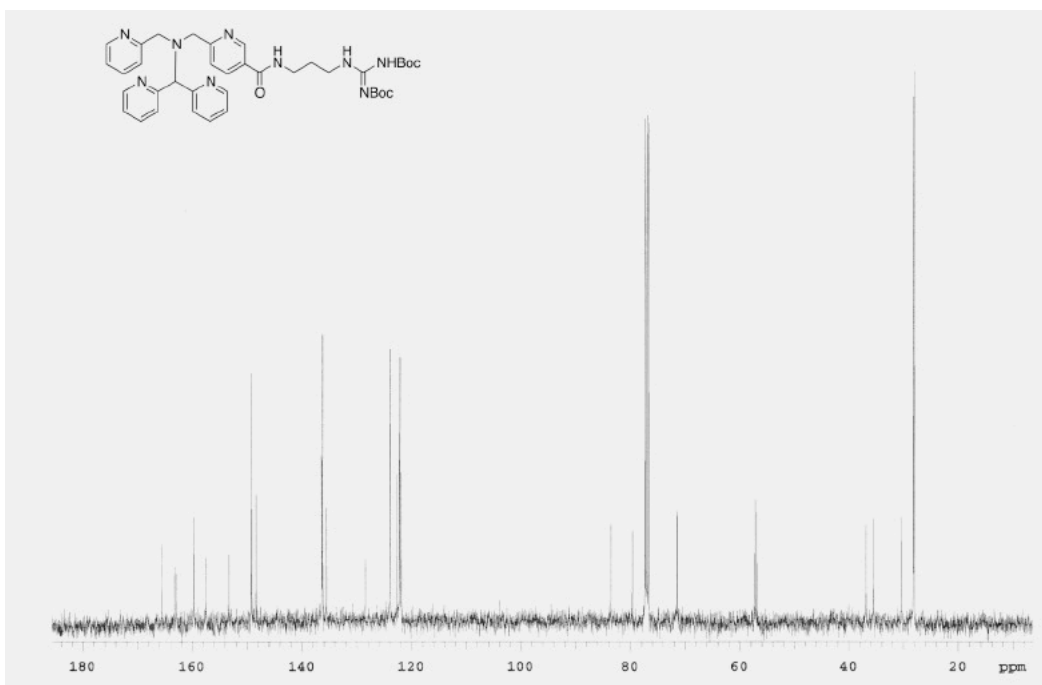
Amino acid	Theoretical composition (%)	Experimental composition (%)	10	9
Ala	9.1	9.90	9.98	9.98
Arg	1.2	1.42	1.41	1.41
Asn/Asp	9.1	9.96	10.06	10.09
Cys	4.1	1.89	1.75	1.79
Gln/Glu	6.2	6.81	6.78	6.73
Gly	9.5	10.24	10.30	10.36
His	0.8	0.84	0.81	0.81
Ile	4.1	3.96	3.97	3.98
Leu	7.9	8.29	8.27	8.23
Lys	5.8	6.44	6.40	6.44
Met	0.8	0.58	0.55	0.56
Phe	2.5	2.82	2.81	2.74
Pro	3.7	4.24	4.33	4.30
Ser	11.2	11.01	11.05	11.05
Thr	9.1	9.49	9.49	9.48
Trp	3.3	0.73	0.80	0.76
Tyr	1.7	1.77	1.41	1.47
Val	9.5	9.40	9.62	9.55

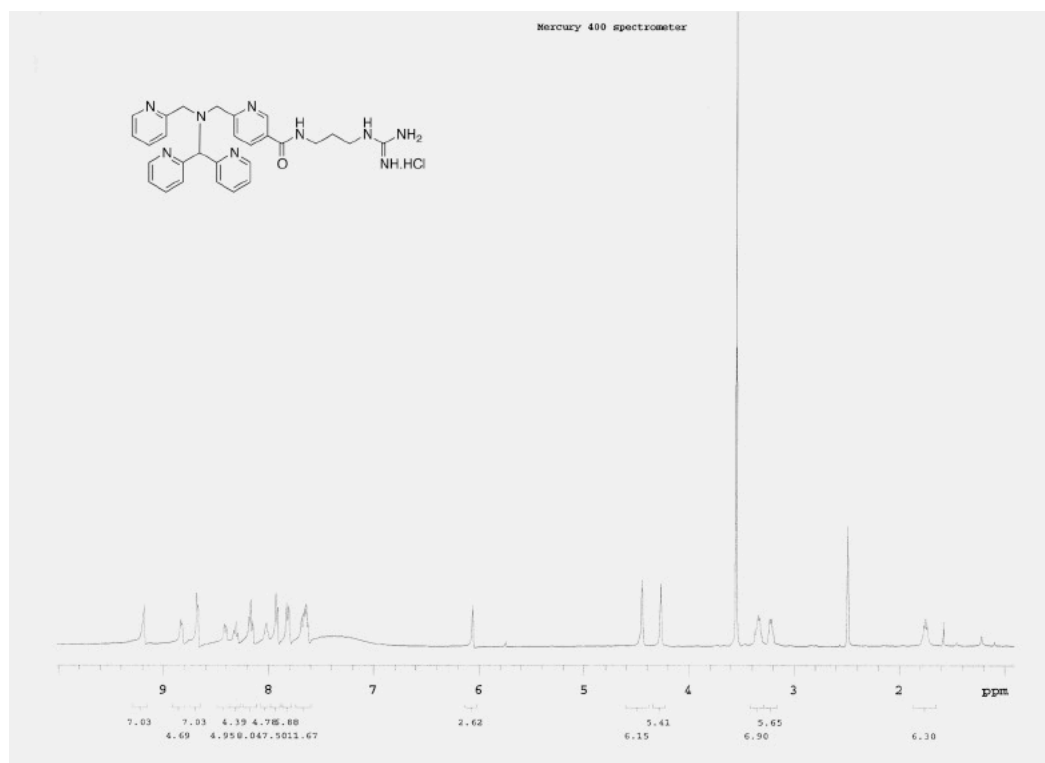
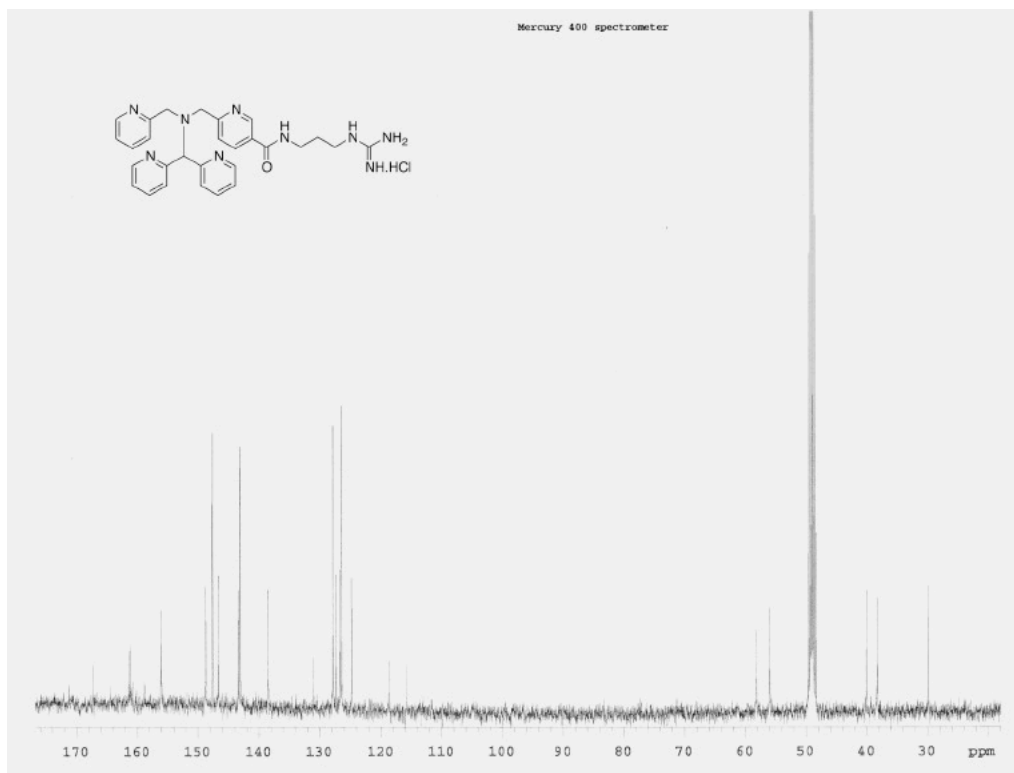
A14. Amino acid analysis of trypsin (20 μM) treated with ferryls **11** or **12** (1000 μM) along with the control

Amino acid	Theoretical composition (%)	Experimental composition (%)	12	11
Ala	6.3	7.11	7.48	7.44
Arg	0.9	1.01	0.98	1.05
Asn/Asp	9.9	10.86	11.58	11.41
Cys	5.4	2.57	0.54	0.81
Gln/Glu	6.3	6.78	6.41	6.76
Gly	11.2	11.91	12.61	12.43
His	1.3	1.34	1.34	1.31
Ile	6.7	6.55	6.93	6.87
Leu	6.3	6.67	6.87	6.86
Lys	6.3	7.14	7.21	6.71
Met	0.9	0.38	0.37	0.41
Phe	1.3	1.48	0.71	1.52
Pro	3.6	4.24	4.41	4.36
Ser	15.2	14.86	15.75	15.51
Thr	4.5	4.52	4.788	4.69
Trp	1.8	0.71	0.84	0.61
Tyr	4.5	4.49	2.92	3.31
Val	7.6	7.22	7.92	7.69

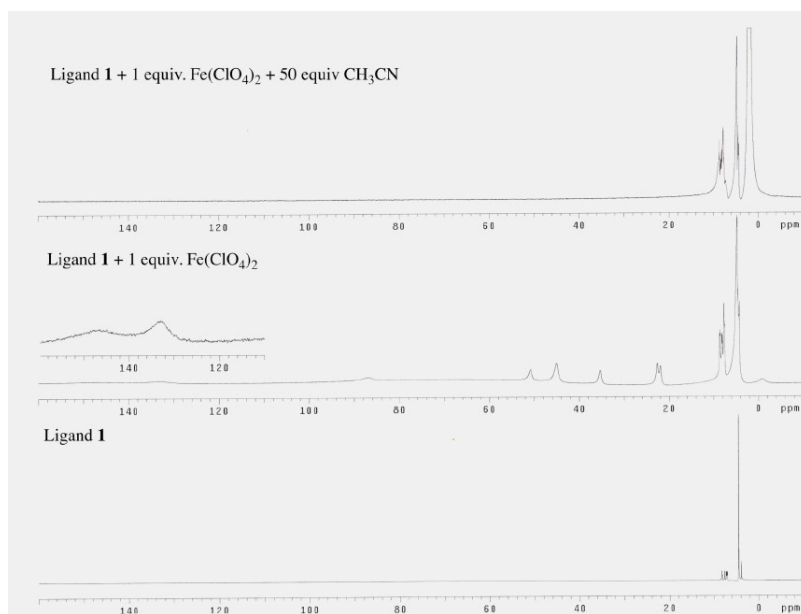
A15. Amino acid analysis of chymotrypsin (20 μ M) treated with ferryls **11** or **12** (1000 μ M) along with control

Amino acid	Theoretical composition (%)	Experimental composition (%)	12	11
Ala	9.1	10.05	10.21	10.17
Arg	1.2	1.38	1.30	1.39
Asn/Asp	9.1	9.98	10.44	10.45
Cys	4.1	1.92	0.85	0.68
Gln/Glu	6.2	6.65	6.36	6.09
Gly	9.5	9.92	10.22	10.22
His	0.8	0.86	0.83	0.83
Ile	4.1	4.01	4.16	4.24
Leu	7.9	8.22	8.37	8.52
Lys	5.8	6.59	6.22	6.01
Met	0.8	0.37	0.38	0.40
Phe	2.5	2.65	2.66	2.75
Pro	3.7	4.35	4.53	4.53
Ser	11.2	11.31	11.78	12.01
Thr	9.1	9.53	9.78	9.89
Trp	3.3	0.67	0.56	0.57
Tyr	1.7	1.62	1.02	1.05
Val	9.5	9.96	10.14	10.11

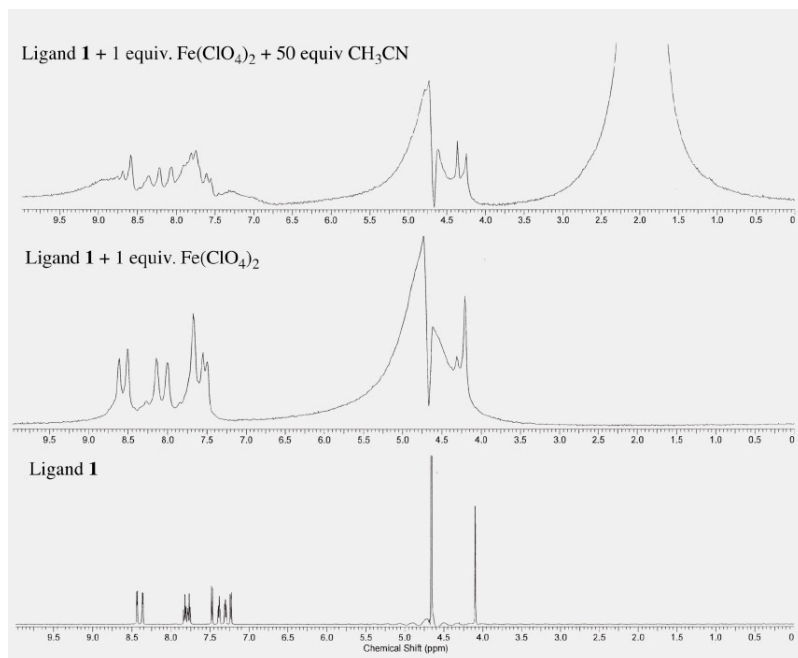
A16. ^1H -NMR spectrum for compound **6****A17.** ^{13}C -NMR spectrum for compound **6**

A18. $^1\text{H-NMR}$ spectrum for compound 7A19. $^{13}\text{C-NMR}$ spectrum for compound 7

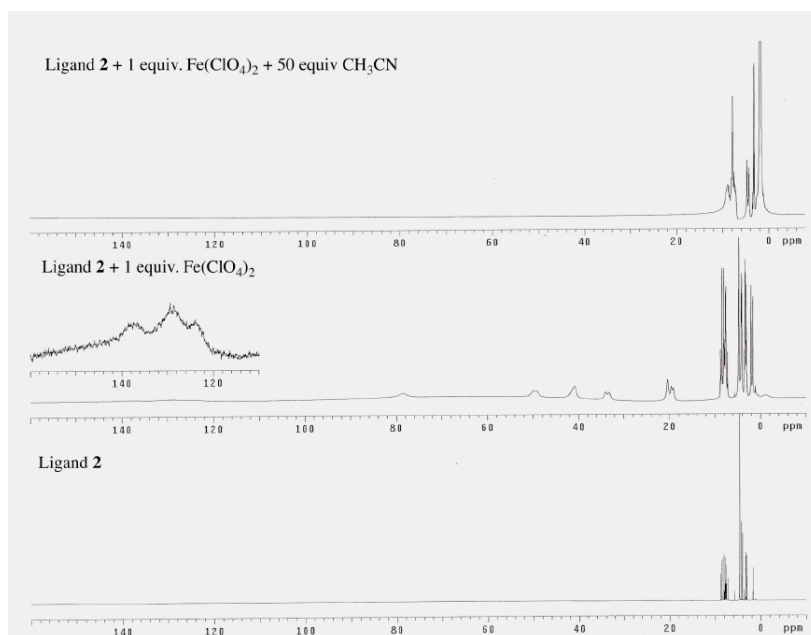
A20. $^1\text{H-NMR}$ (0-160 ppm) of ligand **8** (bottom), ligand **8** treated with 1 equiv. of $\text{Fe}^{\text{II}}(\text{ClO}_4)_2$ (middle) and ligand **8** treated with 1 equiv. of $\text{Fe}^{\text{II}}(\text{ClO}_4)_2$ and 50 equiv. of CH_3CN (top) in D_2O . Inset (middle): Peaks in 110-160 ppm



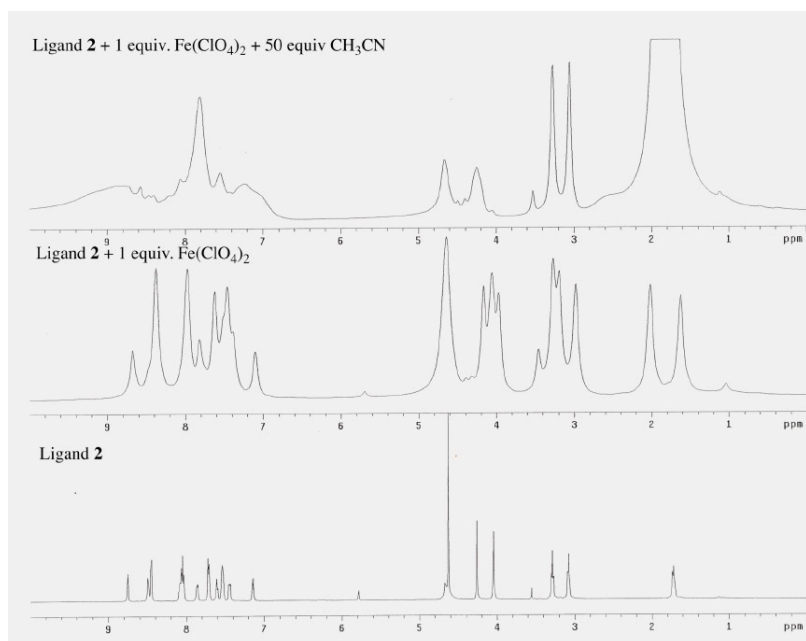
A21. $^1\text{H-NMR}$ (0-10 ppm) of ligand **8** (bottom), ligand **8** treated with 1 equiv. of $\text{Fe}^{\text{II}}(\text{ClO}_4)_2$ (middle) and ligand **8** treated with 1 equiv. of $\text{Fe}^{\text{II}}(\text{ClO}_4)_2$ followed by 50 equiv. of CH_3CN (top) in D_2O



A22. $^1\text{H-NMR}$ (0–160 ppm) of ligand **7** (bottom), ligand **7** treated with 1 equiv. of $\text{Fe}^{\text{II}}(\text{ClO}_4)_2$ (middle) and ligand **7** treated with 1 equiv. of $\text{Fe}^{\text{II}}(\text{ClO}_4)_2$ followed by 50 equiv. of CH_3CN (top) in D_2O . Inset (middle): Peaks in 110–160 ppm region

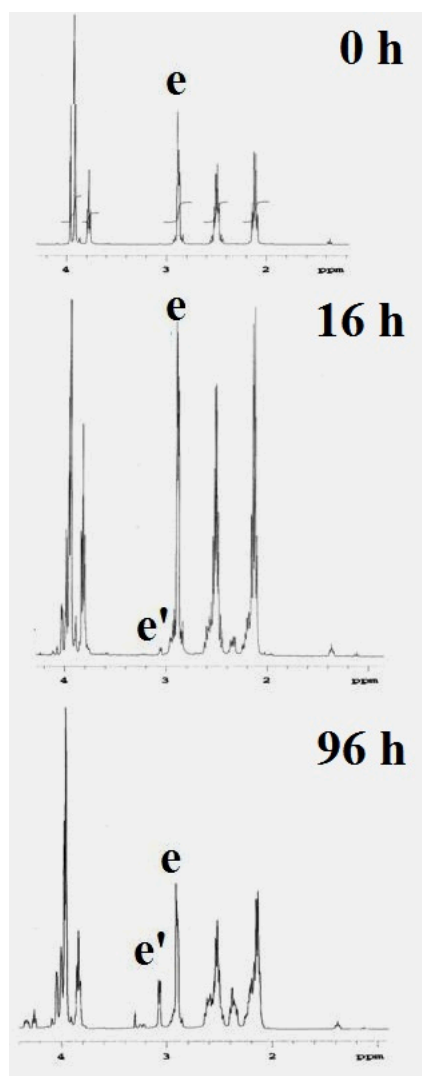


A23. $^1\text{H-NMR}$ (0–10 ppm) of ligand **7** (bottom), ligand **7** treated with 1 equiv. of $\text{Fe}^{\text{II}}(\text{ClO}_4)_2$ (middle) and ligand **7** treated with 1 equiv. of $\text{Fe}^{\text{II}}(\text{ClO}_4)_2$ followed by 50 equiv. of CH_3CN (top) in D_2O



APPENDIX B

B1. $^1\text{H-NMR}$ (1-4 ppm) spectra of reaction mixture containing $[\text{Co}^{\text{III}}(\text{N4PyCO}_2\text{Me})\text{Cl}]\text{Cl}_2$ (**3**; 10 mM) and GSH (40 mM), after a time interval of 0 h (top), 16 h (middle) and 96 h (bottom). The peak **e** (corresponding to Cys- β Hydrogen of GSH) is shifting to **e'** during the course of time showing thiolate coordination with $\text{Co}(\text{III})$ center in glutathionylated product **5**



B2. Crystal data and structure refinement for **3**·MeOH·EtOH

Empirical Formula	$C_{28}H_{33}Cl_3CoN_5O_4$
Formula weight	668.87
Crystal system	Triclinic
Space group	$P\bar{1}$
a (Å)	9.6350(3)
b (Å)	11.5595(4)
c (Å)	15.6403(5)
α (°)	97.695(2)
β (°)	106.955(1)
γ (°)	109.816(2)
V (Å ³)	1514.23(9)
Z	2
D _{calc} (mg/m ³)	1.467
Absorption coefficient, μ (mm ⁻¹)	0.874
F (000)	692
Crystal size (mm ³)	0.29 x 0.26 x 0.18
θ -range for data collection (°)	1.94 to 28.48
Limiting indices	$-12 \leq h \leq 12, -15 \leq k \leq 15$ $0 \leq l \leq 20$
Unique Reflections	36734 / 7571 [R (int) = 0.0342]
Goodness-of-fit on F_o^2	1.033
Final R indices [$I > 2\sigma(I)$]	R1 = 0.0450, wR2 = 0.1227
R indices (all data)	R1 = 0.0530, wR2 = 0.1269
Highest peak and deepest hole (e.Å ⁻³)	1.642 and -0.388

B3. Atomic coordinates ($\times 10^4$) and equivalent isotropic displacement parameters ($\text{\AA}^2 \times 10^3$) for **3**.MeOH.EtOH. U(eq) is defined as one third of the trace of the orthogonalized Uij tensor.

	x	y	z	U(eq)
Co(1)	2942(1)	9263(1)	2722(1)	14(1)
N(1)	2305(2)	9959(2)	1690(1)	15(1)
C(1)	2151(3)	11170(2)	2017(2)	17(1)
C(2)	1979(3)	11239(2)	2937(2)	17(1)
C(3)	1511(3)	12140(3)	3307(2)	23(1)
C(4)	1405(3)	12182(3)	4170(2)	26(1)
C(5)	1748(3)	11319(3)	4645(2)	23(1)
C(6)	2211(3)	10446(2)	4244(2)	19(1)
C(7)	1587(3)	11378(3)	5570(2)	28(1)
O(1)	1009(3)	12039(3)	5865(2)	48(1)
O(2)	2119(2)	10622(2)	6016(1)	30(1)
C(8)	2119(4)	10729(3)	6958(2)	31(1)
N(2)	2320(2)	10406(2)	3399(1)	16(1)
C(9)	785(3)	8991(2)	962(2)	18(1)
C(10)	-38(3)	7997(2)	1372(2)	18(1)
C(11)	-1592(3)	7133(3)	897(2)	25(1)
C(12)	-2267(3)	6217(3)	1302(2)	29(1)
C(13)	-1409(3)	6195(3)	2174(2)	29(1)
C(14)	133(3)	7097(2)	2626(2)	23(1)
N(3)	810(2)	7976(2)	2222(1)	17(1)
C(15)	3722(3)	10177(2)	1396(2)	16(1)
C(16)	5133(3)	11010(2)	2252(2)	16(1)
C(17)	6467(3)	11990(2)	2289(2)	21(1)
C(18)	7675(3)	12609(3)	3143(2)	28(1)
C(19)	7499(3)	12244(3)	3927(2)	29(1)
C(20)	6119(3)	11255(3)	3846(2)	23(1)
N(4)	4971(2)	10642(2)	3018(1)	16(1)
C(21)	3805(3)	8890(2)	1228(2)	17(1)
C(22)	4194(3)	8369(2)	535(2)	21(1)
C(23)	4271(3)	7185(3)	507(2)	25(1)
C(24)	3943(3)	6564(3)	1174(2)	25(1)
C(25)	3561(3)	7142(2)	1855(2)	21(1)
N(5)	3508(2)	8288(2)	1881(1)	17(1)
Cl(1)	3829(1)	8473(1)	3885(1)	21(1)
Cl(2)	4419(1)	13629(1)	1340(1)	24(1)
Cl(3)	1886(1)	9566(1)	-982(1)	23(1)
O(3)	9456(3)	3368(3)	1699(2)	51(1)
C(26)	10146(4)	3945(3)	1101(3)	43(1)
O(4)	1274(6)	4792(4)	4976(3)	37(1)

C(27)	1953(9)	5337(7)	4356(5)	46(2)
C(28)	1184(2)	4951(1)	3404(8)	89(3)
O(5)	3895(6)	4877(5)	2999(4)	49(1)
C(29)	5216(8)	5402(6)	3643(5)	39(1)
C(30)	5815(8)	4596(6)	3512(5)	39(1)

B4. Bond lengths [Å] and angles [deg] for 3.MeOH.EtOH.

Co(1)-N(3)	1.930(2)
Co(1)-N(1)	1.933(2)
Co(1)-N(5)	1.933(2)
Co(1)-N(4)	1.933(2)
Co(1)-N(2)	1.938(2)
Co(1)-Cl(1)	2.222(6)
N(1)-C(1)	1.496(3)
N(1)-C(9)	1.506(3)
N(1)-C(15)	1.518(3)
C(1)-C(2)	1.491(3)
C(2)-N(2)	1.349(3)
C(2)-C(3)	1.390(3)
C(3)-C(4)	1.379(4)
C(4)-C(5)	1.391(4)
C(5)-C(6)	1.383(4)
C(5)-C(7)	1.494(4)
C(6)-N(2)	1.353(3)
C(7)-O(1)	1.205(4)
C(7)-O(2)	1.331(4)
O(2)-C(8)	1.462(3)
C(9)-C(10)	1.496(3)
C(10)-N(3)	1.351(3)
C(10)-C(11)	1.389(3)
C(11)-C(12)	1.378(4)
C(12)-C(13)	1.382(4)
C(13)-C(14)	1.390(4)
C(14)-N(3)	1.350(3)
C(15)-C(21)	1.508(3)
C(15)-C(16)	1.508(3)
C(16)-N(4)	1.357(3)
C(16)-C(17)	1.375(3)
C(17)-C(18)	1.387(4)
C(18)-C(19)	1.386(4)
C(19)-C(20)	1.388(4)
C(20)-N(4)	1.338(3)

C(21)-N(5)	1.354(3)
C(21)-C(22)	1.377(3)
C(22)-C(23)	1.391(4)
C(23)-C(24)	1.393(4)
C(24)-C(25)	1.387(4)
C(25)-N(5)	1.339(3)
O(3)-C(26)	1.412(4)
O(4)-C(27)	1.421(9)
C(27)-C(28)	1.386(1)
O(5)-C(29)	1.252(8)
C(29)-C(30)	1.275(9)
N(3)-Co(1)-N(1)	86.4(8)
N(3)-Co(1)-N(5)	89.5(8)
N(1)-Co(1)-N(5)	83.6(9)
N(3)-Co(1)-N(4)	169.7(9)
N(1)-Co(1)-N(4)	83.4(8)
N(5)-Co(1)-N(4)	87.9(9)
N(3)-Co(1)-N(2)	91.5(8)
N(1)-Co(1)-N(2)	86.4(8)
N(5)-Co(1)-N(2)	169.8(9)
N(4)-Co(1)-N(2)	89.4(8)
N(3)-Co(1)-Cl(1)	96.3(6)
N(1)-Co(1)-Cl(1)	175.8(6)
N(5)-Co(1)-Cl(1)	93.3(6)
N(4)-Co(1)-Cl(1)	93.8(6)
N(2)-Co(1)-Cl(1)	96.7(6)
C(1)-N(1)-C(9)	111.7(2)
C(1)-N(1)-C(15)	112.7(2)
C(9)-N(1)-C(15)	112.9(2)
C(1)-N(1)-Co(1)	110.1(1)
C(9)-N(1)-Co(1)	109.9(1)
C(15)-N(1)-Co(1)	98.9(1)
C(2)-C(1)-N(1)	110.1(2)
N(2)-C(2)-C(3)	121.7(2)
N(2)-C(2)-C(1)	117.2(2)
C(3)-C(2)-C(1)	121.1(2)
C(4)-C(3)-C(2)	118.8(2)
C(3)-C(4)-C(5)	119.7(2)
C(6)-C(5)-C(4)	119.0(2)
C(6)-C(5)-C(7)	122.9(2)
C(4)-C(5)-C(7)	118.0(2)
N(2)-C(6)-C(5)	121.4(2)
O(1)-C(7)-O(2)	124.2(3)
O(1)-C(7)-C(5)	122.3(3)
O(2)-C(7)-C(5)	113.4(2)
C(7)-O(2)-C(8)	115.5(2)

C(2)-N(2)-C(6)	119.4(2)
C(2)-N(2)-Co(1)	112.9(2)
C(6)-N(2)-Co(1)	127.7(2)
C(10)-C(9)-N(1)	110.1(2)
N(3)-C(10)-C(11)	121.9(2)
N(3)-C(10)-C(9)	116.6(2)
C(11)-C(10)-C(9)	121.5(2)
C(12)-C(11)-C(10)	118.6(3)
C(11)-C(12)-C(13)	119.8(3)
C(12)-C(13)-C(14)	119.2(3)
N(3)-C(14)-C(13)	121.1(3)
C(14)-N(3)-C(10)	119.3(2)
C(14)-N(3)-Co(1)	127.1(2)
C(10)-N(3)-Co(1)	113.6(2)
C(21)-C(15)-C(16)	106.4(2)
C(21)-C(15)-N(1)	104.4(2)
C(16)-C(15)-N(1)	104.8(2)
N(4)-C(16)-C(17)	122.2(2)
N(4)-C(16)-C(15)	111.1(2)
C(17)-C(16)-C(15)	126.7(2)
C(16)-C(17)-C(18)	118.1(2)
C(19)-C(18)-C(17)	119.8(2)
C(18)-C(19)-C(20)	119.5(3)
N(4)-C(20)-C(19)	120.5(2)
C(20)-N(4)-C(16)	120.0(2)
C(20)-N(4)-Co(1)	128.6(2)
C(16)-N(4)-Co(1)	111.3(2)
N(5)-C(21)-C(22)	121.9(2)
N(5)-C(21)-C(15)	111.6(2)
C(22)-C(21)-C(15)	126.4(2)
C(21)-C(22)-C(23)	118.5(2)
C(22)-C(23)-C(24)	119.2(2)
C(25)-C(24)-C(23)	119.4(2)
N(5)-C(25)-C(24)	120.8(2)
C(25)-N(5)-C(21)	120.1(2)
C(25)-N(5)-Co(1)	128.9(2)
C(21)-N(5)-Co(1)	110.9(1)
C(28)-C(27)-O(4)	123.2(8)
O(5)-C(29)-C(30)	100.6(6)

B5. Anisotropic displacement parameters ($\text{Å}^2 \times 10^3$) for **3**.MeOH.EtOH. The anisotropic displacement factor exponent takes the form: $-2 \pi^2 [h^2 a^{*2} U_{11} + \dots + 2 h k a^* b^* U_{12}]$

	U11	U22	U33	U23	U13	U12
Co(1)	13(1)	17(1)	13(1)	7(1)	6(1)	7(1)
N(1)	12(1)	20(1)	14(1)	7(1)	6(1)	7(1)
C(1)	18(1)	19(1)	19(1)	8(1)	9(1)	10(1)
C(2)	14(1)	20(1)	18(1)	5(1)	6(1)	6(1)
C(3)	25(1)	25(1)	26(1)	9(1)	11(1)	14(1)
C(4)	29(1)	28(1)	25(1)	4(1)	12(1)	15(1)
C(5)	22(1)	28(1)	19(1)	4(1)	10(1)	11(1)
C(6)	19(1)	24(1)	15(1)	7(1)	7(1)	8(1)
C(7)	28(1)	35(1)	23(1)	6(1)	13(1)	13(1)
O(1)	72(2)	67(2)	35(1)	20(1)	35(1)	49(2)
O(2)	33(1)	42(1)	22(1)	11(1)	16(1)	19(1)
C(8)	29(1)	48(2)	20(1)	11(1)	14(1)	17(1)
N(2)	15(1)	19(1)	16(1)	6(1)	7(1)	7(1)
C(9)	15(1)	23(1)	15(1)	5(1)	4(1)	6(1)
C(10)	16(1)	20(1)	20(1)	5(1)	8(1)	9(1)
C(11)	18(1)	26(1)	26(1)	3(1)	6(1)	7(1)
C(12)	18(1)	25(1)	40(2)	4(1)	11(1)	4(1)
C(13)	25(1)	25(1)	39(2)	12(1)	19(1)	6(1)
C(14)	23(1)	25(1)	28(1)	12(1)	15(1)	10(1)
N(3)	17(1)	18(1)	20(1)	7(1)	10(1)	8(1)
C(15)	13(1)	23(1)	16(1)	8(1)	8(1)	9(1)
C(16)	15(1)	21(1)	18(1)	8(1)	7(1)	10(1)
C(17)	19(1)	23(1)	27(1)	11(1)	12(1)	11(1)
C(18)	17(1)	27(1)	35(2)	11(1)	8(1)	3(1)
C(19)	18(1)	32(1)	27(1)	5(1)	0(1)	5(1)
C(20)	19(1)	29(1)	19(1)	8(1)	4(1)	10(1)
N(4)	14(1)	19(1)	16(1)	6(1)	7(1)	8(1)
C(21)	16(1)	21(1)	17(1)	6(1)	6(1)	8(1)
C(22)	18(1)	26(1)	20(1)	7(1)	10(1)	10(1)
C(23)	25(1)	27(1)	25(1)	4(1)	12(1)	12(1)
C(24)	25(1)	22(1)	31(1)	7(1)	12(1)	12(1)
C(25)	19(1)	21(1)	25(1)	8(1)	9(1)	9(1)
N(5)	15(1)	20(1)	16(1)	6(1)	7(1)	7(1)
Cl(1)	24(1)	26(1)	18(1)	12(1)	9(1)	13(1)
Cl(2)	24(1)	25(1)	29(1)	15(1)	12(1)	12(1)
Cl(3)	18(1)	33(1)	20(1)	9(1)	7(1)	13(1)
O(3)	59(2)	37(1)	61(2)	8(1)	41(1)	10(1)
C(26)	39(2)	34(2)	58(2)	13(2)	28(2)	10(1)

B6. Hydrogen coordinates ($\times 10^4$) and isotropic displacement parameters ($\text{Å}^2 \times 10^3$) for 3.MeOH.EtOH.

	x	y	z	U(eq)
H(1A)	3099	11906	2065	20
H(1B)	1214	11208	1564	20
H(3)	1269	12717	2971	28
H(4)	1099	12797	4438	31
H(6)	2457	9861	4569	23
H(8A)	2847	11586	7345	37
H(8B)	2461	10099	7212	37
H(8C)	1049	10574	6948	37
H(9A)	89	9420	703	22
H(9B)	1016	8586	452	22
H(11)	-2177	7172	304	30
H(12)	-3319	5603	984	35
H(13)	-1867	5571	2461	34
H(14)	720	7094	3230	28
H(15)	3653	10545	849	19
H(17)	6559	12236	1745	25
H(18)	8619	13281	3191	34
H(19)	8319	12667	4515	35
H(20)	5987	11011	4383	27
H(22)	4405	8808	85	25
H(23)	4544	6804	39	30
H(24)	3982	5752	1162	30
H(25)	3333	6719	2309	25
H(103)	8930	2440	1440	54
H(26A)	10474	4869	1294	51
H(26B)	9372	3613	466	51
H(26C)	11072	3755	1126	51
H(104)	434	4899	4914	45
H(27A)	2223	6263	4543	55
H(27B)	2968	5237	4482	55
H(28A)	404	4071	3225	106
H(28B)	1958	5002	3104	106
H(28C)	645	5506	3209	106
H(105)	4025	4790	2489	59
H(29A)	5108	5503	4256	46
H(29B)	5848	6242	3583	46
H(30A)	5316	3846	3713	46
H(30B)	6955	4981	3869	46
H(30C)	5635	4339	2853	46

B7. Torsion angles [deg] for **3**.MeOH.EtOH

N(3)-Co(1)-N(1)-C(1)	107.6(2)
N(5)-Co(1)-N(1)-C(1)	-162.5(2)
N(4)-Co(1)-N(1)-C(1)	-73.9(2)
N(2)-Co(1)-N(1)-C(1)	15.9(2)
Cl(1)-Co(1)-N(1)-C(1)	-121.3(8)
N(3)-Co(1)-N(1)-C(9)	-15.8(2)
N(5)-Co(1)-N(1)-C(9)	74.1(2)
N(4)-Co(1)-N(1)-C(9)	162.6(2)
N(2)-Co(1)-N(1)-C(9)	-107.6(2)
Cl(1)-Co(1)-N(1)-C(9)	115.3(8)
N(3)-Co(1)-N(1)-C(15)	-134.2(1)
N(5)-Co(1)-N(1)-C(15)	-44.3(1)
N(4)-Co(1)-N(1)-C(15)	44.3(1)
N(2)-Co(1)-N(1)-C(15)	134.1(1)
Cl(1)-Co(1)-N(1)-C(15)	-3.1(1)
C(9)-N(1)-C(1)-C(2)	102.9(2)
C(15)-N(1)-C(1)-C(2)	-128.8(2)
Co(1)-N(1)-C(1)-C(2)	-19.6(2)
N(1)-C(1)-C(2)-N(2)	13.7(3)
N(1)-C(1)-C(2)-C(3)	-167.3(2)
N(2)-C(2)-C(3)-C(4)	0.4(4)
C(1)-C(2)-C(3)-C(4)	-178.6(2)
C(2)-C(3)-C(4)-C(5)	-0.7(4)
C(3)-C(4)-C(5)-C(6)	0.9(4)
C(3)-C(4)-C(5)-C(7)	-178.8(3)
C(4)-C(5)-C(6)-N(2)	-0.7(4)
C(7)-C(5)-C(6)-N(2)	178.9(2)
C(6)-C(5)-C(7)-O(1)	-171.2(3)
C(4)-C(5)-C(7)-O(1)	8.5(4)
C(6)-C(5)-C(7)-O(2)	7.9(4)
C(4)-C(5)-C(7)-O(2)	-172.4(2)
O(1)-C(7)-O(2)-C(8)	-6.2(4)
C(5)-C(7)-O(2)-C(8)	174.8(2)
C(3)-C(2)-N(2)-C(6)	-0.2(3)
C(1)-C(2)-N(2)-C(6)	178.8(2)
C(3)-C(2)-N(2)-Co(1)	-179.9(2)
C(1)-C(2)-N(2)-Co(1)	-0.9(3)
C(5)-C(6)-N(2)-C(2)	0.3(4)
C(5)-C(6)-N(2)-Co(1)	-179.9(1)
N(3)-Co(1)-N(2)-C(2)	-95.0(2)
N(1)-Co(1)-N(2)-C(2)	-8.8(2)
N(5)-Co(1)-N(2)-C(2)	0.6(6)
N(4)-Co(1)-N(2)-C(2)	74.7(2)


Cl(1)-Co(1)-N(2)-C(2)	168.4(2)
N(3)-Co(1)-N(2)-C(6)	85.3(2)
N(1)-Co(1)-N(2)-C(6)	171.5(2)
N(5)-Co(1)-N(2)-C(6)	-179.1(4)
N(4)-Co(1)-N(2)-C(6)	-105.1(2)
Cl(1)-Co(1)-N(2)-C(6)	-11.3(2)
C(1)-N(1)-C(9)-C(10)	-103.5(2)
C(15)-N(1)-C(9)-C(10)	128.4(2)
Co(1)-N(1)-C(9)-C(10)	19.0(2)
N(1)-C(9)-C(10)-N(3)	-12.7(3)
N(1)-C(9)-C(10)-C(11)	168.0(2)
N(3)-C(10)-C(11)-C(12)	-1.2(4)
C(9)-C(10)-C(11)-C(12)	178.2(2)
C(10)-C(11)-C(12)-C(13)	1.5(4)
C(11)-C(12)-C(13)-C(14)	-0.4(4)
C(12)-C(13)-C(14)-N(3)	-1.2(4)
C(13)-C(14)-N(3)-C(10)	1.5(4)
C(13)-C(14)-N(3)-Co(1)	-178.1(2)
C(11)-C(10)-N(3)-C(14)	-0.4(4)
C(9)-C(10)-N(3)-C(14)	-179.7(2)
C(11)-C(10)-N(3)-Co(1)	179.3(2)
C(9)-C(10)-N(3)-Co(1)	-0.1(3)
N(1)-Co(1)-N(3)-C(14)	-171.0(2)
N(5)-Co(1)-N(3)-C(14)	105.4(2)
N(4)-Co(1)-N(3)-C(14)	-179.5(4)
N(2)-Co(1)-N(3)-C(14)	-84.8(2)
Cl(1)-Co(1)-N(3)-C(14)	12.1(2)
N(1)-Co(1)-N(3)-C(10)	9.3(2)
N(5)-Co(1)-N(3)-C(10)	-74.2(2)
N(4)-Co(1)-N(3)-C(10)	0.9(6)
N(2)-Co(1)-N(3)-C(10)	95.6(2)
Cl(1)-Co(1)-N(3)-C(10)	-167.5(2)
C(1)-N(1)-C(15)-C(21)	172.0(2)
C(9)-N(1)-C(15)-C(21)	-60.3(2)
Co(1)-N(1)-C(15)-C(21)	55.8(2)
C(1)-N(1)-C(15)-C(16)	60.4(2)
C(9)-N(1)-C(15)-C(16)	-171.9(2)
Co(1)-N(1)-C(15)-C(16)	-55.8(2)
C(21)-C(15)-C(16)-N(4)	-69.9(2)
N(1)-C(15)-C(16)-N(4)	40.3(2)
C(21)-C(15)-C(16)-C(17)	107.6(3)
N(1)-C(15)-C(16)-C(17)	-142.2(2)
N(4)-C(16)-C(17)-C(18)	0.2(4)
C(15)-C(16)-C(17)-C(18)	-177.1(2)
C(16)-C(17)-C(18)-C(19)	-1.0(4)
C(17)-C(18)-C(19)-C(20)	0.4(4)
C(18)-C(19)-C(20)-N(4)	1.0(4)

C(19)-C(20)-N(4)-C(16)	-1.9(4)
C(19)-C(20)-N(4)-Co(1)	-179.0(2)
C(17)-C(16)-N(4)-C(20)	1.3(4)
C(15)-C(16)-N(4)-C(20)	178.9(2)
C(17)-C(16)-N(4)-Co(1)	178.9(2)
C(15)-C(16)-N(4)-Co(1)	-3.5(2)
N(3)-Co(1)-N(4)-C(20)	160.7(4)
N(1)-Co(1)-N(4)-C(20)	152.2(2)
N(5)-Co(1)-N(4)-C(20)	-124.0(2)
N(2)-Co(1)-N(4)-C(20)	65.8(2)
Cl(1)-Co(1)-N(4)-C(20)	-30.8(2)
N(3)-Co(1)-N(4)-C(16)	-16.6(6)
N(1)-Co(1)-N(4)-C(16)	-25.2(2)
N(5)-Co(1)-N(4)-C(16)	58.6(2)
N(2)-Co(1)-N(4)-C(16)	-111.6(2)
Cl(1)-Co(1)-N(4)-C(16)	151.8(2)
C(16)-C(15)-C(21)-N(5)	69.6(2)
N(1)-C(15)-C(21)-N(5)	-40.9(2)
C(16)-C(15)-C(21)-C(22)	-107.7(3)
N(1)-C(15)-C(21)-C(22)	141.7(2)
N(5)-C(21)-C(22)-C(23)	0.4(4)
C(15)-C(21)-C(22)-C(23)	177.5(2)
C(21)-C(22)-C(23)-C(24)	0.4(4)
C(22)-C(23)-C(24)-C(25)	-0.5(4)
C(23)-C(24)-C(25)-N(5)	-0.2(4)
C(24)-C(25)-N(5)-C(21)	1.1(4)
C(24)-C(25)-N(5)-Co(1)	177.7(2)
C(22)-C(21)-N(5)-C(25)	-1.2(4)
C(15)-C(21)-N(5)-C(25)	-178.7(2)
C(22)-C(21)-N(5)-Co(1)	-178.3(2)
C(15)-C(21)-N(5)-Co(1)	4.2(2)
N(3)-Co(1)-N(5)-C(25)	-65.7(2)
N(1)-Co(1)-N(5)-C(25)	-152.1(2)
N(4)-Co(1)-N(5)-C(25)	124.3(2)
N(2)-Co(1)-N(5)-C(25)	-161.5(4)
Cl(1)-Co(1)-N(5)-C(25)	30.6(2)
N(3)-Co(1)-N(5)-C(21)	111.1(2)
N(1)-Co(1)-N(5)-C(21)	24.7(2)
N(4)-Co(1)-N(5)-C(21)	-58.9(2)
N(2)-Co(1)-N(5)-C(21)	15.3(6)
Cl(1)-Co(1)-N(5)-C(21)	-152.6(2)


Symmetry transformations used to generate equivalent atoms

APPENDIX C


C1.



Copyright Clearance Center



[Home](#)
[Create Account](#)
[Help](#)



ACS Publications Title: Selective Inactivation of Serine Proteases by Nonheme Iron Complexes
 Author: Jai Prakash et al.
 Publication: Inorganic Chemistry
 Publisher: American Chemical Society
 Date: May 1, 2011
 Copyright © 2011, American Chemical Society

User ID

Password

Enable Auto Login

[LOGIN](#)

[Forgot Password/User ID?](#)

If you're a copyright.com user, you can login to RightsLink using your copyright.com credentials. Already a RightsLink user or want to [learn more?](#)

PERMISSION/LICENSE IS GRANTED FOR YOUR ORDER AT NO CHARGE

This type of permission/license, instead of the standard Terms & Conditions, is sent to you because no fee is being charged for your order. Please note the following:

- Permission is granted for your request in both print and electronic formats, and translations.
- If figures and/or tables were requested, they may be adapted or used in part.
- Please print this page for your records and send a copy of it to your publisher/graduate school.
- Appropriate credit for the requested material should be given as follows: "Reprinted (adapted) with permission from (COMPLETE REFERENCE CITATION). Copyright (YEAR) American Chemical Society." Insert appropriate information in place of the capitalized words.
- One-time permission is granted only for the use specified in your request. No additional uses are granted (such as derivative works or other editions). For any other uses, please submit a new request.

[BACK](#)[CLOSE WINDOW](#)

C2.



RightsLink®

[Home](#)
[Create Account](#)
[Help](#)


ACS Publications
High quality. High impact.

Title: Synthesis, Characterization, and Glutathionylation of Cobalamin Model Complexes [Co(N4PyCO2Me)Cl]Cl2 and [Co(Bn-CDPy3)Cl]Cl2

Author: Jai Prakash et al.

Publication: Inorganic Chemistry

Publisher: American Chemical Society

Date: Feb 1, 2012

Copyright © 2012, American Chemical Society

User ID
<input type="text"/>
Password
<input type="text"/>
<input type="checkbox"/> Enable Auto Login
<input type="button" value="LOGIN"/>
Forgot Password/User ID?
If you're a copyright.com user, you can login to RightsLink using your copyright.com credentials. Already a RightsLink user or want to learn more?

PERMISSION/LICENSE IS GRANTED FOR YOUR ORDER AT NO CHARGE

This type of permission/license, instead of the standard Terms & Conditions, is sent to you because no fee is being charged for your order. Please note the following:

- Permission is granted for your request in both print and electronic formats, and translations.
- If figures and/or tables were requested, they may be adapted or used in part.
- Please print this page for your records and send a copy of it to your publisher/graduate school.
- Appropriate credit for the requested material should be given as follows: "Reprinted (adapted) with permission from (COMPLETE REFERENCE CITATION). Copyright (YEAR) American Chemical Society." Insert appropriate information in place of the capitalized words.
- One-time permission is granted only for the use specified in your request. No additional uses are granted (such as derivative works or other editions). For any other uses, please submit a new request.

[BACK](#)
[CLOSE WINDOW](#)

Copyright © 2012 [Copyright Clearance Center, Inc.](#) All Rights Reserved. [Privacy statement.](#) Comments? We would like to hear from you. E-mail us at customer care@copyright.com

C3.

Mail :: Inbox: RE: Permission Request Form: Jai Prakash

5/25/12 4:59 AM

Date: Fri, 25 May 2012 09:50:54 +0100 [04:50:54 AM EDT]
From: CONTRACTS-COPYRIGHT (shared) <Contracts-Copyright@rsc.org>
To: 'jprakash@chem.wayne.edu' <jprakash@chem.wayne.edu>
Subject: RE: Permission Request Form: Jai Prakash

Dear Jai

The Royal Society of Chemistry (RSC) hereby grants permission for the use of your paper(s) specified below in the printed and microfilm version of your thesis. You may also make available the PDF version of your paper(s) that the RSC sent to the corresponding author(s) of your paper(s) upon publication of the paper(s) in the following ways: in your thesis via any website that your university may have for the deposition of theses, via your university's Intranet or via your own personal website. We are however unable to grant you permission to include the PDF version of the paper(s) on its own in your institutional repository. The Royal Society of Chemistry is a signatory to the STM Guidelines on Permissions (available on request).

Please note that if the material specified below or any part of it appears with credit or acknowledgement to a third party then you must also secure permission from that third party before reproducing that material.

Please ensure that the thesis states the following:

Reproduced by permission of The Royal Society of Chemistry

and include a link to the paper on the Royal Society of Chemistry's website.

Please ensure that your co-authors are aware that you are including the paper in your thesis.

Regards

Gill Cockhead
Publishing Contracts & Copyright Executive

Gill Cockhead (Mrs), Publishing Contracts & Copyright Executive
Royal Society of Chemistry, Thomas Graham House
Science Park, Milton Road, Cambridge CB4 0WF, UK
Tel +44 (0) 1223 432134, Fax +44 (0) 1223 423623
<http://www.rsc.org><<http://www.rsc.org/>>

-----Original Message-----

From: jprakash@chem.wayne.edu [mailto:jprakash@chem.wayne.edu]
Sent: 24 May 2012 18:39
To: CONTRACTS-COPYRIGHT (shared)
Subject: Permission Request Form: Jai Prakash

Name : Jai Prakash

Address :

5200 Anthony Wayne Dr 48202

Detroit, MI 48202, USA

Tel : 3135163898

Fax :

Email : jprakash@chem.wayne.edu<mailto:jprakash@chem.wayne.edu>

I am preparing the following work for publication:

Article/Chapter Title : PhD Thesis/Dissertation
Journal/Book Title :
Editor/Author(s) : Jai Prakash
Publisher :

I would very much appreciate your permission to use the following material:

Journal/Book Title : Metallomics
Editor/Author(s) : Jai Prakash, Sara M. Schmitt, Q. Ping Dou and Jeremy J. Kodanko
Volume Number : 4
Year of Publication : 2012
Description of Material : Inhibition of the purified 20S proteasome by non-heme iron complexes
Page(s) : 174-178

Any Additional Comments :

Could you please grant me permission to reuse (full article) my own work published in "Metallomics" cited above in my PhD Dissertation ?

DISCLAIMER:

This communication (including any attachments) is intended for the use of the addressee only and may contain confidential, privileged or copyright material. It may not be relied upon or disclosed to any other person without the consent of the RSC. If you have received it in error, please contact us immediately. Any advice given by the RSC has been carefully formulated but is necessarily based on the information available, and the RSC cannot be held responsible for accuracy or completeness. In this respect, the RSC owes no duty of care and shall not be liable for any resulting damage or loss. The RSC acknowledges that a disclaimer cannot restrict liability at law for personal injury or death arising through a finding of negligence. The RSC does not warrant that its emails or attachments are Virus-free: Please rely on your own screening. The Royal Society of Chemistry is a charity, registered in England and Wales, number 207890 - Registered office: Thomas Graham House, Science Park, Milton Road, Cambridge CB4 0WF

C4.

Rightslink Printable License

5/23/1

**JOHN WILEY AND SONS LICENSE
TERMS AND CONDITIONS**

May 23, 2012

This is a License Agreement between Jai Prakash ("You") and John Wiley and Sons ("John Wiley and Sons") provided by Copyright Clearance Center ("CCC"). The license consists of your order details, the terms and conditions provided by John Wiley and Sons, and the payment terms and conditions.

All payments must be made in full to CCC. For payment instructions, please see information listed at the bottom of this form.

License Number	2914851323687
License date	May 23, 2012
Licensed content publisher	John Wiley and Sons
Licensed content publication	Journal of Cellular Biochemistry
Licensed content title	Novel polypyridyl chelators deplete cellular zinc and destabilize the X-linked inhibitor of apoptosis protein (XIAP) prior to induction of apoptosis in human prostate and breast cancer cells
Licensed content author	Jian Zuo, Sara M. Schmitt, Zhen Zhang, Jai Prakash, Yuhua Fan, Caifeng Bi, Jeremy J. Kodanko, Q. Ping Dou
Licensed content date	Mar 13, 2012
Start page	n/a
End page	n/a
Type of use	Dissertation/Thesis
Requestor type	Author of this Wiley article
Format	Electronic
Portion	Figure/table
Number of figures/tables	1
Number of extracts	
Original Wiley figure/table number(s)	Figure 4D
Will you be translating?	No
Order reference number	
Total	0.00 USD

REFERENCES

- (1) Marton, D. H. R.; Martell, A. E.; Sawyer, D. T.; Editors *The Activation of Dioxygen and Homogeneous Catalytic Oxidation. [Proceedings of the Fifth International Symposium on the Activation of Dioxygen and Homogeneous Catalytic Oxidation, held March 14-19, 1993, in College Station, Texas]*, 1993.
- (2) Sheldon, R. A.; Kochi, J. K. *Metal-Catalyzed Oxidations of Organic Compounds*, 1981.
- (3) Feig, A. L.; Lippard, S. J. *Chem. Rev.* **1994**, *94*, 759-805.
- (4) Wallar, B. J.; Lipscomb, J. D. *Chem. Rev.* **1996**, *96*, 2625-2657.
- (5) Que, L., Jr.; Ho, R. Y. N. *Chem. Rev.* **1996**, *96*, 2607-2624.
- (6) Sawyer, D. T.; Sobkowiak, A.; Matsushita, T. *Acc. Chem. Res.* **1996**, *29*, 409-416.
- (7) Meunier, B. *Chem. Rev.* **1992**, *92*, 1411-1456.
- (8) Barton, D. H. R.; Doller, D. *Acc. Chem. Res.* **1992**, *25*, 504-512.
- (9) Walling, C. *Acc. Chem. Res.* **1975**, *8*, 125-131.
- (10) Goldstein, S.; Meyerstein, D. *Acc. Chem. Res.* **1999**, *32*, 547-550.
- (11) MacFaul, P. A.; Wayner, D. D. M.; Ingold, K. U. *Acc. Chem. Res.* **1998**, *31*, 159-162.
- (12) Walling, C. *Acc. Chem. Res.* **1998**, *31*, 155-157.
- (13) Ortiz de Montellano, P. R.; Editor *Cytochrome P450: Structure, Mechanism, and Biochemistry, Second Edition*, 1995.
- (14) Denisov, I. G.; Makris, T. M.; Sligar, S. G.; Schlichting, I. *Chem. Rev.* **2005**, *105*, 2253-2277.

- (15) Sono, M.; Roach, M. P.; Coulter, E. D.; Dawson, J. H. *Chem. Rev.* **1996**, *96*, 2841-2887.
- (16) Alberta, J. A.; Dawson, J. H. *J. Biol. Chem.* **1987**, *262*, 11857-11863.
- (17) Eady, R. R.; Large, P. J. *Biochem. J.* **1969**, *111*, 37-38.
- (18) Hayaishi, O.; Takikawa, O.; Yoshida, R. *Prog. Inorg. Chem.* **1990**, *38*, 75-95.
- (19) Hayaishi, O. *J. Biochem.* **1976**, *79*, 13-21.
- (20) Meunier, B.; de Visser, S. P.; Shaik, S. *Chem. Rev.* **2004**, *104*, 3947-3980.
- (21) Nam, W. *Acc. Chem. Res.* **2007**, *40*, 522-531.
- (22) Lindsey, J. S.; Schreiman, I. C.; Hsu, H. C.; Kearney, P. C.; Marguerettaz, A. M. *J. Org. Chem.* **1987**, *52*, 827-836.
- (23) Groves, J. T.; Nemo, T. E.; Myers, R. S. *J. Am. Chem. Soc.* **1979**, *101*, 1032-1033.
- (24) Groves, J. T.; Haushalter, R. C.; Nakamura, M.; Nemo, T. E.; Evans, B. J. *J. Am. Chem. Soc.* **1981**, *103*, 2884-2886.
- (25) Fujii, H. *Coord. Chem. Rev.* **2002**, *226*, 51-60.
- (26) Hoffmann, P.; Robert, A.; Meunier, B. *Bull. Soc. Chim. Fr.* **1992**, *129*, 85-97.
- (27) Groves, J. T.; Nemo, T. E. *J. Am. Chem. Soc.* **1983**, *105*, 5786-5791.
- (28) Lindsay Smith, J. R.; Mortimer, D. N. *J. Chem. Soc., Chem. Commun.* **1985**, 64-65.
- (29) Lindsay Smith, J. R.; Mortimer, D. N. *J. Chem. Soc., Perkin Trans. 2* **1986**, 1743-1749.

- (30) Iley, J.; Constantino, L.; Norberto, F.; Rosa, E. *Tetrahedron Lett.* **1990**, *31*, 4921-4922.
- (31) Murata, S.; Miura, M.; Nomura, M. *J. Chem. Soc., Chem. Commun.* **1989**, 116-118.
- (32) Groves, J. T.; Viski, P. *J. Org. Chem.* **1990**, *55*, 3628-3634.
- (33) Naruta, Y.; Tani, F.; Maruyama, K. *Tetrahedron Asymmetry* **1991**, *2*, 533-542.
- (34) Labat, G.; Seris, J. L.; Meunier, B. *Angew. Chem.* **1990**, *102*, 1471-1473
(See also *Angew. Chem. Int. Ed. Engl.*, 1990, 1429 (1412), 1488-1490).
- (35) Pautet, F.; Barret, R.; Daudon, M. *Pharm. Acta Helv.* **1988**, *63*, 140-144.
- (36) Labat, G.; Meunier, B. *J. Org. Chem.* **1989**, *54*, 5008-5011.
- (37) Pratviel, G.; Pitie, M.; Bernadou, J.; Meunier, B. *Angew. Chem.* **1991**, *103*, 718-720 (See also *Angew. Chem. Int. Ed. Engl.*, 1991, 1930 (1996), 1702-1994).
- (38) Traylor, T. G.; Hill, K. W.; Fann, W. P.; Tsuchiya, S.; Dunlap, B. E. *J. Am. Chem. Soc.* **1992**, *114*, 1308-1312.
- (39) Dolphin, D.; Traylor, T. G.; Xie, L. Y. *Acc. Chem. Res.* **1997**, *30*, 251-259.
- (40) Rosenzweig, A. C.; Frederick, C. A.; Lippard, S. J.; Nordlund, P. *Nature* **1993**, *366*, 537-543.
- (41) Woodland, M. P.; Dalton, H. *J. Biol. Chem.* **1984**, *259*, 53-59.
- (42) Que, L., Jr. *Adv. Inorg. Biochem.* **1983**, *5*, 167-199.
- (43) Mason, J. R.; Cammack, R. *Annu. Rev. Microbiol.* **1992**, *46*, 277-305.
- (44) Valentine, J. S.; Foote, C. S.; Greenberg, A.; Liebman, J. F.; Editors *Active Oxygen in Biochemistry. [In: Struct. Energ. React. Chem. Ser., 1995; 3]*, 1995.
- (45) Baldwin, J. E.; Bradley, M. *Chem. Rev.* **1990**, *90*, 1079-1088.

- (46) Solomon, E. I.; Decker, A.; Lehnert, N. *Proc. Natl. Acad. Sci. U. S. A.* **2003**, *100*, 3589-3594.
- (47) Bollinger, J. M.; Krebs, C. *J. Inorg. Biochem.* **2006**, *100*, 586-605.
- (48) Hoffart, L. M.; Barr, E. W.; Guyer, R. B.; Bollinger, J. M., Jr.; Krebs, C. *Proc. Natl. Acad. Sci. U. S. A.* **2006**, *103*, 14738-14743.
- (49) Galonic, D. P.; Barr, E. W.; Walsh, C. T.; Bollinger, J. M., Jr.; Krebs, C. *Nat. Chem. Biol.* **2006**, *3*, 113-116.
- (50) Grapperhaus, C. A.; Mienert, B.; Bill, E.; Weyhermueller, T.; Wieghardt, K. *Inorg. Chem.* **2000**, *39*, 5306-5317.
- (51) Rohde, J.-U.; In, J.-H.; Lim, M. H.; Brennessel, W. W.; Bukowski, M. R.; Stubna, A.; Muenck, E.; Nam, W.; Que, L., Jr. *Science* **2003**, *299*, 1037-1039.
- (52) Lim, M. H.; Rohde, J.-U.; Stubna, A.; Bukowski, M. R.; Costas, M.; Ho, R. Y. N.; Muenck, E.; Nam, W.; Que, L., Jr. *Proc. Natl. Acad. Sci. U. S. A.* **2003**, *100*, 3665-3670.
- (53) Kaizer, J.; Klinker, E. J.; Oh, N. Y.; Rohde, J.-U.; Song, W. J.; Stubna, A.; Kim, J.; Muenck, E.; Nam, W.; Que, L., Jr. *J. Am. Chem. Soc.* **2004**, *126*, 472-473.
- (54) Bukowski, M. R.; Koehntop, K. D.; Stubna, A.; Bominaar, E. L.; Halfen, J. A.; Muenck, E.; Nam, W.; Que, L., Jr. *Science* **2005**, *310*, 1000-1002.
- (55) Klinker, E. J.; Kaizer, J.; Brennessel, W. W.; Woodrum, N. L.; Cramer, C. J.; Que, L., Jr. *Angew. Chem., Int. Ed.* **2005**, *44*, 3690-3694.
- (56) Sastri, C. V.; Seo, M. S.; Park, M. J.; Kim, K. M.; Nam, W. *Chem. Commun.* **2005**, 1405-1407.
- (57) Balland, V.; Charlot, M.-F.; Banse, F.; Girerd, J.-J.; Mattioli, T. A.; Bill, E.; Bartoli, J.-F.; Battioni, P.; Mansuy, D. *Eur. J. Inorg. Chem.* **2004**, 301-308.

- (58) Kim, S. O.; Sastri, C. V.; Seo, M. S.; Kim, J.; Nam, W. *J. Am. Chem. Soc.* **2005**, *127*, 4178-4179.
- (59) Thibon, A.; England, J.; Martinho, M.; Young, V. G.; Frisch, J. R.; Guillot, R.; Girerd, J.-J.; Muenck, E.; Que, L., Jr.; Banse, F. *Angew. Chem. Int. Ed.* **2008**, *47*, 7064-7067.
- (60) Hong, S.; Lee, Y.-M.; Shin, W.; Fukuzumi, S.; Nam, W. *J. Am. Chem. Soc.* **2009**, *131*, 13910-13911.
- (61) Prat, I.; Mathieson, J. S.; Guell, M.; Ribas, X.; Luis, J. M.; Cronin, L.; Costas, M. *Nat. Chem.* **2011**, *3*, 788-793.
- (62) Kim, C.; Chen, K.; Kim, J.; Que, L., Jr. *J. Am. Chem. Soc.* **1997**, *119*, 5964-5965.
- (63) Yoon, J.; Wilson, S. A.; Jang, Y. K.; Seo, M. S.; Nehru, K.; Hedman, B.; Hodgson, K. O.; Bill, E.; Solomon, E. I.; Nam, W. *Angew. Chem., Int. Ed.* **2009**, *48*, 1257-1260.
- (64) Nehru, K.; Seo, M. S.; Kim, J.; Nam, W. *Inorg. Chem.* **2007**, *46*, 293-298.
- (65) de Visser, S. P.; Oh, K.; Han, A.-R.; Nam, W. *Inorg. Chem.* **2007**, *46*, 4632-4641.
- (66) Oh, N. Y.; Suh, Y.; Park, M. J.; Seo, M. S.; Kim, J.; Nam, W. *Angew. Chem., Int. Ed.* **2005**, *44*, 4235-4239.
- (67) Burger, R. M. *Chem. Rev.* **1998**, *98*, 1153-1169.
- (68) Claussen, C. A.; Long, E. C. *Chem. Rev.* **1999**, *99*, 2797-2816.
- (69) Armitage, B. *Chem. Rev.* **1998**, *98*, 1171-1200.
- (70) Clarke, M. J.; Zhu, F.; Frasca, D. R. *Chem. Rev.* **1999**, *99*, 2511-2533.
- (71) Wolkenberg, S. E.; Boger, D. L. *Chem. Rev.* **2002**, *102*, 2477-2495.

- (72) Pitie, M.; Pratviel, G. *Chem. Rev.* **2010**, *110*, 1018-1059.
- (73) Jiang, Q.; Xiao, N.; Shi, P.; Zhu, Y.; Guo, Z. *Coord. Chem. Rev.* **2007**, *251*, 1951-1972.
- (74) Cowan, J. A. *Curr. Opin. Chem. Biol.* **2001**, *5*, 634-642.
- (75) Marnett, L. J. *Carcinogenesis* **2000**, *21*, 361-370.
- (76) Umezawa, H.; Maeda, K.; Takeuchi, T.; Okami, Y. *J. Antibiot., Ser. A* **1966**, *19*, 200-209.
- (77) Pogożelski, W. K.; Tullius, T. D. *Chem. Rev.* **1998**, *98*, 1089-1107.
- (78) Hecht, S. M. *J. Nat. Prod.* **2000**, *63*, 158-168.
- (79) Hecht, S. M.; Editor *Bleomycin: Chemical, Biochemical, and Biological Aspects. [Proceedings of a Joint U.S.-Japan Symposium Held in Honolulu, July 18-22, 1978]*, 1979.
- (80) Sam, J. W.; Tang, X.-J.; Peisach, J. *J. Am. Chem. Soc.* **1994**, *116*, 5250-5256.
- (81) Guajardo, R. J.; Hudson, S. E.; Brown, S. J.; Mascharak, P. K. *J. Am. Chem. Soc.* **1993**, *115*, 7971-7977.
- (82) Guajardo, R. J.; Chavez, F.; Farinas, E. T.; Mascharak, P. K. *J. Am. Chem. Soc.* **1995**, *117*, 3883-3884.
- (83) Kittaka, A.; Sugano, Y.; Otsuka, M.; Ohno, M.; Sugiura, Y.; Umezawa, H. *Tetrahedron Lett.* **1986**, *27*, 3631-3634.
- (84) Sugano, Y.; Kittaka, A.; Otsuka, M.; Ohno, M.; Sugiura, Y.; Umezawa, H. *Tetrahedron Lett.* **1986**, *27*, 3635-3638.
- (85) Worth, L., Jr.; Frank, B. L.; Christner, D. F.; Absalon, M. J.; Stubbe, J.; Kozarich, J. W. *Biochemistry* **1993**, *32*, 2601-2609.

- (86) Hecht, S. M. *Acc. Chem. Res.* **1986**, *19*, 383-391.
- (87) Li, Q.; van den Berg, T. A.; Feringa, B. L.; Roelfes, G. *Dalton Trans.* **2010**, *39*, 8012-8021.
- (88) Hegg, E. L.; Burstyn, J. N. *J. Am. Chem. Soc.* **1995**, *117*, 7015-7016.
- (89) Suh, J.; Yoo, S. H.; Kim, M. G.; Jeong, K.; Ahn, J. Y.; Kim, M.-s.; Chae, P. S.; Lee, T. Y.; Lee, J.; Lee, J.; Jang, Y. A.; Ko, E. H. *Angew. Chem., Int. Ed.* **2007**, *46*, 7064-7067.
- (90) Zhu, L.; Qin, L.; Parac, T. N.; Kostic, N. M. *J. Am. Chem. Soc.* **1994**, *116*, 5218-5224.
- (91) Roots, R.; Okada, S. *Radiat. Res.* **1975**, *64*, 306-320.
- (92) Schepartz, A.; Cuenoud, B. *J. Am. Chem. Soc.* **1990**, *112*, 3247-3249.
- (93) Hoyer, D.; Cho, H.; Schultz, P. G. *J. Am. Chem. Soc.* **1990**, *112*, 3249-3250.
- (94) Gallagher, J.; Zelenko, O.; Walts, A. D.; Sigman, D. S. *Biochemistry* **1998**, *37*, 2096-2104.
- (95) Lee, J.; Yu, P.; Xiao, X.; Kodadek, T. *Mol. BioSyst.* **2008**, *4*, 59-65.
- (96) Lee, J.; Udugamasooriya, D. G.; Lim, H.-S.; Kodadek, T. *Nat. Chem. Biol.* **2010**, *6*, 258-260.
- (97) Cuenoud, B.; Tarasow, T. M.; Schepartz, A. *Tetrahedron Lett.* **1992**, *33*, 895-898.
- (98) Gokhale, N. H.; Cowan, J. A. *JBIC, J. Biol. Inorg. Chem.* **2006**, *11*, 937-947.
- (99) Gokhale, N. H.; Bradford, S.; Cowan, J. A. *J. Am. Chem. Soc.* **2008**, *130*, 2388-2389.

- (100) Kakhlon, O.; Cabantchik, Z. I. *Free Radical Biol. Med.* **2002**, *33*, 1037-1046.
- (101) Tenopoulou, M.; Kurz, T.; Doulias, P.-T.; Galaris, D.; Brunk, U. T. *Biochem. J* **2007**, *403*, 261-266.
- (102) Glickstein, H.; Ben El, R.; Link, G.; Breuer, W.; Konjin, A. M.; Hershko, C.; Nick, H.; Cabantchik, Z. I. *Blood* **2006**, *108*, 3195-3203.
- (103) Glickstein, H.; El, R. B.; Shvartsman, M.; Cabantchik, Z. I. *Blood* **2005**, *106*, 3242-3250.
- (104) Petrat, F.; Weisheit, D.; Lensen, M.; De Groot, H.; Sustmann, R.; Rauen, U. *Biochem. J* **2002**, *362*, 137-147.
- (105) Petrat, F.; De Groot, H.; Rauen, U. *Biochem. J* **2001**, *356*, 61-69.
- (106) Petrat, F.; de Groot, H.; Rauen, U. *Arch. Biochem. Biophys.* **2000**, *376*, 74-81.
- (107) Ekkati, A. R.; Kodanko, J. J. *J. Am. Chem. Soc.* **2007**, *129*, 12390-12391.
- (108) Abouelatta, A. I.; Campanali, A. A.; Ekkati, A. R.; Shamoun, M.; Kalapugama, S.; Kodanko, J. J. *Inorg. Chem.* **2009**, *48*, 7729-7739.
- (109) Supuran, C. T.; Scozzafava, A.; Casini, A. *Med. Res. Rev.* **2003**, *23*, 146-189.
- (110) Supuran, C. T.; Scozzafava, A. *Expert Opin. Ther. Pat.* **2000**, *10*, 575-600.
- (111) Briganti, F.; Pierattelli, R.; Scozzafava, A.; Supuran, C. T. *Eur. J. Med. Chem.* **1996**, *31*, 1001-1010.
- (112) Bertini, I.; Luchinat, C.; Scozzafava, A. *Structure and Bonding (Berlin, Germany)* **1981**, *48*, 45-92.

- (113) Kim, G.; Selengut, J.; Levine, R. L. *Arch. Biochem. Biophys.* **2000**, *377*, 334-340.
- (114) Lindahl, M.; Vidgren, J.; Eriksson, E.; Habash, J.; Harrop, S.; Helliwell, J.; Liljas, A.; Lindeskog, M.; Walker, N. *Carbonic Anhydrase, Proc. Int. Workshop* **1991**, 111-118.
- (115) Maren, T. H. *Physiol. Rev.* **1967**, *47*, 595-781.
- (116) Maren, T. H. *Annu. Rev. Pharmacol. Toxicol.* **1976**, *16*, 309-327.
- (117) Owa, T.; Nagasu, T. *Expert Opin. Ther. Pat.* **2000**, *10*, 1725-1740.
- (118) Masereel, B.; Rolin, S.; Abbate, F.; Scozzafava, A.; Supuran, C. T. *J. Med. Chem.* **2002**, *45*, 312-320.
- (119) Rawlings, N. D.; Barrett, A. J. *Methods Enzymol.* **1994**, *244*, 19-61.
- (120) Polgar, L. *Cell. Mol. Life Sci.* **2005**, *62*, 2161-2172.
- (121) Stuerzebecher, J.; Markwardt, F.; Voigt, B.; Wagner, G.; Walsmann, P. *Thromb. Res.* **1983**, *29*, 635-642.
- (122) Stuerzebecher, J.; Stuerzebecher, U.; Vieweg, H.; Wagner, G.; Hauptmann, J.; Markwardt, F. *Thromb. Res.* **1989**, *54*, 245-252.
- (123) Stuerzebecher, J.; Prasa, D.; Wikstroem, P.; Vieweg, H. *J. Enzyme Inhib.* **1995**, *9*, 87-99.
- (124) Stuerzebecher, J.; Prasa, D.; Hauptmann, J.; Vieweg, H.; Wikstroem, P. *J. Med. Chem.* **1997**, *40*, 3091-3099.
- (125) Renatus, M.; Bode, W.; Huber, R.; Stuerzebecher, J.; Stubbs, M. T. *J. Med. Chem.* **1998**, *41*, 5445-5456.
- (126) Krieger, M.; Kay, L. M.; Stroud, R. M. *J. Mol. Biol.* **1974**, *83*, 209-230.

- (127) Brady, K.; Wei, A.; Ringe, D.; Abeles, R. H. *Biochemistry* **1990**, *29*, 7600-7607.
- (128) Ghani, U.; Ng, K. K. S.; Atta Ur, R.; Choudhary, M. I.; Ullah, N.; James, M. N. G. *J. Mol. Biol.* **2001**, *314*, 519-525.
- (129) Harper, J. W.; Powers, J. C. *Biochemistry* **1985**, *24*, 7200-7213.
- (130) Coux, O.; Tanaka, K.; Goldberg, A. L. *Annu. Rev. Biochem.* **1996**, *65*, 801-847.
- (131) Hochstrasser, M. *Curr. Opin. Cell Biol.* **1995**, *7*, 215-223.
- (132) Ciechanover, A. *Cell* **1994**, *79*, 13-21.
- (133) Groll, M.; Ditzel, L.; Loewe, J.; Stock, D.; Bochtler, M.; Bartunik, H. D.; Huber, R. *Nature* **1997**, *386*, 463-471.
- (134) Groll, M.; Huber, R. *Int. J. Biochem. Cell Biol.* **2003**, *35*, 606-616.
- (135) <http://users.rcn.com/jkimball.ma.ultranet/BiologyPages/P/proteasome.gif>
- (136) Seemueller, E.; Lupas, A.; Stock, D.; Loewe, J.; Huber, R.; Baumeister, W. *Science* **1995**, *268*, 579-582.
- (137) Orlowski Robert, Z.; Dees, E. C. *Breast Cancer Res.* **2003**, *5*, 1-7.
- (138) Dou, Q. P.; Goldfarb, R. H. *IDrugs* **2002**, *5*, 828-834.
- (139) Richardson, P. G.; Barlogie, B.; Berenson, J.; Singhal, S.; Jagannath, S.; Irwin, D.; Rajkumar, S. V.; Srkalovic, G.; Alsina, M.; Alexanian, R.; Siegel, D.; Orlowski, R. Z.; Kuter, D.; Limentani, S. A.; Lee, S.; Hideshima, T.; Esseltine, D.-L.; Kauffman, M.; Adams, J.; Schenkein, D. P.; Anderson, K. C. *New Engl. J. Med.* **2003**, *348*, 2609-2617.
- (140) Hindo, S. S.; Frezza, M.; Tomco, D.; Heeg, M. J.; Hryhorczuk, L.; McGarvey, B. R.; Dou, Q. P.; Verani, C. N. *Eur. J. Med. Chem.* **2009**, *44*, 4353-4361.

(141) Frezza, M.; Hindo, S. S.; Tomco, D.; Allard, M. M.; Cui, Q. C.; Heeg, M. J.; Chen, D.; Dou, Q. P.; Verani, C. N. *Inorg. Chem.* **2009**, *48*, 5928-5937.

(142) Chen, D.; Frezza, M.; Shakya, R.; Cui, Q. C.; Milacic, V.; Verani, C. N.; Dou, Q. P. *Cancer Res.* **2007**, *67*, 9258-9265.

(143) Milacic, V.; Chen, D.; Ronconi, L.; Landis-Piwowar, K. R.; Fregona, D.; Dou, Q. P. *Cancer Res.* **2006**, *66*, 10478-10486.

(144) Milacic, V.; Dou, Q. P. *Coord. Chem. Rev.* **2009**, *253*, 1649-1660.

(145) Daniel, K. G.; Gupta, P.; Harbach, R. H.; Guida, W. C.; Dou, Q. P. *Biochem. Pharmacol.* **2004**, *67*, 1139-1151.

(146) Zhang, X.; Frezza, M.; Milacic, V.; Ronconi, L.; Fan, Y.; Bi, C.; Fregona, D.; Dou, Q. P. *J. Cell. Biochem.* **2010**, *109*, 162-172.

(147) Weir, D. G.; Scott, J. M. *Baillieres Clin. Haematol.* **1995**, *8*, 479-497.

(148) Chanarin, I. *Br. J. Haematol.* **2000**, *111*, 407-415.

(149) McCaddon, A.; Regland, B.; Hudson, P.; Davies, G. *Neurology* **2002**, *58*, 1395-1399.

(150) Collin, S. M.; Metcalfe, C.; Refsum, H.; Lewis, S. J.; Zuccolo, L.; Smith, G. D.; Chen, L.; Harris, R.; Davis, M.; Marsden, G.; Johnston, C.; Lane, J. A.; Ebbing, M.; Bonna, K. H.; Nygard, O.; Ueland, P. M.; Grau, M. V.; Baron, J. A.; Donovan, J. L.; Neal, D. E.; Hamdy, F. C.; Smith, A. D.; Martin, R. M. *Cancer Epidemiol. Biomarkers Prev.* **2010**, *19*, 1632-1642.

(151) Kelly, P. J.; Rosand, J.; Kistler, J. P.; Shih, V. E.; Silveira, S.; Plomaritoglou, A.; Furie, K. L. *Neurology* **2002**, *59*, 529-536.

(152) Kawamoto, R.; Kajiwara, T.; Oka, Y.; Takagi, Y. *J. Atheroscler. Thromb.* **2002**, *9*, 121-125.

- (153) Ogawa, M.; Abe, S.; Saigo, M.; Biro, S.; Toda, H.; Matsuoka, T.; Torii, H.; Minagoe, S.; Maruyama, I.; Tei, C. *Thromb. Res.* **2003**, *109*, 253-258.
- (154) Weissbach, H.; Taylor, R. T. *Fed. Proc., Fed. Am. Soc. Exp. Biol.* **1966**, *25*, 1649-1656.
- (155) Taylor, R. T.; Hanna, M. L. *Arch. Biochem. Biophys.* **1975**, *171*, 507-520.
- (156) Gurnani, S.; Mistry, S. P.; Johnson, B. C. *Biochim. Biophys. Acta* **1960**, *38*, 187-188.
- (157) Cannata, J. J. B.; Focesi, A., Jr.; Mazumder, R.; Warner, R. C.; Ochoa, S. *J. Biol. Chem.* **1965**, *240*, 3249-3252.
- (158) Hodgkin, D. C.; Kamper, J.; Mackay, M.; Pickworth, J.; Trueblood, K. N.; White, J. G. *Nature* **1956**, *178*, 64-66.
- (159) Seetharam, B.; Bose, S.; Li, N. *J. Nutr.* **1999**, *129*, 1761-1764.
- (160) Quadros, E. V.; Regec, A. L.; Khan, K. M. F.; Quadros, E.; Rothenberg, S. *P. Am. J. Physiol.* **1999**, *277*, G161-G166.
- (161) Quadros, E. V.; Nakayama, Y.; Sequeira, J. M. *Biochem. Biophys. Res. Commun.* **2005**, *327*, 1006-1010.
- (162) Zhao, R.; Lind, J.; Merenyi, G.; Eriksen, T. E. *J. Chem. Soc., Perkin Trans. 2* **1997**, 569-574.
- (163) Griffith, O. W. *Free Radical Biol. Med.* **1999**, *27*, 922-935.
- (164) Pezacka, E.; Green, R.; Jacobsen, D. W. *Biochem. Biophys. Res. Commun.* **1990**, *169*, 443-450.
- (165) McCaddon, A.; Hudson, P. R. *Future Neurol.* **2007**, *2*, 537-547.
- (166) Brasch, N. E.; Hsu, T.-L. C.; Doll, K. M.; Finke, R. G. *J. Inorg. Biochem.* **1999**, *76*, 197-209.

- (167) Wagner, F.; Bernhauer, K. *Ann. N. Y. Acad. Sci.* **1964**, *112*, 580-589.
- (168) Brasch, N. E.; Xia, L.; (Kent State University, USA). Application: US
US, 2006, pp 5.
- (169) Brown, K. L.; Zou, X.; Savon, S. R.; Jacobsen, D. W. *Biochemistry* **1993**, *32*, 8421-8428.
- (170) Scheuring, E. M.; Sagi, I.; Chance, M. R. *Biochemistry* **1994**, *33*, 6310-6315.
- (171) Randaccio, L.; Geremia, S.; Nardin, G.; Slouf, M.; Srnova, I. *Inorg. Chem.* **1999**, *38*, 4087-4092.
- (172) Randaccio, L.; Furlan, M.; Geremia, S.; Slouf, M.; Srnova, I.; Toffoli, D. *Inorg. Chem.* **2000**, *39*, 3403-3413.
- (173) Randaccio, L.; Geremia, S.; Stener, M.; Toffoli, D.; Zangrando, E. *Eur. J. Inorg. Chem.* **2002**, 93-103.
- (174) Xia, L.; Cregan, A. G.; Berben, L. A.; Brasch, N. E. *Inorg. Chem.* **2004**, *43*, 6848-6857.
- (175) Crumbliss, A. L.; Wilmarth, W. K. *J. Am. Chem. Soc.* **1970**, *92*, 2593-2594.
- (176) Brown, K. L.; Satyanarayana, S. *J. Am. Chem. Soc.* **1992**, *114*, 5674-5684.
- (177) Brown, K. L.; Chernoff, D.; Keljo, D. J.; Kallen, R. G. *J. Am. Chem. Soc.* **1972**, *94*, 6697-6704.
- (178) Marzilli, L. G.; Toscano, P. J.; Randaccio, L.; Bresciani-Pahor, N.; Calligaris, M. *J. Am. Chem. Soc.* **1979**, *101*, 6754-6756.
- (179) Randaccio, L.; Bresciani-Pahor, N.; Toscano, P. J.; Marzilli, L. G. *J. Am. Chem. Soc.* **1980**, *102*, 7372-7373.

(180) Bresciani-Pahor, N.; Randaccio, L.; Toscano, P. G.; Sandercock, A. C.; Marzilli, L. G. *J. Chem. Soc., Dalton Trans.* **1982**, 129-134.

(181) Summers, M. F.; Toscano, P. J.; Bresciani-Pahor, N.; Nardin, G.; Randaccio, L.; Marzilli, L. G. *J. Am. Chem. Soc.* **1983**, *105*, 6259-6263.

(182) Bresciani-Pahor, N.; Marzilli, L. G.; Randaccio, L.; Toscano, P. J.; Zangrando, E. *J. Chem. Soc., Chem. Commun.* **1984**, 1508-1510.

(183) Bresciani-Pahor, N.; Forcolin, M.; Marzilli, L. G.; Randaccio, L.; Summers, M. F.; Toscano, P. J. *Coord. Chem. Rev.* **1985**, *63*, 1-125.

(184) Marzilli, L. G.; Summers, M. F.; Zangrando, E.; Bresciani-Pahor, N.; Randaccio, L. *J. Am. Chem. Soc.* **1986**, *108*, 4830-4838.

(185) Randaccio, L.; Pahor, N. B.; Zangrando, E.; Marzilli, L. G. *Chem. Soc. Rev.* **1989**, *18*, 225-250.

(186) Polson, S. M.; Hansen, L.; Marzilli, L. G. *Inorg. Chem.* **1997**, *36*, 307-313.

(187) Brown, K. L.; Kallen, R. G. *J. Am. Chem. Soc.* **1972**, *94*, 1894-1901.

(188) Pellizer, G.; Tauszik, G. R.; Costa, G. *J. Chem. Soc., Dalton Trans.* **1973**, 317-322.

(189) Berlett, B. S.; Stadtman, E. R. *J. Biol. Chem.* **1997**, *272*, 20313-20316.

(190) Garrison, W. M.; Jayko, M. E.; Bennett, W. *Radiat. Res.* **1962**, *16*, 483-502.

(191) Davies, M. J. *Biochim. Biophys. Acta, Proteins Proteomics* **2005**, *1703*, 93-109.

(192) Stadtman, E. R.; Berlett, B. S. *Chem. Res. Toxicol.* **1997**, *10*, 485-494.

(193) Stadtman, E. R. *Free Radical Biol. Med.* **1990**, *9*, 315-325.

(194) Lee, J.; Yu, P.; Xiao, X.; Kodadek, T. *Mol. BioSyst.* **2008**, *4*, 59-65.

- (195) Jay, D. G. *Proc. Natl. Acad. Sci. U. S. A.* **1988**, *85*, 5454-5458.
- (196) Beck, S.; Sakurai, T.; Eustace, B. K.; Beste, G.; Schier, R.; Rudert, F.; Jay, D. G. *Proteomics* **2002**, *2*, 247-255.
- (197) Yan, P.; Xiong, Y.; Chen, B.; Negash, S.; Squier, T. C.; Mayer, M. U. *Biochemistry* **2006**, *45*, 4736-4748.
- (198) Gokhale, N. H.; Bradford, S.; Cowan, J. A. *J. Am. Chem. Soc.* **2008**, *130*, 2388-2389.
- (199) Gokhale, N. H.; Cowan, J. A. *J. Biol. Inorg. Chem.* **2006**, *11*, 937-947.
- (200) Heyduk, T.; Baichoo, N.; Heyduk, E. *Met. Ions Biol. Syst.* **2001**, *38*, 255-287.
- (201) Heyduk, E.; Heyduk, T. *Biochemistry* **1994**, *33*, 9643-9650.
- (202) Cheal, S. M.; Ng, M.; Barrios, B.; Miao, Z.; Kalani, A. K.; Meares, C. F. *Biochemistry* **2009**, *48*, 4577-4586.
- (203) Traviglia, S. L.; Datwyler, S. A.; Yan, D.; Ishihama, A.; Meares, C. F. *Biochemistry* **1999**, *38*, 15774-15778.
- (204) Greiner, D. P.; Hughes, K. A.; Gunasekera, A. H.; Meares, C. F. *Proc. Natl. Acad. Sci. U. S. A.* **1996**, *93*, 71-75.
- (205) Heilek, G.; Marusak, R.; Meares, C. F.; Noller, H. F. *Proc. Natl. Acad. Sci. U. S. A.* **1995**, *92*, 1113-1116.
- (206) Chen, K.; Que, L., Jr. *J. Am. Chem. Soc.* **2001**, *123*, 6327-6337.
- (207) Fenton, H. J. H. *J. Chem. Soc., Trans.* **1894**, *65*, 899-910.
- (208) Kaizer, J.; Klinker, E. J.; Oh, N. Y.; Rohde, J.-U.; Song, W. J.; Stubna, A.; Kim, J.; Münck, E.; Nam, W.; Que, L., Jr. *J. Am. Chem. Soc.* **2004**, *126*, 472-473.

(209) Yoon, J.; Wilson, S. A.; Jang, Y. K.; Seo, M. S.; Nehru, K.; Hedman, B.; Hodgson, K. O.; Bill, E.; Solomon, E. I.; Nam, W. *Angew. Chem. Int. Ed.* **2009**, *48*, 1257-1260.

(210) Nehru, K.; Jang, Y.; Oh, S.; Dallemer, F.; Nam, W.; Kim, J. *Inorg. Chim. Acta* **2008**, *361*, 2557-2561.

(211) Jeong, Y. J.; Kang, Y.; Han, A.-R.; Lee, Y.-M.; Kotani, H.; Fukuzumi, S.; Nam, W. *Angew. Chem. Int. Ed.* **2008**, *47*, 7321-7324.

(212) Fukuzumi, S.; Kotani, H.; Lee, Y.-M.; Nam, W. *J. Am. Chem. Soc.* **2008**, *130*, 15134-15142.

(213) Nehru, K.; Jang, Y. K.; Seo, M. S.; Nam, W.; Kim, J. *Bull. Korean Chem. Soc.* **2007**, *28*, 843-846.

(214) Krebs, C.; Fujimori, D. G.; Walsh, C. T.; Bollinger, J. M., Jr. *Acc. Chem. Res.* **2007**, *40*, 484-492.

(215) Que, L. *Acc. Chem. Res.* **2007**, *40*, 493-500.

(216) Eser, B. E.; Barr, E. W.; Frantom, P. A.; Saleh, L.; Bollinger, J. M., Jr.; Krebs, C.; Fitzpatrick, P. F. *J. Am. Chem. Soc.* **2007**, *129*, 11334-11335.

(217) Hecht, S. M. *Anticancer Agents from Nat. Prod.* **2005**, 357-381.

(218) Roelfes, G.; Lubben, M.; W. Leppard, S.; Schudde, E. P.; Hermant, R. M.; Hage, R.; Wilkinson, E. C.; Que, L., Jr.; Feringa, B. L. *J. Mol. Catal. A: Chem.* **1997**, *117*, 223-227.

(219) Mialane, P.; Nivorojkine, A.; Pratviel, G.; Azema, L.; Slany, M.; Godde, F.; Simaan, A.; Banse, F.; Kargar-Grisel, T.; Bouchoux, G.; Sainton, J.; Horner, O.; Guilhem, J.; Tchertanova, L.; Meunier, B.; Girerd, J.-J. *Inorg. Chem.* **1999**, *38*, 1085-1092.

(220) Decker, A.; Chow, M. S.; Kemsley, J. N.; Lehnert, N.; Solomon, E. I. *J. Am. Chem. Soc.* **2006**, *128*, 4719-4733.

(221) Stubbe, J.; Kozarich, J. W. *Chem. Rev.* **1987**, *87*, 1107-1136.

(222) Roelfes, G.; Branum, M. E.; Wang, L.; Que, L., Jr.; Feringa, B. L. *J. Am. Chem. Soc.* **2000**, *122*, 11517-11518.

(223) Chakravarty, S.; Kannan, K. K. *J. Mol. Biol.* **1994**, *243*, 198-309.

(224) van den Berg, T. A.; Feringa, B. L.; Roelfes, G. *Chem. Commun.* **2007**, 180-182.

(225) Drago, R. S. *Physical Methods for Chemists*; 2nd ed., 1992.

(226) Campanali, A. A.; Kwiecien, T. D.; Hryhorczuk, L.; Kodanko, J. J. *Inorg. Chem.* **2010**, *49*, 4759-4761.

(227) Jabre, N. D.; Hryhorczuk, L.; Kodanko, J. J. *Inorg. Chem.* **2009**, *48*, 8078-8080.

(228) Louie, A. Y.; Meade, T. J. *Chem. Rev.* **1999**, *99*, 2711-2734.

(229) Brown, K. C.; Yang, S.-H.; Kodadek, T. *Biochemistry* **1995**, *34*, 4733-4739.

(230) Aqueous solutions of **9** and **10** decompose over the course of 2 h at room temperature under an aerobic atmosphere, which indicates that the oxidation of these ferrous complexes with O₂ is a relatively slow process.

(231) Roelfes, G.; Lubben, M.; Hage, R.; Que, L., Jr.; Feringa, B. L. *Chem. Eur. J.* **2000**, *6*, 2152-2159.

(232) Li, F.; England, J.; Que, J. L. *J. Am. Chem. Soc.* **2010**, *132*, 2134-2135.

(233) Makhlynets, O. V.; Das, P.; Taktak, S.; Flook, M.; Mas-Balleste, R.; Rybak-Akimova, E. V.; Que, L., Jr. *Chem. Eur. J.* **2009**, *15*, 13171-13180.

(234) Hazen, S. L.; Zhang, R.; Shen, Z.; Wu, W.; Podrez, E. A.; MacPherson, J. C.; Schmitt, D.; Mitra, S. N.; Mukhopadhyay, C.; Chen, Y.; Cohen, P. A.; Hoff, H. F.; Abu-Soud, H. M. *Circ. Res.* **1999**, *85*, 950-958.

(235) Wever, R.; Bakkenist, A. R. *J. Biochim. Biophys. Acta, Enzymol.* **1980**, *612*, 178-184.

(236) Levine, R. L.; Williams, J. A.; Stadtman, E. R.; Shacter, E. *Methods Enzymol.* **1994**, *233*, 346-357.

(237) Fu, S.; Wang, H.; Davies, M.; Dean, R. *J. Biol. Chem.* **2000**, *275*, 10851-10858.

(238) Bovonsombat, P.; Khanthapura, P.; Krause, M. M.; Leykajarakul, J. *Tetrahedron Lett.* **2008**, *49*, 7008-7011.

(239) Xiong, Y. L.; Park, D.; Ooizumi, T. *J. Agric. Food. Chem.* **2009**, *57*, 153-159.

(240) Ouellet, H.; Ranguelova, K.; LaBarre, M.; Wittenberg, J. B.; Wittenberg, B. A.; Magliozzo, R. S.; Guertin, M. *J. Biol. Chem.* **2007**, *282*, 7491-7503.

(241) Reeder, B. J.; Svistunenko, D. A.; Sharpe, M. A.; Wilson, M. T. *Biochemistry* **2002**, *41*, 367-375.

(242) Irwin, J. A.; Ostdal, H.; Davies, M. J. *Arch. Biochem. Biophys.* **1999**, *362*, 94-104.

(243) Mikkelsen, A.; Skibsted, L. H. *Z. Lebensm.-Unters. Forsch.* **1998**, *206*, 199-202.

(244) Miura, T.; Muraoka, S.; Ogiso, T. *Biochem. Mol. Biol. Int.* **1995**, *36*, 587-594.

(245) Cooper, C. E. *New Compr. Biochem.* **1994**, *28*, 67-111.

(246) Mieyal, J. J.; Gallogly, M. M.; Qanungo, S.; Sabens, E. A.; Shelton, M. D. *Antioxid. Redox Sign.* **2008**, *10*, 1941-1988.

(247) Bian, K.; Gao, Z.; Weisbrodt, N.; Murad, F. *Proc. Natl. Acad. Sci. U. S. A.* **2003**, *100*, 5712-5717.

(248) Suto, D.; Iuchi, Y.; Ikeda, Y.; Sato, K.; Ohba, Y.; Fujii, J. *Arch. Biochem. Biophys.* **2007**, *461*, 151-158.

(249) Das, P.; Que, L., Jr. *Inorg. Chem.* **2010**, *49*, 9479-9485.

(250) Fitzpatrick, P. F. *Biochemistry* **2003**, *42*, 14083-14091.

(251) Kitajima, N.; Ito, M.; Fukui, H.; Morooka, Y. *J. Am. Chem. Soc.* **1993**, *115*, 9335-9336.

(252) Chenault, H. K.; Dahmer, J.; Whitesides, G. M. *J. Am. Chem. Soc.* **1989**, *111*, 6354-6364.

(253) Smith, K. C.; White, R. L.; Le, Y.; Vining, L. C. *J. Nat. Prod.* **1995**, *58*, 1274-1277.

(254) Orłowski, R. Z.; Stinchcombe, T. E.; Mitchell, B. S.; Shea, T. C.; Baldwin, A. S.; Stahl, S.; Adams, J.; Esseltine, D.-L.; Elliott, P. J.; Pien, C. S.; Guerciolini, R.; Anderson, J. K.; Depcik-Smith, N. D.; Bhagat, R.; Lehman, M. J.; Novick, S. C.; O'Connor, O. A.; Soignet, S. L. *J. Clin. Oncol.* **2002**, *20*, 4420-4427.

(255) Orłowski, R. Z.; Eswara, J. R.; Lafond-Walker, A.; Grever, M. R.; Orłowski, M.; Dang, C. V. *Cancer Res.* **1998**, *58*, 4342-4348.

(256) Adams, J.; Palombella, V. J.; Sausville, E. A.; Johnson, J.; Destree, A.; Lazarus, D. D.; Maas, J.; Pien, C. S.; Prakash, S.; Elliott, P. J. *Cancer Res.* **1999**, *59*, 2615-2622.

(257) Dou, Q. P.; Nam, S. *Expert Opin. Ther. Pat.* **2000**, *10*, 1263-1272.

- (258) Almond, J. B.; Cohen, G. M. *Leukemia* **2002**, *16*, 433-443.
- (259) Adams, J. *Drug Discov. Today* **2003**, *8*, 307-315.
- (260) Prakash, J.; Kodanko, J. J. *Inorg. Chem.* **2011**, *50*, 3934-3945.
- (261) Roelfes, G.; Lubben, M.; Chen, K.; Ho, R. Y. N.; Meetsma, A.; Genseberger, S.; Hermant, R. M.; Hage, R.; Mandal, S. K.; Young, V. G., Jr.; Zang, Y.; Kooijman, H.; Spek, A. L.; Que, L.; Feringa, B. L. *Inorg. Chem.* **1999**, *38*, 1929-1936.
- (262) Jackson, C.; Kodanko, J. J. *Metallomics* **2010**, *2*, 407-411.
- (263) van den Berg, T. A.; de Boer, J. W.; Browne, W. R.; Roelfes, G.; Feringa, B. L. *Chem. Commun.* **2004**, 2550-2551.
- (264) van den Heuvel, M.; van den Berg, T. A.; Kellogg, R. M.; Choma, C. T.; Feringa, B. L. *J. Org. Chem.* **2004**, *69*, 250-262.
- (265) Sastri, C. V.; Seo, M. S.; Park, M. J.; Kim, K. M.; Nam, W. *Chem. Commun.* **2005**, 1405-1407.
- (266) Grune, T. *Biogerontology* **2000**, *1*, 31-40.
- (267) Szweda, P. A.; Friguet, B.; Szweda, L. I. *Free Radical Biol. Med.* **2002**, *33*, 29-36.
- (268) Cecarini, V.; Ding, Q.; Keller, J. N. *Free Radical Res.* **2007**, *41*, 673-680.
- (269) Grune, T.; Reinheckel, T.; Joshi, M.; Davies, K. J. A. *J. Biol. Chem.* **1995**, *270*, 2344-2351.
- (270) Meara, J. P.; Rich, D. H. *J. Med. Chem.* **1996**, *39*, 3357-3366.
- (271) Costas, M.; Mehn, M. P.; Jensen, M. P.; Que, L., Jr. *Chem. Rev.* **2004**, *104*, 939-986.
- (272) Lee, Y.-M.; Hong, S.; Morimoto, Y.; Shin, W.; Fukuzumi, S.; Nam, W. *J. Am. Chem. Soc.* **2010**, *132*, 10668-10670.

(273) Zuo, J.; Schmitt Sara, M.; Zhang, Z.; Prakash, J.; Fan, Y.; Bi, C.; Kodanko Jeremy, J.; Dou, Q. P. *J. Cell. Biochem.* **2012**.

(274) Duelund, L.; Hazell, R.; McKenzie, C. J.; Preuss Nielsen, L.; Toftlund, H. *J. Chem. Soc., Dalton Trans.* **2001**, 152-156.

(275) Tang, H.; Arulsamy, N.; Radosz, M.; Shen, Y.; Tsarevsky, N. V.; Braunecker, W. A.; Tang, W.; Matyjaszewski, K. *J. Am. Chem. Soc.* **2006**, *128*, 16277-16285.

(276) Zheng, D.; Birke, R. L. *J. Am. Chem. Soc.* **2002**, *124*, 9066-9067.

(277) Birch, C. S.; Brasch, N. E.; McCaddon, A.; Williams, J. H. H. *Free Radical Biol. Med.* **2009**, *47*, 184-188.

(278) Pezacka, E.; Green, R.; Jacobsen, D. W. *Biochem. Biophys. Res. Commun.* **1990**, *169*, 443-450.

(279) Weissbach, H.; Taylor, R. T. *Fed. Proc.* **1966**, *25*, 1649-1656.

(280) Brasch, N. E.; Hsu, T.-L. C.; Doll, K. M.; Finke, R. G. *J. Inorg. Biochem.* **1999**, *76*, 197-209.

(281) Shevell, M. I.; Rosenblatt, D. S. *Can. J. Neurol. Sci.* **1992**, *19*, 472-486.

(282) Elgy, C. N.; Wells, C. F. *J. Chem. Soc., Dalton Trans.* **1980**, 2405-2409.

(283) Springborg, J.; Schaeffer, C. E. *Acta Chem. Scand.* **1973**, *27*, 3312-3322.

(284) Jackson, W. G.; Dickie, A. J.; Bhula, R.; McKeon, J. A.; Spiccia, L.; Brudenell, S. J.; Hockless, D. C. R.; Willis, A. C. *Inorg. Chem.* **2004**, *43*, 6549-6556.

(285) Poth, T.; Paulus, H.; Elias, H.; Van Eldik, R.; Grohmann, A. *Eur. J. Inorg. Chem.* **1999**, 643-650.

(286) The mean value for Co(III)-N bond lengths in classical complexes, both aliphatic and py, is 1.96(1) Å using survey parameters $(\text{NH}_3)_6\text{Co(III)}^{3+}$, $(\text{en})_3\text{Co(III)}^{3+}$ and

N5Co(III)Cl²⁺. The mean Co-Cl distance in the latter category is 2.26(2) Å. *Cambridge Structural Database*, Cambridge, UK, 2009.

(287) Hammoud, M. M.; McKamie, J. J.; Heeg, M. J.; Kodanko, J. J. *Dalton Trans.* **2008**, 4843-4845.

(288) Bombieri, G.; Forsellini, E.; Del Pra, A.; Tobe, M. L. *Inorg. Chim. Acta* **1981**, *51*, 177-183.

(289) McLachlan, G. A.; Brudenell, S. J.; Fallon, G. D.; Martin, R. L.; Spiccia, L.; Tiekink, E. R. T. *J. Chem. Soc., Dalton Trans* **1995**, 439-447.

(290) Kojima, T.; Weber, D. M.; Choma, C. T. *Acta Crystallogr., Sect. E* **2005**, *E61*, m226-m228.

(291) Geary, W. J. *Coord. Chem. Rev.* **1971**, *7*, 81-122.

(292) Rabenstein, D. L. *J. Am. Chem. Soc.* **1973**, *95*, 2797-2803.

(293) Pellizer, G.; Tauszik, G. R.; Costa, G. *J. Chem. Soc., Dalton Trans* **1973**, 317-322.

(294) Higgs, T. C.; Ji, D.; Czernuszewicz, R. S.; Matzanke, B. F.; Schunemann, V.; Trautwein, A. X.; Helliwell, M.; Ramirez, W.; Carrano, C. J. *Inorg. Chem.* **1998**, *37*, 2383-2392.

(295) Gahan, L. R.; Hughes, J. G.; O'Connor, M. J.; Oliver, P. J. *Inorg. Chem.* **1979**, *18*, 933-937.

(296) This reaction is slower because only a 4-fold excess of GSH is used and pD of reaction mixture was ~ 3.0 in D₂O.

(297) Adler, N.; Medwick, T.; Poznanski, T. J. *J. Am. Chem. Soc.* **1966**, *88*, 5018-5020.

- (298) Brasch, N. E.; Hamza, M. S. A.; Van Eldik, R. *Inorg. Chem.* **1997**, *36*, 3216-3222.
- (299) Thusius, D. *J. Am. Chem. Soc.* **1971**, *93*, 2629-2635.
- (300) Nome, F.; Fendler, J. H. *J. Chem. Soc., Dalton Trans* **1976**, 1212-1219.
- (301) Baldwin, D. A.; Betterton, E. A.; Pratt, J. M. S. *Afr. J. Chem.* **1982**, *35*, 173-175.
- (302) Stochel, G.; Van Eldik, R.; Kunkely, H.; Vogler, A. *Inorg. Chem.* **1989**, *28*, 4314-4318.
- (303) Stochel, G.; Van Eldik, R. *Inorg. Chem.* **1990**, *29*, 2075-2077.
- (304) Hamza, M. S. A.; Duecker-Benfer, C.; Van Eldik, R. *Inorg. Chem.* **2000**, *39*, 3777-3783.
- (305) Randall, W. C.; Alberty, R. A. *Biochemistry* **1967**, *6*, 1520-1525.
- (306) Reenstra, W. W.; Jencks, W. P. *J. Am. Chem. Soc.* **1979**, *101*, 5780-5791.
- (307) Prinsloo, F. F.; Meier, M.; van Eldik, R. *Inorg. Chem.* **1994**, *33*, 900-904.
- (308) Prinsloo, F. F.; Breet, E. L. J.; van Eldik, R. *J. Chem. Soc., Dalton Trans* **1995**, 685-688.
- (309) Meier, M.; van Eldik, R. *Inorg. Chem.* **1993**, *32*, 2635-2639.
- (310) Marques, H. M. *J. Chem. Soc., Dalton Trans.* **1991**, 339-341.
- (311) Marques, H. M.; Bradley, J. C.; Campbell, L. A. *J. Chem. Soc., Dalton Trans.* **1992**, 2019-2027.
- (312) Marques, H. M.; Bradley, J. C.; Brown, K. L.; Brooks, H. *J. Chem. Soc., Dalton Trans.* **1993**, 3475-3478.
- (313) Marques, H. M.; Munro, O. Q.; Cumming, B. M.; de Nysschen, C. *J. Chem. Soc., Dalton Trans.* **1994**, 297-303.

- (314) Drljaca, A.; Hubbard, C. D.; Van Eldik, R.; Asano, T.; Basilevsky, M. V.; Le Noble, W. J. *Chem. Rev.* **1998**, *98*, 2167-2289.
- (315) Van Eldik, R.; Asano, T.; Le Noble, W. J. *Chem. Rev.* **1989**, *89*, 549-688.
- (316) *Inorganic High Pressure Chemistry: Kinetics and Mechanisms*; Van Eldik, R., Ed.; Studies in Inorganic Chemistry; 1986; Vol. 7, p 448.
- (317) Leipoldt, J. G.; Van Eldik, R.; Kelm, H. *Inorg. Chem.* **1983**, *22*, 4146-4149.
- (318) Perry, C. B.; Fernandes, M. A.; Brown, K. L.; Zou, X.; Valente, E. J.; Marques, H. M. *Eur. J. Inorg. Chem.* **2003**, 2095-2107.
- (319) Knapton, L.; Marques, H. M. *Dalton Trans.* **2005**, 889-895.
- (320) Brown, K. L.; Cheng, S.; Zou, X.; Zubkowski, J. D.; Valente, E. J.; Knapton, L.; Marques, H. M. *Inorg. Chem.* **1997**, *36*, 3666-3675.
- (321) Chemaly, S. M.; Florczak, M.; Dirr, H.; Marques, H. M. *Inorg. Chem.* **2011**, *50*, 8719-8727.
- (322) Harney, A. S.; Lee, J.; Manus, L. M.; Wang, P.; Ballweg, D. M.; La Bonne, C.; Meade, T. J. *Proc. Natl. Acad. Sci. U. S. A.* **2009**, *106*, 13667-13672.
- (323) Louie, A. Y.; Meade, T. J. *Proc. Natl. Acad. Sci. U. S. A.* **1998**, *95*, 6663-6668.
- (324) Takeuchi, T.; Bottcher, A.; Quezada, C. M.; Meade, T. J.; Gray, H. B. *Bioorg. Med. Chem.* **1999**, *7*, 815-819.
- (325) Hurtado, R. R.; Harney, A. S.; Heffern, M. C.; Holbrook, R. J.; Holmgren, R. A.; Meade, T. J. *Mol. Pharmaceutics* **2012**, *9*, 325-333.
- (326) Abouelatta, A. I.; Sonk, J. A.; Hammoud, M. M.; Zurcher, D. M.; McKamie, J. J.; Schlegel, H. B.; Kodanko, J. J. *Inorg. Chem.* **2010**, *49*, 5202-5211.
- (327) Sheldrick, G. M. *Acta Crystallogr., Sect. A* **2008**, *A64*, 112-122.

(328) APEX-II collection and processing programs are distributed by the manufacturer. Bruker AXS Inc., M. W., USA 2005.

(329) Van de Bittner, G. C.; Dubikovskaya, E. a.; Bertozzi, C. R.; Chang, C. J. *Proc. Natl. Acad. Sci. U. S. A.* **2010**, *107*, 21316-21321.

(330) Verschoor, M. L.; Wilson, L. A.; Singh, G. *Can. J. Physiol. Pharmacol.* **2010**, *88*, 204-219.

ABSTRACT**METAL COMPLEXES OF NON-HEME LIGANDS: BIOLOGICAL APPLICATIONS**

by

JAI PRAKASH

August 2012

Advisor: Dr. Jeremy J. Kodanko**Major:** Chemistry**Degree:** Doctor of Philosophy

Oxidative inactivation of proteins (carbonic anhydrase-I, trypsin, chymotrypsin and 20S proteasome) by non-heme iron complexes, and glutathionylation of non-heme cobalt complexes mimicking the N5 coordination environment like that of biologically important cofactor cobalamin or B₁₂ (Cbl) are reported. Different non-heme ligand sets or inhibitors were used to inactivate different proteins. Carbonic anhydrase-I (CA-I) and 20S proteasome were inactivated by iron complexes in the presence of O₂ and a reductant (DTT), consistent with a pathway involving the reductive activation of O₂, whereas serine proteases trypsin and chymotrypsin were inactivated by ferryls (single turnover), and by an iron complex in presence of biologically relevant oxidant, H₂O₂ (catalytic conditions). Analysis of the CA-I inactivation products by SDS-PAGE, ESI-MS and LC/MS/MS confirmed that the protein is inactivated by oxidation of amino acid side chains (His, Trp and Met) rather than fragmentation of the protein backbone. On the other hand, amino acid analysis of serine proteases inactivation products confirmed that residues Cys, Tyr, and Trp were oxidized under single turnover condition while the residue tyrosine was oxidized selectively under catalytic conditions. Control experiments preclude the role of ROS, and supported the role of a metal-based oxidant responsible

for protein inactivation in all the cases.

A low spin Co(III) cobalamin model complex derived from a polypyridyl pentadentate N5 non-heme ligand was synthesized and characterized fully by X-ray crystallography, UV-vis, IR, $^1\text{H-NMR}$ and $^{13}\text{C-NMR}$ spectroscopies, and mass spectrometry (HRMS). Kinetic and thermodynamic studies on the reaction of this cobalt complex along with another related congener with glutathione were performed in aqueous buffer to generate biomimetic species of glutathionylcobalamin, an important form of cobalamin found in nature. The reaction follows second order kinetic, with both the rate constants and the observed equilibrium constants smaller than the rate constants and equilibrium constant of the reaction of aquacobalamin and GSH to give glutathionylcobalamin. Glutathionylation showed significant pH dependence, where rates increased with pH. Taken together, these results suggest that glutathionylation is a general reaction for Co(III) complexes related to Cbl.

AUTOBIOGRAPHICAL STATEMENT

JAI PRAKASH

EDUCATION

- **2007-2012:** Ph.D., Organic Chemistry, Wayne State University, Detroit, MI, USA
- **2004-2007:** M.S., Indian Institute of Science, Bangalore, India
- **2001-2004:** B.Sc., St. Stephen's College, Delhi, India

HONORS AND AWARD

- **2012:** Graduate Student Professional Travel Award, WSU
- **2011:** Thomas C. Rumble University Graduate Fellowship, WSU
- **2011:** Summer Dissertation Fellowship, WSU
- **2011:** Graduate School Citation for Excellence in Teaching, WSU
- **2010:** Graduate School Citation for Excellence in Teaching, WSU
- **2009:** Norman A. LeBel Endowed Graduate Award in Organic Chemistry, WSU
- **2008:** Phi Lambda Upsilon (PLU) Honor Society, WSU
- **2006:** Junior Research Fellowship (JRF), Council of Scientific Industrial Research (CSIR), India
- **2004:** Prof. A. C. Jain Merit Scholarship Prize, St. Stephen's College, Delhi, India
- **2004:** Sardar Hansa Singh Memorial Chemistry Prize, St. Stephen's College, India

PUBLICATIONS

- Zuo, J.; Schmitt, S. M.; Zhang Z.; **Prakash, J.**; Fan, Y.; Bi, C.; Kodanko, J. J.; Dou, Q. P. "Novel polypyridyl chelators deplete cellular zinc and destabilize the X-linked inhibitor of apoptosis protein prior to induction of apoptosis in human prostate cancer cells" *J. Cell. Biochem.* **2012**, *accepted*
- **Prakash, J.** and Kodanko J. J. "Synthesis, characterization and glutathionylation of cobalamin (B₁₂) model complexes [Co(N₄PyCO₂Me)Cl]Cl₂ and [Co(Bn-CDPy₃)Cl]Cl₂" *Inorg. Chem.* **2012**, *51*, 2689-2698.
- **Prakash, J.**; Schmitt, S. M.; Dou Q. P. and Kodanko J. J. "Targeting purified 20S proteasome by non-heme iron complexes" *Metallomics*, **2012**, *4*, 174-178.
- **Prakash, J.** and Kodanko, J. J. "Selective inactivation of serine proteases by non-heme iron complexes" *Inorg. Chem.* **2011**, *50*, 3934-3945.
- Singh, A. K.; Kumari, S.; Row, T. N. G.; **Prakash, J.**; Kumar, K. R.; Sridhar, B.; Rao, T. R. "Coordination of a mesogenic Schiff-base with Mn(II), Co(II), Ni(II), Cu(II) and Zn(II): Synthesis, spectral studies and crystal structures" *Polyhedron* **2008**, *27*, 3710-3716.